Prediction of Zone Temperatures, Cooling Loads and Illuminances from Numerical Simulation of the Interaction Between Fluorescent Lighting and HVAC Systems

by

TSE-MING CHUNG

A doctoral thesis submitted in partial fulfilment of the requirements

for the award of

Doctor of Philosophy

of Loughborough University

June 1998

Abstract

of a PhD Thesis on

Prediction of Zone Temperatures, Cooling Loads and Illuminances from Numerical Simulation of the Interaction Between Fluorescent Lighting and HVAC Systems

by

T.M. Chung

A numerical model has been developed for the dynamic simulation of heat and radiation transfer from lamps and ballasts in an enclosure. The model, named LITEAC1, calculates temperatures, cooling loads and illuminances at each simulation time step. LITEAC1 is an improvement upon existing models in the literature in the following aspects: it performs dynamic simulation for all nodes without assuming that some nodes are massless; it calculates illuminances on room surfaces; and it runs faster on a desktop computer. In order to refine the simulation of the two-way interaction between lighting and HVAC systems, a fluorescent lamp positive column discharge model, named LAMPPC, has been incorporated into LITEAC1 to improve calculation of the conversion of input electrical energy into light, thermal radiation and heat. LAMPPC employs established principles in plasma physics to quantify the energy conversion processes. It was tested, as a stand-alone program, using published experimental results. The integration of LAMPPC with LITEAC1 produces a new model called LITEAC2. Predictions of LITEAC1 and LITEAC2 have been shown to give good agreement with experimental and theoretical results in the literature. A laboratory test cell has been constructed for the further validation of LITEAC2. The main contributions to knowledge of this work consist of: the inclusion of a fluorescent lamp discharge model within the numerical simulation of the interaction between lighting and HVAC systems; the methodologies developed for the calculation of heat and radiation transfer from lamps; the ability to calculate light output and lamp power. These afford significant improvements over previous numerical studies of lighting/HVAC interaction through integration of thermal and lighting performance simulation. Designers are now able to predict both the dynamic cooling load due to lighting and the thermal effects on the room illuminance provided by fluorescent lighting installations. This work also introduces a tool for the research community to look seriously into the effect of temperature on the performance of lighting systems and its implication on energy efficiency.

Acknowledgments

The author wishes to express his grateful thanks to his Supervisor, Dr. D.L. Loveday, and his Director of Research, Professor V. Hanby at Loughborough University for their useful discussions, valuable suggestions, critical comments, guidance and encouragement given during the course of this work. Sincere thanks are also due to Professor W.K. Chow for his support, guidance and encouragement.

The author is also grateful to Professor E. Sowell of California State University for providing the LIGHTS program.

This work was supported by The Hong Kong Polytechnic University as a staff development programme for the author and thanks for this support is gratefully acknowledged.

The support and encouragement given by Professor J. Burnett and the author's other colleagues at the Department of Building Services Engineering of The Hong Kong Polytechnic University are very much appreciated.

Table of Contents

Page

List of Tables

List of Figures

Page

Chapter 10

Chapter One

Introduction

1.1 Background

For people to work efficiently and in comfort in modern office buildings, a good visual and thermal environment is essential Provided that adequate glare controls are installed, a good visual environment can be realized using daylight which is preferred by many people both for its quality and its energy saving potential. However, due to the variable nature of daylight, electric lighting is essential in modern office buildings. In Hong Kong, due to the shortage of land, office buildings are high rise and the ceiling height of typical offices is small so that only a shallow perimeter area near windows has sufficient daylight for general illumination. Hence, electric lighting is the main light source in office buildings in Hong Kong and in deep plan buildings worldwide. In the subtropical climate of Hong Kong, summer is long, and hot and humid. Therefore, air-conditioning is essential in office buildings so as to provide a comfortable environment for office workers. Even during winters, air-conditioning is very often necessary to extract the heat generated internally by lighting, equipment and occupants. Heating is not a major requirement in Hong Kong; although heating systems are installed in many first class office buildings, they are in operation for very short periods (less than 10 days on average) each year.

Hence, lighting and HVAC are the two major energy consumers in modern office buildings in Hong Kong as well as in many other parts of the world. The actual proportions of electricity used by lighting and HVAC respectively vary geographically and seasonally with changes in climate. In offices in the UK, lighting often accounts for around 50% of the electricity used (Energy Efficiency Office 1991). In California, U.S.A., lighting accounts for more than 40% of all commercial electric energy use (California Energy Commission 1993). According to the Hong Kong Census and Statistics Department (1996), the commercial sector in Hong Kong consumed 64,751 TJ of electricity in 1996. There is no detailed data about the split of this figure into consumption by lighting, HVAC and other equipment. However, surveys in individual buildings (Chow and Chan 1993; Lam 1995) showed that HVAC accounted for 54% to 60%, and lighting accounted for 21% to 28%, of the total electricity consumption of a building. Therefore, a good estimate is that about 55% (which amounts to about 35,600 TJ) is consumed by HVAC, and about 25% (which amounts to about 16,200 TJ) is consumed by lighting. An energy saving of only 1% of each would be equivalent to 518 TJ, which at present prices would save about HK$ 119 million or UK£ 9.3 million.

Although lighting and HVAC are different systems in a building and provide different functions, they have a mutual effect upon each other when they are operating simultaneously. Lighting produces heat which must be taken away by the air-conditioning in order to maintain thermal comfort. At the same time, air-conditioning affects the lamp temperature which in turn has a strong influence on the light output of fluorescent lamps, these being the major type of light source in use nowadays. In other words, there is a mutual interaction between lighting and HVAC: lighting adds to the cooling load and the ambient temperature affects the lighting output. This mutual interaction is shown schematically in Figure 1.1 and it is discussed in the following paragraphs.

1.1.1 The heating effect of electric lighting

The energy consumed by electric lighting appears as heat in building interiors and thus lighting power is a large source of heat gain in buildings. In fact, in interior zones of typical office buildings where solar heat gain is absent, lighting is the largest source of heat gain. This heat gain may be beneficial to occupants in buildings situated at locations with a cold climate, but for hot climates and for the cooling season of temperate climates this heat gain adds to the cooling load of the air-conditioning system.

Electric lamps convert electrical energy to light. However, even for the most efficient light source, a large proportion of the energy input to the luminaire is converted to heat directly and is sensed as a raised temperature on lamp and ballast surfaces. The remaining energy is radiated out from the lamp as electromagnetic radiation in both the visible and invisible ranges of wavelength. Ultimately, all electric energy input to lighting (less a small proportion which is lost to the outside through windows) becomes heat gain to the space in two forms. One form is the convective and/or conductive heat gain due to the raised temperature on lamp and ballast surfaces; this adds heat to the space instantaneously. The second form is thermal and visible radiation emitted from the lamps which is absorbed by room and furniture surfaces and causes an increase in room and furniture surface temperatures; this temperature increase will, after a time lag, add heat to the space through convection. At steady state, the rate of space heat gain due to lights is equal to the lighting power input if all the lighting radiation are trapped within the space (e g. for an interior zone with no windows). However, in most offices, lights are switched off after office hours and some energy conscious occupants turn off the lights when the room is unoccupied, also, some building management systems (BMS) do this via occupancy detectors; thus, steady state conditions are not normally attained due to these on/off cycles. The instantaneous rate of heat gain from lights therefore depends on a number of factors which include the on/off schedule of the lighting, the configuration of the room, room surfaces and furniture thermal properties and the room ventilation rate.

1.1.2 The effect of the HVAC system on lighting performance

The performance of fluorescent lamps, which are the most widely used lamps in office buildings, is affected by the HVAC system. The luminous flux output, the lighting power and the efficacy of fluorescent lamps are closely related to the minimum lamp wall temperature (IESNA 1993). Figure 1.2 shows the variation of light output, lamp power and efficacy with the minimum lamp wall temperature. For tubular fluorescent lamps inside a box luminaire (the most common configuration in modern office buildings), the minimum lamp wall temperature depends on the following factors: the lamp compartment air temperature; the dimensions of the luminaire; the number of lamps inside the luminaire; the space between lamps; whether the luminaire is vented; the ventilation rate through the lamp compartment. Verderber et al. (1988) quoted statistics in the United States and deduced that about 73% of fluorescent lamps in offices are operating at a temperature 10° to 20°C higher than the optimum temperature for maximum light output and highest efficiency. It would mean, from Figure 1.2, that these lamps give only 70 to 90% of their maximum light output.

Energy for lighting and the number of lamps required to provide the desired illuminance will be minimized if the lamps are operated at their most efficient temperature. The heat gain to the building space from the lamps would also be minimized at this condition, meaning minimum cooling loads from lighting and hence less energy for providing best comfort conditions for the occupants.

1.2 Research motivation

In the preceding section it was stated that there is a two-way interaction between lighting and HVAC systems. Factors affecting these interactions are complex, but it is necessary to consider these interactions in combination. There have been some studies of these interactions reported in the literature. However, most studies so far have treated the interactions in only a 'one-way' manner, i.e. either the heat released from luminaires as a cooling load for the air-conditioning (Kimura and Stephenson 1968; Mitalas and Kimura 1971; Ball and Green 1983; Sowell 1989, 1990), or the effects of air temperature and ventilation around the lamps on the performance of the lamps in respect of light output and efficiency (Siminovitch et al. 1984, 1988). Furthermore, mathematical models of lighting/HVAC interactions in the literature (e.g. Ball and Green 1983; Sowell 1989, 1990) were developed for the calculation of cooling load due to lights but not for the calculation of light output or illuminance on room surfaces in conjunction with the HVAC system. There do not appear to have been any mathematical modelling studies of the effect of the ambient thermal environment on light output or on lighting system efficiency. Studies of how the thermal environment affects the light output of fluorescent lamps have been largely experimental and empirical with little attention to the physical processes that cause the dependence of light output on ambient temperature (Siminovitch et al. 1984; Collins et al. 1992). In order to perform the following tasks: calculation of the transient cooling load from lighting so that effects of changes in the thermal environment on lighting power are taken into account, and calculation of light output and lighting system efficiency during the whole period when air-conditioning is on, it is necessary to study the interaction in a 'two-way' manner, i.e. to model the mutual interaction.

The study of these interactions can be done either theoretically (using analytical or numerical modelling techniques), or experimentally (using purpose-built model rooms or 'real' rooms in existing office buildings). Performing experimental studies is expensive, and usually gives results which are 'system specific', that is, they are only applicable to the building/room configurations investigated. Sowell (1990) argued that full-scale test cells were not the best way to assess the thermal effects of lighting because of problems in obtaining a balance between measured addition and removal of heat. Sowell (1990) also pointed out that errors occurred in the results of the experimental study of Treado and Bean (1992) on lighting/HVAC interaction (details of this experimental study will be described in Chapter 8) due to difficulties encountered in accurate measurement of air mass flow rates and of temperatures, and in elimination of boundary losses. On the other hand, numerical modelling techniques have been developed to a stage such that these can be used to simulate many physical situations, thereby removing the need to carry out an exhaustive range of actual physical experiments. This is particularly true for experiments which require extensive change of parameters to obtain a set of meaningful results. With today's fast and powerful desktop computers, many codes of numerical models can be run conveniently on a desktop machine.

In consideration of the above background, it is proposed to undertake a numerical study of the interaction between lighting and HVAC systems using mathematical modelling techniques, with the aim of predicting not only cooling loads and temperatures but also light output and lighting system performance; it is also proposed to investigate application of the results to reducing energy consumption by lighting and hence to increasing efficiency.

1.3 Research objectives

The objectives of this study are as follows:

(i) Based on fundamental principles of heat transfer, to produce a mathematical model for calculating the conversion of lighting energy into air-conditioning load for the typical lighting systems in office environments.

(ii) To model the conversion of electrical energy to light and heat using a fluorescent lamp positive column model, and thus to investigate the relationship between light output/efficiency of fluorescent lamps and the ambient thermal environment, as well as the effect of different HVAC designs on lighting performance in respect of light output and energy efficiency.

(iii) To validate the models using published results from the literature and experimental data from a simple test cell constructed in the laboratory.

(iv) To assess the implications of the models for the design of lighting and HVAC systems for office buildings.

1.4 Research methodology

Several tasks were identified for this study of the interaction between lighting and HVAC systems. These tasks are described below:

1.4.1 Literature search

A search of the literature on the subject has been undertaken during the initial stage of the research. Developments in the subject have also been regularly reviewed during the course of the project. The major papers reviewed are listed in the Reference section at the end of this thesis. Literature that has been reviewed includes papers on modelling of heat gain or cooling load due to lighting, design guides for the calculation of cooling loads from lighting, articles on the performance characteristics of fluorescent lamps under different ambient thermal conditions and mathematical models of the positive column of fluorescent lamps, as well as experimental studies.

It may be worthwhile to mention that during the early stage of this research, contacts were made with local and international luminaire manufacturers requesting data on the build up of temperature inside luminaires. Some data were obtained relating to the safety of luminaires due to temperature rise. It was found that these data were of little value for this study as the temperatures measured were related to the starter, capacitor, wiring, or lamp holder, but there were no temperature data relating to the lamp surface, luminaire walls or the air inside the luminaire. It can be concluded that the major lamp and luminaire manufacturers do not have useful data for this research. However, this does not suggest that such data are unnecessary but only that current design practice ignores the effect of temperature on light output and efficiency of fluorescent lamps. The problem actually exists as Verderber et al. (1988) deduced from statistics in the United States that about 73% of fluorescent lamps in offices are operating at 10° to 20°C higher than the optimum temperature for maximum light output. It can be deduced from Figure 1.2 that these lamps emit only about 70 to 90% of their maximum light output.

1.4.2 Mathematical modelling

The main task of the research is to produce a detailed mathematical model of a typical fluorescent luminaire within a typical air-conditioned office for the study of both the heat release from the luminaire and the temperature build-up inside the luminaire. This will be a completely new model developed for this research and it will be called LITEAC1. LITEAC1 will be different from existing models and it will treat the heat transfer inside the enclosure in a more comprehensive manner than existing models (Sowell 1989, 1990; Ball and Green 1983).

One shortcoming of existing models is that they do not calculate the conversion of electrical energy into light and heat but assume either that the energy input to lights is divided arbitrarily into light (short-wave radiation), long-wave radiation and convective heat (Ball and Green 1983), or that detailed data in short-wave radiation power output of the lamp is known (Sowell 1989, 1990). Furthermore, in existing models, the effect of lamp-wall temperature on light output and lighting power is either ignored (Ball and Green 1983), or taken into account using empirical curves (Sowell 1989, 1990). Thus, existing mathematical models of lighting/HVAC interaction simulate essentially the effect of lighting on cooling load of HVAC. As mentioned previously, this study focuses on the two-way interaction between lighting and HVAC system design. Hence, the aim of the mathematical model to be developed in this research is to not only simulate and predict the effect of lighting on HVAC cooling load, but also to predict, by theoretical calculations based on the conversion of energy inside the fluorescent lamp, the effect of the ambient thermal environment (which is affected by the HVAC system) on the light output and hence the illuminance on room surfaces. To do the latter, a model of the fluorescent lamp discharge, which simulates the dependence of light output on lamp-wall temperature based on theoretical calculations of the physical processes inside the discharge, will be developed specially for this research. This will be basically a fluorescent lamp positive column model based on similar hypotheses as used in previous positive column models such as Waymouth and Bitter (1956) and Lama et al. (1982). This model will be called LAMPPC and will be incorporated into LITEAC1 as a subroutine for the better simulation of light output and lighting power without the necessity of using empirical data on the temperature dependence of light output. The integration of LAMPPC into LITEAC1 will form a new program called LITEAC2. A schematic diagram showing the energy flow path modelled in LITEAC2 is given in Figure 1.3.

1.4.3 Model validation

In order to fully test the proposed new mathematical model LITEAC2 (which combines the room model LITEAC1 and the fluorescent lamp model LAMPPC), validation of the model is performed in several different ways. Firstly, computer-generated results of the room model LITEAC1 are compared with a simple analytical example which has a closed form solution. Secondly, the fluorescent lamp positive column model LAMPPC is validated against published data from modelling and experimental studies. Thirdly, the combined room and fluorescent lamp model LITEAC2 is validated with experimental data from two different sources which are:

(i) experimental data from a full-scale test performed at the National Institute of Standards and Technology (NIST) in the USA as published in Treado and Bean (1988, 1990 and 1992), and

(ii) the data from measurements inside a laboratory test cell containing a fluorescent luminaire, constructed as part of this research.

In addition to experimental validation, the simulated results of the room model, LITEAC1, and the combined room and fluorescent lamp model, LITEAC2, are compared with that of Sowell's LIGHTS model (Sowell 1989, 1990) for several configurations.

1.5 Outline of thesis

The thesis is organised into 11 chapters. In this chapter, Chapter 1, an introduction to the need for studying the two-way interaction between lighting and HVAC system is given. The background, the motivation, the objectives and the tasks of the research work are established. An overview of the work performed in this study is given and the organisation of the thesis is outlined.

Chapter 2 is the literature survey on the subject of heat from lights in an enclosure. It first gives a summary of the development of theoretical models of lighting heat transfer. Experimental studies on this subject are also reviewed. A review of current design guides then follows. The shortcomings of these models and of the current design guidance are then addressed.

One of the objectives of this study is to develop a fluorescent lamp model suitable for incorporation into the heat transfer model of a room with a luminaire. Therefore, a review of fluorescent lamp models is given in Chapter 3. Experimental studies of the fluorescent lamp positive column are also reviewed. Current design guidance on the treatment of thermal effects on light loss and lamp power is also discussed in Chapter 3.

In Chapter 4, the proposed new mathematical model of an enclosure with luminaires, LITEAC1, is described in detail. The derivation of the model from first principles is presented together with the solution scheme for coding into a computer program. A simple test of LITEAC1 using an enclosure with closed analytical solution is described.

Chapters 5 and 6 contain the main thrust of this research work. In Chapter 5, the new model of a fluorescent lamp positive column, LAMPPC, is elaborated; this model is suitable for incorporation into a heat transfer model of an enclosure for studying the two-way interaction of lighting and HVAC systems. The chapter opens with a discussion of the fluorescent lamp energy balance and the energy conversion processes inside the fluorescent tube. It is followed by a discussion of the balance of the different mercury excited states inside the fluorescent tube.

In Chapter 6, the procedure and approximations used to solve the energy balance and the continuity equations developed in Chapter 5 are described in detail. The algorithm for the calculation of light output from the fluorescent lamps is also described.

Chapter 7 describes the validation of the new fluorescent lamp model, LAMPPC, using experimental results from the literature. The results predicted by the model are compared with experimental results, and with results predicted by more sophisticated models used in plasma physics research; a discussion on the validity of LAMPPC used in this study is given.

Chapter 8 describes the validation of the new lighting/HVAC interaction model, LITEAC2 (which integrates LITEAC1 and LAMPPC), based on experimental results from the literature. The simulated results from LITEAC1 and LITEAC2 are compared with the experimental data of the full-scale test performed at NIST as published in Treado and Bean (1988, 1990 and 1992); the validity of LITEAC1 and LITEAC2 when used as a simulation tool is discussed.

Chapter 9 describes a laboratory test cell constructed for the further validation of LITEAC1 and LITEAC2. Details of the test cell and of the comparison between measured results and simulated results are given. The validity of LITEAC1 and LITEAC2 for use in simulations for small enclosures is tested.

Chapter 10 summarises the comparison of LITEAC1 and LITEAC2 with an existing model, the 'LIGHTS' model, which has been claimed by Sowell (1990) as a "numerical lighting/HVAC test cell". Comparisons are made for one particular experimental configuration of the NIST as well as for the laboratory constructed test cell.

Chapter 11 discusses the possible applications of the new lighting/HVAC interaction model, LITEAC2, in design. Lastly, conclusions of the research work and recommendations for future study are given.

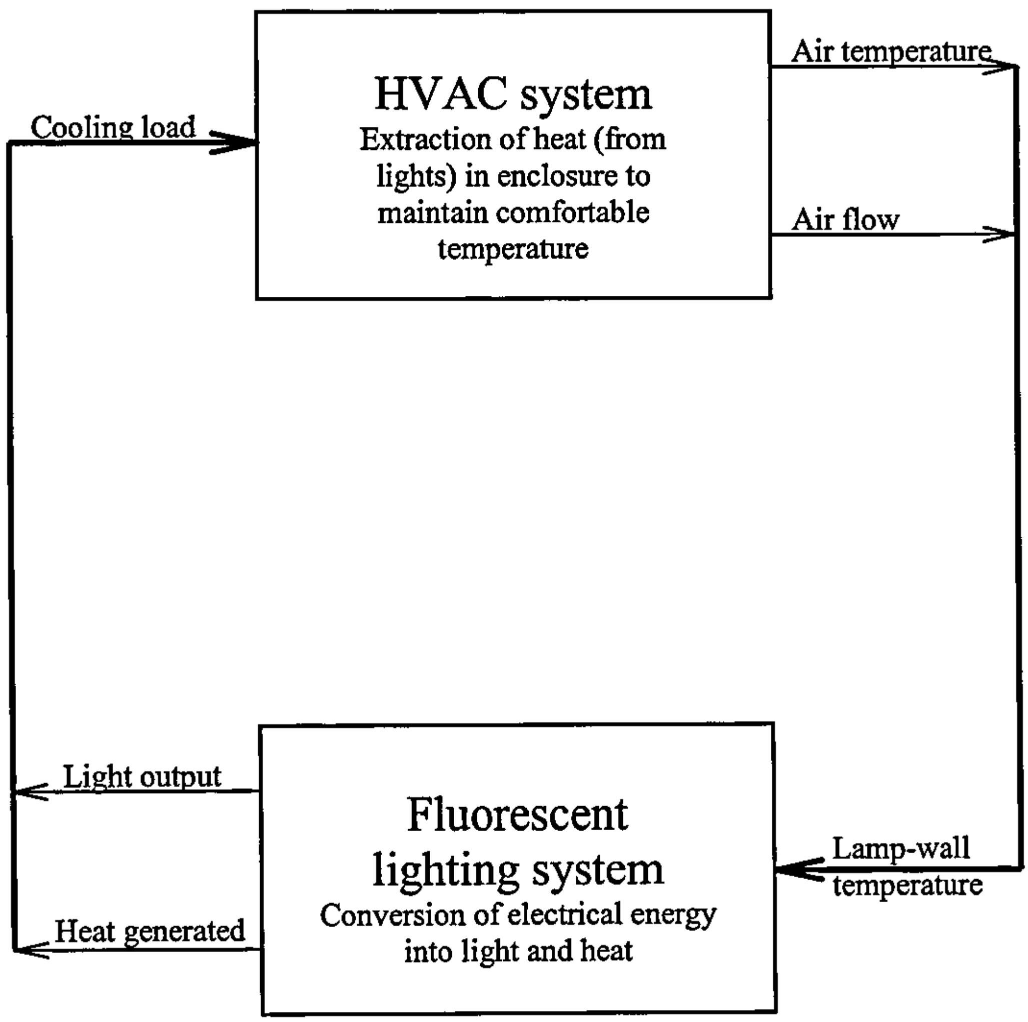

Figure 1.1

Schematic diagram showing the 2-way mutual interaction between HVAC system and fluorescent lighting system.

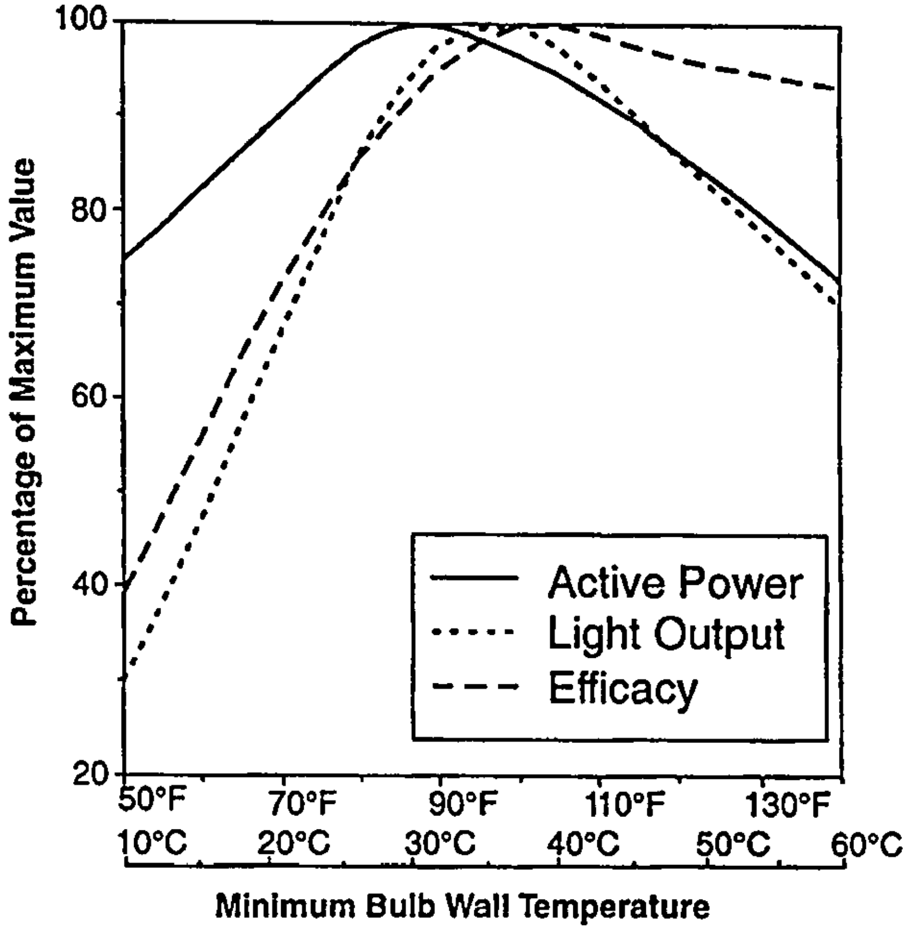

Figure 1.2

Typical fluorescent lamp temperature characteristics (From IESNA 1993).

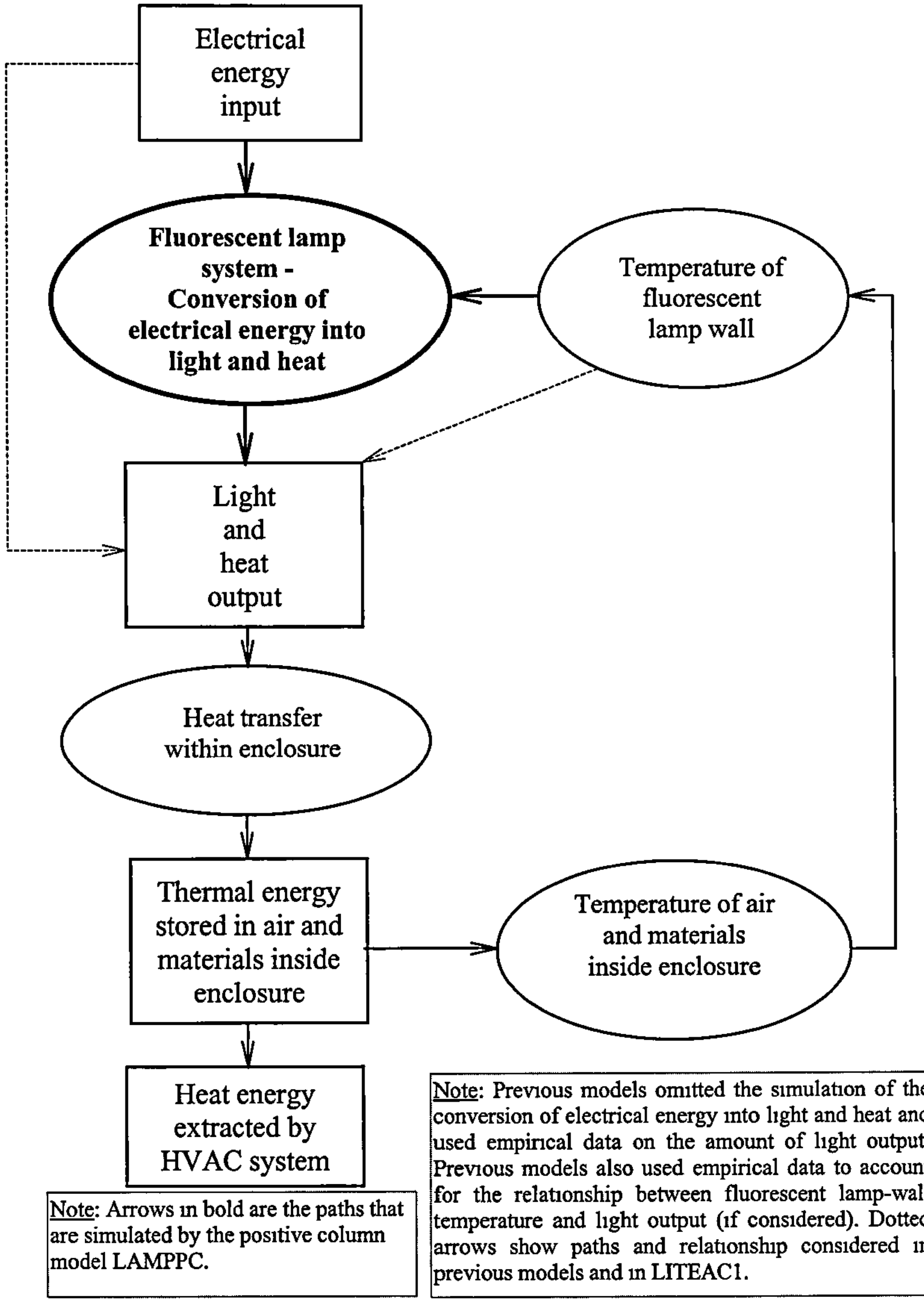

Figure 1.3
Schematic diagram showing the energy flow path of the electrical energy supplied to lighting and the relationship between energy flow and temperature in LITEAC2.

Chapter Two

Heat From Lights in an Enclosure

2.1 Background

The two major research objectives stated in Section 1.3 are as follows: (i) the development of a dynamic heat transfer model of the energy transport of lighting in an enclosure; (ii) the development of a fluorescent lamp positive column model which simulates the conversion by the fluorescent lamp of electrical energy into light and heat. In order to help define the current research so that improvements can be made to previous studies, literature concerning the study of the transport of lighting energy and its effects on the thermal environment and cooling load of an enclosure are reviewed and summarised in this chapter. The literature reviewed include theoretical modelling studies, experimental works and current design guidance.

2.2 Summary of previous studies

It has long been recognized that lighting is a source of indoor heat gain and can cause thermal discomfort to occupants. There have been a number of studies relating to heat gain from lighting, and discomfort due to heat and radiation from lighting.

During the first half of the 20th century, incandescent lamps were the main artificial light source. Incandescent lamps are not efficient in their light production and produce a lot of heat, so heat gain and thermal discomfort produced by incandescent lighting has always been a problem of concern. However, in the early days of this century, artificial lighting did not provide a lighting level as high as we enjoy today, so heat gain from lights was not a significant problem due to these low illuminance levels. The effects of such heat gains began to be seriously studied in the late 1930's when the general illuminance levels were high enough to produce discomfort. The first serious study of lighting heat gain was by Sturrock (1938) who, using measurements in occupied buildings, discussed the heating effects produced by incandescent lamps together with methods for removing this heat before it entered the room space.

During the 1940's, fluorescent lamps became available for general office lighting use. This represented an improvement to the problem of lighting heat gain compared to incandescent lamps because, for the same illuminance, fluorescent lamps produce much less heat. Again, lighting standards at that time did not regard the heating effect from lights as a serious concern, even though the efficiency of fluorescent lamps was not as high as that of today. Air-conditioning was also not as common as it is today, therefore studies of how heat from lighting affects air-conditioning were rare until the late 1960's.

In the late 1960's through to the early 1970's, several analytical models of heat transfer from lighting in a typical office room were developed (Kimura and Stephenson 1968; Nevins et al. 1971; Sowell and O'Brien 1973). The analytical study of Kimura and Stephenson (1968) led to experimental studies which were aimed at determining values of coefficients of the Z-transfer functions used in the analytical study (Nottage and Park 1969; Mitalas and Kimura 1971). Based on these experimental studies, design values of the coefficients used in the transfer function method for cooling load calculation were derived by Mitalas (1973a, 1973b) and these coefficients are still in use in current design guides (ASHRAE 1997).

2.3 Review of models of heat transfer from lighting

The first theoretical modelling study of heat transfer from lighting in a typical office configuration is that of Kimura and Stephenson (1968). They used a simple model of a room with a ceiling plenum, a recessed luminaire and a heat-storing floor slab. Lighting power was split arbitrarily into "upward" (released to plenum space) and "downward" (released to room space) fractions. Each of these fractions was assumed to be equally divided into a convective and a radiative heat transfer component but without any justifications. Using the response factor method developed by Stephenson and Mitalas (1967), they showed that the instantaneous cooling load due to lights can be expressed in terms of two coefficients:

$$\frac{q}{W} = 1 - Ae^{-Bt} \tag{2.1}$$

where q is the instantaneous cooling load at time t caused by lights (W),

W is the power input to lights at time t (W),

A (dimensionless) and B (hour^{-1}) are coefficients to be determined by experiment,

t is the time after the lights are turned on (hours).

Subsequently, the values of coefficients A and B were determined by Mitalas and Kimura (1971) using data from measurements in a full scale room calorimeter. As reported by Mitalas (1973b), results from the experimental study were of limited value for design calculations because they did not cover a sufficiently broad range of room constructions, ventilation apparatus or installation arrangements; all these factors affect the values of the coefficients A and B. Mitalas (1973b) showed, using Z-transfer functions, that the cooling load at time t_n, which is a whole number multiple of a fixed time step after lights on, i.e. $t=t_n=n\Delta$, where n is a whole number and Δ is a time step interval (usually one hour), is given by:

$$q(t_n) = a_1 W(t_{n-1}) + a_2 W(t_{n-2}) + b_1 q(t_{n-1}) \tag{2.2}$$

where $q(t_n)$ = cooling load from lights at $t=n\Delta$ (W),

$W(t_n)$ = power input to lights at $t=n\Delta$ (W),

a_1, a_2 and b_1 are transfer function coefficients (dimensionless).

The a_1 coefficient is the ratio of cooling load one hour after the lights are switched on to the power input to lights. It depends mainly on the short-term thermal storage characteristics of the room. These short-term characteristics depend, in turn, on the proportions of the lighting power that are dissipated by radiation and by convection, the luminaire geometry and lamp arrangement, the ventilation rate, the ventilation air supply and return arrangement, the type of ceiling, and the thermal properties of the surface layer of furniture, walls, floor, etc. The b_1 coefficient is a measure of the rate of cooling load increase or decrease after the lights are switched on or off, respectively. Its value is a strong function of room thermal storage characteristics and it also varies with changes in the heat transfer coefficient between room air and various surfaces in the room. Based on the experimental study of Mitalas and Kimura (1971), design values of a_1 and b_1 were given by Mitalas (1973b) in tabular form. These values are used in the transfer function method for cooling load calculation in the ASHRAE Handbook of Fundamentals (ASHRAE 1997). While a_1 and b_1 are independent coefficients, a_2 is dependent on a_1 and b_1 as follows:

$$a_2 = 1 - b_1 - a_1 \tag{2.3}$$

Sowell and O'Brien (1973) constructed a detailed analytical model representing a building unit cell with a fluorescent fitting recessed into the plenum. The unit cell was discretized into a number of nodes, and heat transfer in the form of conduction, convection and radiation between nodes was considered. For the steady-state condition, a heat balance equation in vector-matrix form was obtained. Sowell and O'Brien (1973) solved this vector-matrix equation numerically, and a set of steady-state nodal temperatures was obtained to enable the prediction of the effects of the lighting system on the thermal environment in the living space. More details of the vector-matrix equation will be given in Chapter 10.

Ball and Green (1983), in an ASHRAE-funded project, made a study using mathematical modelling of the transient energy transfer caused by lighting. Their model was based on heat balance calculation procedures in an explicit transient finite difference formulation and simulated primarily the conditions in a single specific building section with the room, the plenum and the luminaire being considered separately. Ball and Green (1983) compared their model predictions with the experimental results of Mitalas (1973b) and found some good and some poor agreements. Although Ball and Green gave no explanation of the poor agreements, they did mentioned that many assumptions were made regarding the physical properties of the test room facility of Mitalas. These assumptions might contribute to the large discrepancies found in some of the cases. Despite the poor agreement found in some of the test results with experimental data, Ball and Green (1983) developed sets of weighting factors for cooling load calculations and made some recommendations for their use. According to Ball and Green (1983), their aim was for the inclusion of the results of their project in the ASHRAE Handbook. However, results derived from their project were not used (with no reasons given) in revising the design data in the ASHRAE Handbook so that the latest edition of the Handbook (ASHRAE 1997) still uses the results of Mitalas (1973b).

Sowell (1990) added dynamic simulation to his earlier steady-state model (Sowell and O'Brien 1973), so that now the heat balance equation had an additional term comprising the product of heat capacitance and rate of temperature change. The modified equation will be discussed in Chapter 10. Sowell (1990) solved this vector-matrix equation by partitioning the equation into those nodes with finite thermal mass, and those nodes (with actual mass below a certain pre-defined value) declared to be massless. He also included the effect of lamp wall temperature on lamp power, and on luminous output, using empirical curves. Sowell called his model a "numerical lighting / HVAC test cell" and he argued that the use of his numerical test cell had advantages over the use of full-scale physical test cells. His numerical test cell was implemented in the 'C' programming language and was called the LIGHTS program (Sowell 1989). The LIGHTS program predicts temperatures and heat fluxes for all nodes, and cooling loads for the room. More details of the capabilities of LIGHTS will be discussed in Chapter 10. The LIGHTS program was validated by a number of simple examples with known solutions. Comparisons were also made with results from the NIST physical test cell (Treado and Bean 1988, 1990, 1992); however, agreement was generally poor. Sowell attributed the discrepancies between his model and the NIST data to model deficiencies or experimental error.

2.4 Experimental studies

2.4.1 Luminaire calorimeters

There have been several important experimental studies on the thermal performance of lighting systems and the interaction between lighting and HVAC systems. Early experimental works were aimed at the measurement of the energy distribution characteristics of various types of fluorescent luminaires using small calorimeters. Later works measured various interaction parameters using full scale room test facilities. Some of these studies were aimed at getting data for the derivation of values of coefficients (e.g. for the transfer function method) used in design calculations of cooling load due to lighting. Other studies were aimed at the validation of theoretical models of the interaction between lighting and HVAC systems.

Examples of the research efforts using small fluorescent luminaire calorimeters include: Bonvallet (1963), Ballman and Bradley (1964), Sylvester (1964), Ballman and Mueller (1965), and Nevins et al. (1971). These studies used small calorimeters to measure the heat released from a luminaire to the ambient air and/or the heat gained by air circulated through a luminaire. Typically, the calorimeters consisted of insulated boxes, with the luminaire mounted on the bottom face. An external fan attached to a duct allowed air to be drawn through the luminaire into the box and then exhausted from the box, which served as a plenum. The boxes were usually fitted with temperature sensors to measure air and luminaire surface temperatures; luminaire light output and power consumption were measured together with ventilation airflow rate. With the temperature difference between the air before and after passing through the luminaire and the air mass flow rate, the heat given off by the lamps can be deduced. These luminaire calorimeters provided much needed information regarding the heat output of lighting systems.

These luminaire calorimeters did not emulate the environmental conditions in which luminaires are usually installed, i.e. in a room with a plenum. Therefore, the calorimeters had weaknesses, for example, the thermal conditions surrounding the luminaire were not representative of a typical office room environment. This meant that the heat exchange by various modes was likely to be different in an actual installation than in a small calorimeter. Also, heat storage in the room and plenum could not be evaluated by a luminaire calorimeter.

2.4.2 Early full scale room tests

Due to these weaknesses of luminaire calorimeters, several researchers measured the thermal performance of lighting systems in full scale test rooms. Early full scale room tests of the thermal performance of fluorescent luminaires are reported by Boyer (1966, 1967, 1968) and Nottage and Park (1969). Boyer's work was primarily concerned with comparing steady state temperature and airflow conditions for different air handling systems. The work of Nottage and Park was concerned with heat transfer from the luminaire to the room and plenum under steady state conditions.

These full scale tests gave more realistic heat exchange data than the simple luminaire calorimeters, but did not measure the transient lighting thermal performance or the heat storage effects. Two important full scale room tests, which included transient measurements, are the studies performed by Mitalas and Kimura (1971) at the National Research Council of Canada and those performed by Treado and Bean (1988, 1990, 1992) at the National Institute of Standards and Technology (NIST) in the U.S.A. The experiment of Mitalas and Kimura (1971) will be reviewed next, whilst the NIST tests will be reviewed in Chapter 8, together with a discussion of the validation of the model developed in this research.

2.4.3 The experiment of Mitalas and Kimura

The first full scale test room for the measurement of transient lighting thermal performance was built by Mitalas and Kimura (1971) at the National Research Council, Canada. They used the full scale test room to determine the model coefficients for the theoretical model published by Kimura and Stephenson (1968) (equation 2.1). In this full scale test facility, cooling load profiles were measured for a variety of configurations, including different supply and return air locations, with and without furnishings and carpet. These measurements (and the subsequent derivation of the weighting factors for design calculations) represented a great step forward for the calculation of cooling loads due to lighting. Since the set of design data derived from this test facility is still in use in the ASHRAE Handbook (ASHRAE 1997) as will be discussed in Section 2.5, some more details of this full scale test room are given in the following paragraphs.

Mitalas and Kimura's calorimeter was a guarded full scale room of floor dimensions 3.05 by 4.27 m (10 by 14 ft) and ceiling height 2.75 m (9 ft). There was a 1.07 m (3.5 ft) plenum space between the ceiling and the underside of the floor above. The floor to floor distance was 3.97 m (13 ft). Six lighting fixtures each containing two 40 W fluorescent lamps were installed, each being recessed into the ceiling in the room; a duplicate ceiling was installed in the guard space below. This meant the power input from lighting including ballast into the room space was approximately 590 W or a power density of 45.3 W m^{-2} (4.2 W ft^{-2}). Illuminance at desk height was approximately 1400 lux (130 foot-candles). An air-conditioning system was installed such that the supply was through a ceiling diffuser and the return could be either through a high side-wall return grille or through the ceiling plenum space. There was a duplicate ceiling arrangement below the floor of the test room, and the calorimeter room was guarded also by a circulation of air at the same temperature as the inner surface of the walls through the space between the inner and outer walls. To ensure that no high thermal conductivity elements pass from the test room to the surroundings, the floor was a precast concrete slab supported by a timber frame; the floor of the room above was suspended from a structural steel frame. To simulate an area in a large office space in a multi-storey building, all inside wall surfaces of the test room were finished with specularly reflecting aluminium foil. With this calorimeter room, Mitalas and Kimura (1971) determined the coefficients A and B in equation (2.1).

They found that for times greater than 1 hour after turning the lights on, q/W could be represented by an expression with a single time constant, but for times less than 1 hour after switching on, the cooling load was smaller than that calculated by the simple formula. For the case they reported in Mitalas and Kimura (1971), they found that $A = 0.698$ and $B = 0.0924\,hr^{-1}$ which corresponded to a fraction of input power p dissipated into the plenum space of 0.5 and convective heat transfer coefficients h at both the floor and ceiling surfaces of the room of about 5.68 W $m^{-2}K^{-1}$ (1.0 Btu/(ft^2 h °F)).

Subsequently, the results of this experimental study was published in Mitalas (1973a, 1973b). Mitalas did 26 tests with different combinations of the supply and return airflow rates and arrangements, and furnishings in the room to determine the coefficients a_1, a_2, and b_1 in equation (2.2). In these 26 tests, a_1 was found to be between 0.44 and 0.87. The lowest value, 0.44, was for the case where the supply of ventilation air was through a diffuser in the ceiling, the return was through a grille below the ceiling and the room was not furnished. The highest value, 0.87, was for the case where ventilation air was supplied and returned through the luminaires. The experimentally-determined values of b_1 varied between 0 89 and 0.97 which was not due to changes in room construction (as only one room construction was used for all the tests), but instead was due to different ventilation rates, types of luminaires and the manner in which ventilation air was supplied and exhausted. A summary of the experimental values of these coefficients is given in Appendix A. The experimental values by itself had little value for design calculations as they did not cover a broad range of room construction. However, Mitalas (1973a, 1973b) used these experimental results and the calculation methods described by Mitalas and Stephenson (1967) and by Stephenson and Mitalas (1967) to derive a set of design data for cooling loads caused by lights. The experiments were simply grouped into four cases with each case being given a single representative design value of a_1. Calculation was used to derive the design values of b_1 for five types of envelope construction characterised by their specific mass and four different types of room circulation. The calculation for one envelope construction was compared with the experimental value and good agreement was found. This set of design data, given in Appendix A, is still in use in the most recent edition of the ASHRAE Handbook - Fundamentals volume (ASHRAE 1997).

2.4.4 The NIST full scale tests

Since the mid-1980's, building energy analysis computer simulations have been popular for the evaluation of building performance. Computer programs like BLAST (UIUC 1986) and DoE-2 (LBL 1979) have been developed to calculate building energy usage for hourly or other periodic time intervals. These programs calculate cooling, heating and lighting loads for transient heat storage, and heat gains due to building envelope heat transfer, lighting, internal equipment and occupancy factors. Observing the fact that little information was available regarding the lighting energy distribution fractions which were needed as input parameters for these building energy analysis computer programs, Treado and Bean (1988, 1990, 1992) carried out full scale measurements of the interaction between lighting and HVAC systems at the Building and Fire Research Laboratory of the National Institute of Standards and Technology (NIST) in the U.S.A.. The primary objective of the NIST tests was to measure cooling load profiles and to determine lighting energy distribution fractions for various room temperatures, airflow rates and airflow configurations. More details of this NIST test room will be discussed in Chapter 8.

2.5 Present design guidance

The ASHRAE Handbook has some considerations on the cooling load from lights. In the latest edition of the ASHRAE Handbook - Fundamentals Volume (ASHRAE 1997) - the transfer function method (TFM) is used as the fundamental methodology for the calculation of cooling load. ASHRAE (1997) also gives the following simplified methods to be used as alternatives to the TFM method: the cooling load temperature differences (CLTD) method; the solar cooling load (SCL) method; the cooling load factors (CLF) method; the total equivalent temperature difference (TETD) method; and the time averaging (TA) method. Only the TFM method, or alternatively the CLF and TA methods, can be applied in the calculation of cooling load due to lighting. These three methods are summarised next.

In the TFM method, the instantaneous rate of heat gain from electric lighting is calculated first from:

$$q_{el} = WF_{ul}F_{sa} \tag{2.4}$$

where q_{el}= heat gain due to lighting in watts (W),

W= total lamp wattage (W),

F_{ul}= lighting use factor, a value from 0 to 1 to account for the proportion of usage of lighting (dimensionless),

F_{sa}= lighting special allowance factor, a value to account for the power dissipated by the ballast (dimensionless).

The transfer function method can be used for conversion of heat gain to cooling load. If the heat gain q_θ is given at equal time intervals, the corresponding cooling load Q_θ at time θ can be related to the current value of q_θ and the preceding values of cooling load and heat gain by (ASHRAE 1997):

$$Q_\theta = (v_0 q_\theta + v_1 q_{\theta-\delta} + v_2 q_{\theta-2\delta} + \ldots) - (w_1 Q_{\theta-\delta} + w_2 Q_{\theta-2\delta} + \ldots) \tag{2.5}$$

where δ is the time interval (usually 1 hour) and the terms $v_0, v_1, \ldots, w_1, w_2, \ldots$ are the coefficients (dimensionless) of the room transfer function. These coefficients depend on: (1) the size of the time interval δ between successive values of heat gain and cooling load; (2) the nature of the heat gain (how much is in the form of radiation and where it is absorbed); (3) the heat storage capacity of the room and its contents.

For estimating the cooling load due to lighting, only the coefficients w_1, v_1 and v_2 are required. These correspond to the coefficients b_1, a_1 and a_2 in the treatment of Mitalas (1973a, 1973b). Equation (2.5) becomes:

$$Q_\theta = v_1 q_{\theta-\delta} + v_2 q_{\theta-2\delta} - w_1 Q_{\theta-\delta} \tag{2.6}$$

ASHRAE (1997) gives a table (Table 24 of Chapter 28) for the selection of the value of w_1 for the approximate space envelope construction and the range of air circulation; another table (Table 25) permits the selection and calculation of v_1 and v_2 for the appropriate type of furnishing, air supply and return, and type of light fixture. Values given in these tables are based on the experimental results of Mitalas and Kimura (1971).

ASHRAE (1997) also gives a one-step hand calculation procedure called the cooling load factor (CLF) method which is based on the transfer function method. By this method, the instantaneous cooling load due to lighting is given by the following equation:

$$q_{el} = WF_{ul}F_{sa}(CLF) \tag{2.7}$$

where W = total lamp watts from luminaire data (or from electrical plans) (W),

F_{ul} = lighting use factor (dimensionless),

F_{sa} = lighting special allowance factor (dimensionless),

CLF = cooling load factor, by hour of occupancy, which is given in Table 38 of Chapter 28 of ASHRAE (1997). The CLF values given in this table are based on the assumption that the conditioned space temperature is continuously maintained at a constant value and the cooling load and power input to the lights eventually become equal if the lights are on for long enough. If the cooling system operates only during occupied hours, or if the lights are left on for 24 hours a day, then the CLF is equal to 1.0 for all time.

Another method recommended by ASHRAE (1997) to be used as an alternative to the TFM method is the time averaging (TA) technique which recognizes that the cooling load for a space at a given hour is the sum of all convective heat gains and the non-radiant portion of conductive heat gains to that space, plus the amount of previously stored radiant heat released back to the space during the same hour. In other words, the cooling load for the current hour is approximated by averaging the hourly radiant components of heat gain for the previous 1 to 7 or 8 hours with those for the current hour, and then adding the result to the total convective heat gain for the current hour.

The ASHRAE calculation for the cooling load produced by lighting uses the experimental data of Mitalas and Kimura (1971) which is limited to only a few configurations of room construction, ventilation arrangements, and lighting. Also, ASHRAE categories are not inclusive of all combinations of variables. Therefore, sometimes it is not certain which ASHRAE category should be chosen. Using the next incorrect case or slightly inappropriate category would cause 1% to 4% over-prediction of the cooling load according to Rundquist (1990).

2.6 Summary

From the above literature review, the early model of Kimura and Stephenson (1968) provided a useful method of calculation of cooling load from lighting which is still being used. However, coefficients used in the calculation are based on experimental results of only 26 tests performed in one single test room. Moreover, current design guidance on the classification of buildings for selection of coefficients for cooling load calculation does not include all combination of variables. Further experiments can be performed for the determination of coefficients for more configurations, but experiments are expensive and time consuming. Hence, it is considered that a good numerical model can help the design process by performing the cooling load calculation either directly or indirectly by determining coefficients (or weighting factors) for calculations using the conventional methods recommended in some design guides.

Further steady-state and transient models developed previously performed calculations of the cooling load and temperature distribution inside the enclosure. However, these models did not give good agreement with experimental results. These models, although treating the heat transfer from lighting in much detail, did not represent well the heat and radiation output from the lamps which is the only source of heat inside the enclosure. Existing models just assume that a proportion of the input power to the lamps becomes radiation and the rest becomes convective heat loss from the lamps. Furthermore, an existing transient model had to assume that some nodes were massless in order to obtain a solution. Therefore, it is considered that, a new lighting/HVAC interaction model is to be developed in this research to make a better representation of the power flow from lamps inside the enclosure by integrating a fluorescent lamp positive column model into a room heat transfer model.

Chapter Three

Effects of Temperature on Fluorescent Lamp Performance

3.1 Background

The light output of fluorescent lamps depends on the minimum lamp wall temperature (also called the cold spot temperature) which is the temperature of the coldest spot on the surface of the fluorescent tube (IESNA 1993; Elenbaas 1971). It is also known that this dependence is due to the fact that the properties of the lamp discharge depend on the mercury vapour pressure inside the lamp tube, which in turn changes with the minimum lamp wall temperature; this is because mercury vapour condenses on the cold spot of the lamp wall. Studies of thermal effects on light output have been largely empirical (e.g. Siminovitch et al. 1984, 1988; Collins et al. 1992), and have attempted to find the relationship of light output and lighting power with ambient temperature or the lamp wall temperature. These studies obtained empirical results but only for several specific lamp-ballast systems. It is uncertain whether these empirical results can be applied to other types of lamp-ballast combinations.

Sowell's 'LIGHTS' model discussed in Section 2.3 includes a provision for using empirical results for simulating the effect of lamp wall temperature on the light output and lamp power of fluorescent lamps. Despite the fact that 'LIGHTS' permits user input of these temperature-dependent performance data for fluorescent lamps, such data are not normally included in the lamp or luminaire data sheets provided by the manufacturers. In all the sample data files included in the LIGHTS program diskette distributed by Sowell (1989), only one set of data was presented of the dependence of light output and lamp power with lamp wall temperature. This set of data, which consisted of one curve for relative light output and one curve for relative lamp power, was taken from the IES Lighting Handbook (IESNA 1984) and appeared also in Treado and Bean (1988, 1992). Although Treado and Bean (1988) measured the relative light output and relative lighting power of the lamps used in one configuration of the NIST full scale tests, the data presented were incomplete. Therefore, apparently, Sowell (1990) was not able to use these measured data in the validation of LIGHTS using the NIST experimental results. Evidently, due to the lack of other sources of data, the curves that were published in a lighting handbook were used in the numerical experiments described in Sowell (1990). However, neither Sowell (1990) nor Treado and Bean (1988, 1992) discussed the validity of the handbook data for the lamps used in the NIST experiments or in other examples given by Sowell (1990).

Another reason for the importance of investigating into the effect of the thermal environment on the light output of fluorescent lamps is that photometric data for lamps and luminaires are usually obtained under the standard testing condition which is open air at a temperature of 25°C. However, lamps in service are usually operating at an ambient thermal environment different from this standard testing condition. Design calculations of lighting levels on the working plane usually use photometric data measured under this standard testing condition. In practice, lamps housed within luminaires are usually operated at an ambient temperature which is higher than 25°C, and if allowance is not made for this thermal effect in the design calculation, then the actual lighting level will be lower than the calculated design values. This can result in incorrect levels of illuminance, which may, in turn, have an adverse effect on the performance of office workers or may cause visual discomfort to some workers. Hence, the ability to quantify the effect of the thermal environment on the light output of fluorescent lamps is important in the lighting design process in order that a more accurate determination can be made of light output, and hence of illuminance levels, on the working plane or other room surfaces. Furthermore, lamps which are operating at high ambient temperatures do so at lower efficiency, thereby creating more heat while emitting less light; this results in higher cooling loads produced by lights and requiring extraction by the HVAC system. Thus, more accurate calculation of the cooling load from lights requires a better knowledge of the effects of temperature on light output and lamp power. Therefore, it is considered that improvements to the modelling of the interactions between temperature, light output and lamp power are essential, and will help to improve the simulation of lighting and HVAC systems.

In this research, an attempt is made to use a fluorescent lamp positive column model for the simulation of the thermal effect on light output and lighting power. The application of a fluorescent lamp positive column model in the study of lighting/HVAC interaction is discussed in the following chapters. Here, however, a review of the various numerical and analytical positive column models is given in Section 3.2. The simulation results of the positive column model developed in this research will be compared with published experimental data. A summary is therefore given in Section 3.3 of some important experimental measurements from fluorescent lamp discharge experiments. In order to study the current status of design guidance concerning the estimation of thermal effects on light output and lamp power, a literature survey of relevant information has been performed and a summary is given in Section 3.4.

3.2 Review of theoretical studies of the fluorescent lamp positive column discharge

3.2.1 Background

Published theoretical studies of the fluorescent lamp discharge consist of numerical and analytical models that simulate the physical processes occurring in the discharge (Waymouth and Bitter 1956; Cayless 1963; Lama et al. 1982). These models simulate the collision processes that occur between the accelerated electrons and the different species of the mercury atoms. These collision processes occur in a region called the positive column of the discharge (see Appendix B), which occupies over 95% of the length of fluorescent tube; as a result, these models are called positive column models of the mercury-rare-gas discharge. The positive column models also explain how electrical power is converted to ultraviolet (UV) radiation with some power losses in the discharge and via the tube wall. As far as modelling of the interaction between lighting and HVAC systems is concerned, to date, there have been no attempts to employ a positive column model within numerical simulations which describe the variations of light output and lamp power with minimum lamp wall temperature.

In addition to the temperature dependence of light output and lamp power, another important factor which will affect the accuracy of the simulation of lighting/HVAC interaction is the precision in the input data of the proportions of the input electrical energy that would be converted to light, heat, and other radiation. The reason for this is that current lighting/HVAC simulation programs simulate how electrical energy input to the lighting system is finally dissipated as heat, and thus contributes to HVAC cooling load. In the steady state, electric power input to lighting is considered as being equal to the cooling load of HVAC system. Early models such as those of Sowell and O'Brien (1973) were developed for the simulation of the steady state temperature distribution inside the room. As regards the accuracy of the input data on lighting power consumption, the division of lighting power into light and heat would have little effect on the steady state results. However, models developed more recently, such as Ball and Green (1983) and Sowell (1989), attempt to simulate the transient and dynamic cooling loads and temperature distributions due to lighting. The division of lighting power input into light and heat now become important, and will affect the results of transient and steady state cooling loads and temperature distributions. This is because the proportions of light and heat output from the lamps will affect the amount of energy that is transferred to room components before it is sensed as heat and the amount of energy that is sensed as heat immediately. Thus, accurate data on the ratios of light output and of heat generated are essential in obtaining accurate results in dynamic simulations of lighting/HVAC systems. In existing models, data on light output of the lamps is allowed as a user input; the models calculate short-wave radiation power from the input data of lamp light output using a preset constant which is called the luminous efficacy of radiation. The difference between the input data value of the electrical power consumed by the lamps (which is usually assumed to be the rated power of the lamps) and the calculated value of short-wave radiation power is assumed to be dissipated as heat on the lamp surface. If the conversion of electrical energy into light and heat in the fluorescent lamp can be simulated by the model, then user input of light output data will not be necessary. A fluorescent lamp model which requires the input of information which consists only of lamp wattage or lamp current, lamp length and diameter and fluorescent powder type, and which simulates the conversion process of electrical energy into light and heat inside the fluorescent tube, will make improved predictions of the proportions of radiation and convection. In addition, greater insight will be obtained into the physical process of conversion of electrical energy into light and heat.

The conversion of lamp electrical energy into visible light energy can be divided into two major processes. The first process is the conversion of electrical energy into ultra-violet radiation (the resonance lines) in the discharge inside the fluorescent lamp. The second process is the subsequent conversion of the ultra-violet radiation produced by the discharge into visible light; this takes place via the phosphors coated on the inside surface of the fluorescent lamp tube wall. The first process is very temperature sensitive because the discharge properties depend on the mercury vapour pressure inside the tube which in turn depends on the cold-spot temperature of the tube wall (e.g. Elenbaas 1971). In order to calculate the light output and lamp power and to obtain a clearer picture of the effect of the lamp wall temperature on the luminous output and lamp power of the fluorescent lamp, the discharge process inside the fluorescent tube needs to be studied. There have been a number of theoretical and experimental studies of the fluorescent lamp discharge published in the literature. Some of the theoretical modelling studies are discussed in the next sub-section.

3.2.2 Fluorescent lamp positive column models

At the time when the fluorescent lamp became commonly available as an artificial light source, Kenty (1950) carried out a comprehensive quantitative analysis of the positive column of a 40-W fluorescent lamp. In this work, Kenty combined the experimental values of electron temperature, electron density and the densities of the mercury ^3P states, with estimated values of transition rates, to obtain a self-consistent picture of the radiation from the discharge at a single current, tube size, fill pressure, and mercury vapour pressure.

Based on Kenty's results, Waymouth and Bitter (1956) (also, Waymouth 1971) performed a numerical modelling of the positive column of fluorescent lamps. They considered three important relationships between four variables: electron density, electron temperature, axial electric field strength, and current density. In word form, the three relationships are:

(i) Rate of creation of ion-electron pairs = rate of loss of ion-electron pairs

(ii) Rate of energy input to the electron gas from the electric field = rate of loss of energy by electrons

(iii) Current density = electron density times electron mobility times electric field strength.

In seeking a numerical solution to the above equations, Waymouth and Bitter used the following five basic hypotheses:

(i) Only mercury is ionized and excited; inelastic collisions with rare gas atoms can be ignored.

(ii) The type of rare gas determines the mobilities of electrons and ions. The effect of elastic collisions with mercury can be neglected.

(iii) The loss of ions is purely by ambipolar diffusion, with volume recombination being negligible.

(iv) The electron gas has a Maxwellian distribution of velocities, with a temperature determined by the ionization balance equation; the temperature is assumed to be independent of radial position in the discharge tube.

(v) All ionization from the ground state takes place by two-stage processes, i.e. via an intermediate excited state; direct ionization from the ground state can be neglected.

The above assumptions will also be used in the fluorescent lamp positive column model developed in this research. Justifications of the above assumptions will be given in Chapter 5.

Waymouth and Bitter considered a simplified energy level diagram for mercury consisting of only four levels: the ground state, the radiating state, the metastable state and the ionised state. They also used an approximation that radial variations in the discharge tube of all the parameters could be ignored and the average values over the radial position were used for all the parameters. In their analysis, they used two adjustable parameters: the cross-section for ionisation from atoms in radiating and metastable levels; and the effective life time for quanta of the resonance line. By using a cross section for ionisation of the excited states equal to 3.3 times the cross section for ionisation of the ground state, together with a mean life time for ultraviolet photons in the discharge of 3.6 times that employed by Kenty for diffusion in un-ionised vapour, they obtained good agreement with the experimental results of Kenty, Easley and Barnes (1951).

Cayless (1963) produced a more comprehensive positive column model in which the variation of quantities with radial position was considered. Furthermore, Cayless included more mercury excited states then those considered by Waymouth and Bitter. He derived a set of seven simultaneous second-order differential equations. His method of obtaining a solution was to assume radial distributions for several variables and to use these to solve the ionisation balance equation for electron temperature. This value of the electron temperature was then used to solve simultaneously the differential equations for radial dependence of the rest of the variables. The new values of radial distributions were then used to obtain a new value for electron temperature, and the process was repeated to obtain convergence. Cayless also used Kenty's cross sections and obtained a remarkably good fit to experimental data without the use of any arbitrary fitting constants.

Lama et al. (1982) elaborated an analytical model of the low pressure mercury-argon discharge. This model was based essentially on the same approximations as those used by Waymouth and Bitter (1956). In order to obtain analytical expressions for the electron temperature, the resonance radiation and the electric field, four more approximations were made which greatly simplified the analysis. They obtained a fairly good approximation of the parametric dependence on the discharge variables.

In all the above work, a Maxwell-Boltzmann distribution of the electron energy, which is the energy distribution of electrons under thermodynamic equilibrium, was adopted in their calculations. The experimental studies of Kenty (1950) and Easley (1951) were often quoted for justification of the adoption of a

Maxwell-Boltzmann distribution. However, in low-pressure mercury–rare-gas discharges, the local thermodynamic equilibrium conditions are not attained, so that the electron energy distribution function may deviate significantly from the Maxwell-Boltzmann shape (Vriens 1973). Due to this, Vriens (1973) proposed a two-electron-temperature model in which the electrons were assumed to form two groups – the bulk electrons and the tail electrons – with each group described by an electron temperature. Vriens used this two-temperature model to study the energy balance in low-pressure rare-gas discharges.

Winkler et al. (1983) used a collisional-radiative model which included eight mercury levels coupled with the numerical solution of the Boltzmann equation. In this model, argon excitation and ionisation were also included, but the contribution of the argon ions to the charged particle distribution was not taken into account. The model assumed standard radial profiles of particle densities and used Holstein's theory of resonance radiation trapping (Holstein 1947).

Dakin (1986) established a more complete model of radial variations in the low-pressure mercury-argon positive column. In this model, the electron energy distribution function was assumed to follow the two-temperature group model of Vriens (1973). However, argon excitation and ionisation were neglected. The model can be applied to both classical and compact fluorescent tubes.

More recently, Zissis et al. (1992) included argon excitation and ionisation in their collisional-radiative model of the mercury-argon low-pressure discharge positive column. They made no assumptions on the radial profiles and used a non-Maxwell electron energy distribution function proposed by Lagushenko and Maya (1984). Again, this model can be applied to both classical and compact fluorescent tubes.

The model of Waymouth and Bitter (1956), which has become the classical theoretical study of fluorescent lamp discharge, was successful in explaining the general properties of the fluorescent lamp discharge although two adjustable parameters had to be used. Due to the fact that computers were not powerful at the time when Waymouth and Bitter developed their model, they had to use graphical methods for their solution of the dependence of resonance radiation output with discharge variables. It is considered here that, for an initial attempt to integrate a fluorescent lamp positive column model into a numerical lighting/HVAC interaction simulation model, a numerical model based on the same hypotheses as used by Waymouth and Bitter (1956) will be appropriate, but with a different method of solution and written into computer codes. Though more recent fluorescent lamp positive column models have made refinements to the classical model of Waymouth and Bitter, the refinements are mainly for the interest of the plasma physicists who are interested in fine details inside the discharge. These refinements are considered unnecessary for the purpose of this research. A fluorescent lamp positive column model, which is based on established hypotheses with a newly developed solution method, has been developed for this research and the model is described in Chapter 5.

3.3 Review of experimental studies of the fluorescent lamp positive column discharge

A major task of the present work is to incorporate a fluorescent lamp positive column model into a room thermal model for the better simulation of the mutual interaction of lighting and HVAC. The fluorescent lamp positive column model developed as part of this research for this purpose will be validated, as a stand-alone model, by experimental results of the fluorescent lamp discharge reported in the literature. For this reason, a brief review of the experimental studies conducted to date of the fluorescent lamp positive column model is given in this section. The following paragraphs review the measurement techniques, followed by some important experimental studies of the low pressure mercury–rare-gas discharge.

3.3.1 Measurement techniques

Measurements of the physical parameters of the low pressure mercury vapour discharge, such as electric field strength, electron temperature and densities of various mercury species, were performed as early as in the 1920's by a number of workers. These early measurements were carried out before the availability of the fluorescent lamp for general lighting applications. They were directed mainly at investigating the electron mobility and the ionization processes in discharges in pure mercury vapour. In the early 1950's, the fluorescent lamp became available in substantial quantities for lighting applications and, therefore, considerable interest arose in measurements of discharges in mixtures of mercury vapour and rare gas (mainly argon).

Early measurements employed the Langmuir probe technique and its various improvements (reviewed in Verweij (1961)). The probes are small wires (about 1 mm diameter and a few mm long), which are inserted into the plasma and collect a current from the plasma without substantially disturbing its characteristics. Probe techniques yield valuable information on electron temperature, electron energy distribution function, electric field strength, densities of various mercury species in the discharge and other microscopic plasma parameters. Since a probe has to be inserted into the plasma during measurement, some destruction or disturbance to the discharge is unavoidable and this limits the accuracy of probe methods.

Optical techniques which are non-destructive and non-intrusive have been developed for measurements of species densities in the discharge. An example of these optical techniques is the Hook method (reviewed in Marlow (1967)) which employs an interferometer-spectrometer system. More recently, lasers have been used in the diagnostics of low-pressure mercury discharge. There have been a number of measurement techniques using lasers and these techniques have been used successfully in understanding the microscopic processes taking place inside the low-pressure mercury discharge. A good review of laser diagnostics in low-pressure mercury rare-gas discharge is given by Maya and Lagushenko (1990). The following paragraphs summarise some major experimental work on the fluorescent lamp discharge.

3.3.2 Important experimental studies

Kenty et al. (1951) performed an experimental study of the elastic losses in a low-pressure mercury-argon discharge. They measured the electron concentrations and electron temperatures in the axis of the discharge in a tube of 36 mm internal diameter, an argon filling pressure of 465 Pa, a mercury vapour pressure determined by the lamp wall temperature and a discharge current of 420 mA. They used their measured results to deduce the elastic collision losses in the discharge.

Barnes (1960) measured the radiant intensities of the mercury resonance lines just inside the wall of a lamp with an inside diameter of 36 mm for currents 400 mA to 2 A and various lamp wall temperatures and rare gas fillings.

Verweij (1961) carried out several series of measurements of electron temperature, electron concentration and electric field strength using the Langmuir probe method. He used his results to determine the mobility of electrons in the positive column of low-pressure mercury-argon discharges. Verweij's experimental data have been frequently quoted by many authors for comparison with model results.

Koedam and Kruithof (1962) determined the densities of mercury triplet states as a function of discharge parameters using two different methods: (i) by absorption measurements and (ii) by measurements of the 253.7 nm radiation yield. Koedam et al. (1963) measured the radiation output of various lines emitted by the low-pressure mercury-argon positive column. They then used their radiation data together with volume and wall losses calculated from the electron temperature and electron density measured by Verweij (1961) to study the energy balance of the low-pressure mercury-argon discharge.

Denneman et al. (1980) measured the radiation efficiency of 38 mm and 26 mm fluorescent lamps, each for 2 types of rare-gas filling, using a 200 mm ultraviolet integrating sphere. They also measured the electric field strength, electron temperature and axial electron density using probe diagnostics.

Van de Weijer and Cremers (1982, 1985 and 1987) used a pulsed dye laser to measure the lifetimes and densities of excited mercury states of the low-pressure mercury–rare-gas discharge. They then used their results to calculate the UV radiation output of the discharge as a function of mercury vapour pressure or cold-spot temperature.

Bigio (1988) measured the radial distribution and absolute densities of the excited states of mercury with two laser-based diagnostic techniques. His results indicated that the assumption used in early positive column models of a parabolic-type radial density dependence for the excited mercury states were only correct for certain particular discharge conditions. Bigio showed that the radial distributions depend critically on many parameters such as the mercury pressure, the lamp wall temperature, the current, and the argon pressure.

Results of these studies reported in literature will be used for the validation of the fluorescent lamp positive column model developed in this research. Discussion of the validation results will be given in Chapter 7.

3.4 Present design guidance

In order to study the current status of design guidance concerning the estimation of thermal effects on lighting performance, a review of the current design guidance on the treatment of light loss and lamp power changes due to the ambient thermal environment is given in this section.

The standard photometric measurement of fluorescent luminaires is performed at an ambient temperature of 25°C with one type of lamp-ballast combination (IESNA 1993). However, under actual operating conditions, lamps are not usually operated at an ambient temperature of 25°C. Hence, light output and other performance characteristics of the fluorescent luminaire will differ from that given in the test data. To account for this in the design of lighting systems, the calculation of light output from the luminaire involves the use of light loss factors (LLF). The recent (8th) edition of the Lighting Handbook of the Illuminating Engineering Society of North America (IESNA 1993) divides light loss factors into two groups: recoverable and non-recoverable. Recoverable factors are those that can be changed by regular maintenance, such as cleaning and relamping luminaires. Non-recoverable factors are those attributed to equipment and site conditions and cannot be changed with normal maintenance. The total light loss factor is the product of all the applicable factors listed below:

<u>Non-recoverable</u>

Luminaire ambient temperature factor

Heat extraction thermal factor

Voltage-to-luminaire factor

Ballast factor

Ballast-lamp photometric factor

Equipment operating factor

Lamp position (tilt) factor

Luminaire surface depreciation factor

Recoverable

Lamp lumen depreciation factor

Luminaire dirt depreciation factor

Room surface dirt depreciation factor

Lamp burnout factor

Of these light loss factors, the first two of the non-recoverable factors are closely related to ambient temperature and the performance of HVAC systems. They are defined in the Lighting Handbook of the Illuminating Engineering Society (IESNA 1993) as follows:

The *luminaire ambient temperature factor* is the fractional lumen loss of a fluorescent luminaire due to internal luminaire temperatures differing from the temperature at which photometry was performed. This factor should take into consideration any variation in the temperature around the luminaire, the means of, and conditions of, mounting the luminaire, and the use of any insulation in conjunction with the application of the luminaire.

This factor is not normally provided by luminaire manufacturers and IESNA (1993) does not give a method for its determination. However, IESNA (1993) state that the factor can be estimated on the following basis. "*Luminaire photometry is performed in 25°C ambient still air. For each degree of rise in ambient temperature above this value, the cold-spot temperature of the lamp rises by about 0.6°C. The effect of lamp temperature rise can be estimated from the manufacturer's literature, recognizing that lamps in luminaires generally operate at temperatures greater than the optimum. Judgment must be applied to factors such as the effect of open versus enclosed luminaires, possible air movement and the fact that the plenum temperature will have a greater effect than the room temperature on recessed luminaires.*"

The above method of estimating the luminaire ambient temperature thermal factor is very crude. Firstly, the effect of lamp temperature rise on the lamp performance is not given by most lamp manufacturers. Secondly, the lamp may not be operating at its optimum lamp wall cold-spot temperature in 25°C ambient still air.

The *heat extraction thermal factor* is the fractional lumen loss or gain due to the airflow. This factor is useful in assessing the lamp performance in air-handling luminaires in which the fluorescent lamps are integrated with the HVAC system as a means of introducing air to, or removing air from, the zone in question. Airflow across the lamps has a very significant effect on lamp wall temperature and consequently on the light output and other performance characteristics of the lamps. IESNA (1993) state that manufacturers would provide specific luminaire test data for this factor at various air flows; they also state that typically the factor would approach a constant value for air flows in excess of 0.005-0.01 $m^3 s^{-1}$ (10-20 ft^3/min) through the lamp compartment of a luminaire. However, most manufacturers do not supply luminaire test data with respect to thermal effects on lamp performance.

Ji and Davis (1996) recommended the use of three thermal factors in lighting design calculations to account for the change in power and light output of recessed fluorescent luminaires. Two of these factors, named the first and second thermal factors for power (TFW1 and TFW2), are concerned with the change in active power due to temperature changes within the luminaire and within the plenum, respectively. The third factor, named the thermal factor for light output (TFL), is concerned with the change in lumen output due to changes in plenum temperature. The effects which are considered by these thermal factors are presented in Table 3.1 together with their definitions. Ji and Davis (1996) gave values of these factors for different combinations of five luminaire types, three lamp types and three ballast types based on experimental measurements.

According to Ji and Davis (1996), correction for the change in lumen output due to thermal effects within the luminaire is not necessary since the effect is accounted for in photometric measurement of luminaires. This is questionable for the following reason. Luminaire manufacturers usually give photometric data relative to the lumen output of bare lamps, e.g. light output ratios are given in terms of lumen output of luminaire relative to the lumen output of bare lamps, and intensity distribution data are usually given in terms of candela per 1000 lumens of bare lamps. This allows the designer to calculate luminaire light output and intensity distribution when different types of lamps are used. Although it is not clearly defined, it is generally understood by designers that the lumen output of bare lamps used to derive luminaire data is measured when the bare lamps are at an ambient temperature of 25°C. Strictly speaking, thermal effects within the luminaire on light output is taken into account in photometric testing of luminaires only for the type of lamp used in the test. When different types of lamps are put inside a luminaire, there may be a difference in ambient temperature surrounding the lamps and the response of the lamps to different ambient temperatures may be different from the lamps used in photometric testing. Hence, it is still necessary to consider the change in light output due to thermal effects within the luminaire when the lamps installed are different from the lamps used in photometric measurement.

3.5 Summary

Existing numerical models of the interaction between lighting and HVAC systems use only empirical results in dealing with the dependence of lamp performance on minimum lamp wall temperature. However, empirical results are not generally available for all lamp configurations. Lamp manufacturers do not normally supply these data in the lamp data sheet or manual. The validity of simulation results is therefore limited if the variations of lamp power and light output with minimum lamp wall temperature are approximated using handbook curves or data such as those in IESNA (1993). From the literature reviewed in section 3.2, the dependence of light output and lamp power on minimum lamp wall temperature can be calculated using a numerical model of the fluorescent lamp positive column discharge. If a fluorescent lamp positive column model can be integrated into a numerical lighting/HVAC interaction model, then calculations of light output and lamp power can be performed at each time step without the use of empirical curves.

Due to the lack of data for deriving the thermal factors recommended by Ji and Davis (1996) as discussed in Section 3.4, currently the thermal effects on light output are either completely ignored or audaciously assumed in lighting design calculations. The use of correction factors for thermal effects in lighting design calculations is an acceptable approach for obtaining a more accurate prediction of lighting levels during the design stage. However, experimental measurements have to be performed to obtain these factors for each type of lamp-ballast-luminaire combination over a wide range of plenum temperatures. Experimental measurements are expensive and time-consuming and usually are restricted to several configurations only. It is therefore considered that a good numerical model of lighting/HVAC interaction can be used to determine these factors with much less effort. Lighting design calculations can then take the thermal factors into account with the aim to obtain a more accurate calculation of the installed lighting levels.

The research reported in this thesis seeks to apply a numerical fluorescent lamp positive column discharge model as part of the numerical simulation of lighting/HVAC interaction. The heat and light transfer module of the interaction model is described next. The fluorescent lamp positive column discharge model is described in Chapter 5 and its solution methodology is described in Chapter 6.

Table 3.1

Thermal factors recommended by Ji and Davis (1996) for use in lighting design calculations to account for the change in power and light output of recessed fluorescent lamp luminaires.

Factor	Effect	Definition
TFW1 First thermal factor for power	Change in active power due to thermal effect within luminaire.	The ratio of the active power of the lamp/ballast system in the luminaire at 25°C to the active power of the bare lamp/ballast system when operated at 25°C.
TFW2 Second thermal factor for power	Change in active power due to plenum temperature not equal to 25°C.	The ratio of active power of a luminaire at a certain plenum temperature to the active power of the luminaire at 25°C.
TFL Thermal factor for light output	Change in lumen output due to plenum temperature not equal to 25°C.	The ratio of the light output of a luminaire at a certain plenum temperature to the light output of the luminaire at 25°C.
None	Change in lumen output due to thermal effect within luminaire; this effect is accounted for in photometric testing of luminaire.	None

Chapter Four

The Mathematical Model of Light and Heat Transfer in a Room with Luminaires

4.1 Compartmentization of a room

The room model developed in this study is a dynamic mathematical model for simulating transient heat flow and temperature for a room and a plenum with (or without) luminaires. To conform with most modern offices, the room being modelled is considered to have three separate sections or compartments: the luminaire, the plenum (ceiling void) and the occupied space (conditioned space). As most offices have more than one luminaire, the use of only one luminaire compartment means that all luminaires are "lumped" to form a single compartment. Each section is divided into a number of nodes. The model is designed to be flexible so that it can simulate different room configurations, hence the number of nodes in each of the three sections can be varied. Figure 4.1 shows a schematic diagram of the three sections and the distribution of nodes. Dividing the enclosure into three sections has the benefit of simplifying the radiation form factor matrices. However, the computer program developed for the model has the flexibility of defining the number of nodes in any section to be zero. Hence, rooms without a plenum can be modelled using two sections: the luminaire and the occupied space; and rooms in which only batten fittings are used can be modelled by one section only. An example of simulation in an enclosure with a single compartment is given in section 4.4.

4.2 Heat balance equation

The model developed in this research uses fundamental heat transfer principles in the form of heat balance equations about the nodes. It differs from existing models by other researchers in three main aspects. Firstly, it solves the dynamic heat balance equations without assuming any node to be massless; secondly, it calculates illuminance on room surfaces; and thirdly, a fluorescent lamp positive column model can be incorporated to simulate the variation of light output from the lamp with ambient temperature. Hence, the model calculates not only the dynamic temperature variation but also the simultaneous lighting levels in a room with both the air-conditioning and the lighting operational.

Each node is assumed to be isothermal. If any surface deviates significantly from the isothermal condition, then the surface can be divided into smaller elements to form different nodes (each with a different temperature) provided the physical properties of all nodes and the conduction coupling between adjacent nodes are known. For each node, the following heat balance equation holds. This equation relates the temperature rise of each node in one time step to the total net heat gain of that node in that time step:

$$m_i c_{pi} \Delta T_i = q_{Gi} + q_{Li} + q_{Si} + q_{Hi} + q_{Ci} \tag{4.1}$$

where m_i = mass of node i (kg),

c_{pi} = specific heat capacity of node i (J kg^{-1} K^{-1}),

ΔT_i = temperature rise of node i in one time step (K),

q_{Gi} = total (electrical) energy input at node i in one time step (J),

q_{Li} = total (net) long-wave radiation heat gain to node i in one time step (J),

q_{Si} = total (net) short-wave radiation heat gain to node i in one time step (J),

q_{Hi} = total (net) convection heat gain to node i in one time step (J),

q_{Ci} = total (net) conduction heat gain to node i in one time step (J).

As shown in this heat balance equation, the net heat gain to a node consists of five components: energy input (for lamp and ballast nodes only), long-wave (infrared) radiation, short-wave (visible) radiation, convection and conduction. Each of these components is calculated separately as described below.

4.2.1 Energy input at the lamp node(s)

As the purpose of this model is to study the interaction between lighting and air-conditioning, the only energy input to the enclosure considered is the electrical energy consumed at the lamp and ballast nodes, all other energy sources (such as occupants, casual and solar heat gains, for example) are not considered. Electrical energy input to the lamp is dissipated inside the fluorescent lamp tube and converted to light and heat at the lamp tube wall. Therefore, the energy input to the lamp is assumed to be at the lamp surface, i.e. the lamp node.

Figure 4.2 shows a schematic diagram of the major heat transfer paths considered in the model developed in this research. Part of the electrical energy input to the fluorescent lamp is converted to visible radiation by the discharge and fluorescent powder. The rest is dissipated as heat on the lamp tube wall. This heat is then transferred to other luminaire and room components through thermal radiation, convection and conduction.

Fluorescent lamp power input as well as the light output depend on the minimum lamp-wall temperature which in turn depends on the operating environment. Therefore, when modelling the fluorescent lamp power input one cannot simply use the rated power of the lamp. The change of power input to the lamp can be modelled by using an empirical curve such as that published in IES Lighting Handbook (IESNA 1993). This is the approach used in Sowell's LIGHTS model (Sowell 1989, 1990). An empirical curve can also be incorporated in the room heat transfer model being described in this chapter for the calculation of the power input to the lamp node. The computer code written for the room heat transfer model which allows user input of an empirical curve for the calculation of lamp power input and light output is named LITEAC1. In LITEAC1, the power input at the lamp nodes is calculated by multiplying the rated power of the lamp with a fraction (the relative power, user input from empirical data), the latter depending on the minimum temperature of the lamp nodes. The curve of relative power against minimum lamp wall temperature can be obtained from published data in the IES Lighting Handbook (IESNA 1993). It was mentioned in Chapter 3 that this 'handbook curve' may not well represent all the lamps in use. Some more empirical curves can be obtained in Siminovitch et al. (1984); however, data for only a few lamp-ballast combinations are available.

In order that the calculation of power input to the lamp can be carried out without relying on empirical data, a numerical model of the discharge process inside the fluorescent lamp can be used. As the lamp power depends on the intensity of the discharge in a region called the positive column of the fluorescent lamp, the numerical model is referred to as a fluorescent lamp positive column model which relates the total power dissipation in the lamp to the minimum lamp wall temperature. A fluorescent lamp positive column model specially developed for this research (in Chapter 5) will be used to calculate the variation of lamp power under different operating conditions. The positive column model will be integrated with the room heat transfer model to form a lighting/HVAC interaction model and the integrated model will be called LITEAC2.

4.2.2 Energy input at the ballast node

The fluorescent lamp needs a ballast to be connected in series to the mains electricity supply for its operation. The ballast serves two functions: (i) it generates a high electromotive force (e.m.f.) together with a starter for the initial start up of the fluorescent lamp; (ii) it limits the current flowing through the fluorescent lamp discharge after the discharge has been initiated. Conventionally, the fluorescent lamp ballast is an electromagnetic choke consisting of an iron core with wires wound around it. The choke generates an inductance when an alternating current passes through it. This inductance limits the current flowing through the fluorescent lamp discharge. The ballast consumes power itself because: (i) the varying magnetic field generated by the alternating current flowing through the choke also generates current in the iron core which will be dissipated as heat in the iron core; (ii) the wire wounding around the iron core has electrical resistance and current flowing through it generates heat. Recently, some fluorescent lamps can be operated using the high frequency electronic ballast which basically converts the low frequency (50-60 Hz) mains supply to a high frequency alternating current in the range of 20-50 kHz. Under this high frequency, the iron core loss is reduced and hence electronic ballasts are more efficient.

The power consumed at the ballast, i.e. the ballast loss, depends on the type and the quality of the ballast used. In both LITEAC1 and LITEAC2, the rated ballast power loss can be inputted and the ballast power loss is then calculated assuming the ballast loss has the same variation as the lamp power. Alternatively, if the rated power of the ballast is not known, it can be assumed to be a fraction of the lamp power. For common electromagnetic choke ballasts this fraction is between 0.15 and 0.25 (IESNA 1993). The power input at nodes other than the lamp and the ballast is assumed to be zero.

4.2.3 Long-wave radiation

The net rate of long-wave radiation input to node i, $\dot{q}_{Li}$, is obtained by subtracting the radiant exitance (radiosity) of i from the irradiance on i as follows:

$$\dot{q}_{Li} = (E_{Li} - M_{Li})A_i \tag{4.2}$$

where E_{Li}, M_{Li} and A_i are, respectively, the irradiance (W m^{-2}), radiant exitance (radiosity) (W m^{-2}) and area (m^{-2}) with reference to node i (all symbols with a subscript L refer to long-wave radiation). Using form factors F_{ji}, reflectances ρ_{Li} and emissivities ε_i, E_{Li} and M_{Li} are given, respectively, as follows:

$$E_{Li} = \sum_j \frac{A_j F_{ji} M_{Lj}}{A_i} = \sum_j F_{ij} M_{Lj} \tag{4.3}$$

where the last equality in equation (4.3) uses the reciprocity relation of radiation form factors, and

$$M_{Li} = M_{Loi} + \rho_{Li} E_{Li} = M_{Loi} + \rho_{Li} \sum_j F_{ij} M_{Lj} \tag{4.4}$$

where M_{Loi} is the radiant emissive power from a grey surface, and is given by the Stefan-Boltzmann law:

$$M_{Loi} = \varepsilon_i \sigma T_i^4 \tag{4.5}$$

Equation (4.4) is actually a set of simultaneous linear equations which can be solved by an iteration process such as the Jacobi or Gauss-Seidel iteration method to yield the long-wave radiant exitance M_{Li} for all nodes i.

Combining equations (4.2), (4.3), (4.4) and (4.5), gives:

$$\begin{aligned} \dot{q}_{Li} &= (E_{Li} - \varepsilon_i \sigma T_i^4 - \rho_{Li} E_{Li}) A_i \\ &= [(1-\rho_{Li}) E_{Li} - \varepsilon_i \sigma T_i^4] A_i \\ &= A_i (1-\rho_{Li}) \sum_j F_{ij} M_{Lj} - A_i \varepsilon_i \sigma T_i^4 \end{aligned} \tag{4.6}$$

Assuming all surfaces are diffuse grey, then $\rho_{Li} = 1-\varepsilon_i$, and equation (4.6) becomes:

$$\dot{q}_{Li} = A_i \varepsilon_i (\sum_j F_{ij} M_{Lj} - \sigma T_i^4) \tag{4.7}$$

4.2.4 Short-wave radiation

If all surfaces (including the light emitting surfaces) are assumed to be diffuse, then equations similar to equations (4.2), (4.3) and (4.4) above apply also to short-wave radiation. Due to the random orientation of the fluorescent powder coating, fluorescent tubes can be assumed to have more or less a diffuse emission. Also, the assumption of diffuse surfaces is good for all surfaces in a normal office environment except for the situation where there may be a reflector which has a large specular component inside the luminaire. Using symbols similar to the long-wave radiation terms but with a subscript S denoting short-wave radiation, the following equation gives the net short-wave radiation heat gain as:

$$\dot{q}_{Si} = (E_{Si} - M_{Si}) A_i \tag{4.8}$$

E_{Si} and M_{Si} are given respectively by:

$$E_{Si} = \sum_j \frac{A_j F_{ji} M_{Sj}}{A_i} = \sum_j F_{ij} M_{Sj} \tag{4.9}$$

$$M_{Si} = M_{Soi} + \rho_{Si} E_{Si} = M_{Soi} + \rho_{Si} \sum_j F_{ij} M_{Sj} \tag{4.10}$$

where M_{Soi} is the luminous power per unit area emitted from surface i (W m^{-2}), and is zero except for the lamp and diffuser nodes. In a fluorescent lamp, the luminous power emission M_{Soi} is related to the property (quantum efficiency and spectral distribution) of the fluorescent powder in the lamps and to the discharge intensity inside the lamp. The discharge intensity is, in turn, related to the mercury vapour pressure inside the lamp. As mercury vapour inside the lamp condenses at the coldest spot, the discharge intensity and hence the luminous flux emission depend on the minimum lamp wall temperature. In LITEAC2, a fluorescent lamp positive column model will be used to calculate M_{Soi} for the lamp nodes. This positive column model will be described in Chapter 5. In LITEAC1, M_{Soi} for the lamp nodes is calculated from the lumen output of the lamp by assuming a luminous efficacy of radiation emitted from the lamp.

Similar to equation (4.4), equation (4.10) also represents a set of simultaneous equations which can be solved by an iteration process such as the Jacobi or Gauss-Seidel iteration methods to yield the short-wave radiant exitance M_{Si} for all nodes i.

Combining equations (4 8), (4.9) and (4.10), the short-wave radiation heat gain of node i is then given by:

$$\dot{q}_{Si} = A_i[(1-\rho_{Si})\sum_j F_{ij} M_{Sj} - M_{Soi}] \tag{4.11}$$

4.2.5 Convection

For surfaces in contact with an air node there is convection heat exchange between the surface and the air node. The convection heat gain of node i is given by:

$$\dot{q}_{Hi} = A_i h_i (T_a - T_i) \tag{4.12}$$

where h_i is the convective heat transfer coefficient of node i (W m^{-2} K^{-1}), and T_a is the temperature of the air node adjacent to node i (K), T_i is the temperature of the node i (K), and A_i is the area of node i (m^2).

The rate of heat transfer by convection to the air node is then found from:

$$\dot{q}_{Ha} = \sum_i h_i (T_i - T_a) A_i \tag{4.13}$$

where the sum is taken over all nodes in contact with the air node.

Values of the convective heat transfer coefficient used in equations (4.12) and (4.13) will be calculated by the methods described in Appendix C.

If there is air exchange between air nodes in different sections, then the convection heat gain of air node '*ai*' due to this air exchange is calculated from:

$$\dot{q}_{Cai} = \sum_{j \neq i} V_{ij} \rho_a c_{pa} (T_{aj} - T_{ai}) \tag{4.14}$$

where V_{ij} is the volume flow rate of air between air nodes '*ai*' and '*aj*' (m^3 s^{-1}); ρ_a and c_{pa} are the density (kg m^{-3}) and specific heat capacity (J kg^{-1} K^{-1}) of air, respectively, which are assumed to be constant over the range of air temperatures concerned; T_{ai} and T_{aj} are the air temperature (K) of the air nodes '*ai*' and '*aj*', respectively.

4.2.6 Conduction

For nodes in contact with each other, there is conduction heat transfer between them. The total conduction heat transfer rate to node i is calculated by:

$$\dot{q}_{Ci} = \sum_j C_{ji}(T_j - T_i) \qquad (4.15)$$

where C_{ji} is the conductance from node j to node i (W K^{-1}) and the sum is taken over all nodes in contact with node i.

4.3 Solution scheme

In order to obtain a solution to the set of heat balance equations for all nodes (equation 4.1) for the temperature rise of each node in one time step, the mass, specific heat capacity, reflectivity, emissivity and initial temperature of each node must be known or assumed; a time step is then selected. The rates of heat gain by different modes are then calculated one by one using equations (4.2) to (4.15) with nodal temperatures equal to that at the beginning of the time step. In the calculation, consideration is given not only to heat exchange between nodes within a section, but also to heat exchange by short wave radiation transmitted from one section to another, by conduction between adjacent nodes of different sections, and by air exchange between sections. These rates of heat gain to each node by different modes are then added together. This total rate of heat gain to a node is then multiplied by the time step and divided by the heat capacity of the node in order to obtain the temperature change of the node during the time step period according to equation (4.1). This temperature change is then added to the nodal temperature prevailing at the start of the same time step. In other words, the model uses the forward finite difference method in the calculation of the nodal temperatures one time step forward. The calculation scheme also implies that the surface capacitance nodes are placed at the inside of the surface conductance. It is assumed that the room air is kept at a constant temperature by an ideally-controlled air-conditioning system; therefore, the heat convected to the room air node is equal to the cooling load due to lighting. From the short-wave radiation falling on a nodal surface, and from a knowledge (or an assumption) of the spectral distribution of the light, the illuminance on the surface can be calculated using the relative spectral sensitivity curve of the Commission Internationale de L'Eclairage (CIE, International Commission on Illumination) (CIE 1983). The calculation of the short-wave radiation (and hence illuminance) on a nodal surface assumes that all surfaces are perfectly diffusing and that radiation form factors can be used to describe the coupling of radiation between surfaces.

Stability and convergence of the numerical scheme used in the model have caused some concern during the development of the model. In fact, the stability of the numerical scheme depends very much on the input values of the parameters, such as areas, heat capacities and heat transfer coefficients. In Sowell's LIGHTS program (Sowell 1989, 1990), nodal heat capacities smaller than a certain value (user defined) are assumed to be 'massless', so that the transient problem becomes a steady-state one, and in this way the problem of instability due to small mass and large conductances is eliminated. In the present numerical model, no node is assumed to be massless; therefore the time step has to be small: in the validation described in Chapters 8 and 9, a time step of 1.0 second is used to ensure stability. The Gauss-Seidel iteration method is used to solve the simultaneous equations [equations (4.4) and (4.10)] for a faster convergence.

The numerical model is coded in FORTRAN77 and can be compiled using any FORTRAN77 compiler. It has been compiled and has been run successfully on an Intel Pentium desktop computer using Microsoft FORTRAN 5.1 under MS-DOS; it has also been operated using Microsoft FORTRAN PowerStation 1.0 under Windows 3.1, and a Sun SPARCserver 670MP using Sun FORTRAN under UNIX. With very minor modification, it has also been compiled successfully on a VAX machine.

The computer program listing of LITEAC1 is illustrated in Appendix E.

4.4 Test of the room model with a simple analytical example

In order to test the validity of, and to establish confidence in, the room heat transfer model, a two-step validation process was adopted. Firstly, the room model LITEAC1 was tested using a simple configuration with a known analytical solution. Secondly, the results predicted by both LITEAC1 and LITEAC2 are compared with experimental data from the NIST test cell and from a laboratory-constructed test cell. The simple analytical example is discussed in this section while the experimental validation is discussed in Chapters 8 and 9.

4.4.1 Cubic enclosure without light sources

The analytical case studied is a cubic enclosure of unit length of side. Each surface has a unit area and a unit thermal mass. For calculation simplicity, the convection coefficient of each surface is assumed to be 1 W m^{-2} K^{-1}. In order to obtain a closed form analytical solution, the radiation heat exchange must be ignored. In the simulation, all surfaces are assumed to be perfect reflectors in long-wave radiation. Short-wave radiation is absent as there is no light source within the enclosure. These assumptions suppress the radiative heat transfer mechanism, making convection the only heat transfer mechanism within the enclosure.

This case is simulated using LITEAC1 with seven room nodes only, one air node and six identical room surface nodes, while the number of nodes in the luminaire and plenum sections are both zero. In the data file for room nodes, all six room surface nodes are each given an area of 1 m^2, a thermal capacity of 1 J K^{-1}, long-wave emissivity of 0 and long-wave reflectivity of 1. The air node is held at a constant temperature of 37°C while the six surface nodes each have initial temperatures of 25°C.

The analytical solution of this simple configuration can be easily obtained as follows. Let T_a be the air temperature (constant) and T_s be the temperature of a room surface node (a function of time t); then:

$$mc\frac{dT_s}{dt} = hA(T_a - T_s) \tag{4.16}$$

where m, c, h, and A are the mass, specific heat capacity, convective heat transfer coefficient and area of the room surface node, respectively.

Using simple integration, the above equation can be solved analytically for T_s as a function of t and the solution can be written as follows:

$$T_s(t) = T_a - \left[T_a - T_s(0)\right]\exp\left(-\frac{hA}{mc}t\right) \tag{4.17}$$

The solution generated by LITEAC1 can be made to agree with equation (4.17) to any desired accuracy by adjusting the time-step used in the simulation as shown in Table 4.1 and in Figure 4.3.

4.4.2 Cubic enclosure with long-wave radiation

The cubic enclosure with the same dimensions as the one described above has been used again for another simulation in which long-wave radiation is considered. Two opposite surfaces (top and bottom) are assigned a thermal capacity of 2 J K^{-1} while the other four surfaces have each a thermal capacity of 1 J K^{-1}. All six surfaces are assigned an emissivity (and also a reflectivity) of 0.5. The simulated results are shown in Figure 4.4. These results show that the surfaces approach equilibrium slower than the case without radiation. This is explained by the fact that the additional heat loss path due to radiation from the surfaces will extend the time required to reach equilibrium. Figure 4.4 shows also that the surfaces with a higher thermal capacity approach equilibrium slower than the surfaces with a smaller thermal capacity. The reason for this is that surfaces with high thermal capacity need to absorb a larger amount of heat for the same temperature increase as compared with surfaces with a smaller thermal capacity. The results cannot be compared with a corresponding analytical solution since the latter is impossible for the case with radiation introduced (which makes the differential equation non-linear).

One may argue that the above comparisons do not prove how well the model represents physical reality. However, the simple analytical example together with a sensitivity test by including radiation do verify that the computation of heat transfer in an enclosure in LITEAC1 correctly predicts the trends of temperature change of surfaces in the enclosure and hence the analytical test serves to increase confidence in the 'correctness' of the model.

4.5 Summary

A numerical model has been derived for the computation of the heat transfer inside a typical office room with the artificial light source as the only heat and radiation source and an ideally-controlled air-conditioning system as the only heat sink to extract all the heat gain of the air inside the room. In this model, all modes of heat transfer (conduction, convection and radiation) are considered. The model allows the temperature effects on the heat and radiation output of the artificial light source to be taken into account dynamically. The temperature effect on lamp performance can be taken into account either using empirical curves or using a numerical simulation of the fluorescent lamp positive column discharge, to be described in Chapter 5. Computer codes have been written for the model; the code which allows user input of empirical data of temperature effects on lamp performance is named LITEAC1.

The heat transfer computation in LITEAC1 has been verified by comparison with a simple analytical test. This has shown that the model behaves correctly by predicting the correct temperature changes in a simple cubic enclosure with known analytical solution when radiation is ignored. It has also been shown that when radiation is included, although an analytical solution cannot be obtained for comparison, the model behaves as expected by predicting the correct trends of temperature changes.

Therefore, the next stage is to develop a fluorescent lamp positive column model for integration into the dynamic room heat transfer model that has been described in this chapter. The objective is to obtain not only a good prediction of the temperature and cooling load, but also a good prediction of the lighting performance in the room. The fluorescent lamp positive column model is described next (Chapter 5).

Table 4.1

Simulated room surface temperature (T_s) for different time-step values as compared with the calculated temperature using equation (4.17) for the simple cubic enclosure with analytical solution. T_a is the air temperature in the enclosure which is kept constant at 37°C. For small time-steps, the numerically calculated surface temperatures agree very closely with the analytically calculated values.

Time t (s)	T_a (°C)	T_s (°C) by Eq. (4.17)	T_s (°C) at time-step = (in seconds)							
			1.0	0.5	0.25	0.1	0.01	0.001	0.0001	0.00001
0	37	25	25	25	25	25	25	25	25	25
1	37	32.5855	37.0000	34.0000	33.2031	32.8159	32.6076	32.5877	32.5857	32.5855
2	37	35.3760	37.0000	36.2500	35.7986	35.5411	35.3922	35.3776	35.3761	35.3760
3	37	36.4026	37.0000	36.8125	36.6199	36.4913	36.4115	36.4035	36.4026	36.4026
4	37	36.7802	37.0000	36.9531	36.8797	36.8226	36.7846	36.7807	36.7803	36.7802
5	37	36.9191	37.0000	36.9883	36.9619	36.9382	36.9212	36.9193	36.9192	36.9192
6	37	36.9703	37.0000	36.9971	36.9880	36.9784	36.9711	36.9703	36.9703	36.9703
7	37	36.9891	37.0000	36.9993	36.9962	36.9925	36.9894	36.9891	36.9891	36.9891
8	37	36.9960	37.0000	36.9998	36.9988	36.9974	36.9961	36.9960	36.9960	36.9960
9	37	36.9985	37.0000	37.0000	36.9996	36.9991	36.9986	36.9985	36.9985	36.9985
10	37	36.9995	37.0000	37.0000	36.9999	36.9997	36.9995	36.9995	36.9995	36.9995
11	37	36.9998	37.0000	37.0000	37.0000	36.9999	36.9998	36.9998	36.9998	36.9998
12	37	36.9999	37.0000	37.0000	37.0000	37.0000	36.9999	36.9999	36.9999	36.9999
13	37	37.0000	37.0000	37.0000	37.0000	37.0000	37.0000	37.0000	37.0000	37.0000

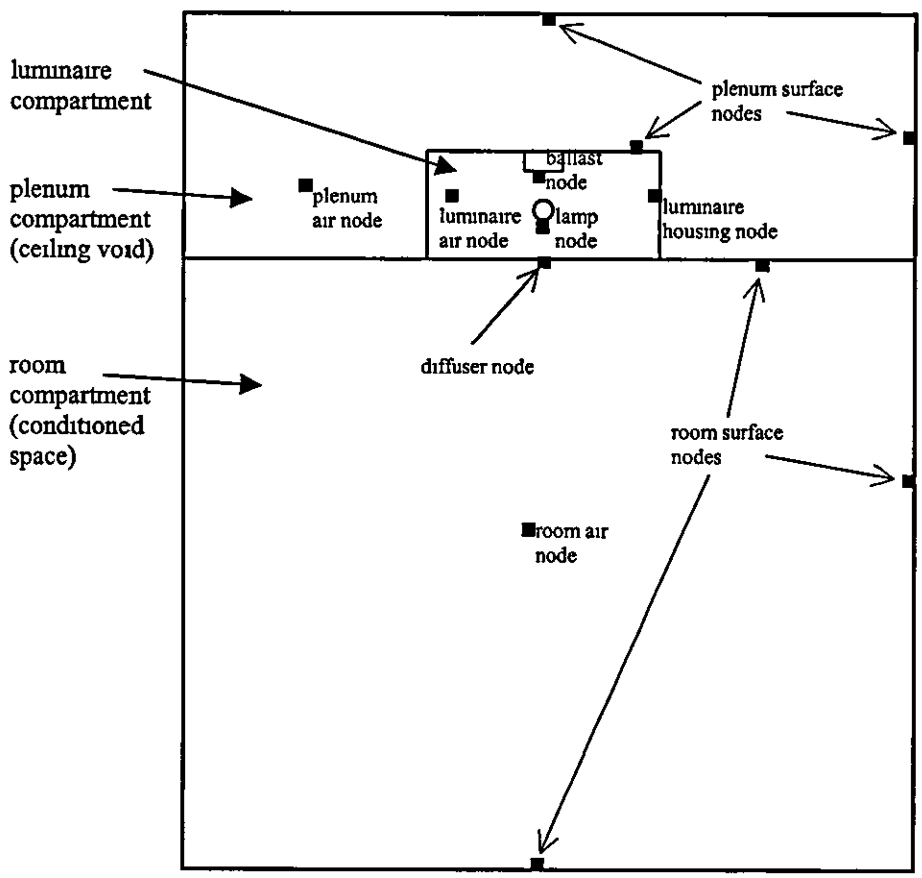

Figure 4.1

Schematic diagram of the three sections and the distribution of some typical nodes.

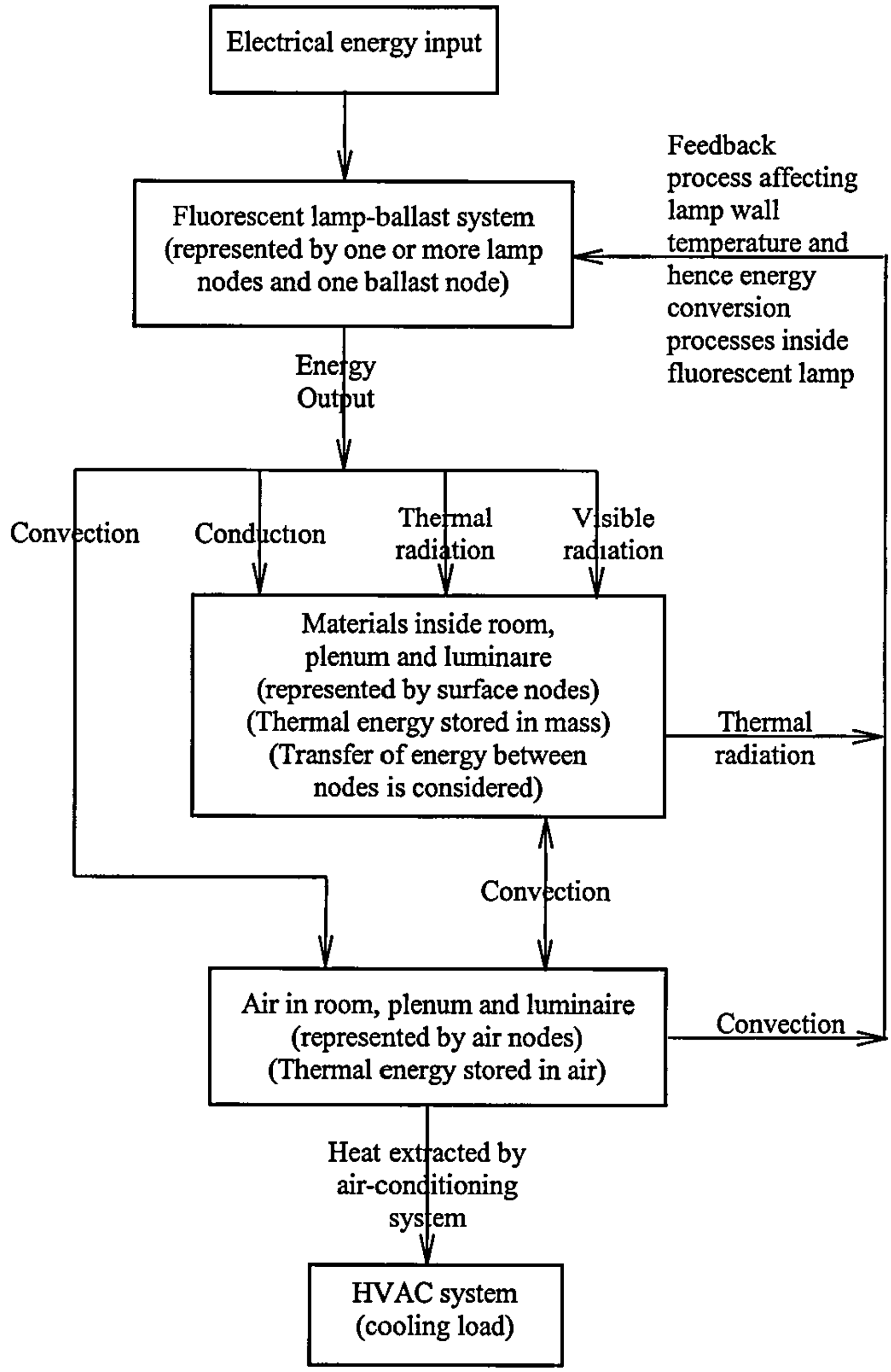

Figure 4.2

Schematic diagram showing major heat transfer paths considered in LITEAC1 and LITEAC2. Thermal radiation and conduction paths between surface nodes are not shown but are considered in LITEAC1 and LITEAC2.

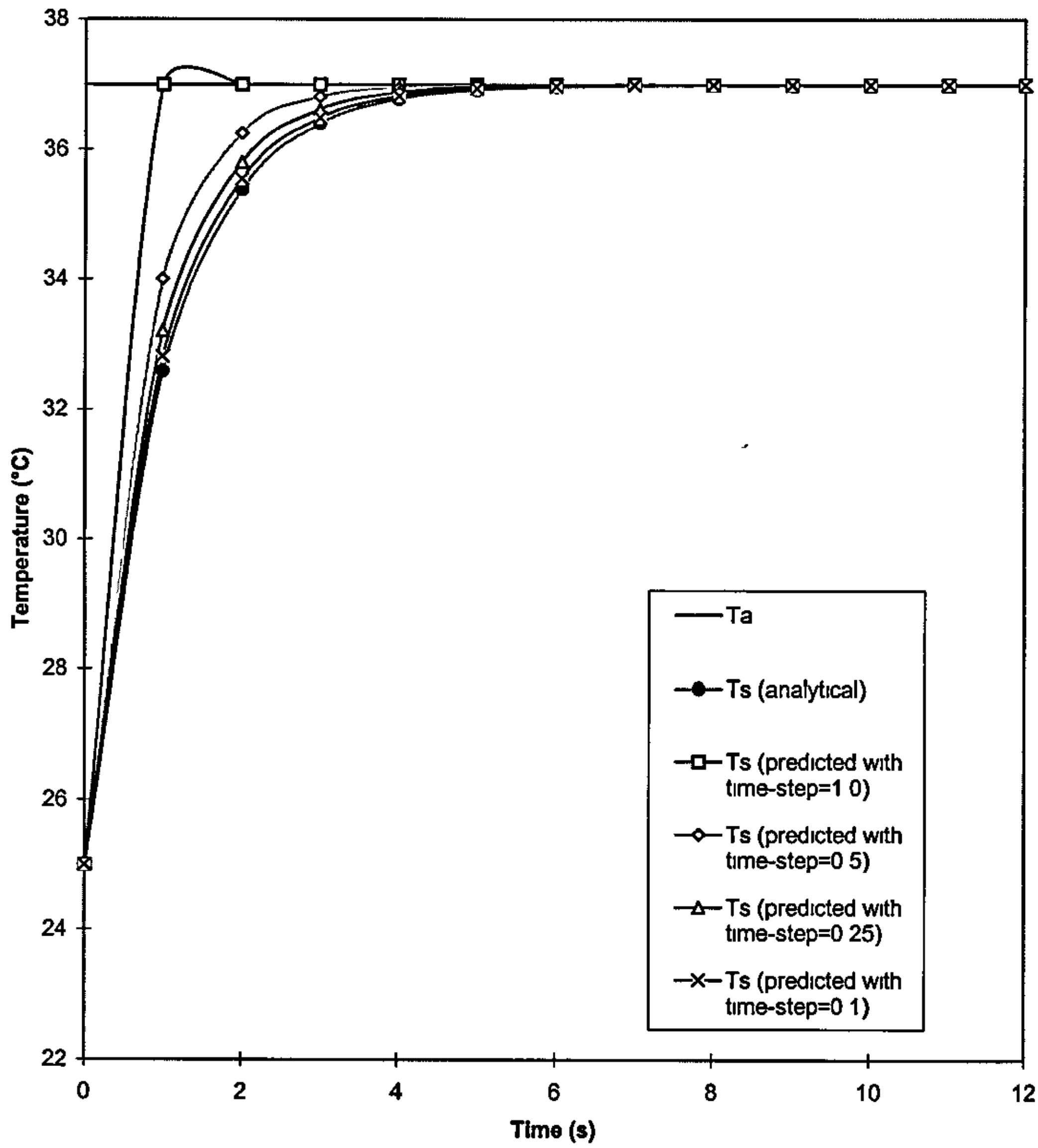

Figure 4.3

Simulated room surface temperature with different time-step values as compared with the calculated temperature using equation (4.17) for the simple cubic enclosure with analytical solution.

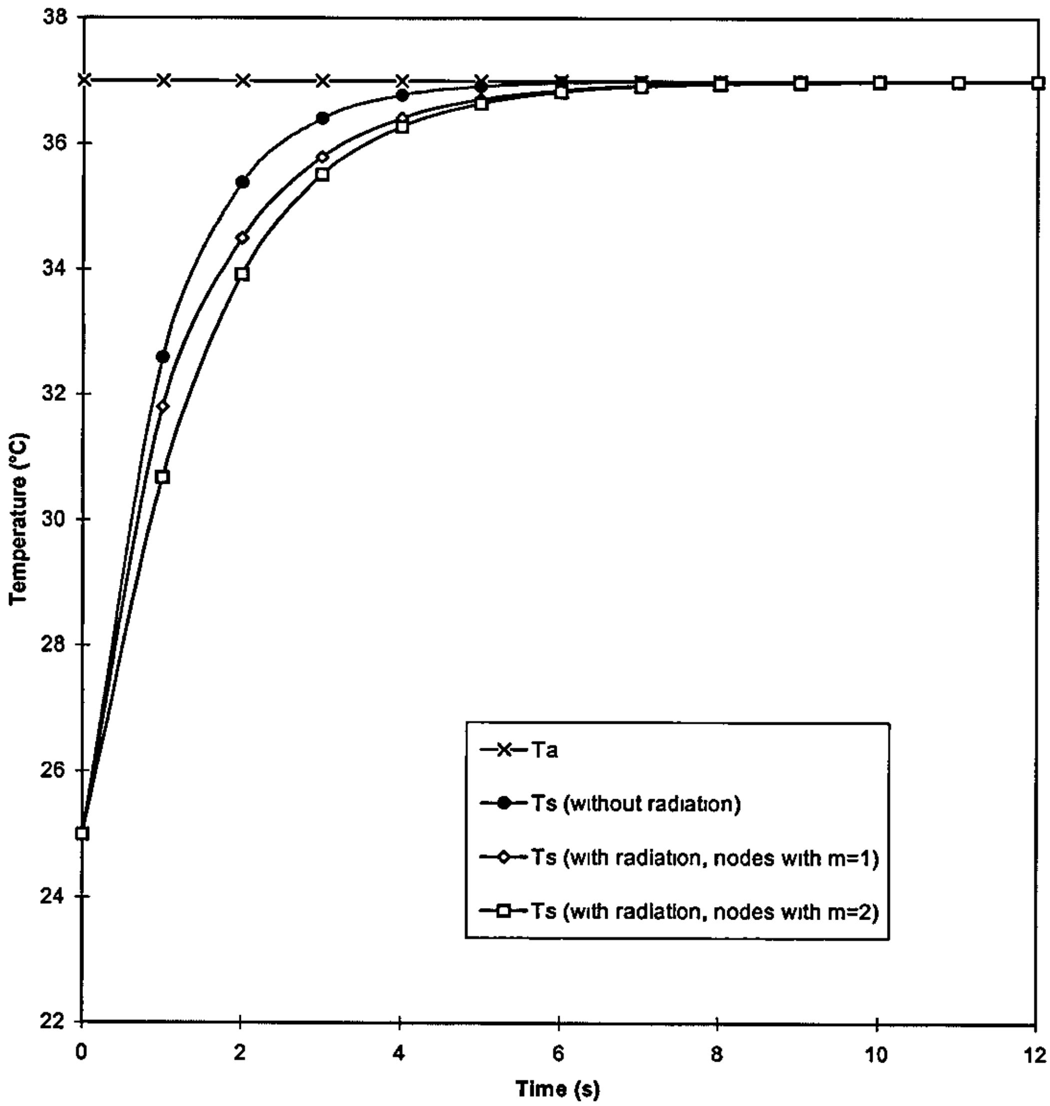

Figure 4.4

Simulated room surface temperature with long-wave radiation considered. Comparison is made between the simulations with radiation considered and that without radiation considered. Comparison is also made between nodes with thermal capacity of 1 J K^{-1} and nodes with thermal capacity of 2 J K^{-1}. All simulations used a time-step of 0 001 s.

Chapter Five

Modelling of the Fluorescent Lamp Positive Column

5.1 Background to using a fluorescent lamp positive column model in this study

In Chapter 4, a numerical model of the heat and radiation transfer in a room enclosure, named LITEAC1, was presented. In this model, the artificial light source is the only source of heat and radiation and all heat gain to the room air is considered to be extracted by an ideally-controlled air-conditioning system so as to keep the room air temperature constant. LITEAC1 calculates, at each time step, the temperatures of nodes (room components) and cooling load due to lighting in an enclosure from user input data of the electrical power rating of lamp, the light output of lamp and the physical properties of nodes: area, thermal capacity, emissivity, reflectance, transmittance, body type, characteristic length, conductance and radiation form factors. In other words, the transient state temperature variations of the nodes and the transient state cooling load profiles are the output of the room heat and radiation transfer model. Other output parameters are the heat and radiation fluxes at the nodes.

The transient state temperature variations of the nodes and the transient state cooling load profiles depend on how much electrical power input to the lamps is converted to radiation and how much is converted to convective/conductive heat. This is because radiation transfer energy directly to the nodes which absorb the radiation energy and can retain the energy for a time period before releasing it to the air to become the cooling load whilst convective heat released by the lamps to the air becomes cooling load instantaneously. In existing models, the proportions of convective heat and radiation output from the lamps have to be assumed arbitrary. In

LITEAC1, the radiation power output from the lamps is calculated using the rated light output of the lamps (from lamp data) and an assumed value (user defined) of the luminous efficacy of radiation to convert the light output in lumens to radiation power in watts. The convective heat is then assumed to be the difference between the input electrical power to the lamps and the radiation power output of the lamps (calculated by dividing the light output by the luminous efficacy of radiation).

The conversion of electrical power into light and heat takes place inside the fluorescent lamp. As reviewed in Chapter 3, there are several existing fluorescent lamp positive column models that calculate the conversion of the input electrical power of a fluorescent lamp into various forms of power output from the positive column of the lamp: UV radiation, other visible and invisible radiation, and heat dissipated inside the lamp and at the lamp wall. These existing models simulate the physical processes inside the fluorescent lamp discharge using established theories in atomic and plasma physics. Most of these models were theoretical studies in physics without clear specific applications. One objective of this research is to apply a fluorescent lamp discharge model to simulate the conversion of electrical power into light and heat. All existing models cannot be applied directly for this purpose. Therefore, a fluorescent lamp positive column model is developed in this work for the integration into the room light and heat transfer model described in Chapter 4. The fluorescent lamp model used here is based on the same hypotheses used by previous workers. However, the equations of the model (to be described in this chapter) are written from first principles and the solution method (to be described in Chapter 6) is developed in this work. This fluorescent lamp positive column model requires only input of the radius of the fluorescent tube and the lamp current from the user (available in lamp data sheets), and the minimum lamp wall temperature from the room heat and radiation transfer model. It calculates the power output of the fluorescent lamp discharge in various forms: UV radiation, other radiation and heat. A method of calculation of the light output (from the fluorescent lamp) from the value of

UV radiation power output calculated by the fluorescent lamp positive column model is also developed in this research. The calculation of light output requires user input of the relative spectral power distribution of the lamp which is a property of the phosphors used in the lamp (Section 6.4). The fluorescent lamp model then returns the light and heat output from the lamps to the room heat and radiation transfer model which will in turn calculate nodal temperatures, heat and radiation fluxes and cooling load in the next time step. The node temperature of the lamp will become again an input to the fluorescent lamp model for the calculation of light and heat output. The calculations repeat for all time steps. Figure 5.1 gives a simple flow diagram showing the flow of data in the integrated room heat and radiation transfer model and fluorescent lamp positive column model.

In this way, the combined model of room heat transfer and the fluorescent lamp discharge calculates not only the effect of heat output from lighting on the cooling load in an enclosure, but also the effect of the ambient thermal environment upon the performance of the lighting system itself. This is because the variations of the light output, lamp power and lamp efficacy with the minimum lamp wall temperature are simulated by the fluorescent lamp positive column model and the variation of the minimum lamp wall temperature with the ambient thermal environment in the enclosure is simulated by the room heat and radiation transfer model. Hence, it can be said that the integration of a fluorescent lamp discharge model with a room heat transfer model produces a numerical model of the mutual interaction between lighting and air-conditioning systems in an enclosure. This chapter is devoted to the discussion of the fluorescent lamp positive column model used in this research. In this section, some background to fluorescent lamp operation is given first.

5.1.1 Operation of a fluorescent lamp

Fluorescent lamps are low pressure mercury discharge lamps. A typical fluorescent lamp consists of a long glass tube of diameter either 38 mm (T12) or 26 mm (T8) with two electrodes, one at each end of the tube. Smaller tube diameters are used in compact fluorescent lamps. The electrodes are coated with alkaline earth oxides to facilitate the emission of electrons. The tube is filled with a rare-gas, such as argon or krypton, or a mixture of argon and krypton, at a pressure of about 300 to 500 Pa. A small amount of liquid mercury is introduced into the tube so that at normal room temperatures there is a mercury vapour partial pressure of about 0.8 to 1.3 Pa. A potential difference applied across the two electrodes accelerates the electrons which are emitted from the electrodes. These accelerated electrons collide inelastically with the mercury atoms in the tube, losing kinetic energy to the mercury atoms which in turn excites the mercury atoms to higher energy levels. As the excited mercury atoms relax back to the ground state or to an intermediate metastable state, the energy which they absorbed during excitation is dissipated as quanta of electromagnetic radiation. This process occurs in a region called the 'positive column' of the discharge. The positive column occupies over 95% of the length of the tube (Elenbaas 1971). The radiation emitted consists mainly of two lines in the ultraviolet (UV) band, at 253.7 nm and at 185.0 nm, which are often called the resonance lines (Elenbaas 1971). The emitted radiation contains also some weak lines in the visible and invisible wavelengths. The output energy of the 253.7 nm line is about 5 to 8 times larger than the output of the 185.0 nm line (Barnes 1960). Fluorescent powder, or phosphor, on the inside surface of the tube wall converts the UV radiation to visible light. The unit can be used for various lighting applications.

The number of inelastic collisions in the discharge depends on the mobility of electrons and on the density of the mercury atoms. The number of mercury atoms being excited to the resonance and upper energy states depends on the energy distribution of the electrons. The radiation emitted during de-excitation of the mercury atoms suffers from self absorption within the positive column. This self absorption is the absorption of the emitted UV radiation quantum by a ground state mercury atom which will then be excited. The excited mercury atom has the same probability of re-emitting the absorbed UV quantum as other excited mercury atoms. This phenomenon is often called radiation trapping or imprisonment of radiation (Holstein 1947, 1951). The self absorption increases with the number of mercury atoms in the gaseous state in the tube. As there is an excess amount of liquid mercury inside the tube, the number of mercury atoms in the gaseous state is determined by the saturated vapour pressure of mercury at the minimum temperature of the tube wall. Hence, for a fixed lamp-ballast system, the variable which affects light output of a fluorescent lamp is the minimum lamp wall temperature (also called the cold spot temperature) which is the temperature of the coldest spot on the lamp wall. The two competing processes, namely increase of UV quanta emitted and increase of self-absorption with density of mercury atoms, give rise to the following phenomenon: the light output increases with minimum lamp wall temperature at first up to a maximum — it then decreases with further rise in the minimum lamp wall temperature. There is thus an optimum minimum lamp wall temperature at which the light output is a maximum.

5.1.2 Modelling of lamp performance

To account for the above effect, previous models of the interaction of lighting and cooling systems such as that of Sowell (1989, 1990) made use of empirical curves to relate light output and lamp power to the minimum lamp wall temperature. However, the use of empirical curves gives no physical insight into the mechanism of conversion of electrical energy into light and heat within the fluorescent lamp. Knowledge of the physical processes inside the fluorescent lamp discharge tube allows the calculation of the division of electrical energy into light and heat, which is important in the dynamic simulation of cooling load (explained in Section 3.2).

Furthermore, it is necessary to use different curves for lamps of different type and of different size which are usually not readily available. In order to obtain a physical insight and to calculate the conversion of electric energy into light and heat from first principles (thus avoiding the need of an arbitrary assumption of the division of light and heat output from the fluorescent lamp), a mathematical model of the discharge process inside the fluorescent tube is necessary. In a fluorescent lamp discharge model, the energy balance is considered in relation to the density of mercury atoms which in turn depends on the ambient temperature.

In this study, the aim is to investigate the macroscopic behaviour of the fluorescent lamp with respect to a change of thermal environment, rather than to investigate the detailed processes occurring inside the fluorescent tube; it will not, therefore, be necessary to use a rigorous and detailed fluorescent lamp positive column model in which the radial variation of mercury excited state densities, for example, is considered. Instead, a model with sufficient details only will be developed. Such a model considers the major mercury excited states, uses published values of transition rates between different states, and treats radiation trapping with a simple formulation, while ignoring the radial variation of discharge properties and the excitation of rare-gas atoms. In this way, the processes taking place within the fluorescent tube will be modelled in sufficient detail so as to advance the current status of HVAC/lighting interaction modelling to beyond the level of reliance upon simple empirical curves which are only available for a few types of lamp.

In this chapter, the fluorescent lamp positive column model developed in this study is described. The discussion begins with statements of the hypotheses and approximations used in deriving the model equations, and is then followed by a detailed description of the fluorescent lamp energy balance and the conservation of different mercury states in the discharge at equilibrium.

5.2 Hypotheses and approximations

The processes which take place inside the fluorescent lamp discharge (described briefly in section 5.1) are complex. In order that these processes can be described in the form of manageable mathematical equations which can be solved to obtain the relationships between the various forms of power dissipation in the discharge and the minimum lamp wall temperature, some hypotheses and approximations have to be employed. Along lines similar to existing models of Waymouth and Bitter (1956) and Lama et al. (1982), the following main hypotheses are employed in this study:

(i) Electron energy distribution is assumed to be Maxwellian and characterized by a constant electron temperature independent of the radial position in the discharge tube.

Probe measurements of Easley (1951) show that this hypothesis is valid in the discharge found in typical fluorescent lamps except at high electron energies. The deviation from the Maxwellian distribution of the high energy electrons brought about the creation of a two-electron-temperature group model of low pressure gas discharges (Vriens 1973). In Vriens' model, the electron energy distribution is characterized by two electron temperatures: one for the low energy electrons and one for the high energy electrons. Although Vriens (1973) showed some improvements of his calculated results over models that considered only a Maxwellian electron energy distribution, he pointed out that his method lacked physical explanation. Furthermore, Vriens (1973) did not give quantitatively the improvement of his model in the calculation of the radiation power output for the mercury-argon discharge compared with earlier models. In more recent models such as that of Zissis et al. (1992), a non-Maxwellian electron-energy distribution function was used but with an analytical approximate solution only. In view of that existing models which assume a Maxwellian electron energy distribution (e.g. Waymouth and Bitter 1956, Cayless 1963 and Lama et al. 1982) give good agreement to experimental results, it is considered that a Maxwellian electron energy distribution with a constant electron temperature throughout the whole positive column is good enough for the purpose of the current research.

(ii) Only mercury is ionised and excited while inelastic collisions with rare-gas atoms can be neglected.

This hypothesis is approximately true because the excitation and ionisation energy of the rare-gas atoms is higher than could be provided by the electrons. The rare-gas serves as a buffer to control the mobility of electrons and to retard the diffusion of electrons to the tube wall. The very weak argon lines observed in the fluorescent lamp discharge justifies this assumption. In some recent works, e.g. Winkler et al. (1983) and Zissis et al. (1992), argon excitation and ionisation were included. However, they all showed that the contribution of rare-gas excitation and ionisation to the energy balance of the fluorescent tube discharge is very small, rare-gas excitation and ionisation will be neglected in this model.

(iii) Loss of electrons and mercury ions is purely by ambipolar diffusion to the tube wall where they recombine. Recombination within the positive column is negligible. Ambipolar diffusion is the diffusion of electrons and positive mercury ions in the positive column plasma to the tube wall at the same rate (see Appendix B).

The maintenance of electrical conductivity in the discharge plasma requires production of electron-ion pairs as fast as they are lost by recombination. In many existing models (e.g. Waymouth and Bitter 1956, Cayless 1963, and Lama et al. 1982), a diffusion-controlled positive column is assumed. The principal loss process is the diffusion of the electron-ion pairs to the tube wall and recombination at the tube wall, rather than volume recombination. If mercury ions only (but not rare-gas ions) are assumed to be present in the positive column, then the diffusive motion of the electrons and ions is governed by the ambipolar diffusion law (see Appendix B).

(iv) The excited mercury atoms are de-excited by spontaneous emission of photons and by superelastic collisions with electrons. Losses due to diffusion of excited atoms to the tube wall and de-excitation by collisions with rare-gas atoms can be ignored.

In the energy balance equation of the positive column [equation (5.1)], the diffusion loss is expressed by the term W_{diff}. This term is simply assumed to be negligible throughout this study. According to Lama et al. (1982), the diffusion rates of the excited atoms are much smaller than the radiation rate and the superelastic collision rate, therefore, ignoring the diffusion loss does not affect the calculation results of radiation power loss, ionisation loss and elastic collision loss.

(v) The positive column is assumed to be uniform and free of striations.

This assumption is very good as the positive column of fluorescent lamp discharge under normal operating conditions are uniform and free of striations. Only under abnormal operating conditions (e.g. when the lamp is near to its end of life or when the voltage is too low) when striations occur, which would appear as alternate light and dark rings running to-and-fro inside the fluorescent tube.

The above hypotheses have been used by other workers in low-pressure mercury-rare-gas positive column models (e.g. Waymouth and Bitter 1956, Waymouth 1971, and Lama et al. 1982) and have been shown to be reasonable assumptions by the good agreement with experimental results (Lama et al. 1982).

5.3 Fluorescent lamp energy balance

The principal function of an electric lamp is to convert electrical energy into light energy. In a fluorescent lamp, this conversion occurs through a number of processes within the lamp discharge tube. The major processes are shown schematically in Figure 5.2.

Electrical energy input to the fluorescent lamp discharge becomes principally the kinetic energy of the electrons due to acceleration of electrons by the electric field within the plasma. The kinetic energy of the electrons is dissipated in one of the following processes (Waymouth 1971):

(i) inelastic collisions with mercury atoms causing excitation to higher energy levels;
(ii) ionization of the mercury atoms;
(iii) elastic collisions with the rare-gas atoms; and
(iv) diffusion to the tube wall and recombination with excited atoms there.

The electrons may also collide with excited mercury atoms causing de-excitation of the excited mercury atoms which results in the excitation energy being released back to become kinetic energy of the electrons. This process is called superelastic collisions or sometimes referred to as elastic collisions of the second kind (Zissis et al. 1992).

An energy balance equation for the electrons in the positive column can be written as follows:

$$E \cdot j - W_{inel} - W_{ion} - W_{el} - W_{diff} + W_{sel} = 0 \tag{5.1}$$

where E is the electric field strength across the discharge tube (V m^{-1}), j is the electric current density (A m^{-2}), and the 'W' terms denote the local energy gains or losses per unit time per unit volume of the positive column (W m^{-3}). The subscripts *inel*, *ion*, *el*, *diff*, and *sel* denote inelastic collision, ionization, elastic collision, diffusion, and super-elastic collisions, respectively. In equation (5.1), it is assumed that the recombination of electrons with ions within the plasma is negligible (hypothesis (iii) of Section 5.2) and that the thermal flux conducted through the electron gas is zero. The last assumption follows from the fact that the electron temperature T_e is taken to be constant throughout the positive column in this study (hypothesis (i) of Section 5.2).

The terms W_{inel}, W_{ion}, W_{el}, W_{diff}, and W_{sel} can be evaluated using the equations described in Appendix D. However, due to mathematical complexity and the difficulty in obtaining reliable data on the cross sections and the electron energy distribution function, approximations are used to evaluate these terms as described in Section 6.1 2.

As the main function of the fluorescent lamp is to produce radiation from which light is obtained by fluorescence, the relationship between radiation in the discharge and the W terms in equation (5.1) is described here. The net radiation loss from the discharge is given by the difference between the inelastic collision loss and the super-elastic collision loss. This is because the excited atoms can either decay spontaneously with emission of radiation or can collide super-elastically with an electron, transferring their extra energy back to the electron. Hence, the net radiation power loss of the positive column per unit volume W_{rad} is given by:

$$W_{rad} = W_{inel} - W_{sel} \tag{5.2}$$

The radiation emission from the discharge contains mainly the two ultra-violet wavelengths 253.7 nm and 185 nm, with some weak lines in the visible and invisible wavelengths. Therefore, the radiation loss can be written as:

$$W_{rad} = W_{254} + W_{185} + W_{vis} + W_{nv} \tag{5.3}$$

where W_{254} and W_{185} are the power losses (per unit volume) due to emissions in the two ultra-violet wavelengths 253.7 nm and 185 nm respectively; W_{vis} and W_{nv} are the power losses (per unit volume) due to weak emissions in the visible and invisible bands resulting from excitations of mercury atoms to energy states higher than the resonance states. These radiation losses occur in the form of emission of quanta of energy and each quantum has an energy equal to the product of the electronic charge and the energy level difference in electron volts between the excited state and the final state after the transition. The number of quanta that can escape the plasma in unit time per unit volume is equal to the number density (number per unit volume) of the excited state in the plasma divided by the effective life time of the state in the plasma. The radiation power is then equal to the number of quanta escaping the plasma per unit time per unit volume multiplied by the energy gap of the transition. Expressions giving the radiation power losses will be given in equations (6.10) to (6.13) in Chapter 6. A diagram showing the flow of energy in a fluorescent lamp is shown in Figure 5.2.

As can be seen in equations (D.1)-(D.5) of Appendix D, the power loss terms (W terms) each depend on the density of all species of mercury atoms, cross-sections of ionisation and excitation of mercury atoms, the rate of re-combination at the tube wall and the density of rare-gas in the tube. A continuity equation can be set up for each species of the mercury atom; the set of continuity equations for all species of the mercury atom, together with the energy balance equation, form the equation set of a positive column model of the fluorescent lamp. Simplifications and approximations (to be described in Chapter 6) have to be made in order that the set of model equations becomes solvable for the power loss terms (W terms) in equation (5.1) as functions of the minimum lamp wall temperature. Details of the mercury levels considered and the continuity equations used in this study are discussed in the following sections.

5.4 Mercury atom energy levels

In the fluorescent lamp mercury-rare-gas discharge plasma, ten species of the mercury atom are considered to be important in the generation of radiation quanta (e.g. Kenty 1950). These are the ground state (6^1S_0), the two metastable states (6^3P_0 and 6^3P_2), the two resonance states (6^3P_1 and 6^1P_1), the four upper states (7^3S_1, 6^3D_1, 6^3D_2, and 6^3D_3), and the ionised state (Hg^+). In the model developed in this research, following the treatment of Cayless (1963), the three upper states 6^3D_1, 6^3D_2, and 6^3D_3 are lumped into a fictitious level which gives out quanta of invisible radiation (with wavelength between 297 nm to 366 nm) upon decay. The eight mercury atom energy levels considered in this model are summarised in Table 5.1 and these are shown, together with the transitions taken into account, in Figure 5.3.

5.5 Balance of mercury states at equilibrium

Following the nomenclature used by many previous workers (e.g. Waymouth and Bitter 1956; Lama et al. 1982; Zissis et al. 1992), the 'density' of electrons or mercury states refers to the number of electrons or mercury states, respectively, per unit volume of the positive column. It is also noted that some authors (e.g. Cayless 1963) used the term 'concentration' to mean the same thing (i.e. 'density'). At equilibrium, the rate of creation of a species of mercury is equal to the rate of loss of the species; hence, a mercury state density balance equation which describes this equality can be written for each mercury state. These balance equations are often referred to as continuity equations (Zissis et al. 1992).

5.5.1 *Ground state density*

At equilibrium, the rate of change of the ground state density is equal to zero:

$$-\sum_{j=1}^{6} K_{0j} N_e N_0 - K_{0i} N_e N_0 + \sum_{j=1}^{6} K_{j0} N_e N_j + \sum_{j=1}^{6} \frac{N_j}{\tau_{j0}^{*}} + \frac{D_a N_e}{\Lambda^2} = 0 \tag{5.4}$$

where K_{jk} (j,k=0,1,…,6) are the transition rate coefficients ($m^3\ s^{-1}$), defined as the number of transitions from state j to state k per state j atom per electron per second; K_{0i} is the ionisation rate coefficient of the ground state ($m^3\ s^{-1}$), defined as the rate of ionisation per electron per mercury ground state atom; τ_{jo}^{*} is the effective life time of the spontaneous decay from the j^{th} state to the ground state (s); D_a is the ambipolar diffusion coefficient ($m^2\ s^{-1}$); Λ is the diffusion length (m); N_e, N_j (j=0,1,…,6) are the densities (number per unit volume of the positive column) of electrons and the j^{th} mercury state, respectively.

In the above equation, the first term represents the excitation of the ground state to the six excited states, the second term represents ionization from the ground state, the third term represents the super-elastic decay of the six excited states to the ground state, the fourth term represents the spontaneous decay of the six excited states to the ground state with emission of a photon, and the last term represents the rate of recombination of ions and electrons which is assumed to be purely an ambipolar diffusion phenomenon.

5.5.2 *Excited state density*

Again, at equilibrium, for the k^{th} (k = 1,…,6) excited state:

$$-\sum_{j=k+1}^{6} K_{kj} N_e N_k - K_{ki} N_e N_k + \sum_{j=0}^{k-1} K_{jk} N_e N_j + \sum_{j=k+1}^{6} K_{jk} N_e N_j - \sum_{j=0}^{k-1} K_{kj} N_e N_k - \sum_{j=0}^{k-1} \frac{N_k}{\tau^*_{kj}} = 0 \tag{5.5}$$

where τ^*_{kj} is the effective life time of the spontaneous decay of the k^{th} state to the j^{th} state (s); and all other symbols have the same meaning as those defined in equation (5.4).

Equation (5.5) represents a set of 6 equations, one for each of the 6 excited states k=1 to 6. The first term represents loss of the k^{th} state due to inelastic collisions causing excitation to higher levels. The second term represents loss due to ionization. The third and fourth terms represent the increase to the k^{th} energy state due to excitation from lower states and to super-elastic de-excitation of higher states, respectively. The fifth term represents loss due to super-elastic de-excitation of the k^{th} state. The last term represents the spontaneous decay of the k^{th} state with emission of a photon, and is written in a general form in equation (5.5) that includes decay transitions to all lower states; however, there are only several 'permissible' transitions that emit photons.

5.5.3 Electron density and ionised state density

During ionisation of mercury, one electron escapes from each mercury atom. Hence, the electron density and the ionised state density are equal. Hypothesis (iii) in Section 5.2 states that loss of electrons and ions is purely by ambipolar diffusion to the tube wall, where they recombine. Therefore, at equilibrium, the rate of creation of electron-ion pairs is equal to their rate of loss due to recombination at the tube wall which is the same as the rate of ambipolar diffusion to the tube wall.

$$\sum_{j=0}^{6} K_{ji} N_e N_j - \frac{D_a N_e}{\Lambda^2} = 0 \tag{5.6}$$

where all symbols have the same meaning as those defined in equation (5.4).

Equation (5.6) is called the ambipolar diffusion equation (see Appendix B). The first term is the sum of the rate of ionization from the ground state and the six excited states. The second term is the ambipolar diffusion rate to the tube wall.

5.6 Electric current density

Electric current inside the fluorescent lamp discharge is carried mainly by electrons. The current carried by ions is very small and can be neglected (Elenbaas 1971). This is due to the fact that the ions have a much larger mass than the electrons and hence the mobility of ions in the discharge is very small compared with the electrons. In this study, the electric current inside the fluorescent lamp discharge is assumed to be carried completely by the flow of electrons.

The electric current density j (A m^{-2}) is equal to the product of the electron density N_e (m^{-3}), the electronic charge e (C) and the electron drift velocity v (m s^{-1}) which is governed by the electron mobility μ_e (m^2 V^{-1}s^{-1}) and the electric field strength E (V m^{-1}) across the positive column. It is expressed as:

$$j = N_e e v = N_e e \mu_e E \tag{5.7}$$

5.7 Summary

A fluorescent lamp positive column model has been derived for the integration into a room heat transfer model with a fluorescent lamp system as the only heat source and an ideally-controlled air-conditioning system for keeping the room air temperature constant. This fluorescent lamp positive column model employs the same established hypotheses used by previous workers (Waymouth and Bitter 1956; Lama et al. 1982). These hypotheses have been described here with justifications. The equations describing the positive column model are the energy balance equation (5.1), the continuity equations (5.4)-(5.6), and the electrical conductivity equation (5.7).

In this chapter, the energy balance of the fluorescent lamp discharge have been described with some details of how the input electrical energy to the fluorescent lamp is dissipated inside the tube. The most important form of the energy dissipation inside the fluorescent tube is the inelastic collisions which excite mercury atoms to higher energy levels and when these excited atoms relax back to the ground state or some intermediate metastable levels radiation is emitted. The radiation power loss have been described and explained.

Based on the conservation of the densities of mercury states at equilibrium, continuity equations (5.4)-(5.6) have been derived. These continuity equations are written in a general form that include all transitions: inelastic excitation, super-elastic de-excitation, ionisation, and spontaneous decay with photon emission. However, not all transitions are 'permitted', and some transitions are small enough to be ignored. In the next chapter, chapter 6, simplifications to the continuity equations will be described.

The set of model equations, i.e. the energy balance equation (5.1), the continuity equations (5.4)-(5.6) and the electrical conductivity equation (5.7), are written here in more comprehensive forms then those in previous works such as Waymouth and Bitter (1956) and Waymouth (1971). Furthermore, six excited mercury energy states are considered in this study as oppose to only two excited states (the resonance states) were considered in the work of Waymouth and Bitter (1956).

The aim of using a fluorescent lamp positive column model is to obtain the functions describing the variations of light output and lamp power with minimum lamp wall temperature. The formulation of the fluorescent lamp positive column model has been described in this chapter. The scheme of solution for these equations so that the light output and lamp power can be calculated for different minimum lamp wall temperatures will be described in the next chapter.

Table 5.1

Mercury energy levels considered in the positive column model used in this research.

Mercury energy level	**Index**	**Threshold potential (eV)**
Ground level 6^1S_0	0	0
First metastable level 6^3P_0	1	4 66
Triplet resonance level 6^3P_1	2	4.87
Second metastable level 6^3P_2	3	5 43
Singlet resonance level 6^1P_1	4	6.68
Upper level of the 404.7-546.1 nm group (7^3S_1)	5	7.70
A fictitious level lumping all upper levels ($6^3D_{1,2,3}$)	6	8.85
Ionised state	7 or i	10.44

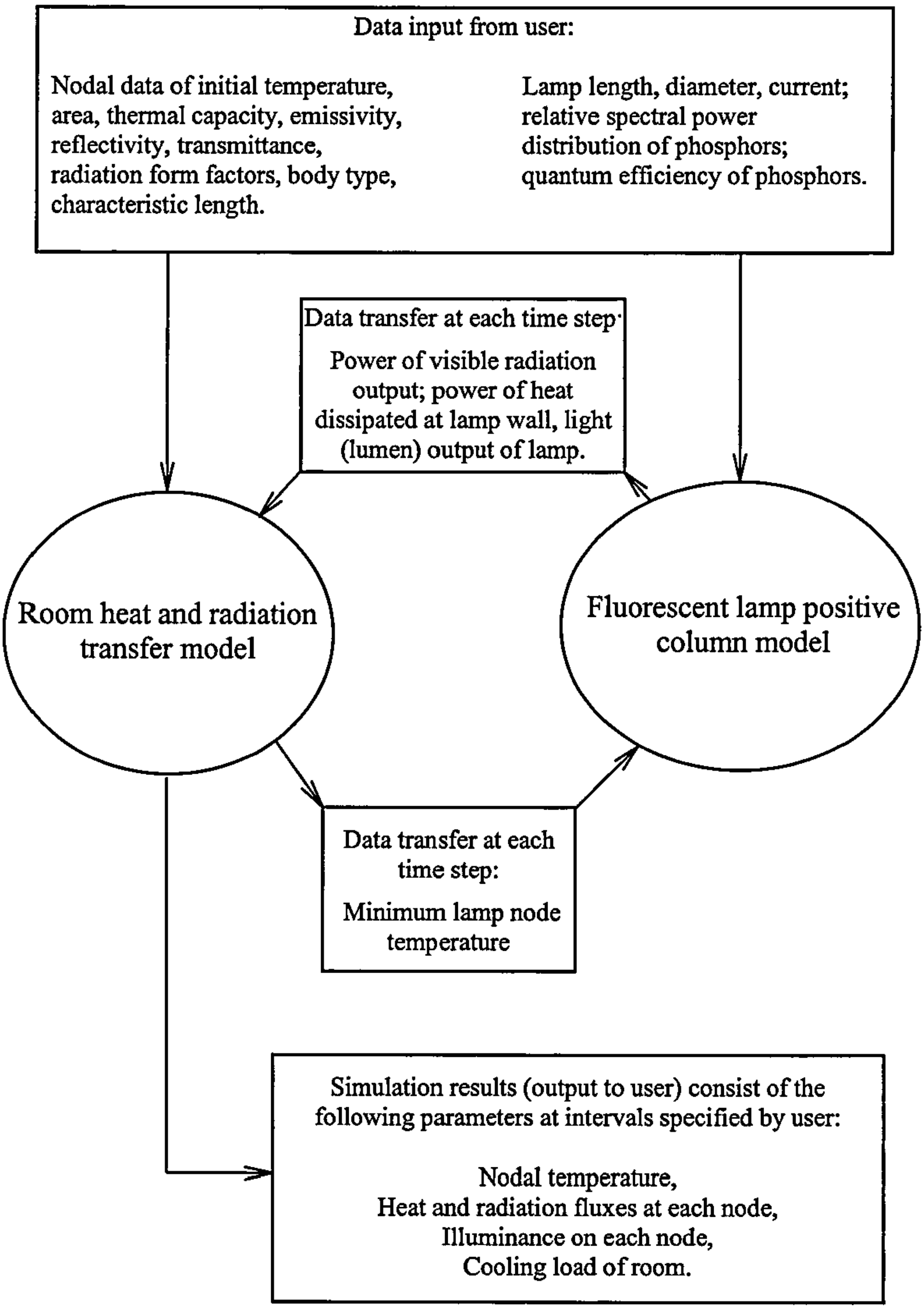

Figure 5.1

Simple flow diagram showing the data flow in the program LITEAC2.

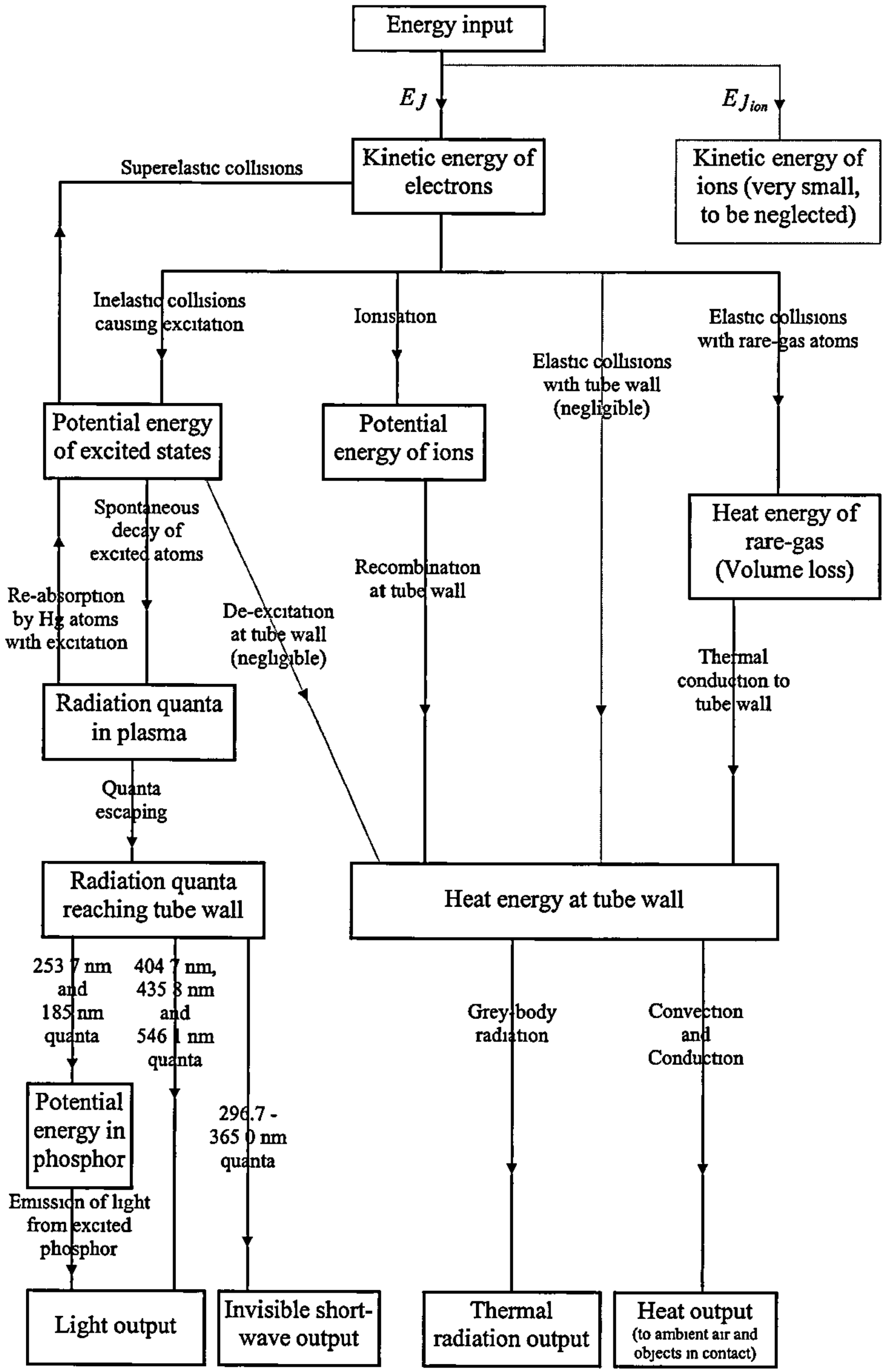

Figure 5.2
Schematic diagram showing the energy conversion processes in a fluorescent lamp.

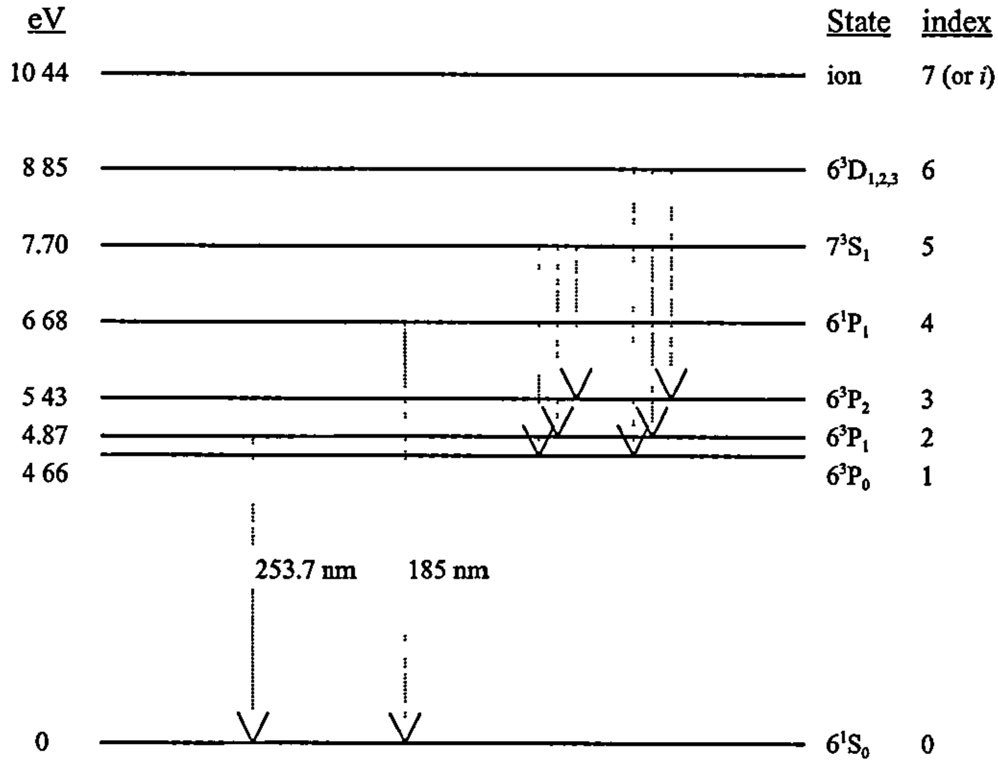

Figure 5.3

Simplified energy level diagram of the mercury atom. Transitions that produce radiation are shown as dotted lines with arrow heads. No other transitions are shown.

Chapter Six

Methodology for Solving the Fluorescent Lamp Positive Column Model

6.1 Approximations used to solve the equations

The set of equations that comprise the fluorescent lamp positive column model was described in Chapter 5. This set of equations is comprised of the energy balance equation (5.1), the continuity equations (5.4)-(5.6) and the electron current density equation (5.7). In order to solve this set of equations to obtain relationships between light output, lamp power and minimum lamp wall temperature, some further approximations are necessary. These approximations, which are discussed in the following sub-sections, have been specially designed for this study and they differ from the approximations used in existing positive column models.

6.1.1 Approximations for simplifying the continuity equations

The first approximation is that the mercury ground state density N_0 is assumed to be equal to the density of mercury atoms N_{Hg} in the positive column. This approximation is justified because the mercury ground state density is much (about 2 to 3 orders of magnitude) greater than the densities of the excited states (Kenty 1950).

$$N_0 = N_{Hg} \tag{6.1}$$

The second approximation is to assume that direct ionisation from the ground state, and ionisation from the levels higher than the 6^3P_2 metastable level, can all be neglected. The approximation that direct ionisation from the ground state can be ignored was also used by Waymouth and Bitter (1956), and by Lama et al. (1982). Direct ionisation from the ground state is unlikely because of the high value of the mercury ionisation energy compared with the electron energy. Due to the high population densities of the $6^3P_{0,1,2}$ states compared with the higher energy states, ionisation from the higher energy states is very low compared with the ionisation from the $6^3P_{0,1,2}$ levels; therefore, all ionisation from higher energy states are neglected. In other words, the transition rates K_{0i}, K_{4i}, K_{5i} and K_{6i} in equations (5.5) and (5.6) are all equal to zero.

It is further assumed that excitation to the 7^3S_1 and $6^3D_{1,2,3}$ levels comes only from the ground and the triplet $6^3P_{0,1,2}$ levels, and that the decay of these levels can only take place with the release of quanta of radiation. It is also assumed that the transitions between the triplet $6^3P_{0,1,2}$ levels and both the 7^3S_1 and $6^3D_{1,2,3}$ levels have insignificant contributions to the balance of the triplet $6^3P_{0,1,2}$ levels and therefore that these transitions can be ignored in the continuity equations of the triplet $6^3P_{0,1,2}$ levels. Furthermore, both the 7^3S_1 and $6^3D_{1,2,3}$ states decay to the three triplet $6^3P_{0,1,2}$ levels, resulting in the emission of several lines in the visible and invisible wavelengths, respectively. As these emissions are weak, in order to simplify the continuity equations for the 7^3S_1 and $6^3D_{1,2,3}$ states, it is assumed that the decays of the 7^3S_1 and $6^3D_{1,2,3}$ states to the triplet $6^3P_{0,1,2}$ levels can be treated as if these decays were to a single fictitious level with an energy equal to the triplet resonance state, i.e. level 2.

Using these approximations, equations (5.4) to (5.6) can be rewritten as:

$$-\sum_{j=1}^{6} K_{0j} N_e N_0 + \sum_{j=1}^{6} K_{j0} N_e N_j + \frac{N_2}{\tau^*_{20}} + \frac{N_4}{\tau^*_{40}} + \frac{D_a N_e}{\Lambda^2} = 0 \tag{6.2}$$

$$\begin{aligned} &K_{01} N_e N_0 + K_{21} N_e N_2 + K_{31} N_e N_3 + K_{41} N_e N_4 \\ &\qquad -\left(K_{10} + \sum_{j=2}^{4} K_{1j} + K_{17}\right) N_e N_1 = 0 \end{aligned} \tag{6.3}$$

$$K_{02}N_eN_0 + K_{12}N_eN_1 + K_{32}N_eN_3 + K_{42}N_eN_4 - \left(K_{20} + K_{21} + \sum_{j=3}^{4} K_{2j} + K_{27} \right) N_eN_2 - \frac{N_2}{\tau_{20}^*} = 0 \tag{6.4}$$

$$K_{03}N_eN_0 + K_{13}N_eN_1 + K_{23}N_eN_2 + K_{43}N_eN_4 - \left(\sum_{j=0}^{2} K_{3j} + K_{34} + K_{37} \right) N_eN_3 = 0 \tag{6.5}$$

$$K_{04}N_eN_0 + K_{14}N_eN_1 + K_{24}N_eN_2 + K_{34}N_eN_3 - \sum_{j=0}^{3} K_{4j}N_eN_4 - \frac{N_4}{\tau_{40}^*} = 0 \tag{6.6}$$

$$K_{05}N_eN_0 + K_{15}N_eN_1 + K_{25}N_eN_2 + K_{35}N_eN_3 - \frac{N_5}{\tau_5^*} = 0 \tag{6.7}$$

$$K_{06}N_eN_0 + K_{16}N_eN_1 + K_{26}N_eN_2 + K_{36}N_eN_3 - \frac{N_6}{\tau_6^*} = 0 \tag{6.8}$$

$$K_{17}N_eN_1 + K_{27}N_eN_2 + K_{37}N_eN_3 - \frac{D_aN_e}{\Lambda^2} = 0 \tag{6.9}$$

where all symbols have the same meanings as previously defined in equations (5 4)-(5.6).

6.1.2 Approximations for energy terms

For the purpose of this study, it is not necessary to evaluate the energy terms using the forms given in Appendix D [equations (D.1)-(D.5)]. The following approach is used to evaluate, at equilibrium, the radiation power loss, the ionisation loss and the elastic collision loss of the positive column.

In equation (5.2) the difference between inelastic collision power loss and super-elastic collision power loss is equated to the net radiation power loss. This net radiation power loss consists of power losses due to the emission of the two ultra-violet lines, 253.7 nm and 185 nm, from the decay of the two resonance states, and due to emission of several weak lines in the visible and invisible wavelengths from the decay of the upper states. The net radiation loss is calculated as the sum of these four 'types' of emissions as given in equation (5.3). All these radiation losses occur in the form of emission of quanta of energy and each quantum has an energy equal to the product of the electronic charge and the energy gap in electron volts between the excited state and the final state of the transition. The number of quanta that can escape the plasma in unit time per unit volume is equal to the density of the excited state in the plasma divided by the effective life time of the state in the plasma. The radiation power is then equal to the number of quanta escaping the plasma per unit time per unit volume multiplied by the energy gap of the transition. The radiation power losses of the two resonance lines are as given below:

$$W_{254} = eV_2 \frac{N_2}{\tau_2^*} \tag{6.10}$$

$$W_{185} = eV_4 \frac{N_4}{\tau_4^*} \tag{6.11}$$

where W_{254} and W_{185} are the power losses (per unit volume) (W m^{-3}) due to emissions in the two ultra-violet wavelengths 253.7 nm and 185 nm, respectively; e is the electronic charge (C); V_2 and V_4 are the energy level (eV) of the 6^3P_1 and 6^1P_1 mercury states respectively; N_2 and N_4 are the number of the 6^3P_1 and 6^1P_1 mercury atoms, respectively, per unit volume of the positive column (m^{-3}); and τ_2^* and τ_4^* are the average effective life time of the 6^3P_1 and 6^1P_1 mercury atoms, respectively.

For the emissions of weak visible and invisible lines resulting from decays of the upper states, it is assumed, as discussed in section 6.1.1, that these upper states decay to a single fictitious level having an energy equals to the triplet resonance state 6^3P_1, i.e. level 2. With this assumption, a single effective life time for each upper state is used in the following expressions for the weak visible and invisible power losses.

$$W_{vis} = e(V_5 - V_2)\frac{N_5}{\tau_5^*} \tag{6.12}$$

$$W_{nv} = e(V_6 - V_2)\frac{N_6}{\tau_6^*} \tag{6.13}$$

where W_{vis} and W_{nv} are the power losses (per unit volume) (W m^{-3}) due to weak emissions in the visible and invisible bands, respectively, resulting from excitations of mercury atoms to energy states higher than the resonance states; e is the electronic charge (C); V_2, V_5 and V_6 are the energy levels (eV) of the 6^3P_1, 7^3S_1 and $6^3D_{1,2,3}$ mercury states respectively; N_5 and N_6 are the number of the 7^3S_1 and $6^3D_{1,2,3}$ mercury atoms, respectively, per unit volume of the positive column (m^{-3}); and τ_5^* and τ_6^* are the average effective life time of the 7^3S_1 and $6^3D_{1,2,3}$ mercury atoms, respectively.

For the ionisation loss, as ionisation from states other than the triplet $6^3P_{0,1,2}$ states are ignored, only three terms under the summation sign in equation (D.2) of Appendix D need to be considered. As the mercury atoms are ionised, they attain energy higher than the minimum energy of the ionised state V_i. Following Hoyaux and Sucov (1969), the average energy level V_i' corresponding to the ionised state is assumed to be given by:

$$V_i' = V_i + \frac{3kT_e}{2e} \tag{6.14}$$

where k is the Boltzmann constant, T_e is the electron temperature (K) and e is the electronic charge (C).

This is the average energy loss for each ionisation. The ionisation energy loss for each mercury state is the product of the number of ionisations from the state and the average energy loss for each ionisation. Then, using the transition rate coefficients K_{17}, K_{27}, K_{37}, the ionisation loss W_{ion} is calculated from the following equation:

$$\begin{aligned} W_{ion} = {} & K_{17} N_e N_1 e\left(V_i + \frac{3kT_e}{2e} - V_1\right) + K_{27} N_e N_2 e\left(V_i + \frac{3kT_e}{2e} - V_2\right) \\ & + K_{37} N_e N_3 e\left(V_i + \frac{3kT_e}{2e} - V_3\right) \end{aligned} \tag{6.15}$$

where N_e is the electron density (m^{-3}) in the positive column; N_1, N_2 and N_3 are the densities (m^{-3}) of the 6^3P_0, 6^3P_1 and 6^3P_2 states, respectively; and V_i, k, T_e and e have the same meanings as defined in equation (6.14).

Elastic collisions in the positive column refer to the collision between the electrons and the rare-gas atoms resulting in a transfer of momentum from the electrons to the rare-gas atoms. This means that the electrons lose energy while the rare-gas atoms gains energy resulting in an increase in temperature of the rare-gas. The elastic collision loss rate is the product of energy loss per electron per collision, the collision frequency and the electron density. According to Waymouth (1971), the electron loses, in an elastic collision, on average a fraction of its energy equal to $\frac{8m_e}{3m_{rg}}$, where m_e and m_{rg} are the masses of the electron and the rare-gas atom, respectively. Since the average electron kinetic energy is kT_e, the mean energy loss per collision, E_{el}, is given by:

$$E_{el} = \frac{8m_e}{3m_{rg}} kT_e \tag{6.16}$$

The average collision frequency ν_c per rare-gas atom is the average electron velocity divided by the electron mean free path λ_e, as follows:

$$\nu_c = \frac{1}{\lambda_e}\left(\frac{3kT_e}{m_e}\right)^{1/2} \tag{6.17}$$

Therefore, the total elastic collision loss is:

$$W_{el} = E_{el}\nu_c N_{rg} N_e = \frac{8\left(\frac{m_e}{3}\right)^{1/2} N_{rg} N_e (kT_e)^{3/2}}{m_{rg}\lambda_e} \tag{6.18}$$

6.2 Transition rate coefficients

The transition rate coefficients K_{jk} in equations (6.2)-(6.9) can be obtained by an integration of the collision cross section $Q_{jk}(E_e)$ over the electron energy distribution function (EEDF) $f(E_e)$ as follows:

$$K_{jk} = \left(\frac{2e}{m_e}\right)^{1/2} \int_0^\infty E_e Q_{jk}(E_e) f(E_e) dE_e \tag{6.19}$$

To simplify the solution process, and realising the facts that:

(i) reliable data on the cross sections for transitions between the various mercury states are sparse, and

(ii) the EEDF is not well known for many cases, the transition coefficients used in the present study were not obtained by the above integral. Instead, the method of Hoyaux and Sucov (1969) is followed and the transition rate coefficients K_{jk} are assumed to be dependent on the electron temperature T_e as given in equation (6.10) for ascending transitions ($k>j$):

$$K_{jk} = C_{jk}\left(\frac{kT_e}{e}\right)^{\frac{3}{2}}\left(1+\frac{e(V_k - V_j)}{2kT_e}\right)\exp\left(-\frac{e(V_k - V_j)}{kT_e}\right) \tag{6.20}$$

where the coefficients C_{jk} are constants to be determined using experimental values of transition rates and electron temperature quoted in literature.

Hoyaux and Sucov (1969) used a simple inverse dependence of transition rates on electron temperature for all descending transitions:

$$K_{kj} = A_{kj}\frac{e}{kT_e} \tag{6.21}$$

where the coefficients A_{kj} are constants derived by Hoyaux and Sucov (1969) using the results of Kenty (1950). However, in the present study it is considered not necessary to use another set of coefficients A_{kj} since there is the Klein-Rosseland relationship between the downward transition coefficient and the corresponding upward transition coefficient as follows (Hoyaux and Sucov 1969; Lama et al. 1982):

$$K_{kj} = \frac{g_j}{g_k}\exp\left(\frac{e(V_k - V_j)}{kT_e}\right)K_{jk} \tag{6.22}$$

The above relationship is based on detailed balancing of excitation and de-excitation by electron collisions (Hoyaux and Sucov 1969), this relationship is generally valid as long as the electron energy distribution is Maxwellian which is one of the hypotheses (hypothesis (i) of Section 5.2) used in this study. The relationship was used successfully by Lama et al. (1982).

The transition rates obtained from the literature are those corresponding to a minimum lamp wall temperature of 42°C and are taken from Winkler et al. (1983). Using the experimentally measured electron temperature of 11500 K for a lamp-wall temperature of 42°C, the set of modified continuity equations (6.2)-(6.9) for the particle densities is solved iteratively to obtain convergence on a solution of the particle densities at the lamp wall temperature of 42°C. These particle densities are then used to calculate the constant coefficients C_{jk}. These constants C_{jk} are then used to calculate the transition rate coefficients K_{jk} at different electron temperatures.

6.3 Effective life times

The effective life times of the radiating states are also very important in the adequate explanation of the observed emission of radiation from the discharge. The resonance states emit photons which suffer from self-absorption while travelling through the discharge plasma. The repeated absorptions and re-emissions of photons on the way to the tube wall increase the effective mean life times of the mercury resonance states. Accurate knowledge of the effective life times is important in the numerical modelling of the emission, absorption and re-emission of radiation by the resonance states. In the model developed here, the effective life times for the resonance states 6^3P_1 and 6^1P_1 as well as the 7^3S_1 and $6^3D_{1,2,3}$ states are needed in order to solve the set of simplified continuity equations (6.2)-(6.9).

The magnitude of the effective life time is influenced by many factors among which are the mercury atom density, the broadening of the hyperfine structure of the resonance lines due to thermal motion of the atoms (Doppler broadening) and the interaction of the mercury atoms with mercury and argon atoms (collision broadening) (Holstein 1947, 1951). Holstein performed an analysis of the effective life time by considering Doppler broadening and collision broadening separately and obtained different relations for the two cases. Walsh (1959) investigated the combined effects of both Doppler and collision broadening. However, there are still unsolved problems concerning the hyperfine structure of the lines and researchers are still active in this subject; examples of recent works include those of van de Weijer and Cremers (1985, 1987), Post (1986) and Post et al. (1986).

In order to keep the analysis as simple as possible, Holstein's theory for a pure Doppler broadening (Holstein 1951) is adopted here in the calculation of the effective life time. The expression giving the effective life time of a radiating state is as follows:

$$\tau_{eff} = \frac{k_o R(\pi \ln(k_o R))^{1/2} \tau}{16} \tag{6.23}$$

where k_o is the absorption coefficient at the centre of the resonance line (m^{-1}), R is the radius of the discharge tube (m) and τ is the natural life time of the radiating state (s). Following Winkler et al. (1983), use is made of the following expressions for the absorption coefficient of the two resonance lines 253.7 nm and 185 nm:

$$k_{02} = 2.23 \times 10^{-16} N_0 T^{-1/2} \text{ m}^{-1} \tag{6.24}$$

$$k_{04} = 71.8 \times 10^{-16} N_0 T^{-1/2} \text{ m}^{-1} \tag{6.25}$$

The values of the natural life time are discussed in various articles such as Van de Weijer and Cremers (1985, 1987). In this work the values of natural life time used in the calculation are the measured values of Van de Weijer and Cremers (1987), which are 120 ns and 1.3 ns for the 6^3P_1 and 6^1P_1 states, respectively.

6.4 Light output

Existing positive column models calculate the UV radiation output from the fluorescent lamp discharge but not the visible light output of the fluorescent lamp. The aim of using a fluorescent lamp positive column model in this work is to calculate the light output and lamp power at different minimum lamp wall temperatures. The following is a description of the method of calculation of light output from the fluorescent lamp developed during this study.

The light output of a fluorescent lamp is mainly from the fluorescence of the phosphors after excitation by the UV radiation emitted from the discharge. Hence, the light output from the lamp can be derived from a knowledge of the relative spectral power output $S(\lambda)$ of the phosphors in the lamp. In this work, the relative spectral power output $S(\lambda)$ is defined such that:

$$\int_{vis} S(\lambda)d\lambda = 1 \qquad (6\ 26)$$

where the integral sign $\int_{vis}$ denotes integration over all visible wavelengths. Then, the power output in wavelength interval λ to λ+dλ is

$$W(\lambda) = S(\lambda) \cdot W_{phos} \qquad (6.27)$$

where W_{phos} is the total output power of the emitted radiation from the phosphors in the lamp.

Suppose the number of quanta in the wavelength interval λ to λ+dλ emitted per second is n_λ, then the power output in this wavelength interval is:

$$W(\lambda) = \frac{n_\lambda \overline{hc}}{\lambda} \tag{6.28}$$

where $\bar{h}$ is the Planck's constant (= 6.626×10^{-24} Js) and $\bar{c}$ is the velocity of light (= 3.0×10^{8} m s^{-1}).

According to Elenbaas (1971), it is observed that for the present-day phosphors, only one quantum of visible light is emitted if a phosphor is excited by one quantum of UV radiation. However, there is a small loss of UV quanta which do not excite any phosphor. Define the quantum efficiency of the lamp phosphor η as the ratio of the total number of quanta of visible radiation emitted per second from the phosphors to the number of quanta of the UV radiation (253.7 nm and 185 nm) emitted per second from the discharge:

$$\eta = \frac{\int_{vis} n_\lambda d\lambda}{n_{254} + n_{185}} \tag{6 29}$$

where n_{254} and n_{185} are the number of quanta emitted per second of the 253.7 nm line, and of the 185.0 nm line, from the positive column, respectively.

From equations (6.27) and (6.28), the number of visible light quanta emitted per second can be written as:

$$n_\lambda = \frac{W_{phos} S(\lambda)\lambda}{\overline{hc}} \tag{6.30}$$

Therefore,

$$\int_{vis} n_\lambda d\lambda = \frac{W_{phos}}{\overline{hc}} \int_{vis} S(\lambda)\lambda d\lambda \tag{6.31}$$

The number of quanta emitted per second of the UV emission from the discharge can be expressed in terms of the power of the emission as follows:

$$n_{254} = \frac{253.7W_{254}}{\overline{hc}} \tag{6.32}$$

$$n_{185} = \frac{185.0W_{185}}{\overline{hc}} \tag{6.33}$$

Adding equations (6.32) and (6.33), the sum of the UV quanta emitted per second is:

$$n_{254} + n_{185} = \frac{253.7W_{254} + 185.0W_{185}}{\overline{hc}} \tag{6.34}$$

Combining equations (6.29), (6.31) and (6.34), it can be shown that the quantum efficiency η is given by the following expression

$$\eta = \frac{W_{phos}}{W_{uv}} \int_{vis} S(\lambda) \frac{\lambda}{253.7} d\lambda \tag{6.35}$$

where $W_{uv} = \dfrac{253.7W_{254} + 185.0W_{185}}{253.7}$ (6.36)

According to CIE (1983), visible light flux is radiant power weighted according to the spectral sensitivity of the human eye. Therefore, the visible light output Φ, in lumens, from the phosphors due to UV radiation emitted from the positive column is given by:

$$\Phi = F \cdot 683 \cdot W_{phos} \int_{vis} S(\lambda)V(\lambda)d\lambda \tag{6.37}$$

Substituting for η with the expression given in equation (6.35):

$$\Phi = F \cdot 683 \cdot \eta \cdot W_{uv} \frac{\int_{vis} S(\lambda)V(\lambda)d\lambda}{\int_{vis} S(\lambda)\frac{\lambda}{253.7}d\lambda} \tag{6.38}$$

In the above two equations, F is a factor to correct for loss of radiation and emitted light at the ends of the lamp and absorption of light by the phosphor and glass bulb. F is quoted by Jerome (1953) to be 0.75 which is a representative value for most lamps. The factor 683 is the maximum luminous efficacy of radiation, i.e. the maximum luminous flux per watt of radiant power, which is equal to 683 lm/W occurring at a wavelength of 555 nm. $V(\lambda)$ is the CIE relative spectral luminous efficiency for photopic vision of the human eye (CIE 1983).

CIE publication No. 15.2 (CIE 1986) gives the relative spectral power distributions of 12 types of typical fluorescent lamps representing standard, broad-band and three-narrow-band fluorescent lamps. From these spectral power distributions, the integrals $\int_{vis} S(\lambda)V(\lambda)d\lambda$ and $\int_{vis} S(\lambda)\frac{\lambda}{253.7}d\lambda$ can be evaluated. Using literature values of the quantum efficiency (Jerome 1953), the light output due to UV radiation Φ can be calculated by equation (6.38).

There is a small light output due to the visible emission of the discharge directly. This is calculated by assuming that half of the visible emission can escape through the phosphor coating and that the only visible lines emitted are 404.6 nm, 435 8 nm and 546.1 nm so that the mean V(λ) is 0.334. Hence, the total luminous flux output of the fluorescent lamp is calculated by the following formula:

$$\Phi = 683 \cdot \left(0.75 \cdot \eta \cdot W_{uv} \frac{\int S(\lambda) V(\lambda) d\lambda}{\int S(\lambda) \frac{\lambda}{253.7} d\lambda} + 0.5 \cdot W_{vis} \cdot 0.334 \right) \tag{6.39}$$

In the above equation, the first term is the light output from the UV activated phosphors and the second term is the light output due to the visible lines in the discharge.

6.5 Solution scheme

The following steps describe the solution scheme developed in this work for solving the fluorescent lamp positive column model to obtain the light output and lamp power at different minimum lamp wall temperatures.

1. Calculate the ground state density N_0 by using equation (6.1) and Dalton's Law of partial pressure:

$$N_0 = N_{Hg} = \frac{p_{Hg}}{kT_g} \tag{6.40}$$

where p_{Hg} is the mercury vapour partial pressure (Pa) at the minimum lamp wall temperature, and T_g is the gas temperature inside the lamp in K.

The mercury vapour partial pressure (Pa) at the minimum lamp wall temperature is calculated using the following correlation equation (Antoine equation, quoted in Dean (1992)) derived from the data of mercury vapour pressure in Dean (1992):

$$p_{Hg} = 10^{\left(10.025 - \frac{3110.14}{MLWT+267.42}\right)} \tag{6.41}$$

where $MLWT$ is the minimum lamp wall temperature in °C.

The gas temperature inside the lamp is assumed to be given by the elevation ΔT above the minimum lamp wall temperature using the indirectly measured values of Kenty et al. (1951). ΔT is larger for a lower minimum lamp wall temperature (MLWT), e.g. ΔT=15.8°C when MLWT=60°C and ΔT=42.7°C when MLWT=17°C.

2. Calculate the electron density N_e using equation (5.7) in the following form and an initially guessed value (for iteration purpose) of electric field strength E:

$$N_e = \frac{I}{e\mu_e E\pi R^2} \tag{6.42}$$

where I is the electric current (A) in the positive column, e is the electronic charge (C), μ_e is the electron mobility (m^2 V^{-1}s^{-1}), R is the radius (m) of the discharge tube.

In the above equation, the positive column current I is assumed to be constant and for a typical 40-W (diameter 38 mm, length 1.2 m) fluorescent lamp, I=420 mA. The electron mobility μ_e depends on the density of the rare-gas. Following Lama et al. (1982), μ_e is calculated by an inverse dependence of the rare-gas density N_{rg} as follows:

$$\mu_e = \frac{1.24\times 10^{25}}{N_{rg}}\ \mathrm{m^2V^{-1}s^{-1}} \tag{6.43}$$

3. Calculate the electron temperature T_e by an iteration method. An initial value of T_e is guessed, then all the transition rates K_{jk} and K_{kj} are calculated using this guessed value of T_e and the equations (6 20) and (6.22).

4. Using the set of transition rates obtained from step 3 above, solve the set of simultaneous equations (6.3)-(6.8) for the number densities of the six excited mercury states N_1, N_2, N_3, N_4, N_5 and N_6. In the computer code LAMPPC, the Gauss elimination method is used for solving the set of simultaneous equations (6.3)-(6 8).

5. Calculate T_e using the ambipolar diffusion equation (6.9) and the densities of the mercury triplet states N_1, N_2 and N_3 obtained from step 4. This equation is rewritten by removing the common factor of the first three terms $exp(-4.97e/kT_e)$:

$$\left(K_{17}' N_1 + K_{27}' N_2 + K_{37}' N_3\right) \exp\left(-\frac{4.97e}{kT_e}\right) = \frac{D_a}{\Lambda^2} \tag{6.44}$$

where

$$K_{17}' = C_{17}\left(\frac{kT_e}{e}\right)^{\frac{3}{2}}\left(1+\frac{5.76e}{2kT_e}\right)\exp\left(-\frac{0.79e}{kT_e}\right) \tag{6.45}$$

$$K_{27}' = C_{27}\left(\frac{kT_e}{e}\right)^{\frac{3}{2}}\left(1+\frac{5.54e}{2kT_e}\right)\exp\left(-\frac{0.57e}{kT_e}\right) \tag{6.46}$$

$$K_{37}' = C_{37}\left(\frac{kT_e}{e}\right)^{\frac{3}{2}}\left(1+\frac{4.97e}{2kT_e}\right) \tag{6.47}$$

Rearrangement of equation (6.44) gives the following expression for T_e:

$$T_e = \frac{4.97e}{k\log\left(\dfrac{K'_{17}N_1 + K'_{27}N_2 + K'_{37}N_3}{D_a/\Lambda^2}\right)} \tag{6.48}$$

6. Compare the newly calculated value for T_e from equation (6.48) with the guessed value for T_e. If their difference is larger than a pre-set value, say 1 K, then the new T_e is used to calculate again all the transition rates K_{jk} and K_{kj} by equations (6 20) and (6.22). This new set of transition rates is used to calculate the densities of the mercury excited states as described in step 4. Using the new triplet state densities, a new value of T_e is calculated again as described in step 5. Repeat this process until T_e converges.

7. Use the converged value for T_e to calculate the transition rates according to equations (6.20) and (6 22). Using these transition rates, solve the set of equations (6.3)-(6.8) for the mercury excited state densities, N_1, N_2, N_3, N_4, N_5 and N_6.

8. Combining equations (5.1), (5.2) and (5.3), the energy balance equation can be re-written as:

$$E \cdot j = W_{254} + W_{185} + W_{vis} + W_{nv} + W_{ion} + W_{el} \tag{6.49}$$

After obtaining T_e, N_e, N_0, N_1, N_2, N_3, N_4, N_5 and N_6, the above energy balance equation (6.49) is used to calculate the electric field strength E again. This value of E is then compared with the initially assumed electric field strength (in step 2). If the difference between the newly calculated and the initial assumed value of electric field strength is greater than a preset value, say 0.1 V/m, then the calculations are repeated from step 2 until convergence.

9. On convergence of both E and T_e, the set of equations are solved and all the unknowns E, T_e, N_e, N_0, N_1, N_2, N_3, N_4, N_5 and N_6 are found. Then the power of UV lines 253.7 nm and 185 nm are calculated by equations (6.10) and (6.11).

The visible and non-visible radiation output power from the 7^3S_1 and $6^3D_{1,2,3}$ states are estimated by equations (6.12) and (6.13). The ionisation loss and elastic collision loss are then estimated by equations (6.15) and (6.18), respectively. The sum of these power terms gives the total lamp power.

10. The light output is then calculated by equation (6.39) with values of W_{uv} and W_{vis} from equations (6.36) and (6.12) respectively. The illuminance on room surfaces can then be calculated by multiplying the light output with the ratio of short-wave radiation falling on the surface to that emitted from the lamps.

A set of computer codes is written in FORTRAN, and is named LAMPPC, for the solution scheme described above. LAMPPC is included in the program LITEAC2 as a subroutine which gets an input of minimum lamp wall temperature and returns to the main program the following variables: total lamp power, power of visible radiation output from the lamp and total light output of the lamps. The program listing of LAMPPC is included in LITEAC2 in Appendix F.

6.6 Summary

Due to the complexity of the equations of the fluorescent lamp positive column discharge described in Chapter 5, approximations have been made to simplify the equations so that a solution giving the light output and lamp power as functions of minimum lamp wall temperature can be obtained. The approximations for simplifying the continuity equations are mainly to neglect those transitions which are considered small. Approximations are also used in the calculation of the energy terms in the energy balance equations. A method modified from Hoyaux and Sucov (1969) is used in the derivation of transition rate coefficients for use in the continuity equations. For the effective life times of the mercury excited states, the Holstein theory (Holstein 1951) is adopted in this work.

Using the minimum lamp wall temperature (calculated in the room heat and light transfer model) as an input to the fluorescent lamp positive column model, an iteration method is adopted for the calculation of the electron temperature and the densities of electron and mercury states. The different components of the energy loss from the fluorescent lamp are then calculated. The light output from the lamps are then calculated by knowing the spectral emission of the phosphors used in the fluorescent lamp. The lamp power can also be calculated by multiplying the electric field strength with the current in the positive column. The power loss due to ionisation and elastic collisions of the electrons with the rare-gas atoms can also be calculated and these are treated as heat dissipated from the fluorescent lamp. This positive column model, which is named LAMPPC, will be integrated into the room heat transfer model for the calculation of the conversion of electrical energy into light, radiation and heat.

Chapter Seven

Validation of the Positive Column Model with Published Experimental Results

7.1 Introduction

The fluorescent lamp positive column model, LAMPPC, elaborated in Chapters 5 and 6, can be validated on its own using the results of experimental measurements of mercury–rare-gas discharge reported in the literature. Comparison of the values for various parameters predicted by LAMPPC with corresponding experimental data quoted in the literature is essential before LAMPPC could be used with confidence for the modelling of lighting / HVAC interaction. There are a number of fluorescent lamp positive column parameters which have been measured experimentally. The parameters which will be used here for the comparison are: electron temperature, electric field strength, electron and mercury state densities, radiation output, volume losses (elastic collision loss) and wall losses (ionisation loss).

A review of experimental measurements of mercury–rare-gas discharge has been given in Chapter 3. In the next section a summary of the experimental results will be given. Results calculated using LAMPPC will then be compared with the corresponding experimental results.

7.2 Summary of experimental results in the literature

In order to facilitate the comparison of experimental results with calculated values, published results of some important experimental measurements of low-pressure mercury–rare-gas discharge are tabulated in Tables 7.1-7.3. Table 7.1 gives the results of measurements of electric field strength, electron temperature and axial electron density. The experimental data listed in this table are taken from Kenty et al. (1951), Verweij (1961), and Denneman et al. (1980). There is reasonably good agreement between the sets of measured data from different work. These data are plotted on Figure 7.1-7.3 where they are compared with values calculated using LAMPPC.

Table 7.2 gives the results of measurements of the energy balance of low-pressure mercury–rare-gas discharge, i.e. the power dissipation by radiation, power dissipation inside the positive column (volume losses) and power dissipation at the lamp wall (wall losses) at different lamp wall temperatures. The volume losses are mainly due to elastic collision of the rare-gas atoms by electrons; therefore, the values for elastic collision loss calculated by LAMPPC will be compared with the experimental data of volume losses reported by Koedam et al. (1963). The wall losses are mainly due to energy released at the lamp wall when mercury ions recombine with electrons at the lamp wall; therefore, the values for ionisation power calculated by LAMPPC will be compared with the experimental data of wall losses reported by Koedam et al. (1963). As there are not many direct measurements of the radiation output, volume losses and wall losses reported in the literature, the data of Koedam et al. (1963) only are listed in this table with the total lamp power output data measured by Verweij (1961) listed in the same table for reference. The two sets of total power output measurements are in good agreement with each other, differing by less than 10% for lamp wall temperatures of at least up to 60°C.

Table 7.3 gives the results of measurement of the axial densities of mercury excited states at different lamp wall temperatures. The experimental data listed in this table are from Koedam and Kruithof (1962), Van de Weijer and Cremers (1987), and Bigio (1988). It can be seen that some large discrepancies occur in these sets of experimental data.

Despite the discrepancies occurring between different measurements, these experimental results provide good data for the validation of LAMPPC as a stand alone model. The experimental results shown in Tables 7.1-7.3 will be compared with the calculated results of LAMPPC. The comparison is discussed in the following section.

7.3 Comparison of results calculated using LAMPPC with published experimental results

7.3.1 Electron temperature

Figure 7.1 shows the variation of electron temperature with minimum lamp wall temperature as predicted using LAMPPC. Also plotted in this figure are the two sets of measured data as obtained by Kenty et al. (1951) and by Verweij (1961). The agreement between the LAMPPC model prediction and both sets of measured data is seen to be remarkably good.

7.3.2 Electric field strength

Figure 7.2 shows electric field strength plotted against minimum lamp wall temperature as predicted by LAMPPC and as measured by Verweij (1961). Agreement between the LAMPPC prediction and the measured values is very good, with differences remaining within 5%. Moreover, LAMPPC predicts the general trend in change of electric field strength with minimum lamp wall temperature, and the order of magnitude of the predicted electric field strength is correct. Shown also in this figure is a curve of the calculated results of a recent model by Dakin (1986). Dakin gave only results for the range of lamp wall temperatures between 20°C and 60°C. Comparing the agreement LAMPPC-calculated results and Verweij's experimental data, the LAMPPC model is better than and is valid over a wider range than Dakin's model.

7.3.3 Electron density

Figure 7.3 shows the average electron density plotted against minimum lamp wall temperature. The figure shows the results predicted by LAMPPC, and also two sets of measured data, one by Kenty et al. (1951) and the other by Verweij (1961); also shown are the predictions by the model of Dakin (1986). The measured data plotted in the figure have been converted to average density by assuming a parabolic radial distribution of electron density, i.e. $\text{average density} = \frac{\text{axial density}}{2.4}$ (Dakin 1986). The figure shows that there is good agreement between the results predicted by LAMPPC and the experimental data, and also that the results predicted by LAMPPC offer a closer fit to both sets of experimental data than those of Dakin (1986).

7.3.4 Mercury resonance state density

LAMPPC calculates the densities of all mercury excited states considered in the model. The density of the mercury resonance state 6^3P_1 is used here for a comparison of LAMPPC-calculated values with published data of mercury state density measurement. Figure 7.4 compares the calculated mercury resonance state density with three sets of measured data: Koedam and Kruithof (1962), Van de Weijer and Cremers (1985) and Bigio (1988); also shown are the model-based predictions of Dakin (1986). All three sets of published data were originally given as the on-axis densities of the resonance state, but the points plotted in Figure 7.4 are the average densities (assuming a parabolic radial distribution of the resonance state). The figure shows that the LAMPPC-calculated resonance state density agrees well with the three sets of measured data for lamp wall temperatures lower than 40°C with discrepancies being less than 17%. There is, however, a higher discrepancy between the calculated resonance state density and the experimental data for lamp wall temperatures above

40°C. Results predicted by LAMPPC agree well with those of Dakin (1986) for lamp wall temperatures up to 50°C after which some divergence occurs.

7.3.5 Radiation output power

As the aim of using LAMPPC is to simulate the effect of ambient temperature on light output, a good agreement between the predicted radiation output and experimental data is important, perhaps more important than the fit of mercury state densities. In Figure 7.5, the radiation output power predicted by LAMPPC is compared with both the measured values of Koedam et al. (1963) and the model predictions of Dakin (1986). The figure shows that the predictions of LAMPPC agree with the experimental data reasonably well; both the shape and the magnitude of the curve are similar to those of the experimental data. However, LAMPPC predictions are generally higher than the measured values for all lamp wall temperatures. For lamp wall temperatures between 30° and 80°C, LAMPPC predictions are 10-15% higher than the measured values. In view of the complexity of the low pressure mercury discharge, it can be considered that LAMPPC simulates the radiation output to a reasonable degree of accuracy.

7.3.6 Volume losses

"Volume losses" is the term used in Koedam et al. (1963) to mean the power losses which come mainly from the elastic collisions within the positive column. Figure 7.6 compares the elastic collision loss as predicted by LAMPPC with the experimental data of Koedam et al. (1963). The figure shows that the calculated curve fits the experimental data closely except perhaps at low lamp wall temperatures.

7.3.7 Wall losses

"Wall losses" is again the term used in Koedam et al. (1963) to mean the power losses at the walls of the positive column discharge. Wall losses are due mainly to the energy release when mercury ions recombine with electrons at the lamp wall. Figure 7.7 compares the calculated ionisation power using LAMPPC with the experimental data of wall losses as measured by Koedam et al. (1963). The figure shows that the calculated curve fits very closely to the experimental data. The calculated curve also predicts correctly that minimum wall losses occur within the range of minimum lamp wall temperature of 40° to 60°C.

7.4 Summary

From Figures 7.1-7.7, it can be seen that there is, in general, very good agreement between values predicted by the fluorescent lamp positive column model LAMPPC and published experimental results. It can be concluded that LAMPPC is able to simulate well the fluorescent lamp positive column, and can be used to calculate the conversion of electrical energy into light, radiation and heat to an acceptable degree of accuracy. Therefore, LAMPPC will be integrated into the room heat and light transfer model described in Chapter 4 so as to form a model, named LITEAC2, for the simulation of lighting/HVAC interaction. Such a model will then be able to simulate the effects of air-conditioning on light output in greater detail than is currently possible with existing models. Validation of the combined model LITEAC2 is discussed in the next chapter.

Table 7.1

Published data of measured electric field strength, electron temperature and axial electron density in low-pressure mercury–rare-gas discharge by several authors.

Author	Lamp wall temperature (°C)	Electric field strength ($V\ m^{-1}$)	Electron temperature (K)	Axial electron density ($\times 10^{17} m^{-3}$)
Kenty, Easley and Barnes (1951)	17		15000	5.44
Internal diameter: 36 mm;	30		13300	4.79
Filling gas: A at 465 Pa;	40		11300	5.00
Current: 420 mA	50		10100	5.77
	60		9800	5.77
Verweij (1961)	11	79	16300	6.20
Internal diameter: 36 mm;	20	83	15200	5.50
Filling gas: A at 400 Pa;	30	86	13700	5.00
Current. 400 mA	42	81	11400	4.90
	50	73	10200	5.20
	60	65	9300	6.20
	70	60	8600	7.70
	80	58	8100	10.50
Denneman et al. (1980)	42	81±1	12900±500	5±5%
Internal diameter: 36 mm;				
Filling gas A at 400 Pa;				
Current: 400 mA				

Table 7.2

Published data of measured radiation power output, volume losses, wall losses, total power output and power input of low-pressure mercury–rare-gas discharge at different lamp wall temperatures by several authors.

Author	Lamp wall temperature (°C)	Radiation output (W m^{-1})	Volume losses (W m^{-1})	Wall losses (W m^{-1})	Power output (W m^{-1})	Power input (W m^{-1})
Verweij (1961)	11				31.6	
Internal diameter. 36mm;	20				33.2	
	30				34.2	
Filling gas: A at 400 Pa,	42				32.5	
Current· 400 mA	50				29 2	
	60				25 8	
	70				23 8	
	80				23 0	
Koedam, Kruithof and Riemens (1963)	10	8.1	19 5	2.9	30 5	31 4
	20	15 9	14.5	2 3	32.7	33 2
Internal diameter. 36mm;	30	21.9	9.8	1.9	34 1	34.2
Filling gas A at 400 Pa;	42	22.3	5.9	1.5	29.7	32.5
	50	20 0	4.7	1.5	26 2	29.5
Current· 400mA	60	17.2	4 4	1.5	23 1	25.8
	70	14.5	4 5	1.7	20.7	23 8
	80	11.3	5 5	2.2	19.0	23.0

Table 7.3

Published data of measured on axis mercury state densities in low-pressure mercury–rare-gas discharge positive column at different lamp wall temperatures by several authors.

Author	Lamp wall temperature (°C)	Axial 6^3P_0 density ($\times10^{17}$ m^{-3})	Axial 6^3P_1 density ($\times10^{17}$ m^{-3})	Axial 6^3P_2 density ($\times10^{17}$ m^{-3})
Koedam and Kruithof (1962) Internal diameter: 36 mm; Filling gas: A at 372 Pa; Current: 400mA,	5	0.2	-	0.6
	10	0.8	-	1.5
	15	1.3	0.1	2.4
	20	1.8	0.5	3.2
	25	2.4	0.8	4.3
	30	3.0	1.4	5.3
	35	3.7	2.3	6.3
	40	4.3	3.3	6.9
	42	4.5	3.8	-
	45	5.0	-	7.5
	50	-	5.9	7.8
	55	5.9	7.8	-
	60	6.3	10.8	8.1
	67	6.5	12.5	8.1
	70	-	15.5	-
van de Weijer and Cremers (1987) Internal diameter: 36 mm; Filling gas: A at 400 Pa; Current: 400 mA.	30	3.6	1.8	6.4
	40	4.7	3.9	7.9
	50	5.6	6.9	8.8
	60	6.3	9.6	9.5
	70	6.9	11.7	9.8
	80	7.3	13.6	10.2
Bigio (1988) Internal diameter: 34 mm; Filling gas: A at 374 Pa, Current: 400mA SLA method	20	1.72	0.42	3.88
	30	2.89	1.71	6.94
	40	3.87	3.83	9.30
Same as above Hook method	20	1.80±0.13	0.35±0.25	3.14±0.12
	30	3.30±0.35	1.90±0.15	5.9±0.3
	40	4.80±0.25	4.4±0.1	8.5±0.3

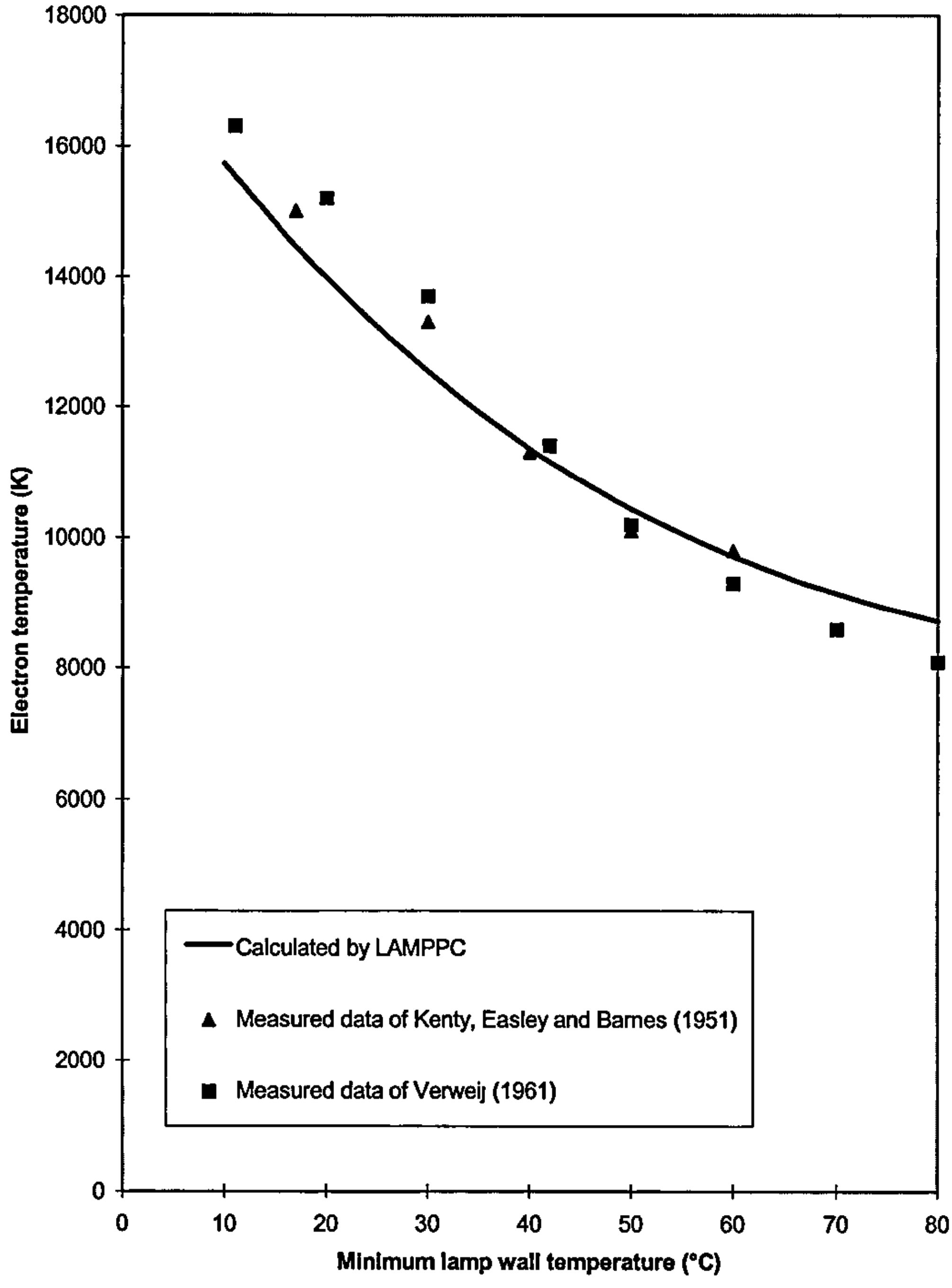

Figure 7.1

Electron temperature vs minimum lamp wall temperature.

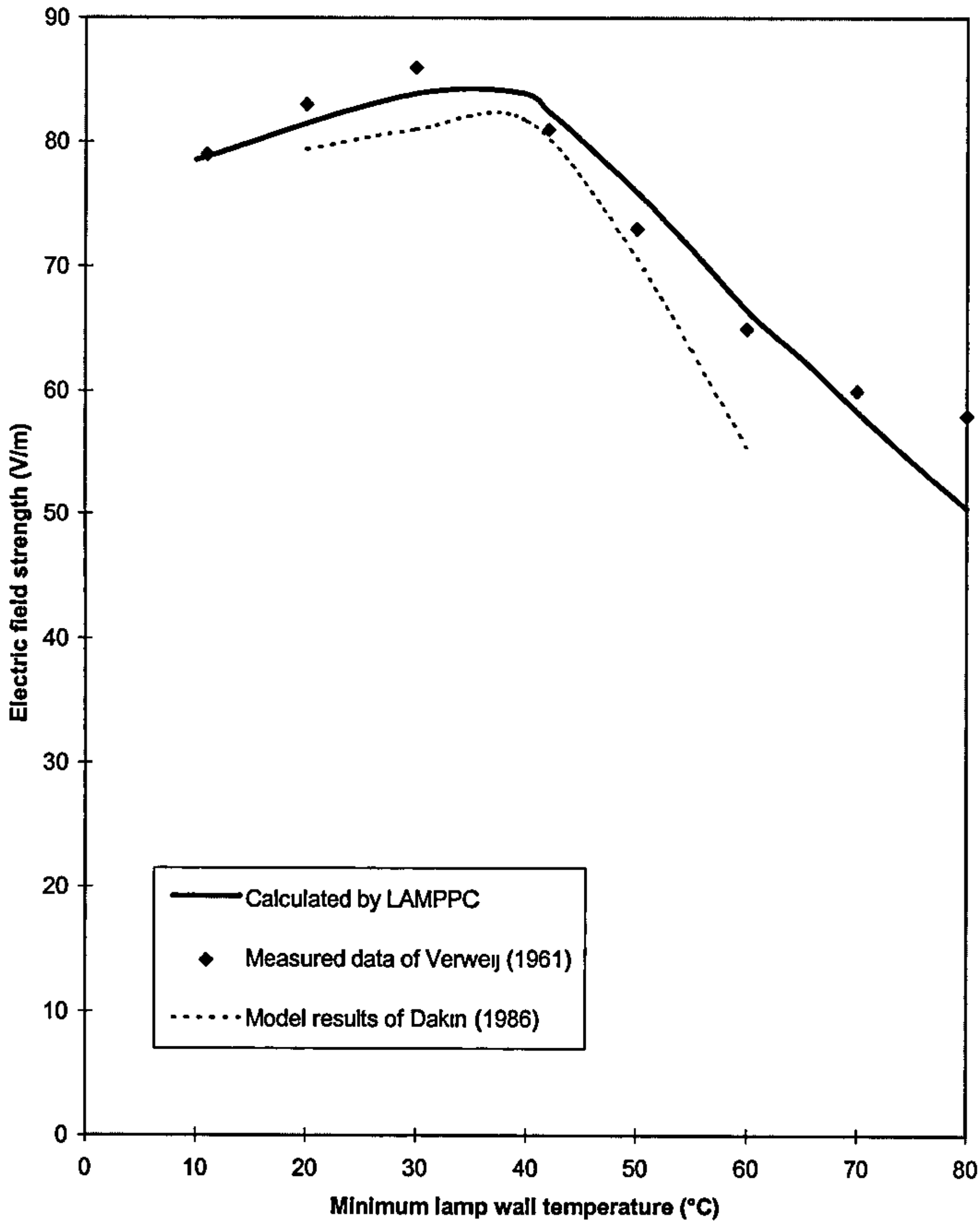

Figure 7.2

Electric field strength vs minimum lamp wall temperature.

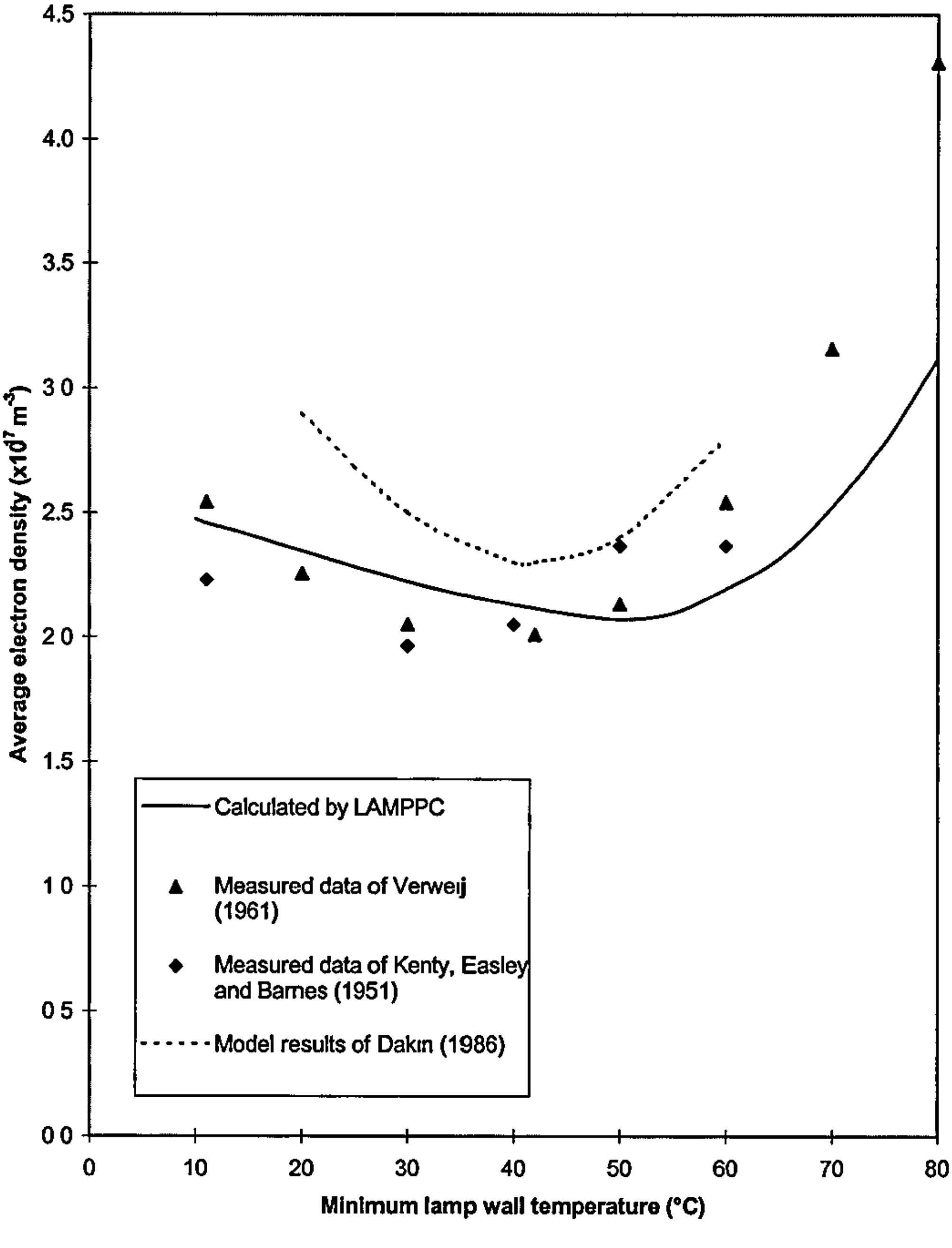

Figure 7.3

Electron density (average) vs minimum lamp wall temperature.

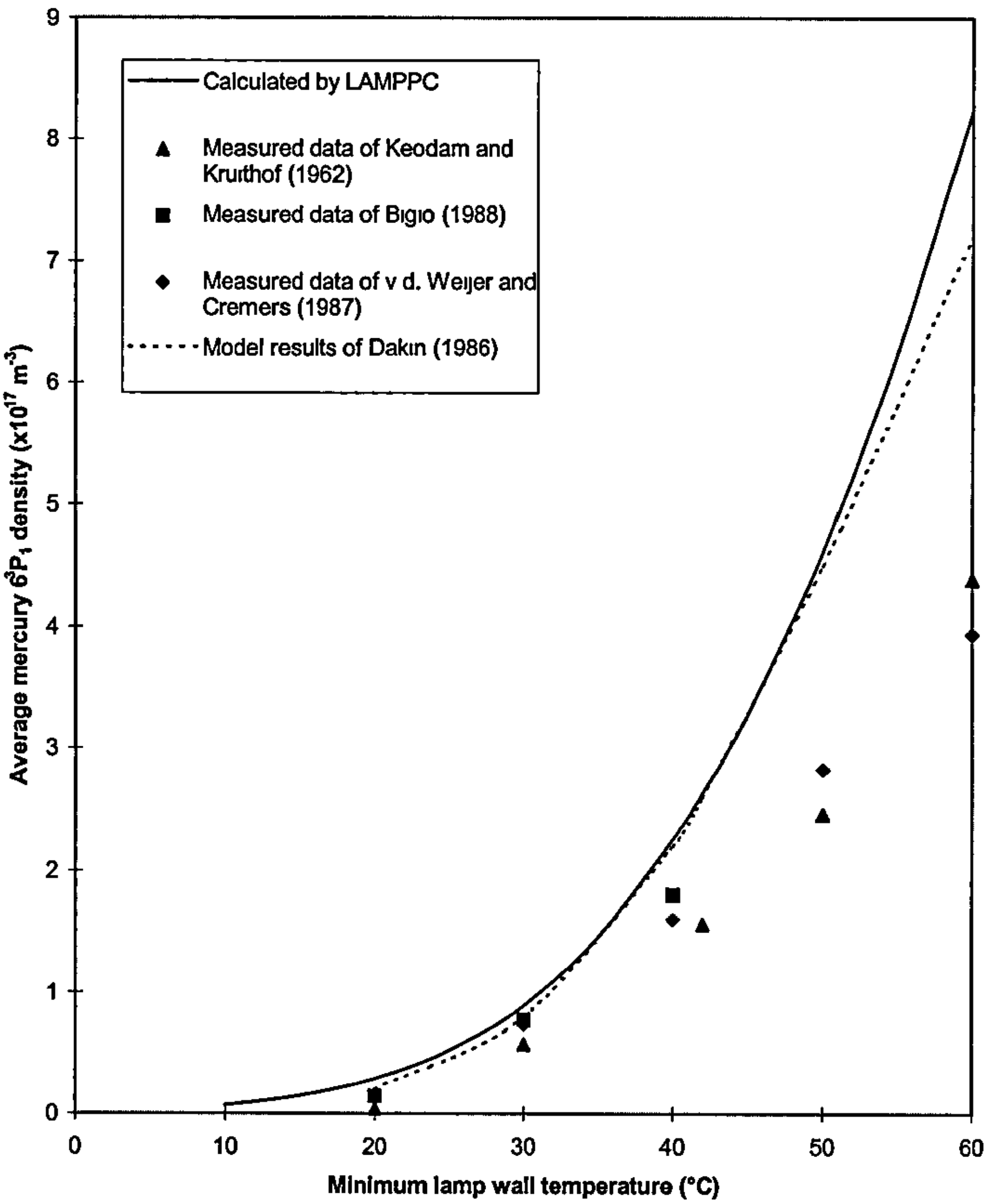

Figure 7.4

Mercury 6^3P_1 density (average) vs minimum lamp wall temperature.

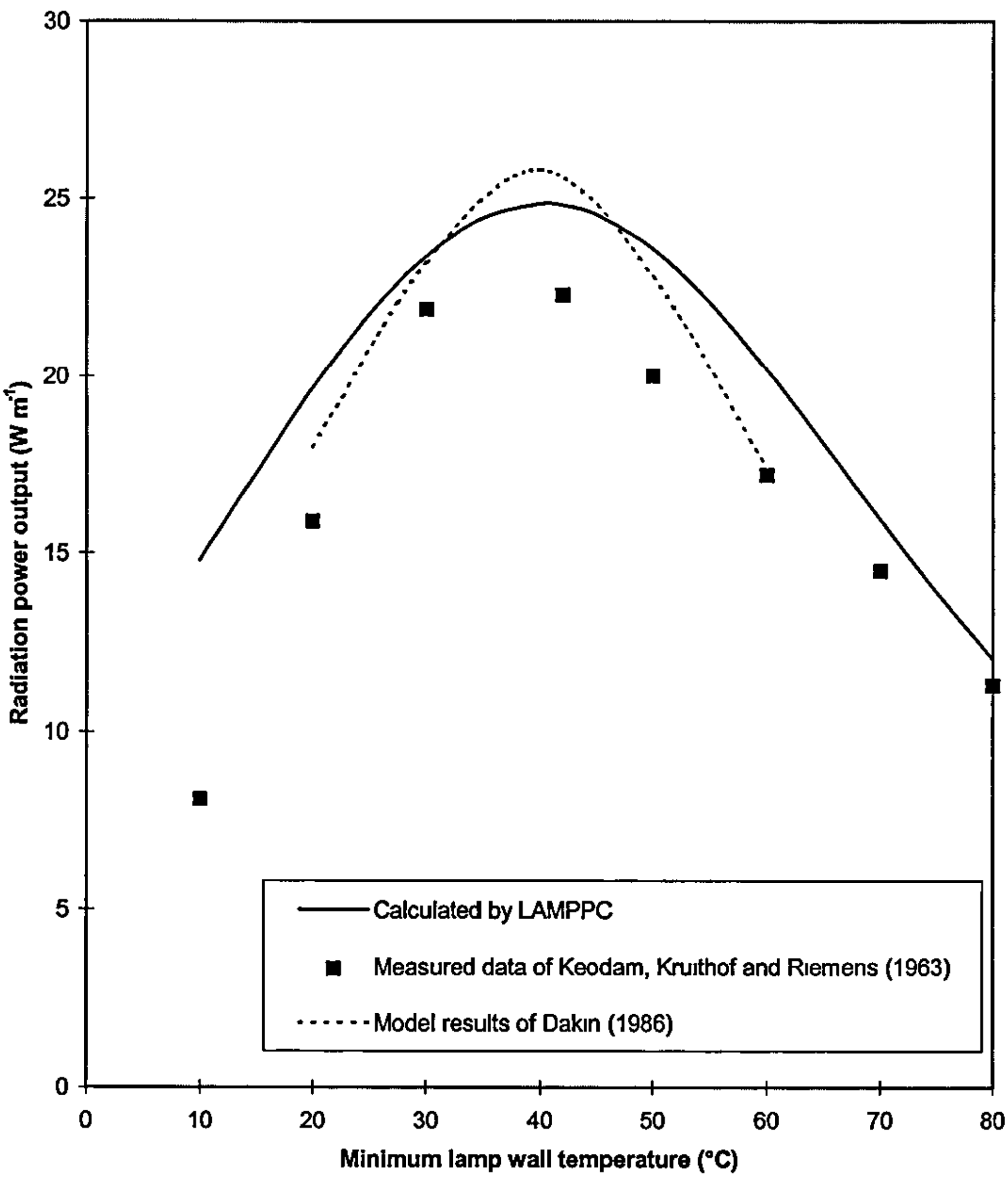

Figure 7.5

Total radiation power output vs minimum lamp wall temperature.

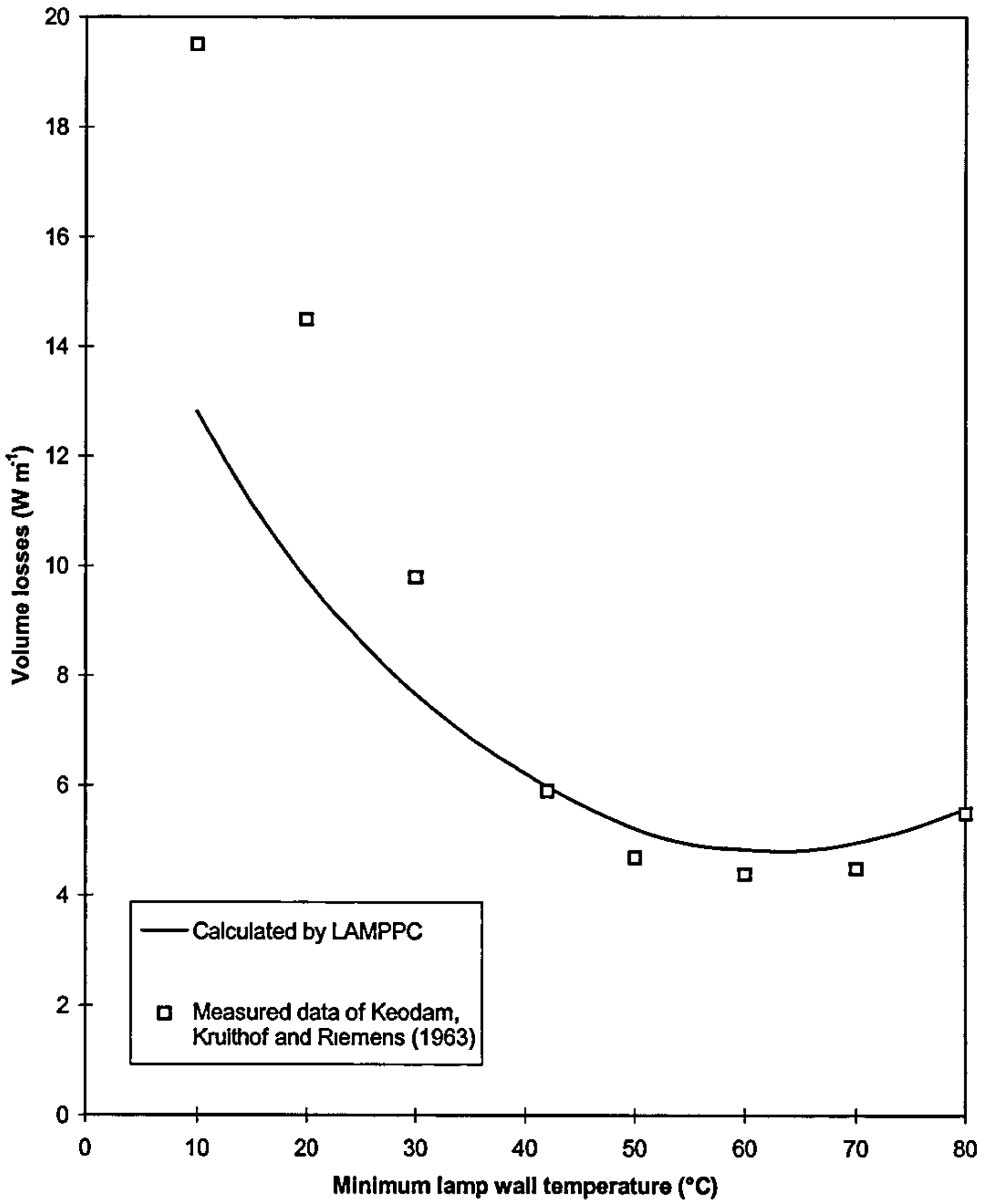

Figure 7.6

Volume losses (elastic collision loss) vs minimum lamp wall temperature.

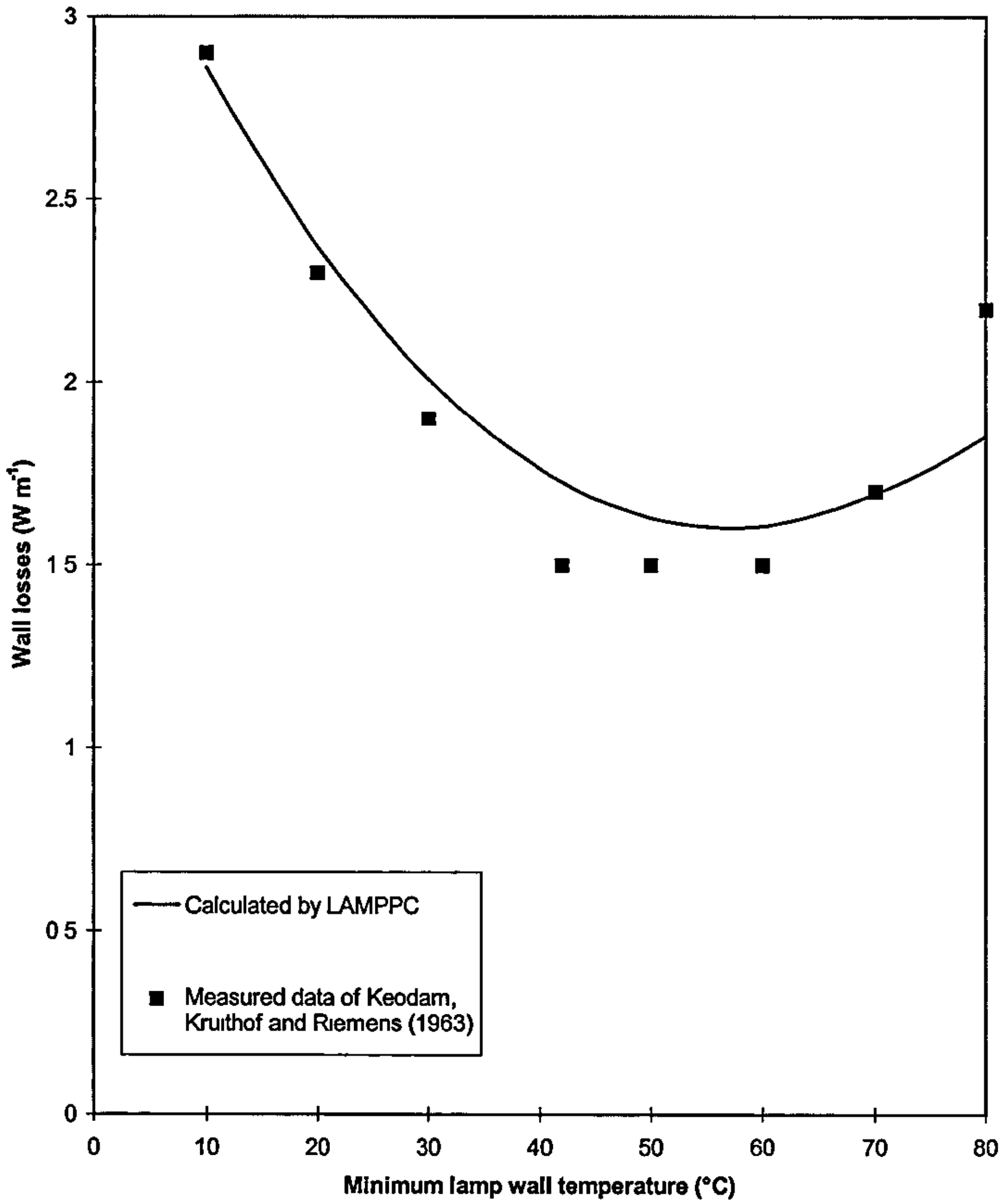

Figure 7.7

Wall losses (ionisation power) vs minimum lamp wall temperature.

Chapter Eight

Validation of the Lighting/HVAC Interaction Model with Published Experimental Results

8.1 Introduction

In Chapter 2, a brief summary of the experimental works on lighting thermal performance and lighting/HVAC interaction has been given. The NIST test cell reviewed briefly in Chapter 2 gave valuable data on the study of lighting/HVAC interaction. These data include steady-state temperatures, lighting energy distribution fractions, and transient cooling load profiles, for various room temperatures, airflow rates and airflow configurations. In spite of the fact that relatively little measured data is available on lighting performance, such as lighting power and light output, in the NIST reports (Treado and Bean 1988, 1992), the published experimental data on the NIST full-scale test cell are most suitable for the validation of the models LITEAC1 and LITEAC2 developed in this study (Chapters 4-6). The limited amount of detailed measured light output data reported in the NIST reports permits only partial validation of the model LITEAC2 on the prediction of light output and illuminance under different ambient temperatures. The validation using a laboratory constructed test cell (to be described in Chapter 9) will supplement this by making comparison between predicted illuminance and measured values. Before the validation of the models LITEAC1 and LITEAC2 is discussed, some more details of the NIST test room are given first in the following section.

8.2 The NIST test cell

Treado and Bean (1988, 1990, 1992) reported on full-scale measurements of the interaction between lighting and HVAC carried out at the Building and Fire Research Laboratory of the National Institute of Standards and Technology (NIST) in the U.S.A. The NIST test facility was constructed within a large environmental chamber and was divided into two sections: a large insulated shell enclosing the test room area, and a smaller attached control room for housing instrumentation. It was extensively instrumented to allow the measurement of cooling load, lighting power, airflow rate, surface and air temperatures, heat flow rate and lighting level.

The test room was of dimensions 4.27 m in length and 3.66 m in width, with a conditioned room space height of 2.44 m and a plenum height of 0.76 m. The test room floor slab was elevated to accommodate a lower plenum beneath the floor. All other room surfaces were adjacent to temperature-controlled guard air spaces. Duplicate lighting and HVAC systems were installed in both the test room plenum and the lower plenum.

Identical lighting systems were installed in the room plenum and the lower plenum. During the initial stage of measurements, each plenum had four recessed luminaires, 0.6 m wide by 1.2 m long. Each of the luminaires contained four 40 W fluorescent lamps and a parabolic diffuser. During the later stages of measurements, the type and number of luminaires were varied as test parameters, namely, acrylic lens (prismatic diffusers), 2 lamp luminaires and 34 W lamps were tested.

The HVAC system consisted of three air handling units which serviced seven individually controlled zones, including the test room and surrounding spaces. Chilled water for cooling were drawn from the environmental chamber supplies. Each air handling unit consisted of a fan and chilled water coil, with separate electric duct heaters for each supply duct. Independent temperature control was allowed for each of the seven supply systems. One air handling system was dedicated to the test room only. The second air handling unit serviced the east, south, west and upper guard air spaces. The third air handling unit serviced the lower plenum and north guard air space.

Measurements of test room temperatures were made using an array of 64 thermocouples, in a 4 by 4 by 4 grid. The upper 16 thermocouples were in the plenum while the 48 thermocouples below the suspended ceiling measured the room temperature. Surface temperatures were measured throughout the test room and inside the luminaires by thermocouples affixed on wall surfaces, at the centre and around the perimeter. Heat flux transducers were mounted on each room surface for the measurement of heat flow through the walls.

Thermopiles were used to control the test room boundary conditions. To maintain a boundary condition such that the test room is surrounding by similar spaces, the temperature difference across each wall was sensed by thermopiles with the control system keeping the thermopile readings equal to zero; this was done by varying the power supplied to the appropriate electric duct heater which was used to control the room and air space temperatures. In this way, the boundary condition of no net heat flow through taking place the walls was maintained. Thermopiles were also used to maintain equal surface temperatures at the top of the ceiling and the top of the floor, and also equal temperatures at the bottom of the floor and the bottom of the ceiling.

Light (illuminance) levels in the test room were measured continuously at the centre of each surface using colour corrected silicon photovoltaic cells. Periodically, detailed light distribution measurements were also taken using an array of photocells.

Full details of the NIST test room facilities with detailed drawings are given in Treado and Bean (1988). Several of these drawings are reproduced in Figures 8.1-8.3 to help the reader to understand the experimental setup.

Both steady state and transient tests were run in the test cell. Steady state tests involved establishing a test configuration and allowing conditions to stabilize; then, measurements of temperatures, lighting power and lighting levels were taken. To make a transient test, the lighting system was switched either suddenly on or suddenly off and then the response of the cooling load was measured.

There were two stages of measurements reported by Treado and Bean (1988, 1992). The first stage tests were described in an interim report by Treado and Bean (1988). During this stage of measurements, the primary parameters varied were airflow configuration, airflow rate and room air temperature, and the tests were aimed at evaluating the effects of these parameters on the transient and steady state performance of the lighting and HVAC systems. Tests were executed for 27 basic configurations consisting of combinations of three variations of each of the primary parameters as follows:

Airflow return:
- ceiling grille
- luminaire side slots
- lamp compartment

Airflow rate:
- 0.0566 $m^3 s^{-1}$ (120 cfm);
  [i.e. 0.0142 $m^3 s^{-1}$ (30 cfm) per luminaire]
- 0.0755 $m^3 s^{-1}$ (160 cfm);
  [i e. 0.0189 $m^3 s^{-1}$ (40 cfm) per luminaire]
- 0.0944 $m^3 s^{-1}$ (200 cfm);
  [i.e. 0.0236 $m^3 s^{-1}$ (50 cfm) per luminaire]

Room air temperature:
- 21.1°C (70 °F)
- 23.9°C (75 °F)
- 26.7°C (80 °F)

The 27 combinations of basic configurations were tested with only one type of luminaire; this was a fluorescent luminaire with four 40 W lamps, standard choke ballasts and parabolic reflectors. Return air was directed either through the lamp compartment, through slots in the sides of the luminaire, or through the ceiling grille return. The first stage tests were carried out with constant supply air volume and with carpet on the floor.

In the second stage of measurements (Treado and Bean 1992), in addition to the three test parameters described above, the luminaire type (i.e. the number of lamps in each luminaire and the type of diffusers used), the number of luminaires and the lamp wattage were also test parameters which were varied. In addition to the four-40W-lamp parabolic luminaire used in the first stage measurements, three other different luminaire types were used, namely, four-40W-lamp with acrylic lens, two-40W-lamp with acrylic lens, and two-34W-lamp with acrylic lens. The number of luminaires was also varied, with two of the configurations consisting of three luminaires only for the 2-lamp cases (40 W or 34 W). These combinations were included to enable comparison of identical luminaire configurations with lamps of different wattage, and identical luminaire types with different numbers of luminaires. The combinations of different luminaire types were tested with or without carpet and with or without furnishings. Airflow rate was also varied through five ranges in the second stage of measurements instead of only three variations used in the first stage tests.

8.3 Validation of LITEAC1 and LITEAC2

In modelling the NIST test room using LITEAC1 and LITEAC2, 23 nodes are used. These consist of 5 luminaire nodes, 9 plenum nodes and 9 room nodes. This division is similar to that used in the NIST numerical model (Treado and Bean 1988), except that 2 nodes are added: the carpet surface and the base of the luminaire diffuser. In addition, 4 NIST nodes are eliminated: floor middle and ceiling middle, which are actually the same node and considered unnecessary in the current validation exercise; ceiling top and floor surface, which are actually the same node and are combined into a single node; ceiling bottom and floor bottom, which are also the same node and are also combined into a single node in this validation exercise. Defining nodes in a similar way as in the NIST numerical model would ensure that the physical data of the nodes stated in the NIST reports (Treado and Bean 1988, 1992) can be used as the input data in the validation runs conducted in this study.

Data concerning the dimensions, the heat capacity, the emissivity and the reflectivity of nodes were obtained either from the NIST reports (Treado and Bean 1988, 1992) or were calculated from data in the ASHRAE Handbook (ASHRAE 1993) using information given in the NIST reports. Radiation form factors were calculated using the view factor programs 'VF' and 'FACTS' included in 'LIGHTS' (Sowell 1989). Convective heat transfer coefficients were determined from correlations given in Holman (1992). Conductance values of the materials used in the construction of the NIST test cell were obtained from ASHRAE Handbook (ASHRAE 1993). The set of nodal data used in the validation are given in Appendix G.

Validation runs were performed using both the simulation programs LITEAC1 and LITEAC2. In the case of LITEAC1, since the fluorescent lamp positive column model was not included in it, changes in light output and lighting power were accounted for by empirical curves, with lamp data concerning the relative power and relative light output being obtained from Siminovitch et al. (1984). Lamp power balances and luminous efficacies were obtained from Dorleijn and Jack (1985). The transmittance values of the prismatic diffusers used in the NIST test cell are not available in the published reports. According to IESNA (1993), the transmittance of a clear prismatic lens has a range between 0.7 and 0.92, and it is reasonable in the simulations here to assume the transmittance to be 0.8.

Steady-state and transient test results published in the NIST reports were compared with results predicted from simulations using LITEAC1 and LITEAC2. For the steady-state runs, calculations were performed with lights turned on at the start until temperatures and illuminance levels at all nodes attained constant values. Details of the comparison of steady-state test results are discussed in section 8.4.

For transient tests, comparison is made for profiles of node temperatures and cooling load between the NIST experimental results and the simulation results from LITEAC1 and LITEAC2. Results of two kinds of simulation tests, namely, the 'lights on test' and 'lights on/off cycles test', will be reported in section 8.5.

8.4 Steady-state comparisons

Steady-state test results reported in the two NIST reports (Treado and Bean 1988, 1992) consisted mainly of measurement of the parameters needed for the evaluation of lighting system performance. These test data included minimum lamp wall temperature, elevation of minimum lamp wall temperature above room temperature, relative lighting power, relative light output and relative lighting efficacy. These data were published in Treado and Bean (1988, 1992) in the form of graphs. Numerical values were directly read from the graphs for this comparison exercise.

For the minimum lamp wall temperature, the 'average' value was given for each configuration tested. According to Treado and Bean (1988), the 'average' minimum lamp wall temperature for a certain test was calculated by simply taking the arithmetic average of the lamp temperature minima for each luminaire. The elevation of minimum lamp wall temperature above room temperature reported by Treado and Bean (1992) was the difference between the measured minimum lamp wall temperature and the measured room air temperature. The measured room air temperature could be different from the controlled 'set-point' room air temperature which was used as a test parameter.

In Treado and Bean (1992), results on the relative performance of the lighting system were given as plots of the relative lighting power, relative light output and relative lighting efficacy against the minimum lamp wall temperature for each luminaire type and air return configuration. The reference values for deriving the relative lighting performance parameters were the corresponding individual maximum values in each combination of luminaire type and air return configuration. For all the tests reported, absolute values of lighting power, light output and efficacy were not published and these values cannot be deduced from the published relative values. The only test configurations for which measured values of lighting power are obtainable from Treado and Bean (1988) are those with 4 × 4 lamp parabolic diffuser and lamp compartment return. No data on measured light output and lighting power are available for other configurations.

Comparison is therefore made between simulation results from LITEAC1 and LITEAC2 and the NIST measured steady-state results (reported in Treado and Bean 1992) for the minimum lamp wall temperature and its elevation above room temperature for all 40 configurations (to be described below). Comparison between simulation results and measured results for the relative light output, relative lighting power and relative lighting efficacy can only be made for the 9 (out of the 40) configurations with the 4 × 4 lamp parabolic diffuser and lamp compartment return. The 40 configurations consist of combinations of the following four varied parameters:

Luminaire types: - 4 × 4 lamp 40 W, parabolic diffuser
4 × 4 lamp 40 W, prismatic diffuser (acrylic lens)
4 × 2 lamp 40 W, prismatic diffuser (acrylic lens)

Airflow return: - ceiling grille

- lamp compartment

Airflow rate: - 0.0944 $m^3 s^{-1}$ (200 cfm);

[i.e. 0.0236 $m^3 s^{-1}$ (50 cfm) per luminaire]

- 0.0755 $m^3 s^{-1}$ (160 cfm);

[i.e. 0.0189 $m^3 s^{-1}$ (40 cfm) per luminaire]

- 0.0566 $m^3 s^{-1}$ (120 cfm);

[i.e. 0.0142 $m^3 s^{-1}$ (30 cfm) per luminaire]

- 0.0378 $m^3 s^{-1}$ (80 cfm);

[i.e. 0.00944 $m^3 s^{-1}$ (20 cfm) per luminaire]

Room air temperature: - 26.7°C (80 °F)

- 23.9°C (75 °F)

- 21.1°C (70 °F)

Tables 8.1-8.3 show the comparison between predicted results and experimental results for all the 40 different configurations. Configurations with the same luminaire type are grouped into one table for convenience of presentation of results. For ease of reference to the NIST configurations in the presentation of results here, each NIST configuration is given a number consisting of 5 digits: $d_1d_2d_3d_4d_5$. The digit d_1 gives the number of luminaires in the test room; d_2 gives the number of lamps in each luminaire; d_3 is either 1 or 2 and represents the type of diffuser used in the luminaire (1 = prismatic diffuser, 2 = parabolic diffuser); d_4d_5 is a 2-digit serial number representing different configurations within the group with the same luminaire type. For example, the configuration number 44101 represents the first configuration in the series with 4 luminaires in the test room, 4 lamps in each luminaire and prismatic diffuser. The 40 configurations considered in this validation exercise are all listed in Tables 8.1-8.3. Treado and Bean (1988, 1992) did not use any numbering system in their reports so that the configuration numbers used here cannot be referred directly to the NIST reports.

Table 8.1(a) shows the comparison between results of minimum lamp wall temperature and its elevation above room temperature for the 12 configurations with the luminaire type 4 × 4-lamp 40 W parabolic reflector. The percentage deviations of the calculated value from the measured value are also given in this table. It can be seen from the table that there are good matches between predicted and measured minimum lamp wall temperatures (MLWT). Comparing the results of LITEAC1 with LITEAC2, LITEAC2 always gives a slightly higher MLWT than LITEAC1. This can be explained by the fact that lighting power calculated by LITEAC2 is always higher (and closer to the measured lighting power) than that calculated by LITEAC1. For five of the 12 configurations both LITEAC1 and LITEAC2 predicted lower values of MLWT than those measured, while for the other 7 configurations both LITEAC1 and LITEAC2 predicted higher values of MLWT than those measured.

Table 8.1(b) compares the measured and predicted values of lighting power, relative lighting power (RLP), relative light output (RLO) and relative lighting efficacy (RLE). Only the 9 configurations for which Treado and Bean (1988) give absolute measured values of lighting power are included in this table. It can be seen from this table that there is an excellent match between the LITEAC2-predicted lighting power and the measured lighting power. LITEAC1 predicts a lighting power which is 5-6% lower than the measured values. This is probably due to the use of an inappropriate empirical curve for the change of lighting power with minimum lamp wall temperature in LITEAC1. The lower lighting power predicted by LITEAC1 also explains why values of the MLWT calculated by LITEAC1 are lower than those predicted by LITEAC2. The comparison between measured and calculated values of relative lighting power, relative light output and relative lighting efficacy is not meaningful because the reference maximum values for the calculation of the relative values of the measured data are not known. However, the relative values are given in Table 8.1(b) for completeness.

Table 8.2 shows the comparison between results of minimum lamp wall temperature and its elevation above room temperature for the 19 configurations with the luminaire type 4 × 4-lamp 40 W prismatic diffuser (acrylic lens). It can be seen that for all but 2 of the 19 configurations, there is excellent agreement between the predicted values (both LITEAC1 and LITEAC2) and the corresponding measured values. The relatively large discrepancy between the predicted and measured results for the case labelled with a configuration number 44113 may be due to errors in measurement. This configuration had all settings exactly the same as those of configuration number 44103 except for the airflow rate, which was 0.0566 $m^3 s^{-1}$ for configuration 44113 and 0.0944 $m^3 s^{-1}$ for configuration 44103. It is illogical for configuration 44113, which had a lower airflow rate, to have a lower measured lamp wall temperature (47.8°C) than configuration 44103 (49.8°C), which had a higher airflow rate. When comparing the measured MLWT for configurations 44113 and 44114, it is also illogical to have a lower lamp wall temperature for a ceiling grille return than that for lamp compartment return with all other settings exactly the same. Thus, it is believed that errors occur in the measured results of configuration 44113.

Table 8.3 shows the comparison between results of minimum lamp wall temperature and its elevation above room temperature for the 9 configurations with the luminaire type 4 × 2-lamp 40 W prismatic diffuser (acrylic lens). The match between predicted and measured values for these 9 configurations is, in general, very good. Typical deviations are to within 2% while only one configuration (42103) shows a larger discrepancy of about 9%. This larger discrepancy is for the configuration with a high return airflow rate through the lamp compartment and the discrepancy is thought to be due to an error in the assumed model convection coefficients.

8.5 Transient test results

Transient tests were run in the NIST test cell by Treado and Bean (1988, 1992) to determine the response of the cooling load to a step change in lighting power, i.e. switching on or switching off of lamps. Starting from a steady-state condition with the lights off for a long period of time, the lighting system was switched on and the cooling load monitored until equilibrium conditions were attained. After the steady-state condition had been attained with the lights on, the lighting system was switched off and again the cooling load was monitored until equilibrium conditions were again attained. As described by Treado and Bean (1988), the lighting system was the only planned heat source in the test room. Under ideal conditions, the measured cooling load would be zero with the test room at equilibrium and the lights off. At equilibrium with the lights on, the cooling load would be equal to the lighting power if the NIST test cell was well insulated. However, there were small heat gains to the test room which caused slight cooling loads with the lights off. Treado and Bean (1988) assumed this zero offset to be constant for the duration of a test, and the measured cooling loads were adjusted accordingly. The typical zero offset was less than 20 W, compared to the smallest lighting power tested (of the order of 350 W). According to Treado and Bean (1988), the measured cooling loads were also adjusted so that the equilibrium cooling load was equal to the measured lighting power with the lights on and the test room at equilibrium. Treado and Bean (1988) estimated that this correction factor was less than four percent, and it varied with airflow rate, increasing slightly as airflow increased. Transient tests were run in the NIST test cell with the combinations described in section 8.4. However, the actual cooling load data were not published and they are not available. Results were published as cooling load regression curves only in Treado and Bean (1992). These curves are regression curves based on the double exponential regression model as described in Treado and Bean (1988). Most of the curves are very similar to one another with only small differences for different configurations.

Transient simulations were conducted using LITEAC1 and LITEAC2 for all the configurations described in tables 8.1-8.3. However, because most of the measured data are not available for comparison, this validation exercise considers only the one configuration for which the experimental data can be obtained from Sowell (1990). Measured data which are available include cooling load, lighting power, air temperature, lamp temperature as well as room surface temperatures. Sowell (1990) made the criticism that problems existed with the NIST experimental data, so that meaningful comparisons could not be made with calculated results and that only one single set of data could be used for comparison with calculated results. This set of data was the transient test results for the configuration number 42101 in Table 8.3. This was the configuration in which the test room was installed with 4 static luminaires (i.e. air return not through luminaire) with a prismatic diffuser (acrylic lens) and two 40 W lamps each. The air return was through a ceiling grille to a plenum above an acoustic tile suspended ceiling with a nominal supply airflow rate of 0.0944 m^3s^{-1}. Room air temperature was kept at 23.9°C. The floor was covered with carpet. 'Lights-on' and 'lighting on-off cycle' tests were modelled with LITEAC1 and LITEAC2. Comparisons with measurements are discussed below.

8.5.1 Lights ON test

For the 'lights on' simulation, tests were conducted with all the lamps switched on at time zero, and then are kept on at all times. In the simulations, the node temperatures, cooling load and lighting power were calculated for each time step. The results of the test runs for the configuration 42101 are plotted in figures 8.4-8.8.

Figure 8.4 shows the LITEAC1 and LITEAC2 simulated lighting power and cooling load, compared with the NIST test results. From Figure 8.4, it can be seen that both simulated lighting power curves match the experimental one excellently with deviations of only about 1.5%. It is not surprising that there is good agreement between the LITEAC1 simulated lighting power and the measured lighting power, since the lighting power is an input in LITEAC1. However, the lighting power in LITEAC2 is calculated by the fluorescent lamp positive column model LAMPPC and a good agreement between predicted and measured values shows that LAMPPC is capable of simulating the lamp power correctly.

Figure 8.4 also shows that there is good agreement between the two predicted cooling load curves and the experimental one. It appears in Figure 8.4 that, for the initial five hours, both LITEAC1 and LITEAC2 predict cooling loads lower than experimental results whilst both models predict cooling loads higher than experimental results after hour 7, with errors within 5-6% for most hours. The predicted shape of the cooling load curve for the initial hours is sensitive to the convective heat transfer coefficients; hence, a small error in the convection coefficients would cause an error in the calculation of cooling load. This partly explains the discrepancy in the initial hours. The discrepancy in the later hours is due mainly to experimental difficulty in minimising net heat loss rate from the test cell. At equilibrium, the cooling load should theoretically equal the lighting power, because lighting power was the only heat source inside the test cell. The two simulated cooling load curves approach the corresponding lighting power line with cooling load equal to lighting power after about hour 20. However, as can be seen from Figure 8.4, the measured cooling load is always lower than the measured lighting power. According to Treado and Bean (1988), despite the use of an active guard space control system, small heat losses from the test cell to the surroundings occurred during the tests. Treado and Bean (1988) did mention that corrections were made to the measured cooling load so that cooling load equalled measured lighting power with the lights on and with the test room at equilibrium, but this correction was assumed to be constant throughout the whole test. It can be seen from Figure 8.4 that there were fluctuations in the measured cooling load and it is not clear whether the set of data used in this validation exercise had been corrected or not. This experimental error, due to small heat gains/losses from other sources, would be the main cause for the discrepancy in later hours.

Figure 8.5 shows the predicted lamp temperature plotted against time for simulations using LITEAC1 and LITEAC2. Also shown in this figure is the curve of measured lamp temperatures in the NIST test cell as reported by Sowell (1990). This figure shows that the lamp temperature rises to its equilibrium value within the first two hours. There is very good agreement between the simulation results of LITEAC2 and the NIST experimental results, with differences of less than 0.6°C in 45°C between simulated and experimental temperatures. The differences between predicted lamp temperatures by LITEAC1 and the measured lamp temperatures are slightly higher but are still within about 1°C.

Figure 8.6 shows the plenum wall temperatures predicted by both LITEAC1 and LITEAC2 with the NIST measured results plotted on the same graph. There is no significant difference between the simulated results of LITEAC1 and LITEAC2. When the simulation results are compared with the NIST data, however, the simulated plenum wall temperatures are about 1°C higher than the NIST test results at equilibrium. Curves of the plenum ceiling temperature (not shown for conciseness) exhibit similar behaviour to those of the plenum wall temperature. This discrepancy of about 1°C in 24°C – which is actually not large for a model that considers all modes of heat transfer – may be due to small errors in the input heat transfer coefficients and/or radiation form factors. Another possible cause of discrepancy between model-predicted and experimental results is error in the measurement of temperatures. Treado and Bean (1988) reported that the NIST temperature measurements were accurate to within 0.28°C (or 0.5°F, as reported). However, this error might be just the error of the thermocouple junction temperature (Sowell 1990). Treado and Bean (1988) did not discuss any error that might have been caused by a possible difference between junction temperature and the true surface temperature (the result of imperfect contact between the thermocouple and surface, for example).

Figures 8.7 and 8.8 show the temperatures of two room nodes: walls and floor, respectively. Again, there is no significant difference between the simulated results of LITEAC1 and LITEAC2. The simulated temperatures are all higher than the corresponding measured results by about 1°C for the wall and about 1.2°C for the floor. This discrepancy can be attributed to either error in the input convective heat transfer coefficients or experimental error due to imperfect contact between thermocouple and surface. It can be noted from Figures 8.7 and 8.8 that both LITEAC1 and LITEAC2 correctly predicted that the floor temperature was slightly higher than the wall temperature.

8.5.2 Lights ON/OFF cycles

For 'lights on/off cycles' tests, no experimental data on temperature profiles were published. Only cooling load profiles for some configurations are obtainable from Treado and Bean (1992). Since the cooling load profiles for various configurations are similar in shape, only the configuration number 42101 is used for comparison between simulated and experimental data.

For 'lights on/off cycles' tests, simulations were conducted for a period of five days with lamps on for 12 hours (lamp switched on at hour 0) and lamps off for 12 hours (lamps switched off at hour 12) each day. Test simulations were also conducted for periods longer than five days and simulation results showed almost exactly the same daily cooling load profile repeated from day 3 onwards; hence, it is considered a period of 5 days is long enough to obtain the daily transient cooling load profile for 'lights on/off cylces' tests. Figure 8.9 shows the LITEAC1 and LITEAC2 simulation results for the profile of cooling load as a fraction of the lighting power for configuration 42101 over a 24-hour period, starting at hour 18 of day 3. Also shown in Figure 8.9 are the NIST test results (Treado and Bean 1992) for the same configuration. The figure shows that there is no significant difference between simulated results of LITEAC1 and LITEAC2 and these results agree well with the NIST test results. The small discrepancy between simulated and experimental results can be attributed to errors in the input convective heat transfer coefficients.

8.6 Discussion

8.6.1 Minimum lamp wall temperature

In all simulations described in this chapter, the mean lamp wall temperature is assumed to be equal to the minimum lamp wall temperature. This may have introduced errors in the simulation results. Sowell (1990) quoted that experimental data of lamp wall temperature generally showed a difference of 5.5°C between the hottest and coldest parts of the lamp wall. Assuming that there is an even distribution of temperature between the highest and lowest values, the minimum lamp wall temperature is about 2.5° to 3°C below the average lamp wall temperature. From Figure 7.5, this difference means that LAMPPC predicts a radiation output 3 to 4% higher if the average lamp wall temperature is taken to be equal to the minimum lamp wall temperature.

The error due to the difference between mean lamp wall temperature and minimum lamp wall temperature can be reduced by dividing the lamp wall into more than one node with the lowest of the simulated temperatures of the lamp nodes taken to be the minimum lamp wall temperature. In the simulation of a laboratory test cell to be described in Chapter 9, the lamp wall is divided into an upper half node and a lower half node. The lower of the simulated lamp node temperatures is taken as the minimum lamp wall temperature. It will be shown in chapter 9 that this improves the prediction of the minimum lamp wall temperature. The prediction of minimum lamp wall temperature can be even better if the lamp wall is further divided into more nodes. However, there will be difficulties in obtaining accurate radiation form factors and convection heat transfer coefficients for all the lamp nodes due to the more complicated geometries.

8.6.2 Change in convective heat transfer coefficients

In sections 8.4 and 8.5, the convective heat transfer coefficients were ascribed to be one of the source of modelling errors. As described in Appendix C, the convective heat transfer coefficient for each node is calculated according to empirical correlation equations published recently. The correlation equation used for each node is selected in accordance of the geometry of the node (see Table C.1) and the temperature difference between the node and the adjacent air. However, as the heat transfer coefficients of the NIST test cell surfaces under actual operating conditions are not available, it is thought that errors may occur in the heat transfer coefficients and these errors could be a reason for the discrepancies found between modelling and experimental results. There is a temptation of trying to adjust the heat transfer coefficients (and other model variables) to obtain agreement with the experimental results. However, to do this would be pointless unless experimental measurements could be used to 'validate' the adjusted coefficients and correlations could be developed to extend the adjusted coefficients to other room configurations.

In order to test the sensitivity of the model predictions to variations in the heat transfer coefficients, tests have been performed by using heat transfer coefficients different from those calculated by the correlations as described in Appendix C. A test run was performed using heat transfer coefficients 30% lower than those used for the configuration 42101 as described in section 8.5. A better fit of the cooling load curve was obtained as shown in Figure 8.10. However, poorer agreements with experimental results were obtained for the lamp node temperature and other room surface temperatures. Figure 8.11 shows the result for the lamp node temperature. Hence, adjustments of the heat transfer coefficients may give better agreement with experimental results for one parameter but poorer agreement for another parameter.

8.7 Summary

In this chapter, both steady-state and transient simulation results of both LITEAC1 and LITEAC2 are compared with experimental results of tests conducted in NIST. For the 40 configurations considered, predicted steady-state results, which include minimum lamp wall temperature, elevation of minimum lamp wall temperature above room temperature, relative lighting power, relative light output and relative lighting efficacy, of both LITEAC1 and LITEAC2 compare well with experimental data. For most cases, predicted results deviate from experimental data by less than 5%. There are a few cases with higher deviations. Inter-comparison between experimental results show that experimental error existed in the case with exceptionally high deviation. Another author, Sowell (1990), commented also that problems existed in the NIST test data. Detailed properties of the materials used in the NIST test cell and values for the heat transfer coefficients are not known, so that errors in the model input data could be one cause of the deviation between predicted and experimental results.

Transient temperatures and cooling load profiles predicted by both LITEAC1 and LITEAC2 also compare well with experimental data. Deviations of the calculated cooling load from the experimental results during the initial hours of transient operation can be attributed to errors in the estimation of heat transfer coefficients. Discrepancy in the later hours is due mainly to experimental error in minimizing heat gains/losses from other sources and the magnitude of the corrections made to the measured data. In general, the simulated temperature profiles and the corresponding experimental profiles are in good agreement. Those discrepancies found can be attributed to experimental errors in the measurement of temperature due to improper contact between thermocouple and surface as commented by Sowell (1990).

Detailed data on light output and lighting levels were not published in the NIST reports (Treado and Bean 1988, 1992) and are not available for comparison with predicted results. Comparison between the only set of measured lighting power data available and the corresponding predicted values shows good agreement especially for LITEAC2. This good agreement between LITEAC2 simulated lighting power with the experimental data shows that the positive column model in LITEAC2 is capable of simulating the power consumed by fluorescent lamps without the need for input data on lamp power.

In view of the complexity of the models and the uncertainty in input parameters, the agreement between the simulated results and the experimental data is generally considered to be good. It can be concluded that both the models LITEAC1 and LITEAC2 are suitable numerical models for simulating the interaction between lighting and HVAC operation. Both models behave similarly in the simulation of cooling load and temperature. However, when LITEAC1 is used, a good empirical curve is required as input data to represent the variation of lamp power and of light output with lamp wall temperature. Lamp manufacturers do not normally include these data in the lamp data sheet or manual. On the other hand, LITEAC2 requires input concerning the relative spectral power output of lamps which is more often given in lamp data sheets.

The fact that LITEAC2 gives a better simulation of lighting power and light output than LITEAC1 is encouraging, and this shows that LITEAC2 can simulate the effect of temperature changes on lighting power and light output without the use of empirical curves.

In order to test the validity of LITEAC1 and LITEAC2 for an enclosure with different dimensions and to compare predicted illuminances with measurements, further experimental validation using a laboratory constructed test cell has been carried out. The construction of the laboratory test cell and the validation results are described in the next chapter.

Table 8.1(a)

Minimum lamp wall temperature and elevation of minimum lamp wall temperature above room temperature. Comparison between NIST measurements and predicted results from LITEAC1 and LITEAC2 for the configurations with the luminaire type 4 × 4 lamp parabolic diffuser.

Configuration No	Airflow rate (m^3/s)	Airflow return type	'Set-point' Room air temperature (°C)	Measured MLWT (°C)	Measured elevation (°C)	Predicted MLWT by LITEAC1 (°C)	Predicted elevation by LITEAC1 (°C)	Predicted MLWT by LITEAC2 (°C)	Predicted elevation by LITEAC2 (°C)	Percentage deviation LITEAC1 vs measured	Percentage deviation LITEAC2 vs measured
44201	0 0944	LC	26 7	40 9	13 8	41 4	14 7	41 7	15 0	6 52%	8 70%
44202	0 0944	CG	23 9	44 9	20 6	44 0	20 1	44 5	20 6	-2 43%	0 00%
44203	0 0944	LC	23 9	38 4	14 2	39 0	15 1	39 2	15 3	6 34%	7 75%
44204	0 0944	LC	21 1	36 0	14 6	36 5	15 4	36 6	15 5	5 48%	6 16%
44205	0 0755	LC	26 7	43 8	16 6	41 9	15 2	42 3	15 6	-8 43%	-6 02%
44206	0 0755	CG	23 9	45 9	21 9	44 5	20 6	45 1	21 2	-5 94%	-3 20%
44207	0 0755	LC	23 9	38 7	14 5	39 6	15 7	39 8	15 9	8 28%	9 66%
44208	0 0755	LC	21 1	36 2	14 8	37 1	16 0	37 5	16 4	8 11%	10 81%
44209	0 0566	LC	26 7	44 3	17 2	42 7	16 0	43 0	16 3	-6 98%	-5 23%
44210	0 0566	CG	23 9	46 1	21 8	45 1	21 2	45 7	21 8	-2 75%	0 00%
44211	0 0566	LC	23 9	39 2	15 0	40 3	16 4	40 6	16 7	9 33%	11 33%
44212	0 0566	LC	21 1	37 6	16 1	38 0	16 9	38 1	17 0	4 97%	5 59%

MLWT = Minimum lamp wall temperature
Measured elevation = Measured MLWT – measured room air temperature (see note below)
LC = lamp compartment return
CG = ceiling grille return

Note: The measured elevation of minimum lamp wall temperature above room temperature is the difference between the measured minimum lamp wall temperature and the measured room air temperature The measured room air temperature could be different from the controlled 'set-point' room air temperature which was used as a test parameter (Treado and Bean 1992).

Table 8.1(b)

Lighting power, relative lighting power (RLP), relative light output (RLO) and relative lighting efficacy (RLE). Comparison between NIST measurements and predicted results from LITEAC1 and LITEAC2 for the configurations with the luminaire type 4 × 4 lamp parabolic diffuser and lamp compartment return.

Config-uration No	Lighting power NIST expt. (W)	RLP NIST expt	RLO NIST expt	RLE NIST expt	Lighting power by LITEAC1 (W)	RLP by LITEAC1	RLO by LITEAC1	RLE by LITEAC1	Lighting power by LITEAC2 (W)	RLP by LITEAC2	RLO by LITEAC2	RLE by LITEAC2
44201	743	0 969	-	-	704	0 982	0 980	0 997	748	0 982	0 997	0 991
44203	754	0 983	0 963	0 969	711	0 992	0 992	0 999	755	0 991	0 987	0 973
44204	767	1	0 964	0 953	717	1	1	0 999	762	1	0 972	0 949
44205	737	0 961	0 943	0 970	702	0 979	0 976	0 997	746	0 979	0 998	0 996
44207	753	0 982	-	-	710	0 990	0 990	0 999	754	0 990	0 990	0 977
44208	764	0 996	1	0 994	716	0 998	0 999	1	759	0 996	0 978	0 959
44209	730	0 952	0 948	0 985	699	0 975	0 971	0 996	744	0 976	1	1
44211	753	0 982	0 965	0 973	708	0 987	0 986	0 999	752	0 987	0 993	0 982
44212	757	0 987	0 998	1	714	0 995	0 996	0 999	757	0 993	0 982	0 965

Table 8.2

Minimum lamp wall temperature and elevation of minimum lamp wall temperature above room temperature. Comparison between NIST measurements and predicted results from LITEAC1 and LITEAC2 for the configurations with the luminaire type 4 × 4 lamp prismatic diffuser (acrylic lens).

Configuration No	Airflow rate (m^3/s)	Airflow return type	'Set-point' Room air temperature (°C)	Measured MLWT (°C)	Measured elevation (°C)	Predicted MLWT by LITEAC1 (°C)	Predicted elevation by LITEAC1 (°C)	Predicted MLWT by LITEAC2 (°C)	Predicted elevation by LITEAC2 (°C)	Percentage deviation LITEAC1 vs measured	Percentage deviation LITEAC2 vs measured
44101	0.0944	CG	26.7	51.9	25.9	52.5	25.8	53.1	26.4	-0.39%	1.93%
44102	0.0944	LC	26.7	48.4	22.4	49.0	22.3	49.5	22.8	-0.45%	1.79%
44103	0.0944	CG	23.9	49.8	26.6	50.2	26.3	50.8	26.9	-1.13%	1.13%
44104	0.0944	CG	21.1	47.6	27.2	47.9	26.8	48.5	27.4	-1.47%	0.74%
44105	0.0944	LC	21.1	42.9	22.5	44.0	22.9	44.5	23.4	1.78%	4.00%
44106	0.0755	CG	26.7	52.3	26.3	53.3	26.6	53.9	27.2	1.14%	3.42%
44107	0.0755	LC	26.7	49.3	23.3	49.4	22.7	49.9	23.2	-2.58%	-0.43%
44108	0.0755	LC	23.9	47.5	23.1	46.9	23.0	47.5	23.6	-0.43%	2.16%
44109	0.0755	CG	21.1	48.4	28.0	48.7	27.6	49.4	28.3	-1.43%	1.07%
44110	0.0755	LC	21.1	44.4	23.9	44.5	23.4	45.0	23.9	-2.09%	0.00%
44111	0.0566	CG	26.7	52.7	26.7	54.4	27.7	54.9	28.2	3.75%	5.62%
44112	0.0566	LC	26.7	50.2	24.2	50.0	23.3	50.6	23.9	-3.72%	-1.24%
44113	0.0566	CG	23.9	47.8	23.6	52.1	28.2	52.7	28.8	19.49%	22.03%
44114	0.0566	LC	23.9	48.2	23.8	47.6	23.7	48.2	24.3	-0.42%	2.10%
44115	0.0566	CG	21.1	49.2	28.1	49.8	28.7	50.5	29.4	2.14%	4.63%
44116	0.0566	LC	21.1	45.5	24.9	45.2	24.1	45.7	24.6	-3.21%	-1.20%
44117	0.0378	CG	26.7	53.5	26.6	55.8	29.1	56.2	29.5	9.40%	10.90%
44118	0.0378	LC	26.7	50.8	24.8	51.1	24.4	51.7	25.0	-1.61%	0.81%
44119	0.0378	LC	23.9	49.2	24.9	48.7	24.8	49.3	25.4	-0.40%	2.01%

MLWT = Minimum lamp wall temperature
Measured elevation = Measured MLWT – measured room air temperature (see note below)
LC = lamp compartment return
CG = ceiling grille return

Note. The measured elevation of minimum lamp wall temperature above room temperature is the difference between the measured minimum lamp wall temperature and the measured room air temperature. The measured room air temperature could be different from the controlled 'set-point' room air temperature which was used as a test parameter (Treado and Bean 1992).

Table 8.3

Minimum lamp wall temperature and elevation of minimum lamp wall temperature above room temperature. Comparison between NIST measurements and predicted results from LITEAC1 and LITEAC2 for the configurations with the luminaire type 4 × 2 lamp prismatic diffuser (acrylic lens).

Configuration No	Airflow rate (m^3/s)	Airflow return type	'Set-point' Room air temperature (°C)	Measured MLWT (°C)	Measured elevation (°C)	Predicted MLWT by LITEAC1 (°C)	Predicted elevation by LITEAC1 (°C)	Predicted MLWT by LITEAC2 (°C)	Predicted elevation by LITEAC2 (°C)	Percentage deviation LITEAC1 vs measured	Percentage deviation LITEAC2 vs measured
42101	0 0944	CG	23 9	47 4	23 2	46 1	22 2	46 6	22 7	-4 31%	-2 16%
42102	0 0944	LC	23 9	40 3	16 5	40 4	16 5	40 6	16 7	0 00%	1 21%
42103	0 0944	LC	21 1	35 7	15 3	37 8	16 7	37 9	16 8	9 15%	9 80%
42104	0 0755	CG	23 9	46 9	22 5	46 5	22 6	47 1	23 2	0 44%	3 11%
42105	0 0755	LC	23 9	40 7	17 0	40 7	16 8	41 3	17 4	-1 18%	2 35%
42106	0 0755	LC	21 1	37 2	16 7	38 1	17 0	38 6	17 5	1 80%	4 79%
42107	0 0566	CG	23 9	48 2	23 7	47 2	23 3	47 7	23 8	-1 69%	0 42%
42108	0 0566	LC	23 9	42 4	19 1	41 9	18 0	42 2	18 3	-5 76%	-4 19%
42109	0 0566	LC	21 1	38 8	18 3	39 3	18 2	39 6	18 5	-0 55%	1 09%

MLWT = Minimum lamp wall temperature
Measured elevation = Measured MLWT – measured room air temperature (see note below)
LC = lamp compartment return
CG = ceiling grille return

Note: The measured elevation of minimum lamp wall temperature above room temperature is the difference between the measured minimum lamp wall temperature and the measured room air temperature. The measured room air temperature could be different from the controlled 'set-point' room air temperature which was used as a test parameter (Treado and Bean 1992).

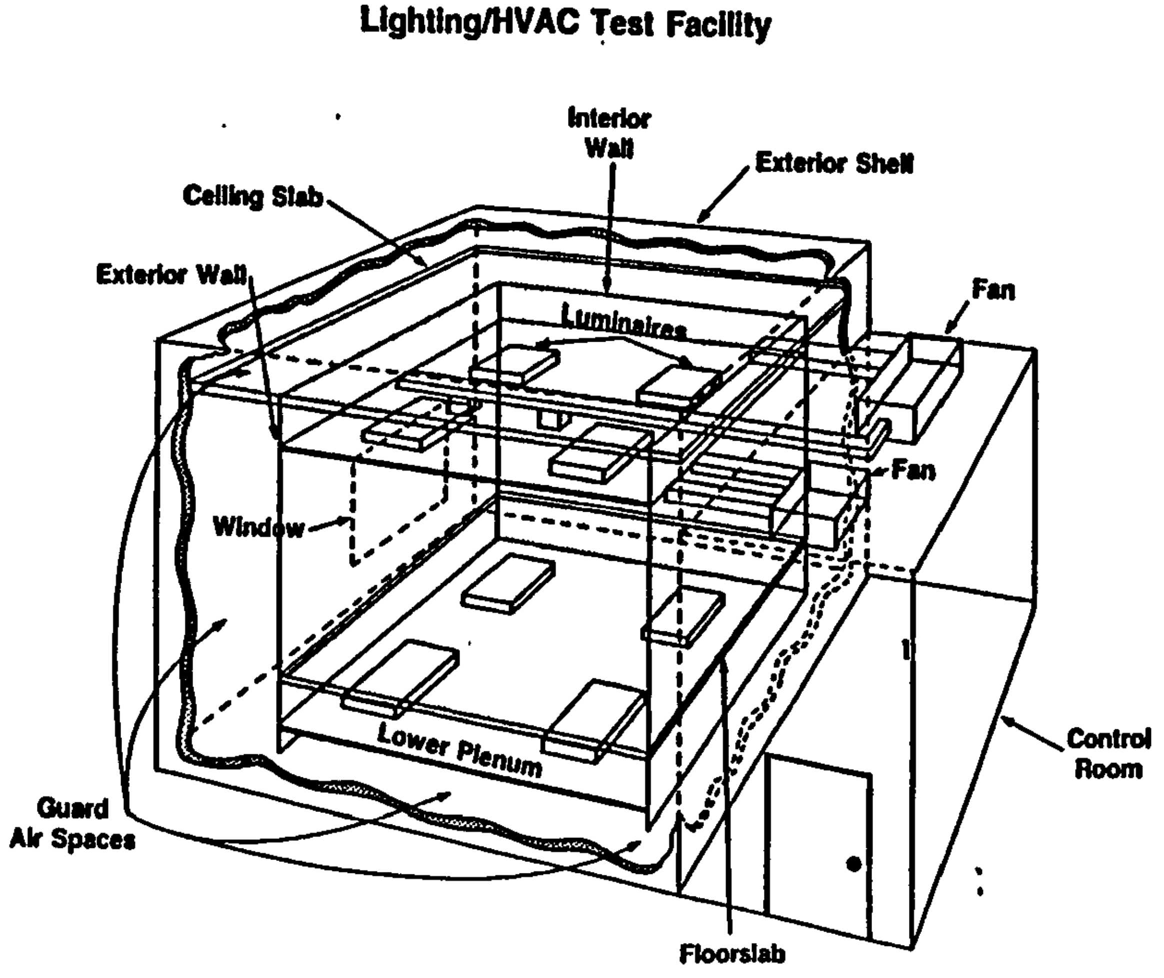

Figure 8.1

Cut-away schematic view of the NIST test facility (From Treado and Bean 1988).

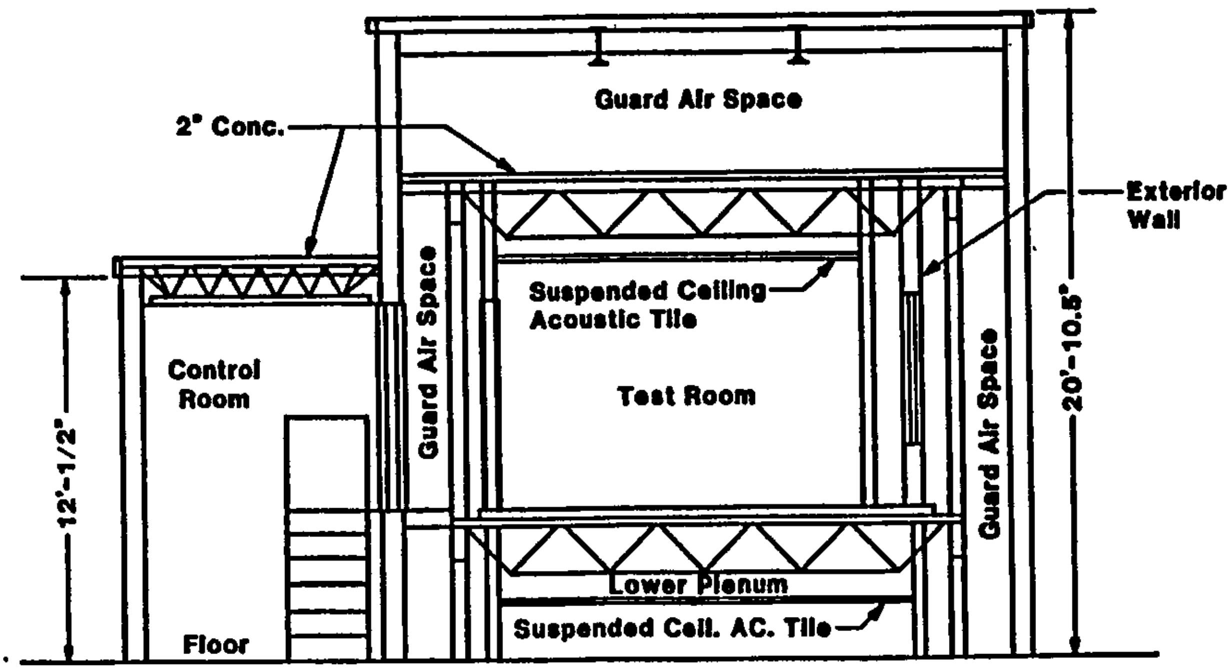

Figure 8.2

Elevation view of the test room (From Treado and Bean 1988).

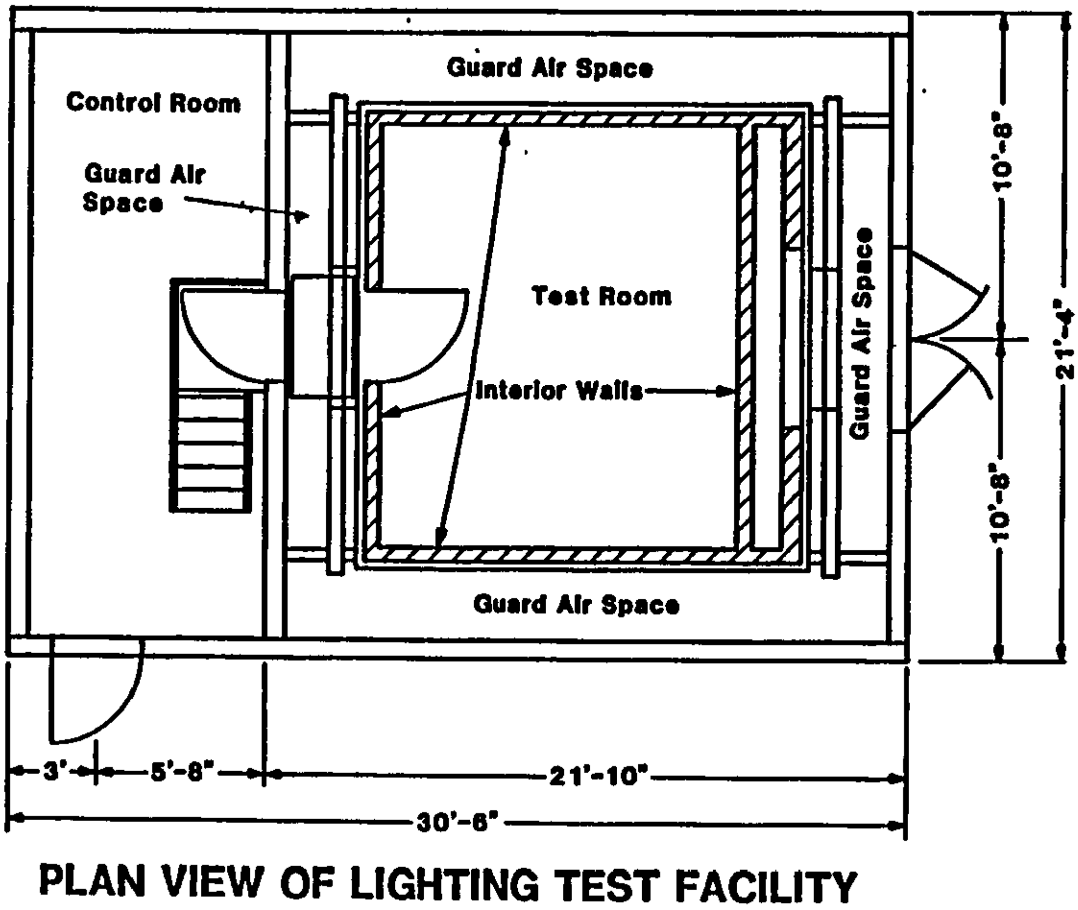

Figure 8.3

Plan view of the NIST test room showing guard air spaces surrounding the test room (From Treado and Bean 1988).

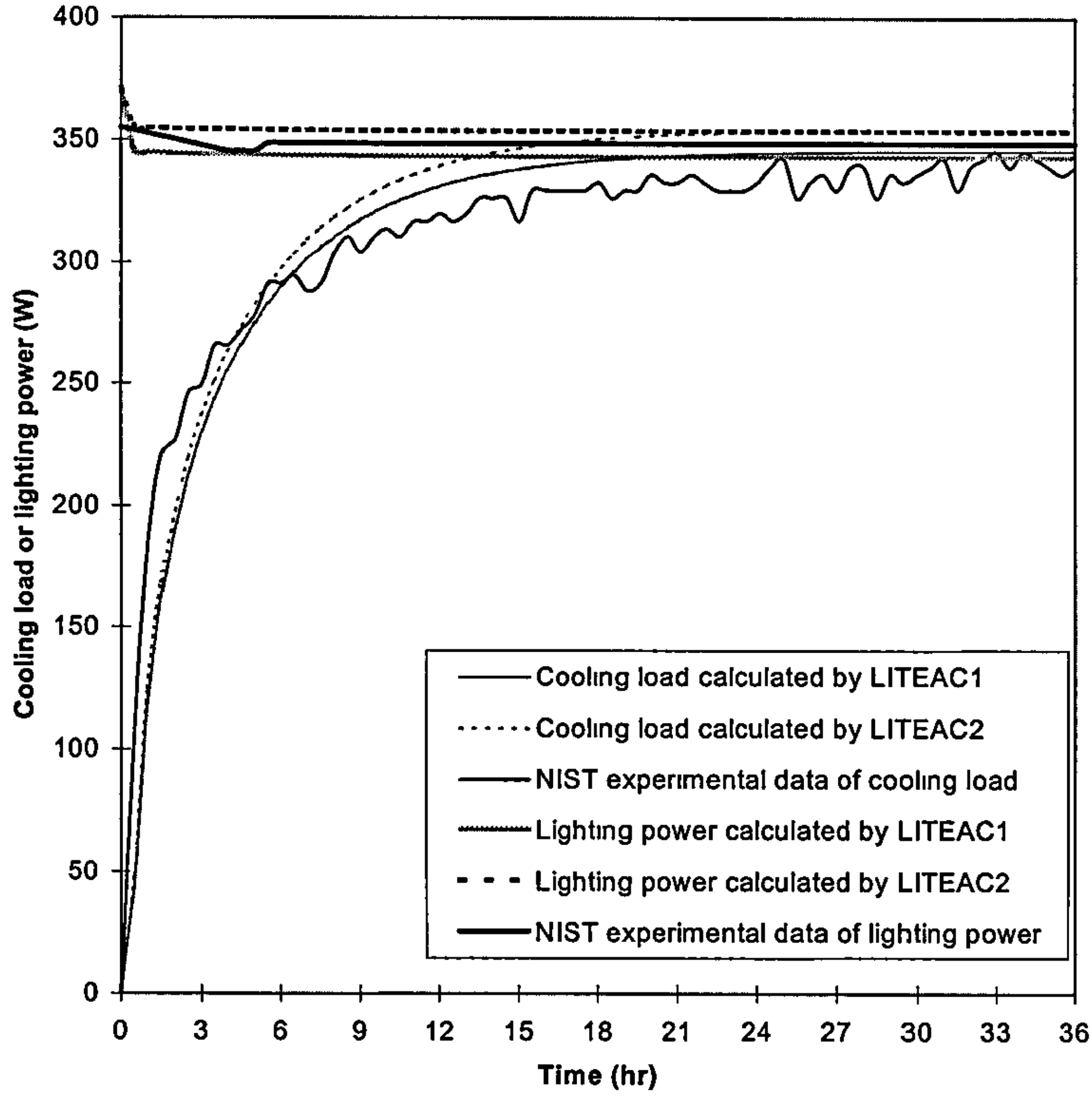

Figure 8.4

Cooling load and lighting power of NIST test cell for lights-on test with the configuration of 4 × 2 lamp prismatic diffuser, ceiling grille return, airflow rate 0.0944 m^3s^{-1} and room air temperature 23.9°C. Comparison between LITEAC1, LITEAC2 and measured results.

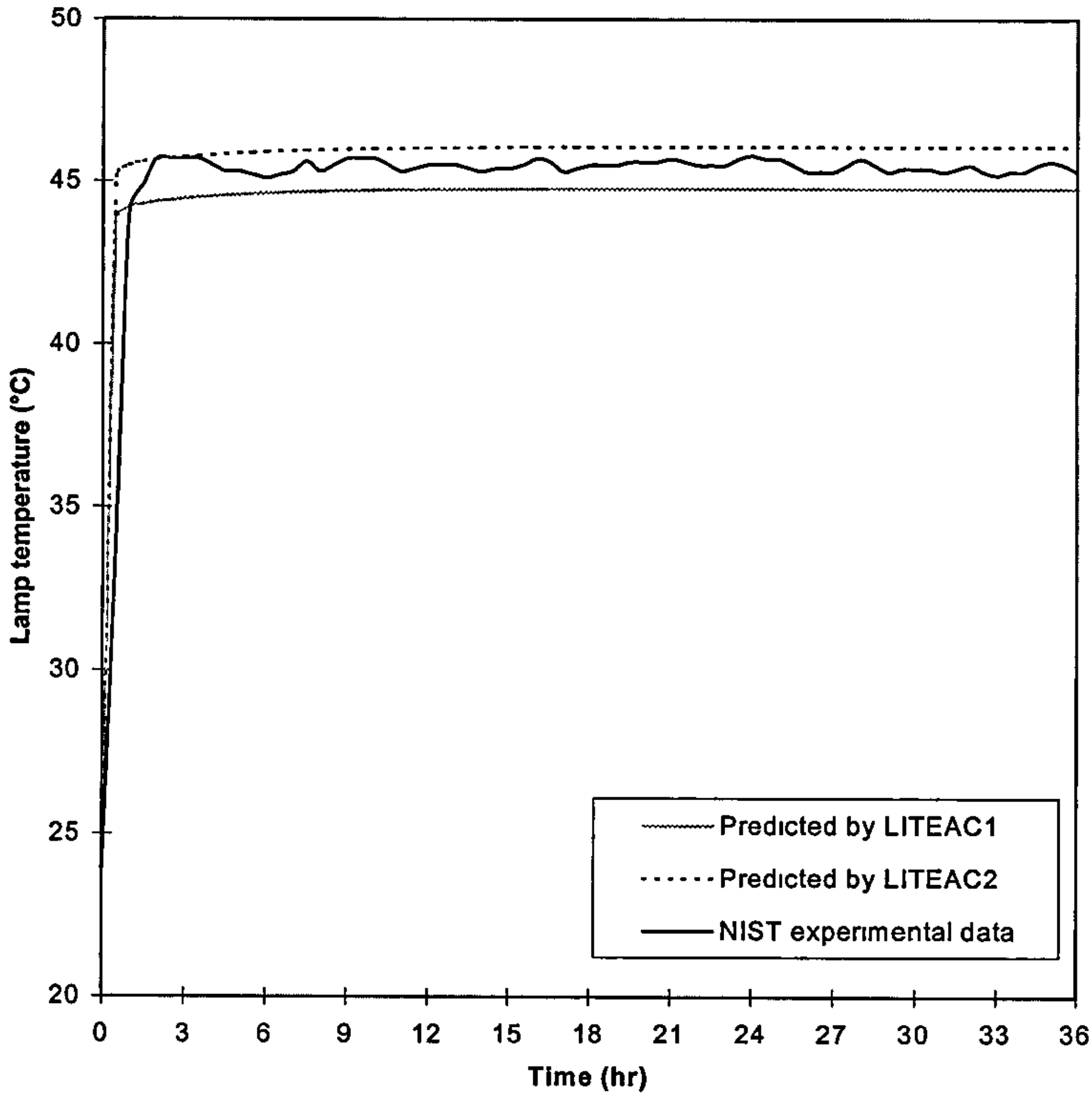

Figure 8.5

Lamp node temperature of NIST test cell for lights-on test with the configuration of 4 × 2 lamp prismatic diffuser, ceiling grille return, airflow rate 0.0944 m^3s^{-1} and room air temperature 23.9°C. Comparison between LITEAC1, LITEAC2 and measured results.

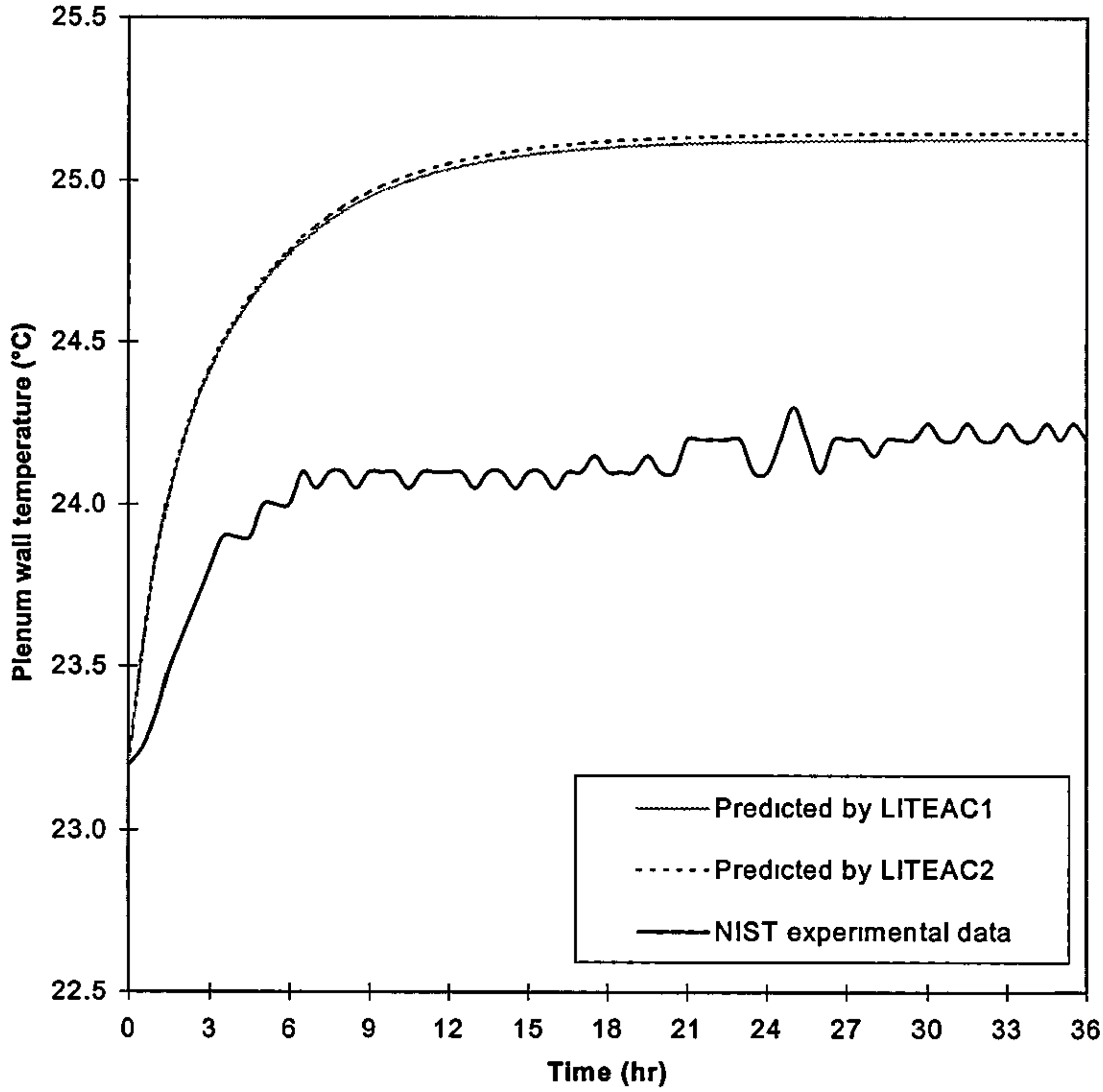

Figure 8.6

Plenum wall node temperature of NIST test cell for lights-on test with the configuration of 4 × 2 lamp prismatic diffuser, ceiling grille return, airflow rate 0.0944 m^3s^{-1} and room air temperature 23.9°C. Comparison between LITEAC1, LITEAC2 and measured results.

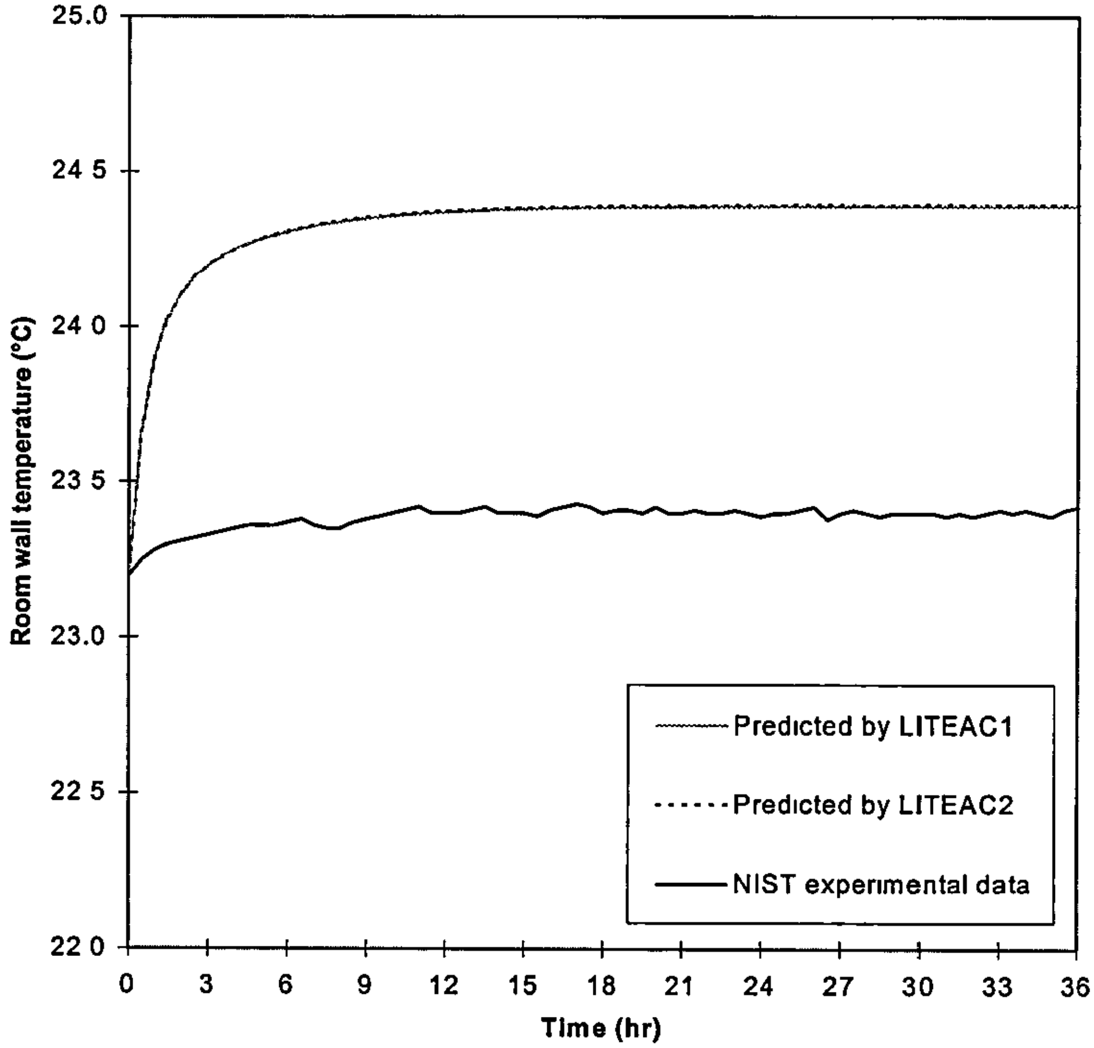

Figure 8.7

Room wall temperatures of NIST test cell for lights-on test with the configuration of 4 x 2 lamp prismatic diffuser, ceiling grille return, airflow rate 0.0944 m^3s^{-1} and room air temperature 23.9°C. Comparison between LITEAC1, LITEAC2 and measured results.

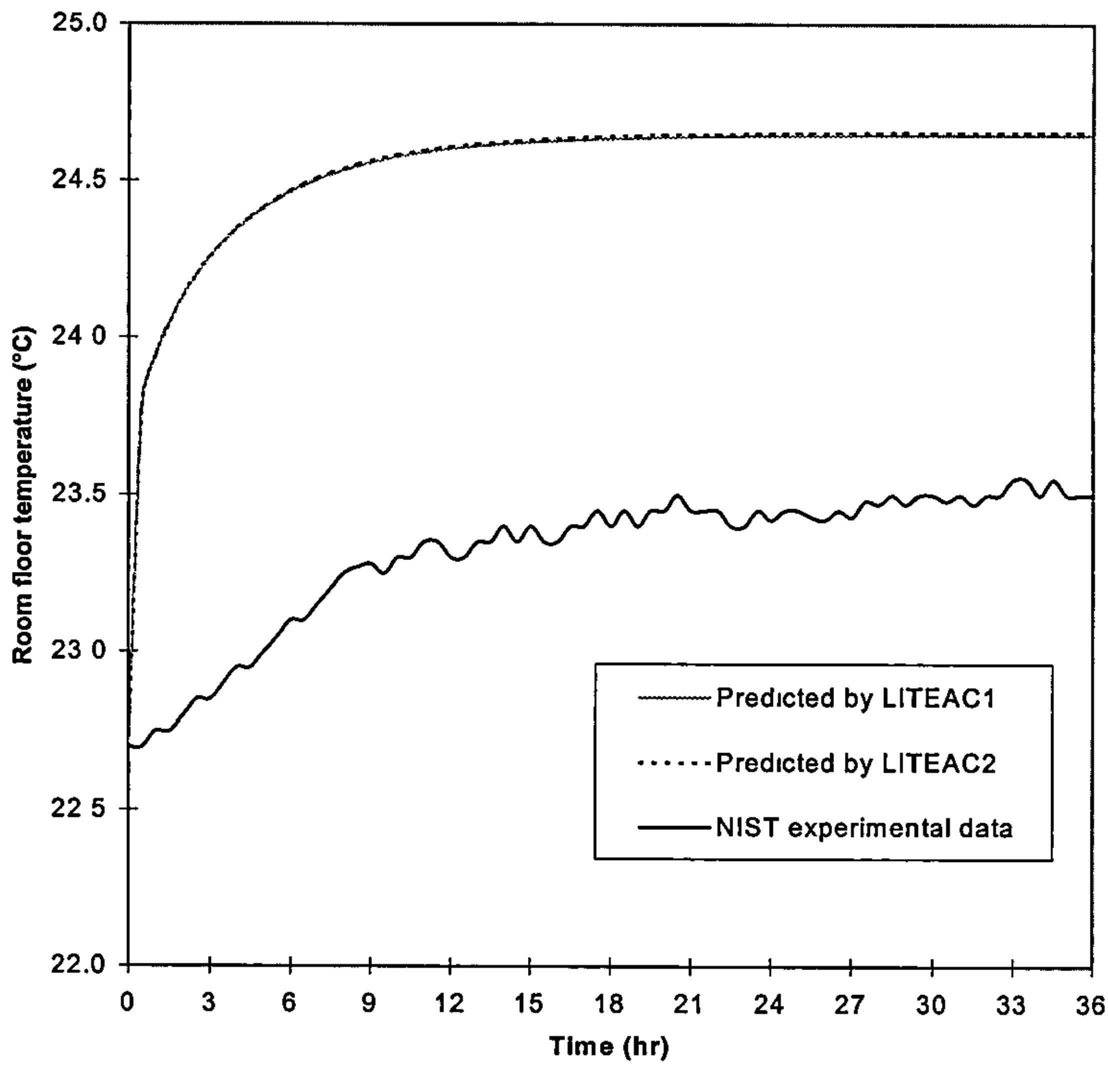

Figure 8.8

Room floor temperatures of NIST test cell for lights-on test with the configuration of 4 × 2 lamp prismatic diffuser, ceiling grille return, airflow rate 0 0944 m^3s^{-1} and room air temperature 23.9°C. Comparison between LITEAC1, LITEAC2 and measured results.

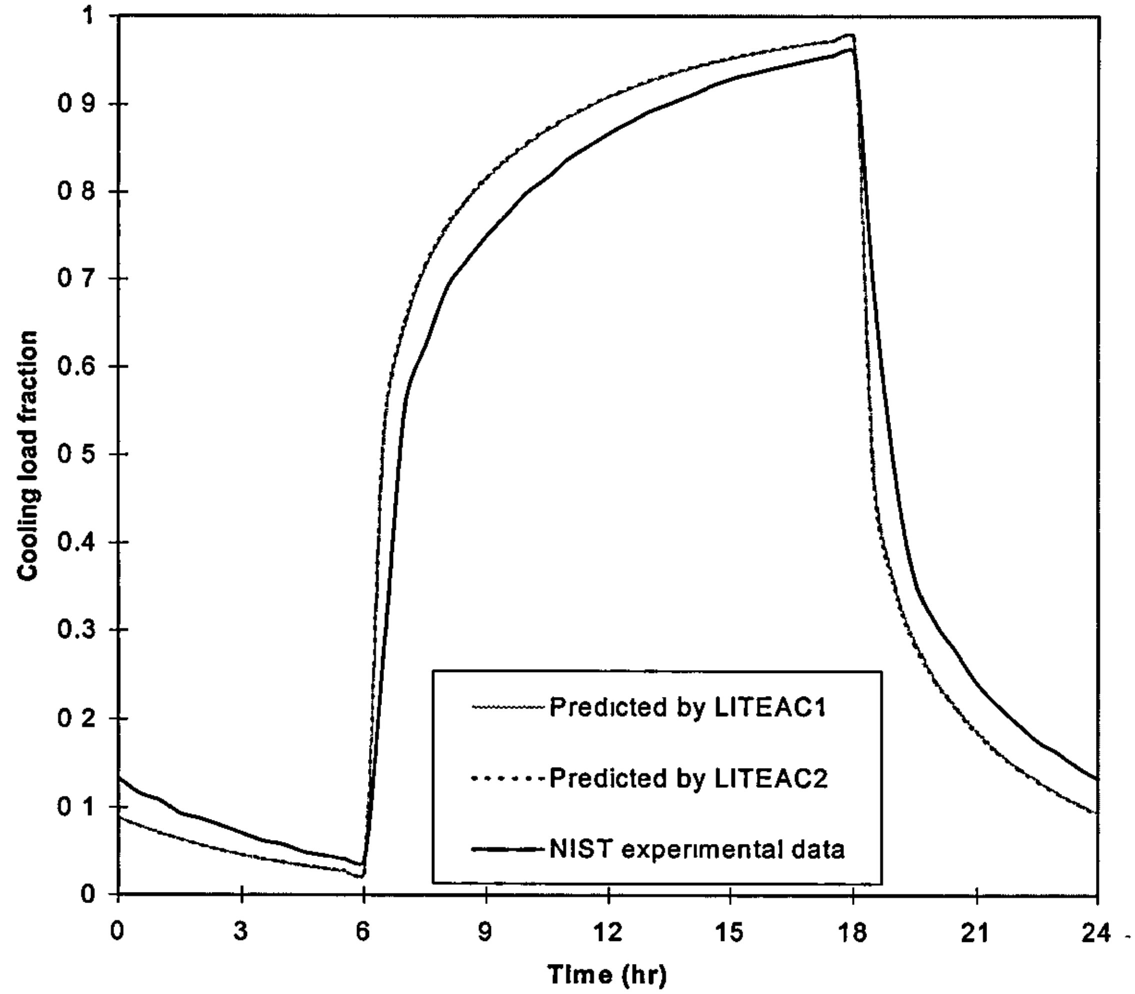

Figure 8.9

Cooling load fraction of NIST test cell for 'lights on/off cycles' test with the configuration of 4 × 2 lamp prismatic diffuser, ceiling grille return, airflow rate 0.0944 m^3s^{-1} and room air temperature 23.9°C. Comparison between LITEAC1, LITEAC2 and measured results.

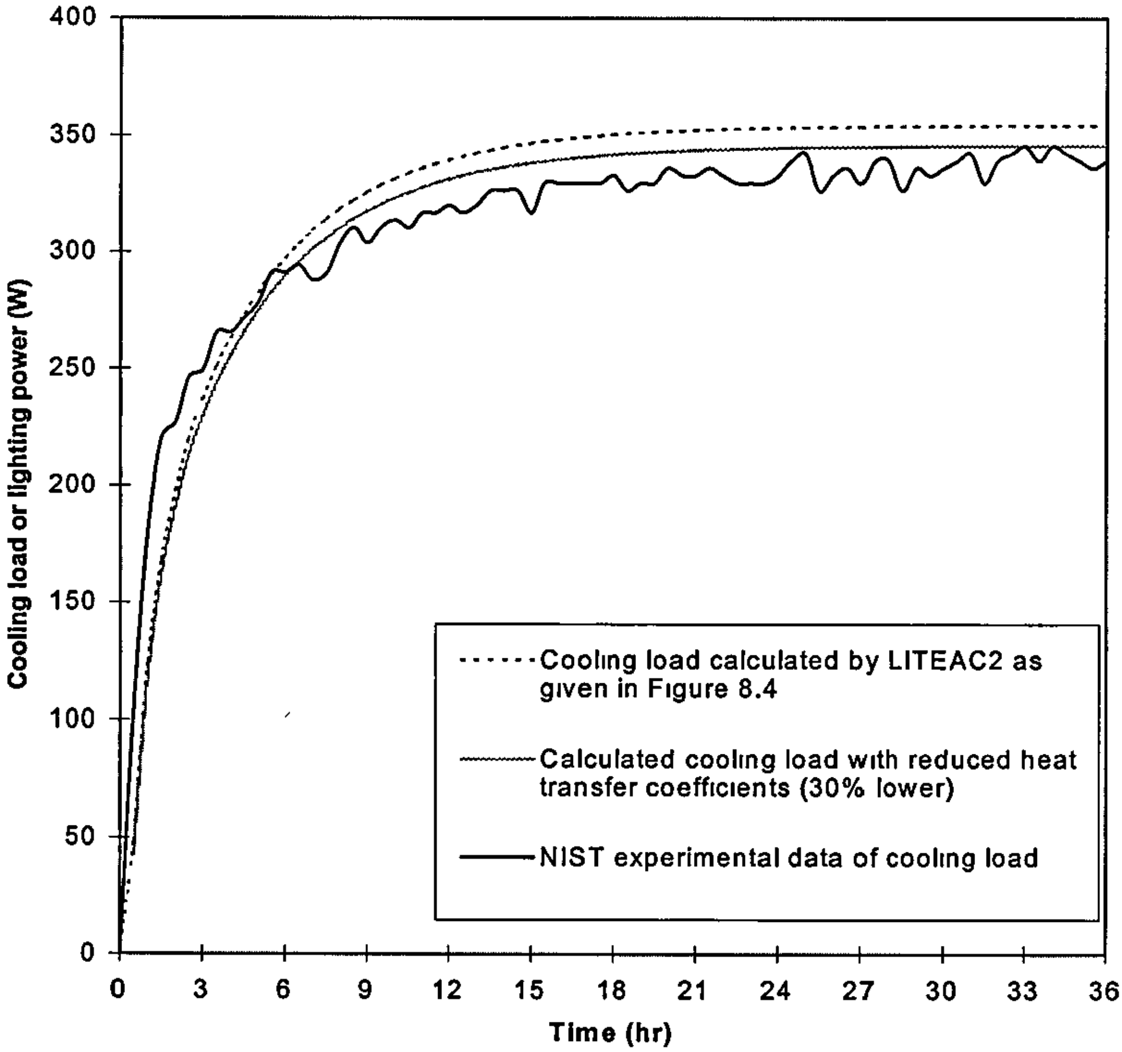

Figure 8.10

Effect on predicted cooling load with the convective heat transfer coefficients in the model data lowered by 30%.

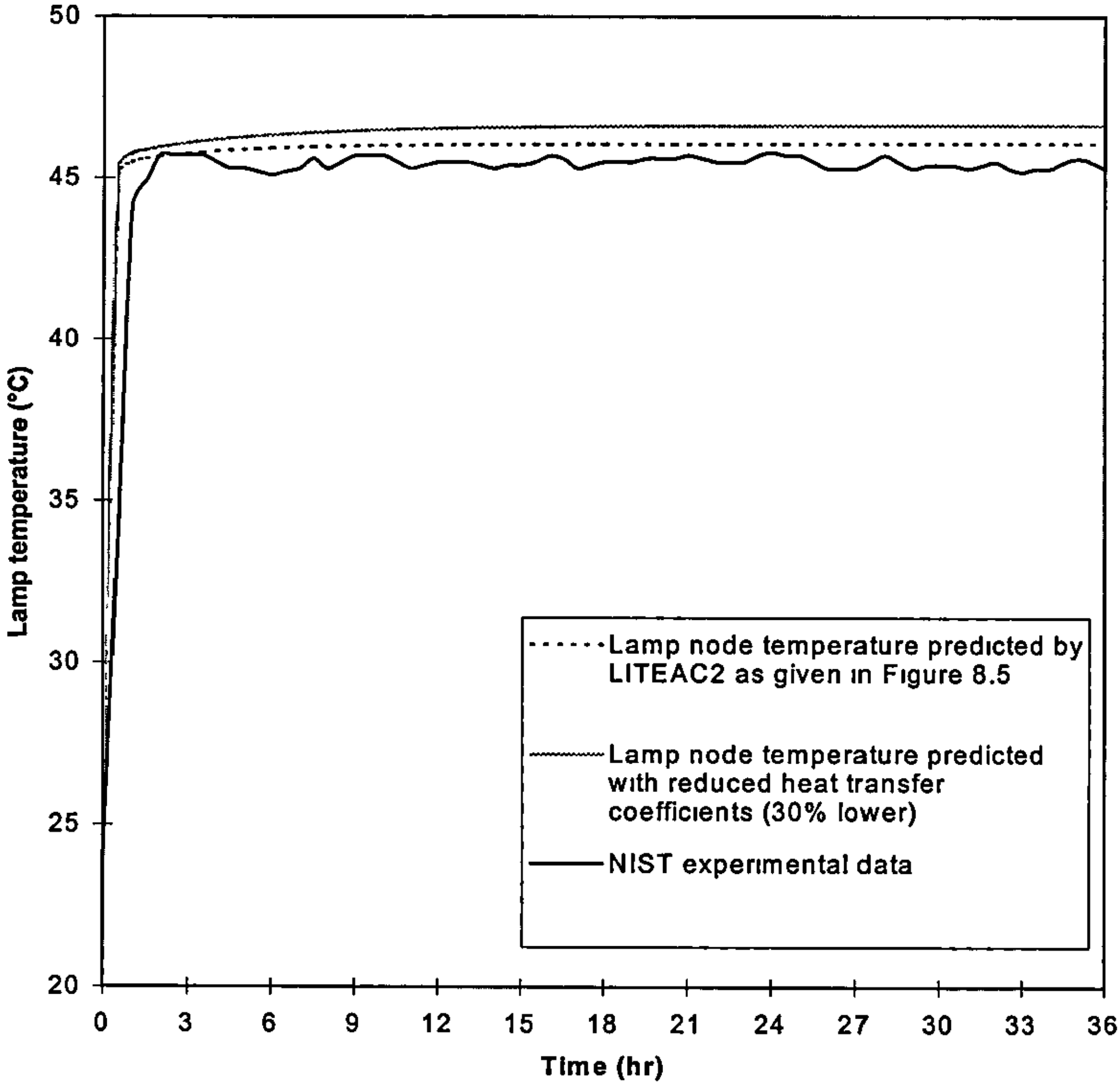

Figure 8.11

Effect on predicted lamp node temperature with the convective heat transfer coefficients in the model data lowered by 30%.

Chapter Nine

Further Experimental Validation of LITEAC1 and LITEAC2

9.1 The laboratory test cell

In the previous chapter, validation of the two models LITEAC1 and LITEAC2 using the published experimental data measured in the NIST full-scale test cell (Treado and Bean 1988, 1992) has been discussed. The dimensions of the NIST full-scale test cell were fixed, and although there is generally good agreement between simulated and experimental results, it would be useful to investigate whether the models give a similarly good agreement with experimental data for a cell of different dimensions.

The reasons for undertaking a further validation exercise using a laboratory test cell are:

(i) to test the validity of LITEAC1 and LITEAC2 in predicting illuminances for which data is not available in the NIST tests;

(ii) to measure the change of illuminance with respect to lamp wall temperature (by providing a wide range of supply air temperature into the test cell) so that illuminance predictions by LITEAC2 under different lamp wall temperatures can be validated.

(iii) to test the validity of LITEAC1 and LITEAC2 using an enclosure of non-typical dimensions.

A laboratory test cell containing a fluorescent luminaire, a 'plenum' or ceiling void, and a 'room space' was constructed for this further validation exercise. This cell was not intended to be a scaled down model of an office, but rather a room with small dimensions. This can be used to further validate the models LITEAC1 and LITEAC2 because the models are designed such that it can be used for different dimensions; suitable values for convective heat transfer coefficients and radiation form factors are required of course, as appropriate.

The cell is 1.5 m long, 1 m wide and 1 m high. It is constructed of plywood of thickness 9.5 mm, and insulated on the outer faces with expanded polystyrene of thickness 15 mm. The height of the cell is divided by a 'suspended ceiling' into a 'ceiling void' 0.2 m in height and a 'room space' 0.8 m in height. A 1200 mm × 300 mm fluorescent luminaire was installed at the centre of the 'suspended ceiling', with its axis along the length of the cell. The luminaire holds a 1200 mm long fluorescent lamp. Figure 9.1 illustrates the arrangement. Thermocouples were attached to the lamp and luminaire surfaces and to the walls, floor and ceiling surfaces as shown in Figure 9.1, for the measurement of node temperatures. One thermocouple was used for each node. An air-conditioning laboratory unit (manufactured by P.A. Hilton Ltd.) was used to supply cool air to the cell, for cooling load removal.

From the cell physical dimensions and its construction materials, data for the heat capacity, emissivity and reflectivity of the nodes were obtained from the ASHRAE Handbook (ASHRAE 1993). Radiation form factors were calculated from the physical dimensions using the view factor programs 'VF' and 'FACTS', which are included in 'LIGHTS' (Sowell 1989). Approximations were used in the calculation of form factors for surfaces inside the luminaire. Convective heat transfer coefficients were estimated for the geometries concerned using correlations given in Holman (1992). Conductance values were obtained from the ASHRAE Handbook (ASHRAE 1993). These data are shown in Appendix H.

9.2 Transient test results

To include both the 'lights on' and 'lights off' tests, experimental measurements were made for the case with the lamp switched on for 23 hours and then switched off. Measurements of temperatures at node surfaces were taken every minute for the first ten minutes after the lamp was switched on, then at every 10 minutes throughout the rest of the 'lamp on' period; this was repeated at every minute for the first ten minutes after the lamp was switched off and then at every 10 minutes for up to 10 hours after the lamp was switched off.

The preceding situation was simulated using both the LITEAC1 and LITEAC2 models, and the comparisons of the simulated results with the measured results are shown in figures 9.2 to 9.6. Figure 9.2 shows the temperatures of the two lamp nodes (upper and lower) plotted against time as measured and as predicted by LITEAC1 and LITEAC2. It can be seen from this figure that the lamp node temperatures predicted by LITEAC1 and LITEAC2 are very much the same as each other. The temperatures for the lamp upper node predicted by both LITEAC1 and LITEAC2 are very close to the experimentally measured values. However, the predicted lamp lower node temperatures of both models are about 2.8°C higher than the measured values. This can be explained by the fact that the predicted lamp lower node temperature represents the average temperature over the entire lower half of the lamp, while the measured lamp lower node temperature is the temperature measured at one point only. The discrepancy may also be partly due to uncertainty in the convection coefficient assumed for the lamp lower node.

Figure 9.3 shows the predicted and measured temperatures of two other luminaire nodes: luminaire air and luminaire housing. LITEAC1 and LITEAC2 gave almost identical results to one another for luminaire air and luminaire housing temperatures. The predicted temperatures are lower than the corresponding experimental values by 2 to 2.5°C. The discrepancy is believed to be due partly to experimental error in the measurement and partly to inaccuracy in the input data for heat transfer coefficients used in the simulations.

Figure 9.4 shows the predicted and measured temperatures for three plenum nodes: plenum air, luminaire housing top and ceiling. The figure shows again that the temperatures predicted by the two models LITEAC1 and LITEAC2 are very close to each other. The figure shows also that both the LITEAC1 and LITEAC2 models predicted values for plenum air temperatures which agree very closely with the measured values. The predicted luminaire housing top temperatures are about 1°C lower than the measured values, whilst the predicted ceiling temperatures are about 3.5°C lower than the measured values. The discrepancy between predicted and measured temperatures can be attributed to experimental error or to inaccuracy in the input data for heat transfer coefficients used in the simulations. The larger discrepancy of the calculated ceiling temperatures from the measured values may be due to the fact that the ceiling was not isothermal with the centre portion of the ceiling (which was just above the luminaire and subjected to higher radiation) being at a higher temperature. The ceiling temperature was measured by a thermocouple at its centre so that its reading could be considerably higher than the average temperature.

Figure 9.5 shows the temperature of three room nodes: room air, walls and floor. This figure shows again that there is no significant difference between the predicted temperatures by the two models. The figure shows also that there is good agreement between the simulated results of both models and the measured results, with differences of less than 0.3°C. The simulated results correctly predicted that the room air temperature was higher than the floor temperature which was in turn higher than the wall temperature.

Figure 9.6 shows a comparison of the floor illuminance predicted by LITEAC2 with that predicted by LITEAC1, and with the measured floor illuminance.

It can be seen from this figure that LITEAC2 gives a excellent agreement with the experimental data, while LITEAC1 gives illuminance values which are about 10% lower than the experimental values. This provides clear evidence that the positive column model in LITEAC2 can simulate the light output accurately even without input data of the total luminous flux output of the lamps. The discrepancy between the illuminance values predicted by LITEAC1 and the measured illuminance is considered to be due mainly to the inaccuracy in the input data for light output of the lamp and its variation with temperature.

9.3 Prediction of the change of illuminance with lamp wall temperature

In order to test the performance of LITEAC2 in predicting illuminance on room surfaces under different temperature conditions, experiments have been carried out using the laboratory constructed test cell with different supply air temperatures. In these experiments, the lamp wall temperatures were measured using three thermocouples attached to the lamp wall; the lowest of these three readings was taken to be the minimum lamp wall temperature. The minimum lamp wall temperatures that were obtained ranged from 17.4°C to 62.7°C. The corresponding average illuminances on the floor were measured using six lux meters. Simulations were then carried out using LITEAC2 for three cases with the test cell air temperature kept constant at 10°C, 25°C and 40°C. Predicted illuminance values at different minimum lamp wall temperatures ranging from 15°C to 65°C were extracted from the output data files. The predicted and the measured illuminances are plotted together in Figure 9.7. This figure shows that there is good agreement between the measured and the predicted illuminances. The illuminance values shown in Figure 9.7 for lamp wall temperatures of around 45°C were higher than those shown in Figure 9.6 because the prismatic diffuser (which was used in the tests shown in Figure 9.6) was removed for the experiments in which the data in Figure 9.7 were extracted from. The results from

Figures 9.6 and 9.7 therefore show that LITEAC2 predicts illuminance sufficiently well for different situations.

9.4 Summary

From the results presented, it can be concluded that both lighting and air-conditioning interaction models, LITEAC1 and LITEAC2, give predictions which are generally in good agreement with experimental data. Those discrepancies found have been attributed to experimental errors or inaccurate input data especially in terms of the convection coefficients. The assumption of isothermal surfaces in the measurement as well as simulation might also be a cause of the discrepancies between calculated and experimental data.

For LITEAC1 to give good predictions, good empirical curves to represent the change of lamp power and light output with lamp wall temperature must be obtained as input data. Lamp manufacturers do not normally include these data in their lamp data sheets or manuals. The incorporation of a fluorescent lamp positive column model into the lighting and air-conditioning interaction model LITEAC2 avoids the use of such empirical curves and gives improved predictions of the luminous flux output from lamps and hence room surface illuminances; predictions of temperature remain the same. The positive column model also permits a better understanding of the conversion of electrical energy into visible and invisible radiation, and then into heat.

The use of a laboratory-constructed test cell in this validation exercise shows that the models LITEAC1 and LITEAC2 can be applied to the simulation of lighting/HVAC interactions in a small enclosure. From the validation exercises described in chapter 8 and in the present chapter, there is evidence that the two models LITEAC1 and LITEAC2 are valid not only for a particular test cell or configuration, but also for different-sized enclosures in general. The validity of any model depends on the accuracy of its input data; for many cases, accurate input data such as that for heat transfer coefficients is difficult to obtain.

It is impossible and impractical to test the models for all types of dimensions of rooms found in practical cases. Even if time and resources permit extensive experimental measurements to be carried out for validation of theoretical models, discrepancies between experimental and theoretical results will always exist and it is never certain whether these discrepancies are due to experimental errors or model deficiencies.

In view of the good results obtained thus far, together with difficulties and expense encountered in experimentation, further validation of the models was considered unnecessary. The validation exercises carried out so far have already built confidence in the validity of the numerical models to be used as a tool for the simulation of lighting/HVAC interaction in enclosures.

In order to compare the performance of LITEAC2 with an existing model LIGHTS (Sowell 1989, 1990), which was validated using data from the NIST full-scale test facility, simulations were carried out using LITEAC2 and LIGHTS for the NIST configuration used in the validation of LIGHTS, and also for the laboratory test cell. The results of these simulations will be discussed in the next chapter.

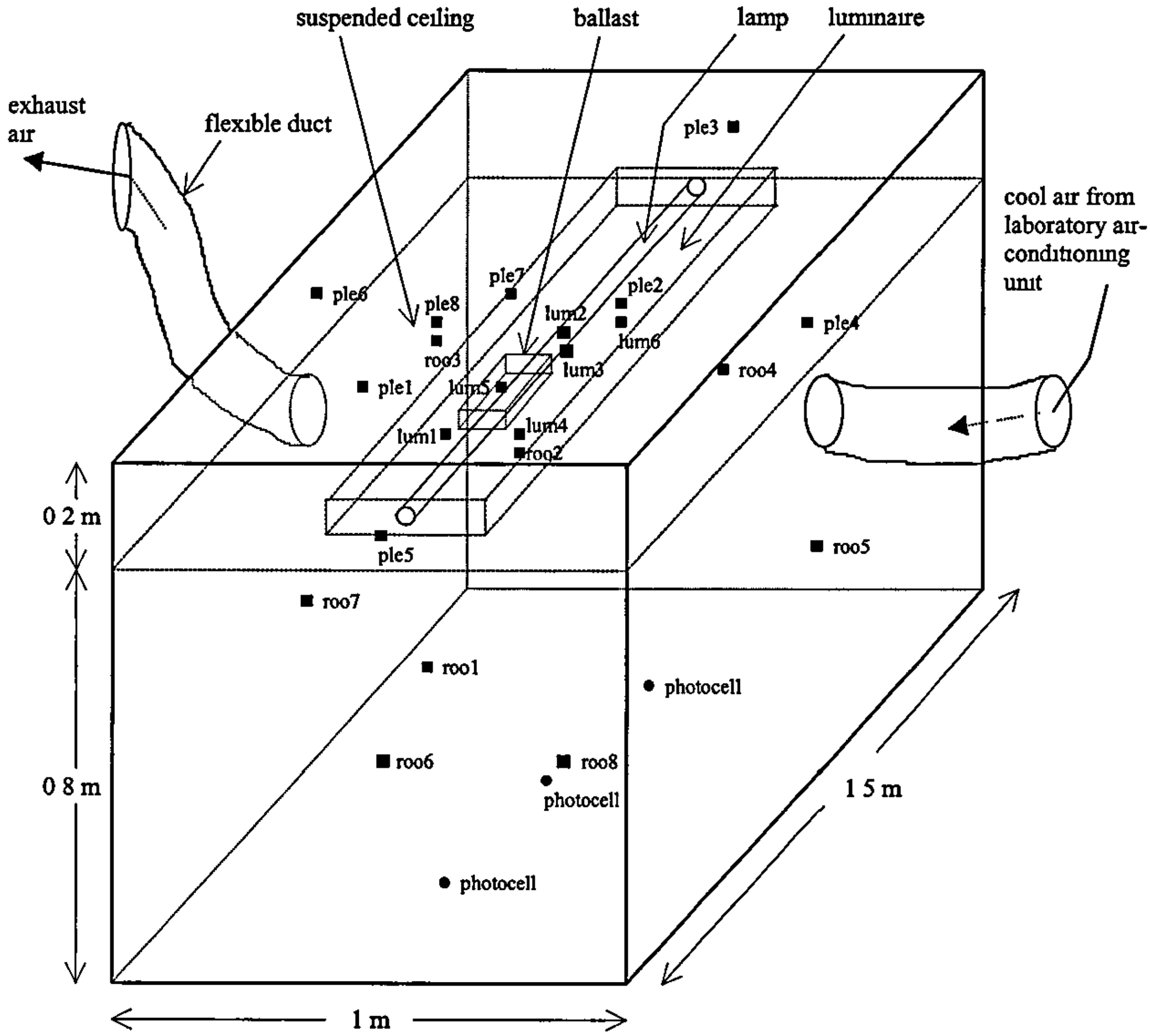

■ Positions of thermocouples for measurement of node temperatures with node code indicated

● Positions of photocells for measurement of floor illuminance

Nodes

lum1	luminaire air	roo1	conditioned space air
lum2	lamp upper	roo2	luminaire diffuser bottom (outside luminaire)
lum3	lamp lower	roo3	suspended ceiling bottom
lum4	luminaire diffuser top (inside luminaire)	roo4	east wall
lum5	ballast	roo5	south wall
lum6	luminaire housing bottom (inside luminaire)	roo6	west wall
ple1	plenum air	roo7	north wall
ple2	luminaire housing top (outside luminaire)	roo8	floor surface
ple3	east plenum wall		
ple4	south plenum wall		
ple5	west plenum wall		
ple6	north plenum wall		
ple7	ceiling		
ple8	suspended ceiling top (plenum side)		

Figure 9.1
Schematic diagram of the laboratory test cell with positions of the thermocouples and photocells indicated.

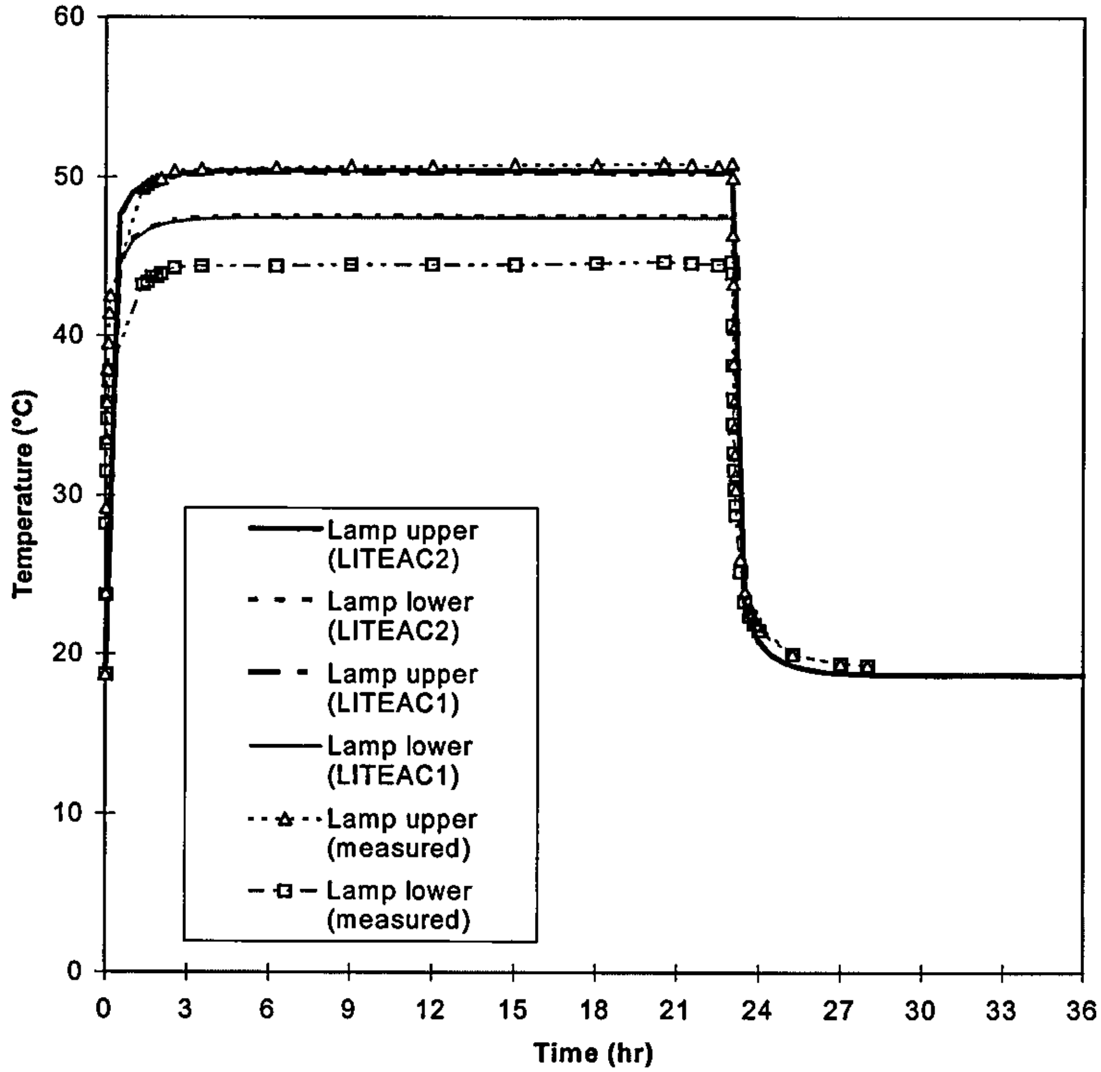

Figure 9.2

Lamp node temperatures in laboratory constructed test cell - comparison between LITEAC1 and LITEAC2 predictions, and measured results.

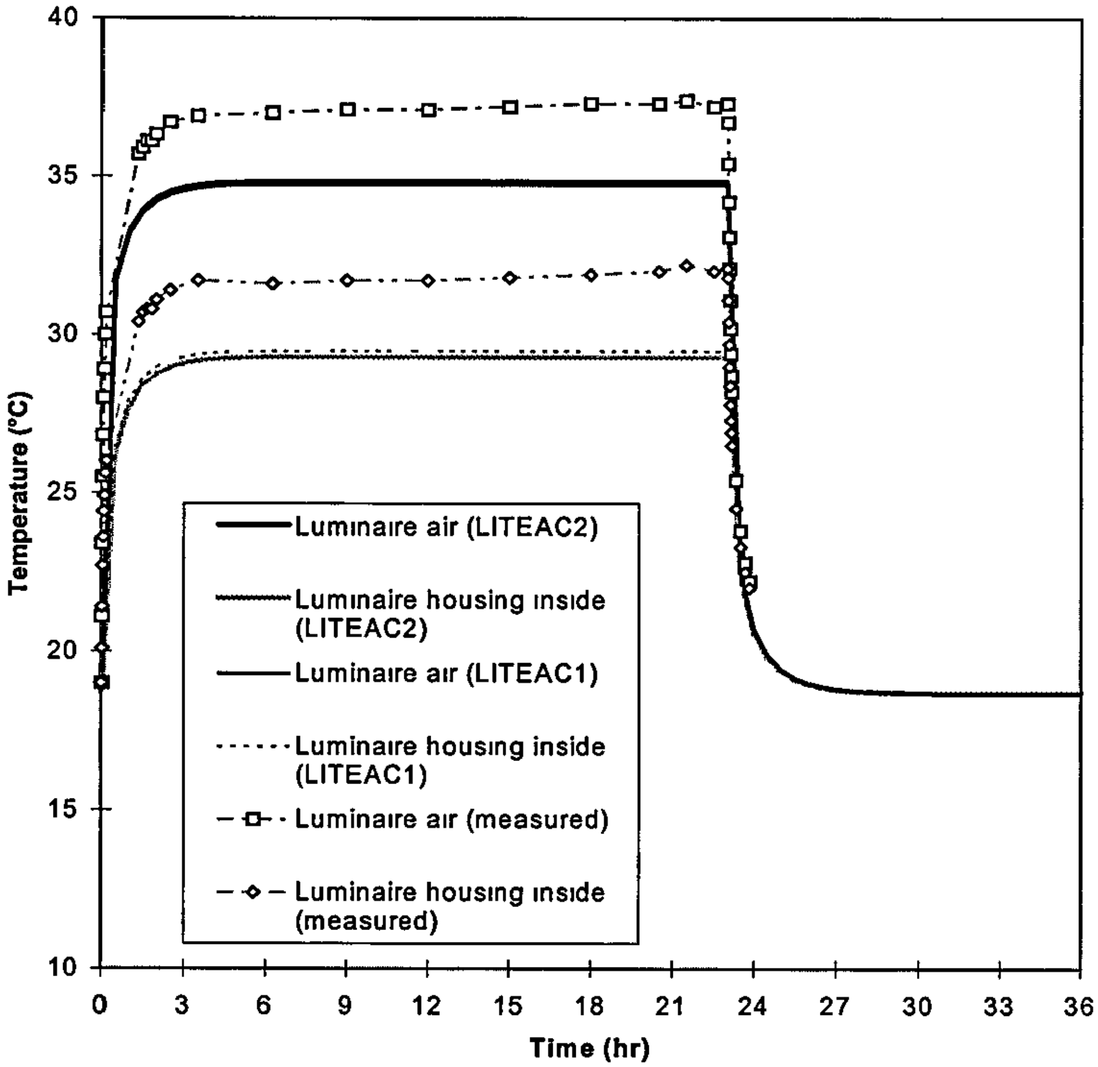

Figure 9.3

Luminaire air and housing temperatures of laboratory test cell - comparison between LITEAC1 and LITEAC2 predictions, and measured results.
(Note: Luminaire temperatures predicted by LITEAC1 and by LITEAC2 are very close and therefore appear almost as a single line in this figure.)

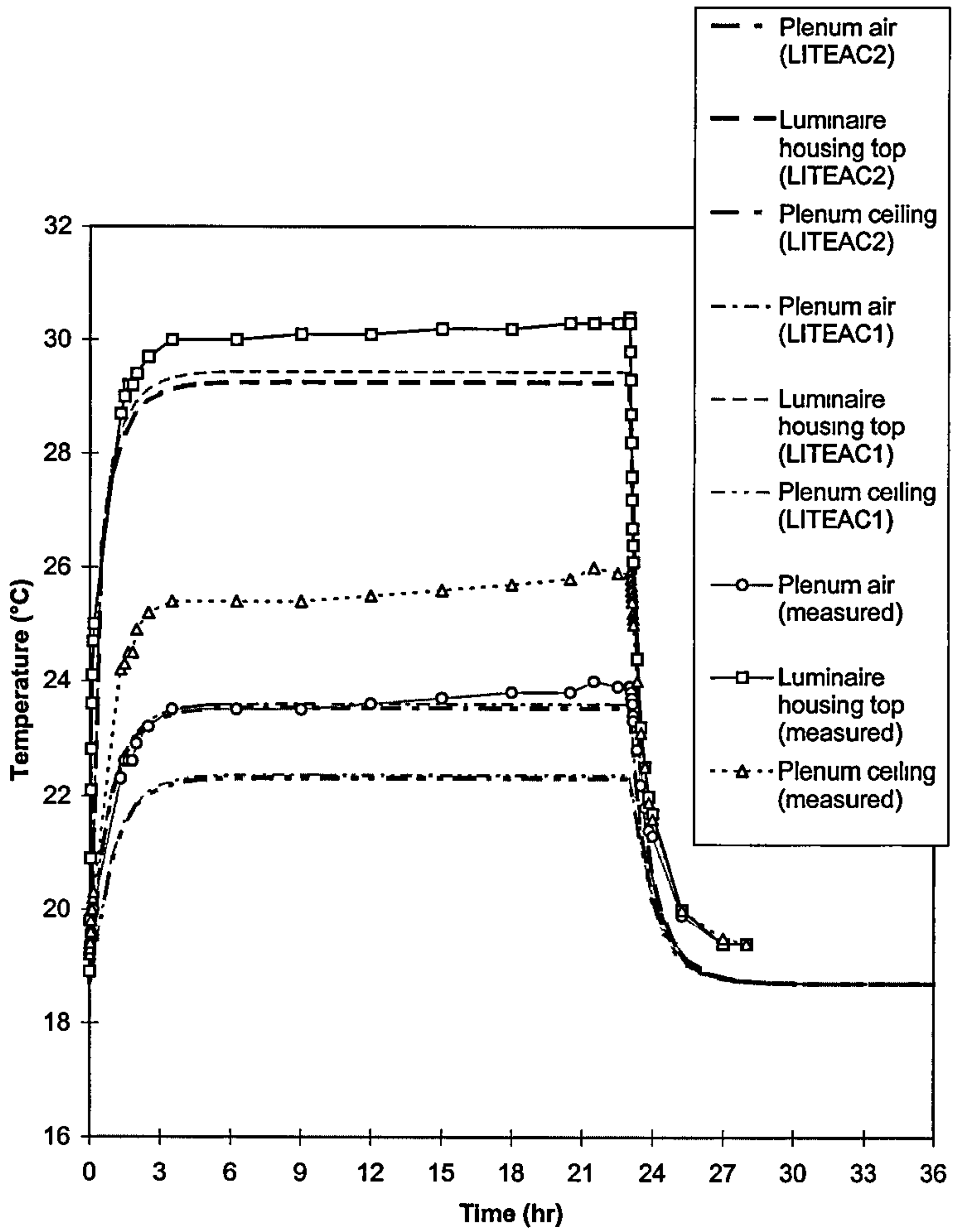

Figure 9.4

Plenum node temperatures of laboratory test cell - comparison between LITEAC1 and LITEAC2 preedictions, and measured results.

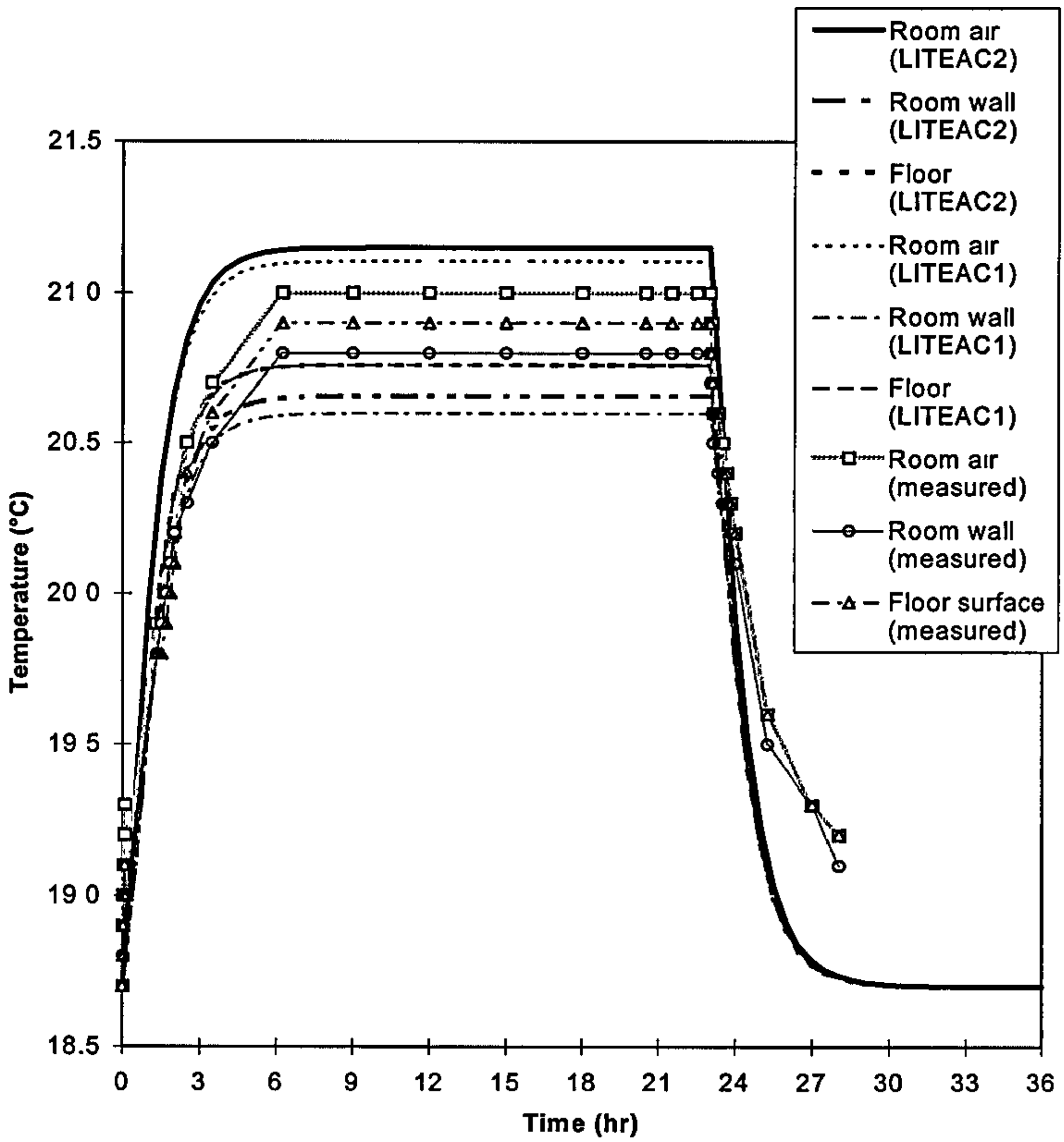

Figure 9.5

Room node temperatures of laboratory test cell - comparison between LITEAC1 and LITEAC2 predictions, and measured results.

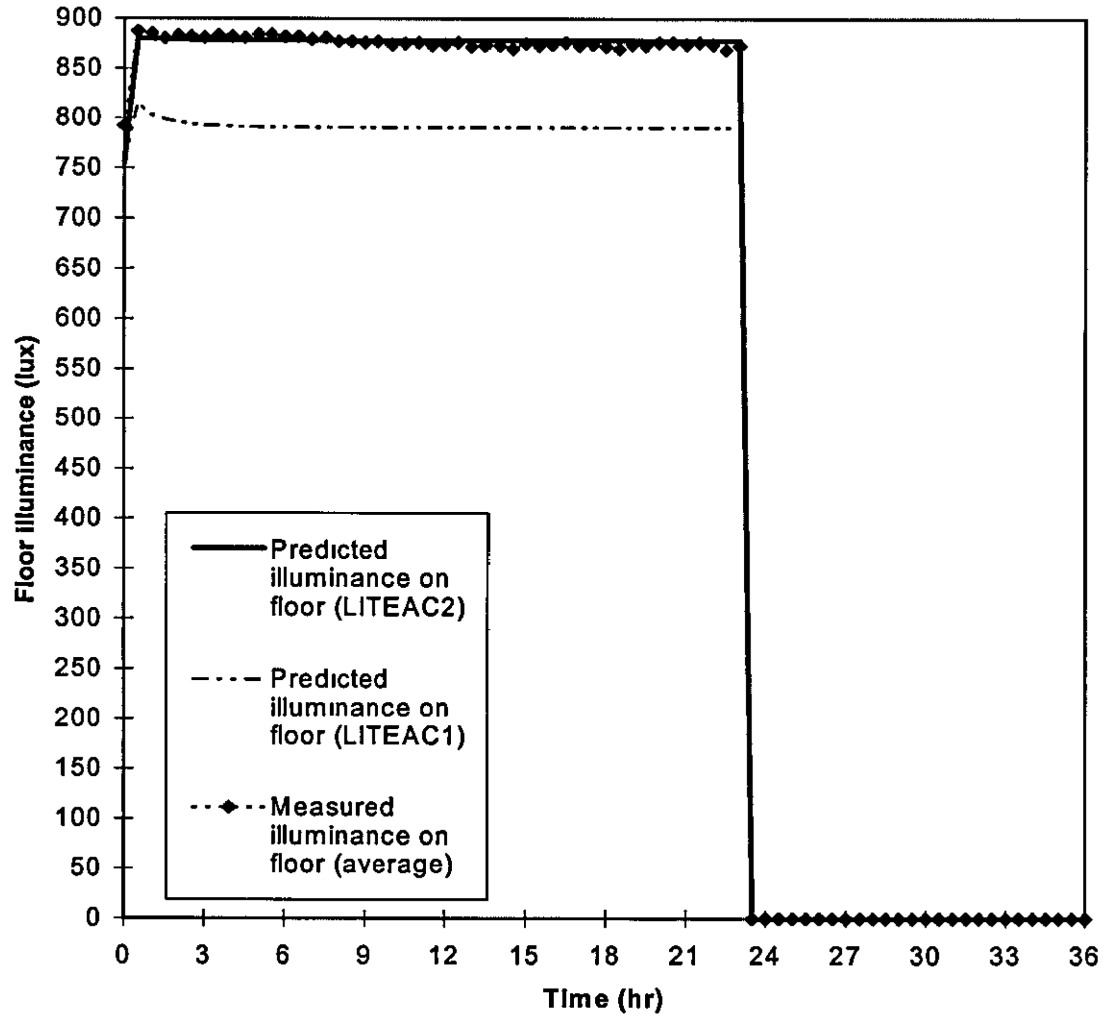

Figure 9.6

Floor illuminance of laboratory test cell - comparison between LITEAC1 and LITEAC2 predictions, and measured results.

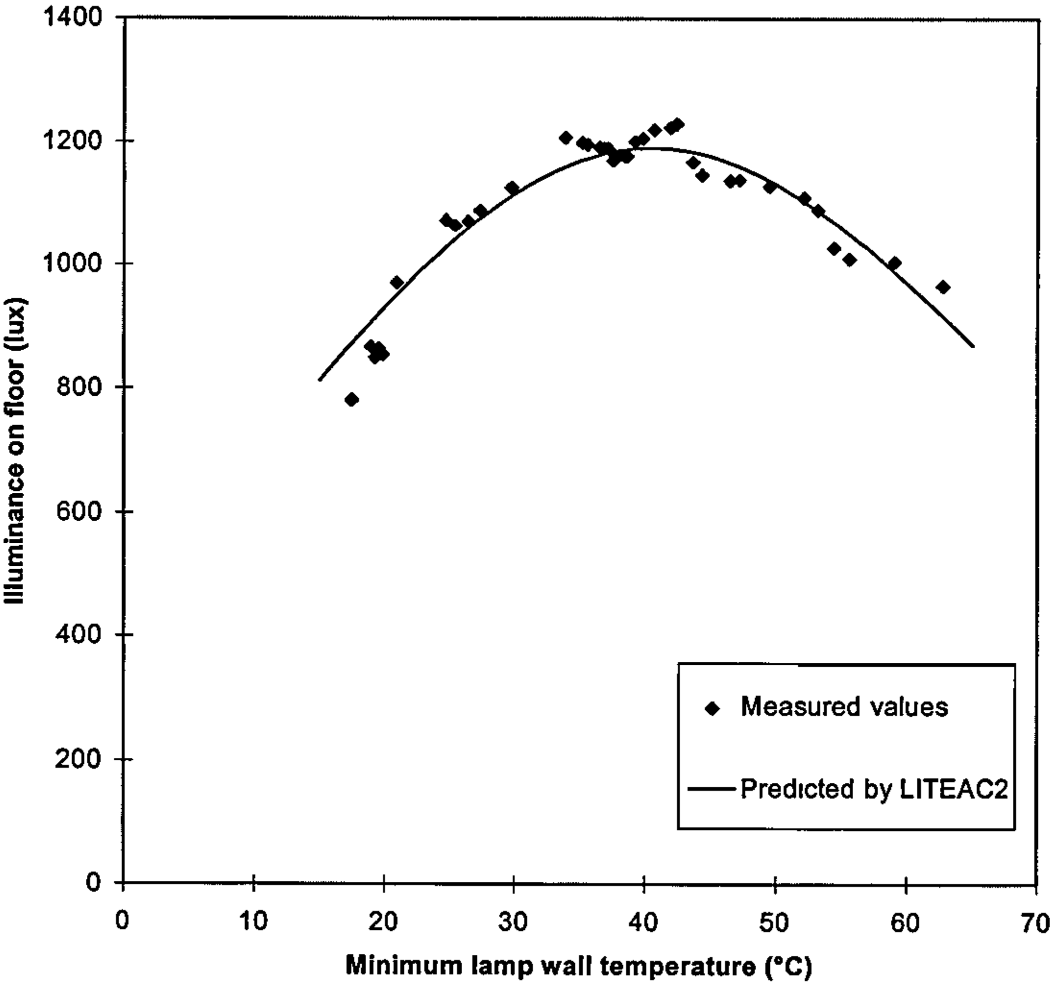

Figure 9.7

LITEAC2-predicted and measured illuminance at various minimum lamp wall temperatures for the laboratory test cell configuration.

Chapter Ten

Comparison with LIGHTS

- a Published Lighting/HVAC Numerical Model

10.1 Introduction

In Chapters 8 and 9, details of the validation of the two models LITEAC1 and LITEAC2 have been presented for the cases of a full-scale test room and a laboratory constructed test cell. To investigate the performance of the models developed in this research, LITEAC1 and LITEAC2 are compared with an existing numerical model called LIGHTS (Sowell 1989, 1990) which has been claimed to qualify as a "numerical lighting/HVAC test cell". The comparison was carried out using a particular configuration of the NIST tests and also the experimental data obtained from the laboratory constructed test cell.

10.2 Summary of LIGHTS

It was already mentioned in Chapter 2 that Sowell (1989, 1990) developed the numerical lighting/HVAC test cell which is called 'LIGHTS'. The LIGHTS program was designed to allow modelling of the thermal and luminous performance of lighting systems in buildings. According to Sowell (1989), LIGHTS is sufficiently general to allow representation of almost any lighting configuration, room construction or size, and HVAC airflow path. Once a room has been defined, its dynamic operation can be simulated by LIGHTS over a specified period. The results of the simulation include temperatures of surfaces and air masses, heat flows at various places in the room, and short wave (luminous) and long wave (thermal) radiation flux flow rates at all surfaces.

Sowell (1989) stated that LIGHTS was intended primarily for researchers interested in modelling the thermal and luminous processes in a room at a relatively high level of detail. Similar to LITEAC1 and LITEAC2, LIGHTS requires a considerable amount of input data. For example, the required input data for a detailed representation includes short and long wave radiative properties of all surfaces, convection coefficients at all air/surface boundaries, conduction and mass properties of all solid elements, and lamp performance as a function of wavelength and temperature. Additionally, the initial temperatures must be given or assumed for all surfaces and air masses. However, for most configurations detailed input data are not always available and some approximations and/or estimations have to be made in the input data.

According to Sowell (1989), the mathematics of LIGHTS is rigorous. LIGHTS is a completely general, lumped parameter thermal and luminous representation of the building zone, including the lighting and HVAC systems. LIGHTS is based on an earlier steady state model developed by Sowell and O'Brien (1973). In this steady state model, the basic equation employed is, in vector-matrix form:

$$Q^o - U^c(T)\cdot T - A^m \cdot V^s \cdot J^{os} - A^m \cdot V^l \cdot J^{ol}(T) = 0 \tag{10.1}$$

In the above equation, the first term Q^o represents the vector of source powers at each node, and the term $U^c(T)\cdot T$ represents conductive/convective heat transfer away from each of these nodes. T is the vector of nodal temperatures which must satisfy this equation. The other two terms represent net radiative transport away from each node in the short- and long-wave ranges, respectively. Each of these can be further sub-divided into a number of bands for more detailed analysis if the radiative properties are known for each individual band. In these terms A^m is a diagonal matrix of surface areas, V^s and V^l are special transfer matrices describing inter-reflections and transmissions within the enclosure(s) for the short- and long-wave bands, respectively, and J^{os} and J^{ol} are matrices of source radiation terms at each node in the short- and long-wave bands, respectively. The right hand side is a zero vector, indicating a power balance at steady state. This equation is non-linear due to temperature dependence of the terms Q^o, U^c and J^{ol}.

LIGHTS, as a dynamic model, is an extension of the steady state model of Sowell and O'Brien (1973). The transient state is taken into account by adding finite heat capacitance for some nodes. Then, equation (10.1) becomes:

$$M \cdot \dot{T} = Q^o - U^c \cdot T - A^m \cdot \sum_{j}^{m} V_j \cdot J_j^o \tag{10.2}$$

where M is a diagonal matrix of heat capacitances and $\dot{T}$ is the time derivative of the nodal temperature vector. To facilitate solution, Sowell (1989) partitioned the vector of nodes into nodes with finite thermal mass and those declared to be massless. Then the above equation becomes:

$$\begin{bmatrix} 0 & 0 \\ 0 & M_d \end{bmatrix} \cdot \begin{bmatrix} \dot{T}_s \\ \dot{T}_d \end{bmatrix} = \begin{bmatrix} Q_s^o \\ Q_d^o \end{bmatrix} - \begin{bmatrix} U_{11}^c & U_{12}^c \\ U_{21}^c & U_{22}^c \end{bmatrix} \begin{bmatrix} T_s \\ T_d \end{bmatrix} - \begin{bmatrix} A_{11} & 0 \\ 0 & A_{22} \end{bmatrix} \sum_j \begin{bmatrix} V_{11} & V_{12} \\ V_{21} & V_{22} \end{bmatrix} \begin{bmatrix} J_s^o \\ J_d^o \end{bmatrix} \tag{10.3}$$

where the subscripts s and d denote steady-state quantities and dynamic quantities, respectively.

Matrix algebra then leads to an equation exactly like the steady state equation (10.1) but with the temperature vector representing only the nodes which are assumed to be massless (called algebric nodes in Sowell 1990), and a specially defined Q^o term, Q_d^o which represents the effect of net heat transfer from the dynamic nodes. The remainder of the partitioned set is exactly like equation (10.2), but involves only the dynamic nodes in the time derivative temperature vector. That is,

$$M_d \cdot \dot{T}_d = Q_d^o - U_{21}^c \cdot T_s - U_{22}^c \cdot T_d - A_{22} \cdot \sum_j \left(V_{21} \cdot J_s^o + V_{22} \cdot J_d^o\right) \tag{10.4}$$

The result of the partitioning is a set of algebraic equations representing nodes which are assumed to be massless and a set of differential equations governing massive nodes. These two sets of equations are coupled through the temperature vector.

LIGHTS uses the following solution scheme as described by Sowell (1989). With initial conditions defined, the algebraic set is solved using Newton-Raphson iteration. The differential set is then solved after the next time step, using a variable time step, predictor-corrector method. In each corrector step, the algebraic set is solved again, since the temperature of the algebraic nodes must be updated as the dynamic node temperatures adjust to their new values. Also, because lamp and ballast power and luminous output depend on lamp wall temperature, the luminous flux calculations must be repeated at each step toward convergence. The process is then repeated throughout the period of interest. Truncation error is controlled within a user-specified range by automatic adjustment of the integration time step.

LIGHTS reads zone geometric, thermal, and radiative properties from an input file. Also, the input file includes definition of which nodes are to be held at constant temperature, and which are to be held at specified net heat transfer rates. LIGHTS uses a convenient scheme to specify nodal power versus time so that various on/off tests can be simulated. The input file also includes a user defined thermal mass threshold so that any node with thermal mass less than the threshold is treated as massless. In this way, LIGHTS allows steady state solutions to be obtained without a long dynamic simulation, and without changes to the model itself; one merely sets a high mass threshold so that all nodes are treated as massless.

LIGHTS gives output to a file which can consist of input echo, user-defined intermediate reports, and final state reports of temperature, net heat flux, and radiative and convective transfer rates at each node and through each path. User-defined reports allow output of requested quantities (temperatures, heat fluxes, etc.) at selected nodes and at selected times.

By modern standards, LIGHTS is not considered to be a "user friendly" program. The user must know exactly how to create the input file. He/she must also know how to avoid program instability. For these reasons, it is unlikely that LIGHTS will satisfy the requirements of lighting and/or HVAC designers for performing design calculations using simple-to-use practical software. Sowell (1989) classified LIGHTS as a research tool for the study of the interaction between lighting and HVAC systems.

10.3 Comparison of LIGHTS and LITEAC2 simulations of the NIST test cell

Since the simulation results of node temperatures using LITEAC1 and LITEAC2 are found to be very similar to those presented in Chapter 8, only the results of LITEAC2 will be compared here with the results of LIGHTS. The same configuration (configuration number 42101) as that described in Section 8.5 is used for this comparison exercise. Details of this configuration have been described in Section 8.5 and therefore will not be repeated. This particular configuration is selected for the comparison exercise because more details are available for this configuration than for the others and Sowell (1990) himself used this configuration for validation of the LIGHTS model.

Figure 10.1 shows the LITEAC2 and LIGHTS simulated lighting powers and cooling loads, together with the NIST test results. This figure shows that LITEAC2 and LIGHTS give very close results for the lighting power and both simulated lighting power curves fit the experimental data excellently. It is not surprising that there is good agreement between the LIGHTS simulated lighting power and the measured lighting power as the lamp power is an input to LIGHTS. On the other hand, the lamp power in LITEAC2 is calculated by the fluorescent lamp positive column model and the good agreement between predicted and measured values here shows that the positive column model is capable of simulating the lamp power correctly.

Figure 10.1 shows also that there is good agreement between the cooling load curves predicted by LITEAC2 and by LIGHTS, and that these predictions fit closely the experimental data. The small difference between the two predicted curves is insignificant in view of the possible experimental error as discussed in Section 8.6.

Figure 10.2 shows the lamp node temperature plotted against time from simulations using LITEAC2 and LIGHTS. Also shown in this figure are the measured lamp temperatures in the NIST test cell as reported by Sowell (1990). The two simulation-based curves agree closely with each other, and both fit the experimental data well. The lamp node temperatures predicted by LITEAC2 are closer to the measured results than are the LIGHTS-predicted values, by about 0.2°C.

Figure 10.3 shows the plenum ceiling temperatures predicted both by LITEAC2 and by LIGHTS, together with the measured results. LIGHTS-predicted plenum temperatures are about 0.2°C closer to the measured data than are the LITEAC2-predicted temperatures. However, this small difference is insignificant in view of the possible experimental error as discussed in Section 8.6.

Figure 10.4 shows the temperatures of the room floor surface. Both LITEAC2 and LIGHTS give simulated temperatures slightly higher than the measured results.

LITEAC2-predicted floor temperatures are about 0.5°C higher than those predicted by LIGHTS. Again, the difference is within experimental error and LITEAC2 and LIGHTS are as good as each other.

As shown in Figures 10.1-10.4, there is no significant difference between the simulation results using LITEAC2 and that using the LIGHTS model. However, significant differences did occur between the computation times required: using a fixed time step of 1 second and a simulated period of 96 hours, and running on a personal computer with an Intel Pentium-100MHz processor, LITEAC2 required 12 minutes of computation time whilst LIGHTS required 3 hours and 37 minutes of computation time. The LIGHTS model can run faster if the time step is allowed to vary between a minimum and a maximum. Even with a minimum time step of 0.36 seconds and a maximum time step of 18 seconds, 15 minutes of extra computation time (compared with LITEAC2) was required for LIGHTS to complete a simulation run with the same configuration.

10.4 The laboratory test cell

The laboratory-constructed test cell described in Chapter 9 was also simulated using LIGHTS. Simulation results using LITEAC2 are already described in Chapter 9, and are compared here with those from LIGHTS.

Figure 10.5 shows the temperature of the two lamp nodes as predicted by LITEAC2 and by LIGHTS, together with the measured values. The figure shows that LITEAC2 gives a better fit to the measured lamp node temperatures than does LIGHTS. The LIGHTS-simulated temperatures are much higher than the measured temperatures. The difference between LITEAC2-simulated temperatures and LIGHTS-simulated temperatures is larger in this case than in the NIST case (Figure 10.2).

Figure 10.6 shows the comparison between LITEAC2 and LIGHTS in respect to two other luminaire node temperatures: luminaire air and luminaire housing. It can be seen from the figure that both LITEAC2 and LIGHTS give very similar results with differences of less than 0.5°C. Both results fit the experimental data reasonably well, with reasons for small discrepancies explained in Section 9.2.

Figure 10.7 shows the comparison between LITEAC2 and LIGHTS in respect to three nodes in the plenum compartment: plenum air, luminaire housing top and plenum ceiling. For these nodes, LITEAC2 and LIGHTS simulations are very close to each other, with differences of less than 0.8°C. For plenum air and luminaire housing top temperatures, simulated results from both LITEAC2 and LIGHTS fit the experimental data reasonably well. The reasons for the relatively larger discrepancy between model-predicted and experimentally-measured results of plenum ceiling temperatures have been explained in Section 9.2.

Figure 10.8 shows the comparison between LITEAC2 and LIGHTS in respect to three room nodes: room air, room walls and floor. The scale of this figure is magnified for clarity because temperatures between hour 5 and hour 23 fall within the one degree range 20.6° to 21.6°C. It can be seen from the figure that there is good agreement between the simulated temperatures from both LITEAC2 and LIGHTS and the measured values. Both models correctly predicted that the room air had the highest temperature amongst the three nodes followed by the floor and then the room wall. However, while LITEAC2 predicted temperatures that are closer to the experimental data, LIGHTS predicted temperatures that are about 0.5°C higher than the LITEAC2-predicted temperatures.

LIGHTS does not give output of illuminance on surfaces directly, whereas LITEAC2 is able to do this. A comparison between the LITEAC2-predicted illuminance and the measured illuminance was already discussed in Section 9.2 (Figure 9.6).

10.5 Summary

In this chapter, the performance of LITEAC2 is compared with the existing model LIGHTS which has been claimed to be a "numerical lighting/HVAC test cell". The comparison is performed with respect to a selected configuration of the NIST tests, and also the test configuration carried out in the specially made laboratory test cell.

Figures 10.1-10.8 show that the simulation results of LITEAC2 and LIGHTS are close to each other. These results show that both models are similar in respect to simulation of lighting power, cooling load and temperature. However, for all cases simulated, LITEAC2 runs faster than LIGHTS on a personal computer. More importantly, LITEAC2 gives good predictions for illuminance on room surfaces, a capability which LIGHTS does not process.

Based on the comparisons made between the two models LITEAC2 and LIGHTS, it can be said that both models give reasonably good predictions of lighting power, cooling load and temperatures. However, LITEAC2 is superior to LIGHTS in at least two respects; firstly, it runs faster on a personal computer and, secondly, it calculates with reasonable accuracy the illuminance on room surfaces.

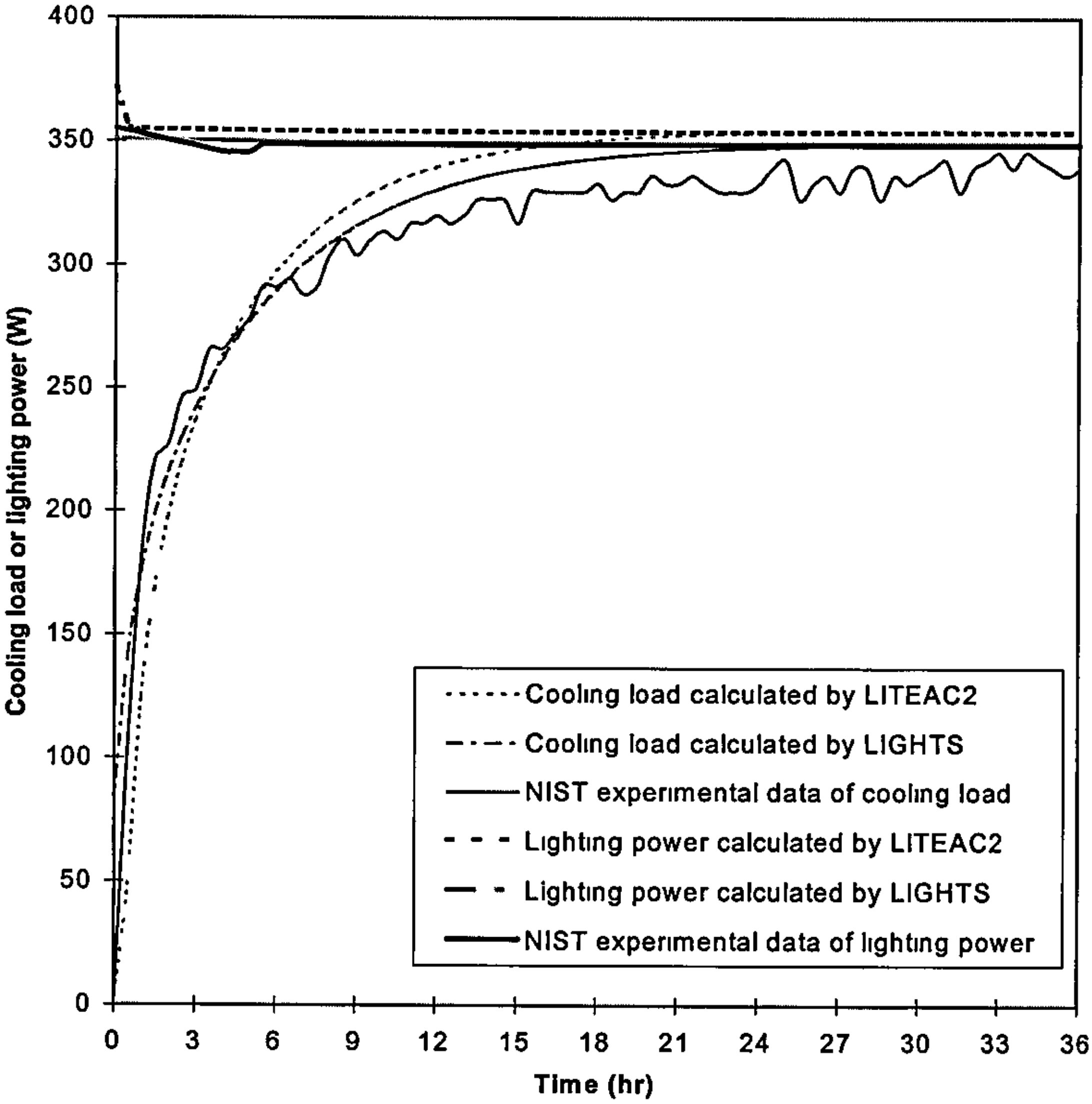

Figure 10.1

Lighting power and cooling load in NIST test cell - comparison between LITEAC2 and LIGHTS predictions, and measured results.

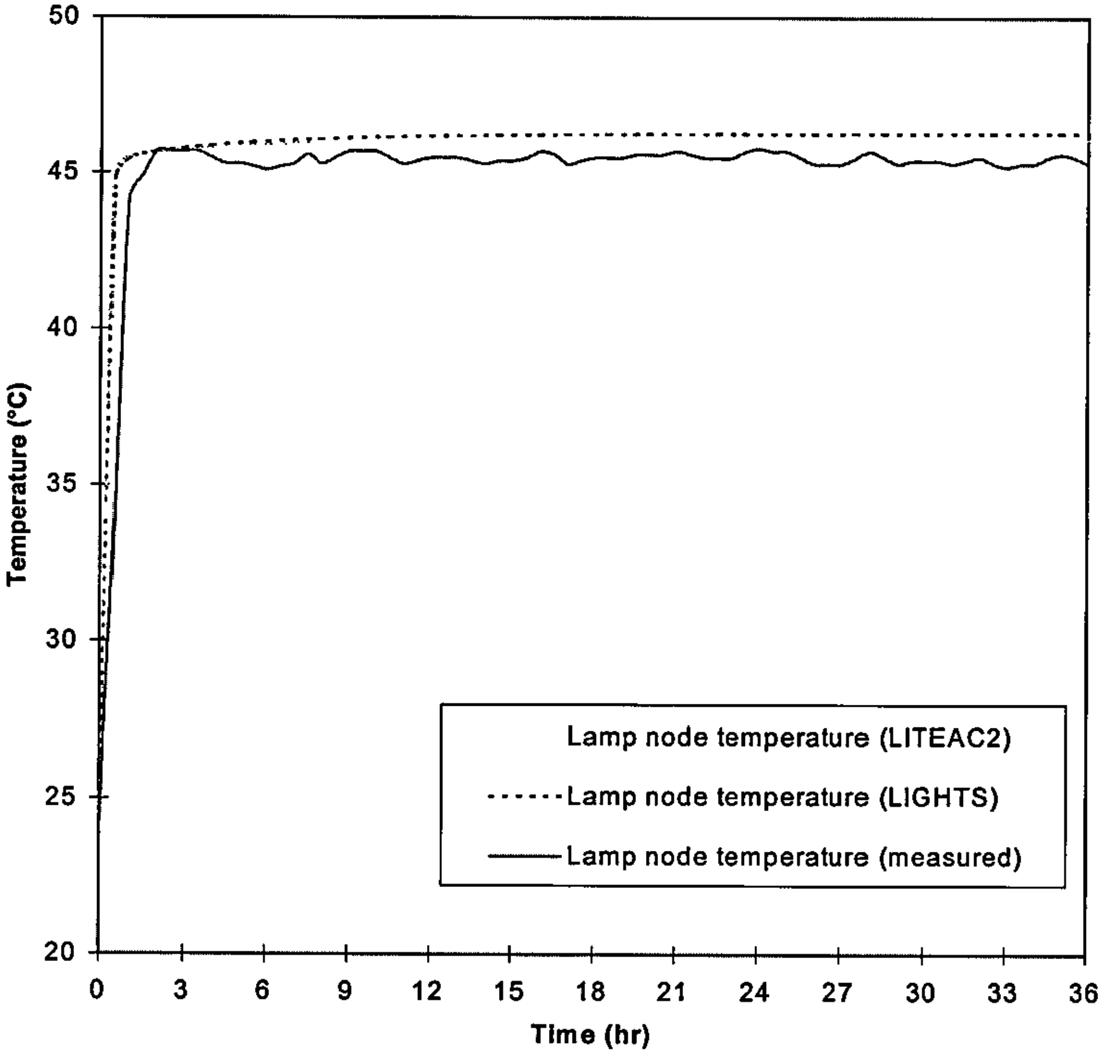

Figure 10.2

Lamp node temperatures in NIST test cell - comparison between LITEAC2 and LIGHTS predictions, and measured results.

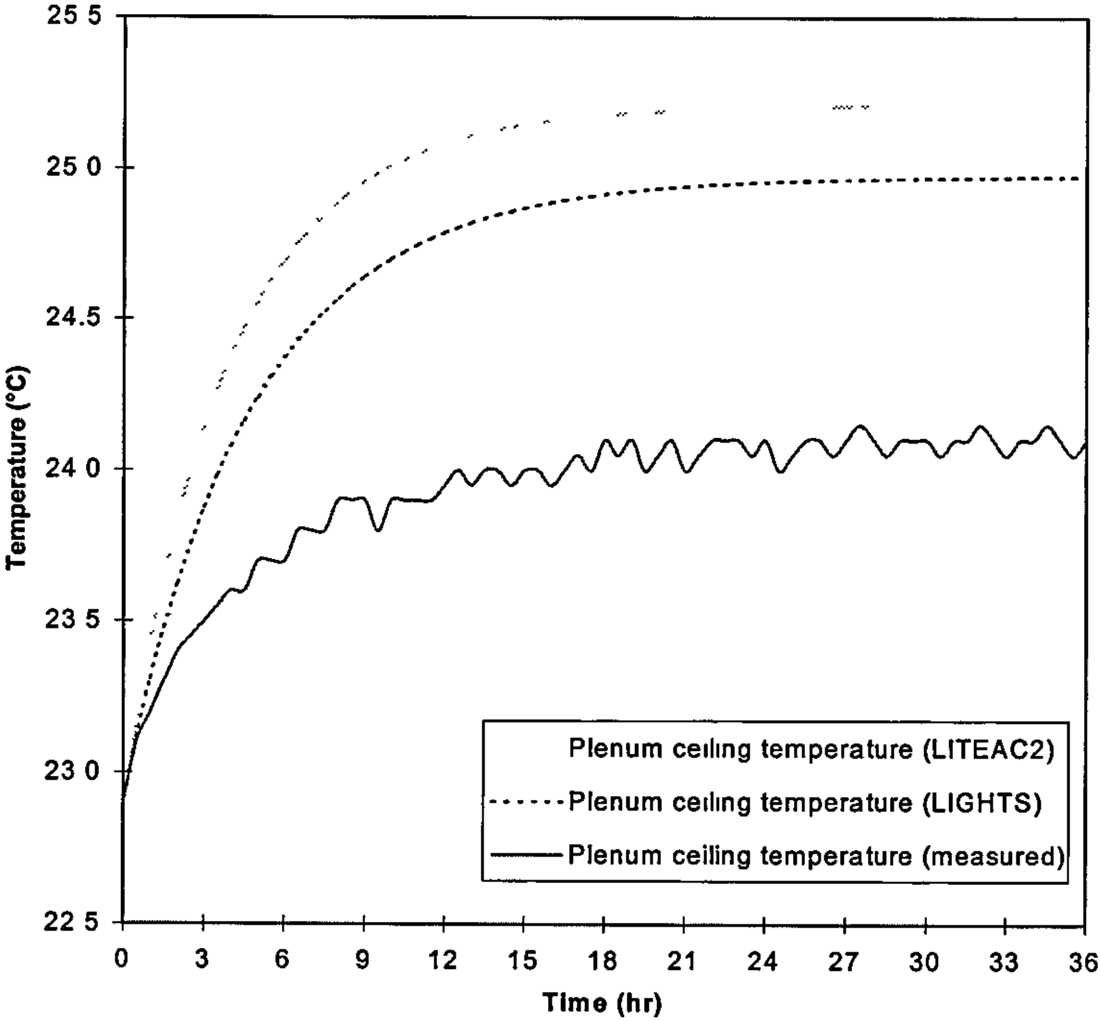

Figure 10.3

Plenum ceiling temperatures in NIST test cell - comparison between LITEAC2 and LIGHTS predictions, and measured results.

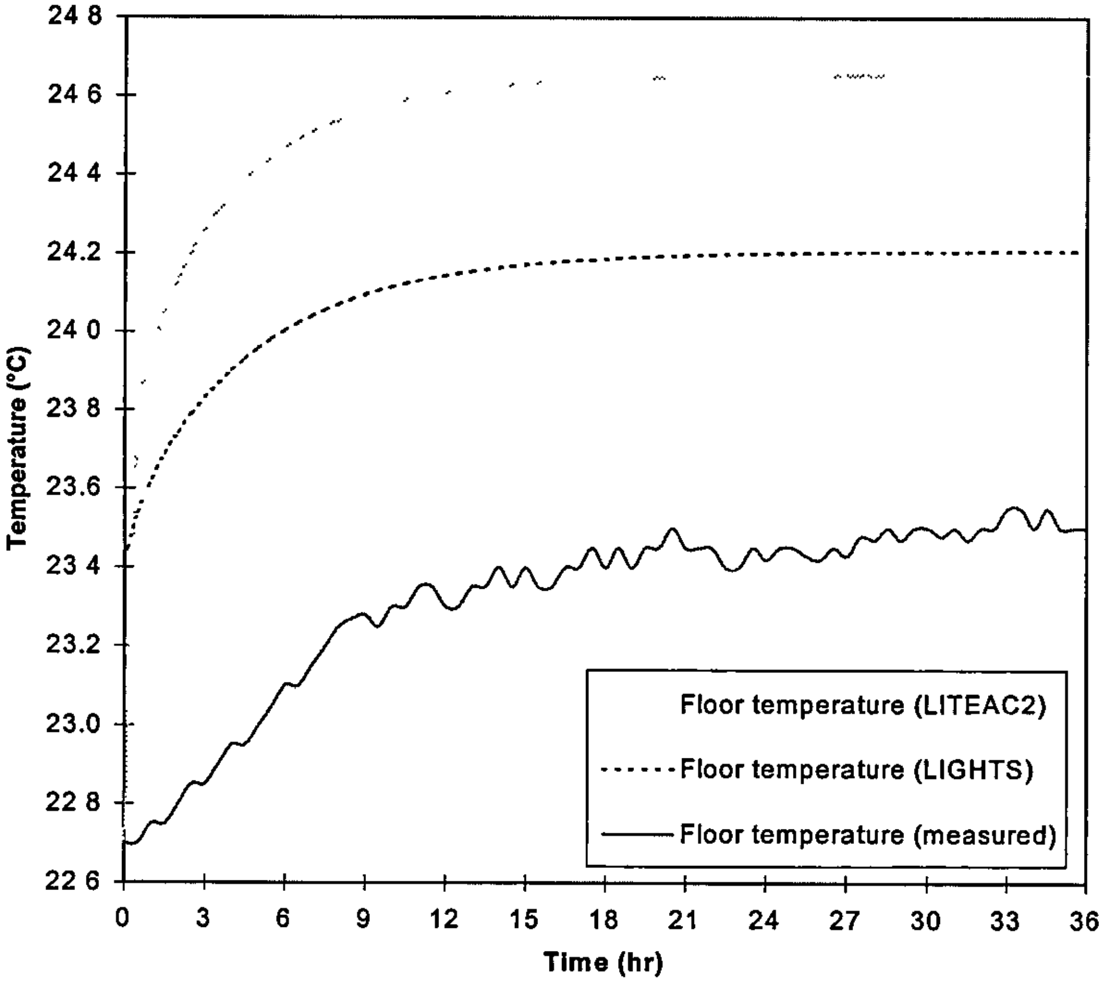

Figure 10.4

Floor surface temperatures in NIST test cell - comparison between LITEAC2 and LIGHTS predictions, and measured results.

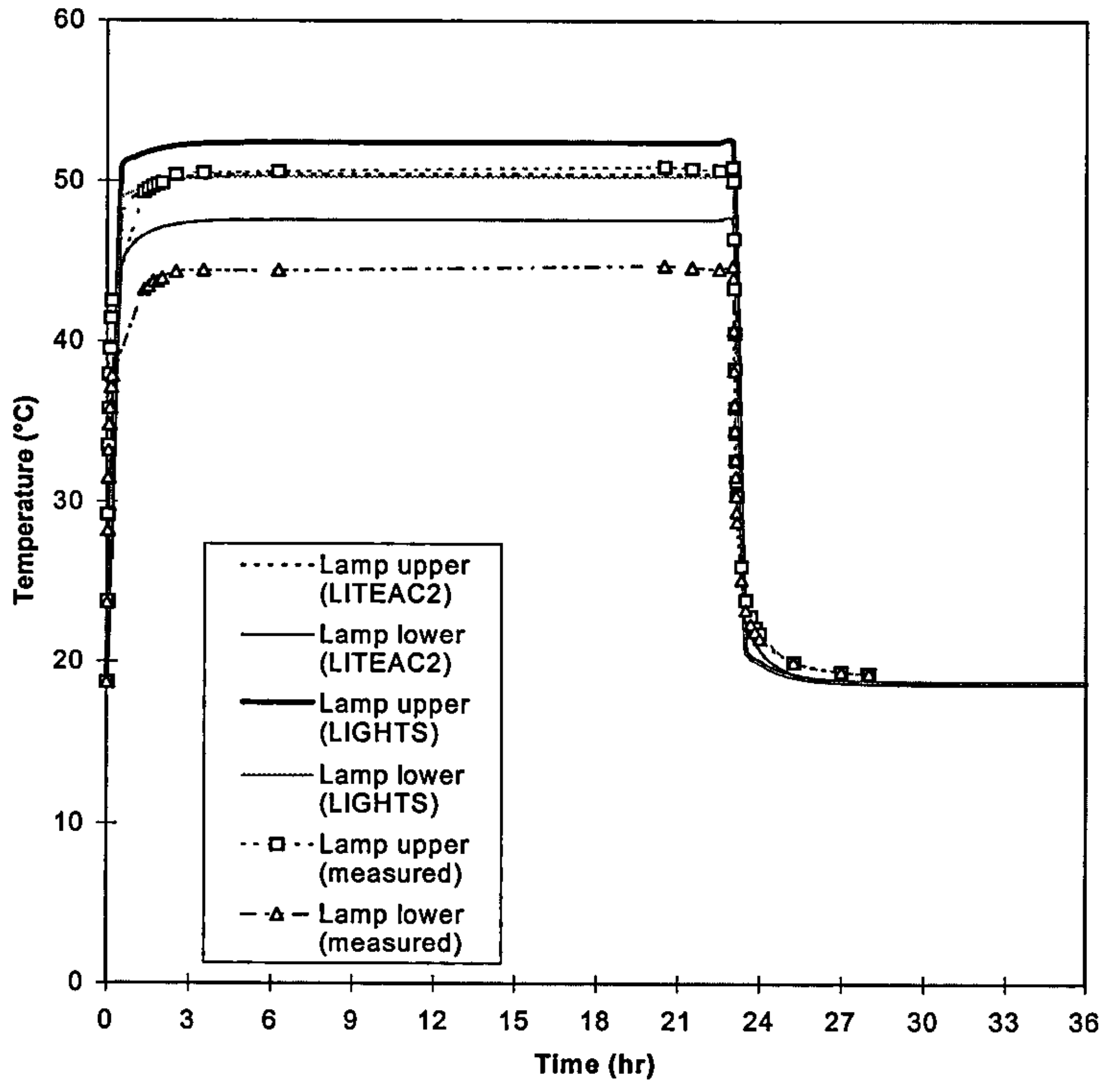

Figure 10.5

Lamp node temperatures in laboratory constructed test cell - comparison between LITEAC2 and LIGHTS predictions, and measured results.

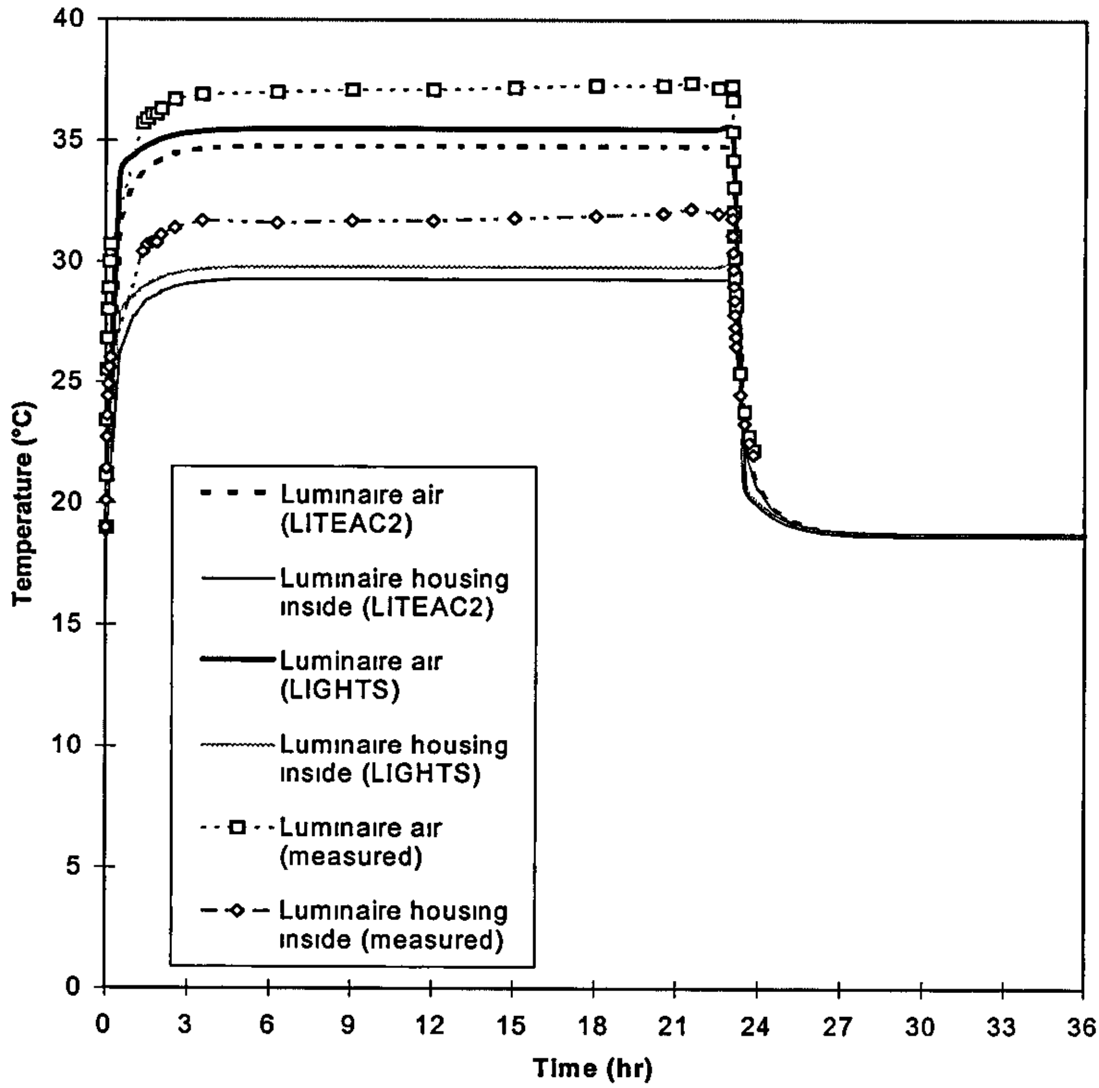

Figure 10.6

Luminaire air and housing temperatures in laboratory constructed test cell - comparison between LITEAC2 and LIGHTS predictions, and measured results.

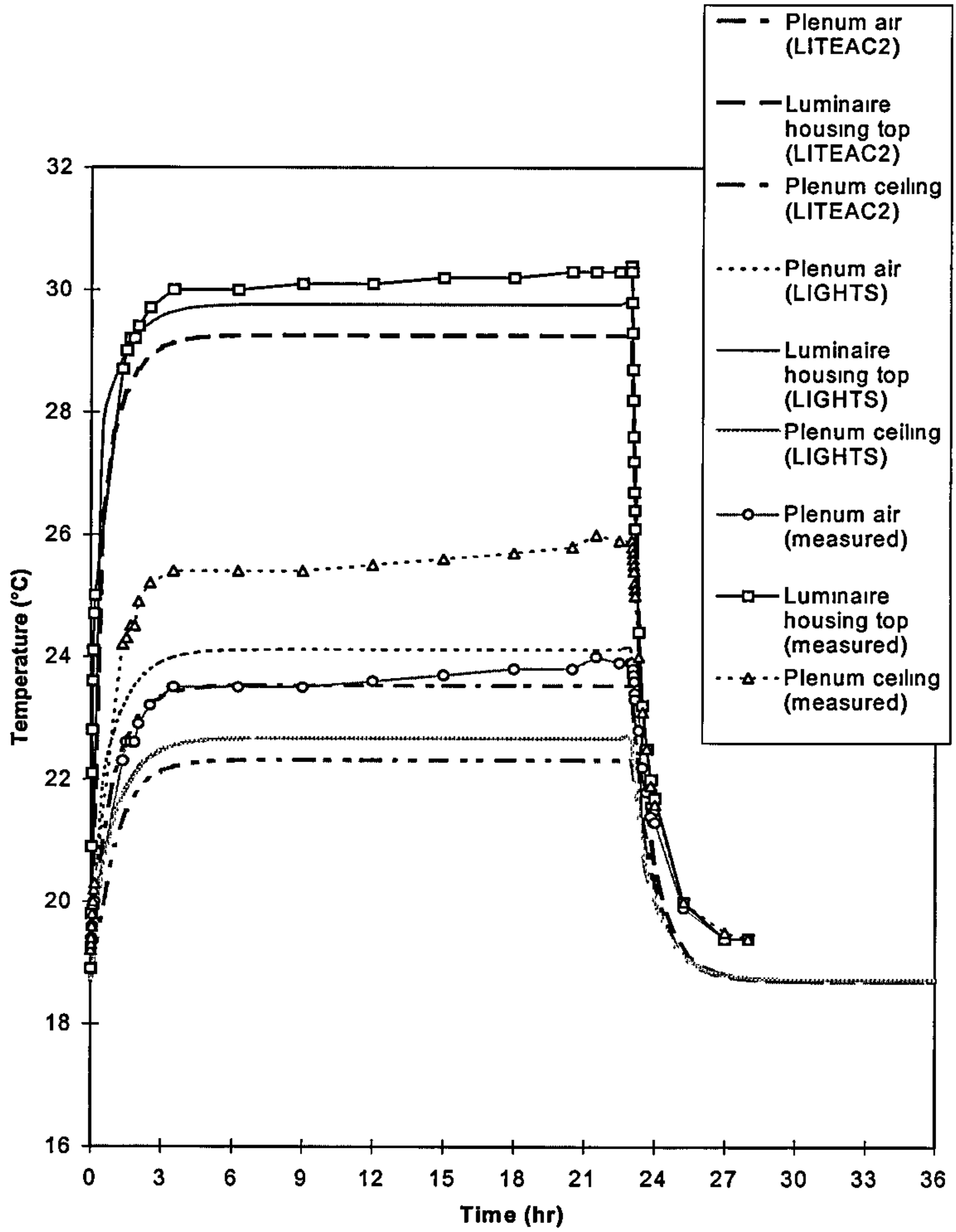

Figure 10.7

Temperatures of three plenum nodes: plenum air, luminaire housing top and plenum ceiling, in laboratory constructed test cell - comparison between LITEAC2 and LIGHTS predictions, and measured results.

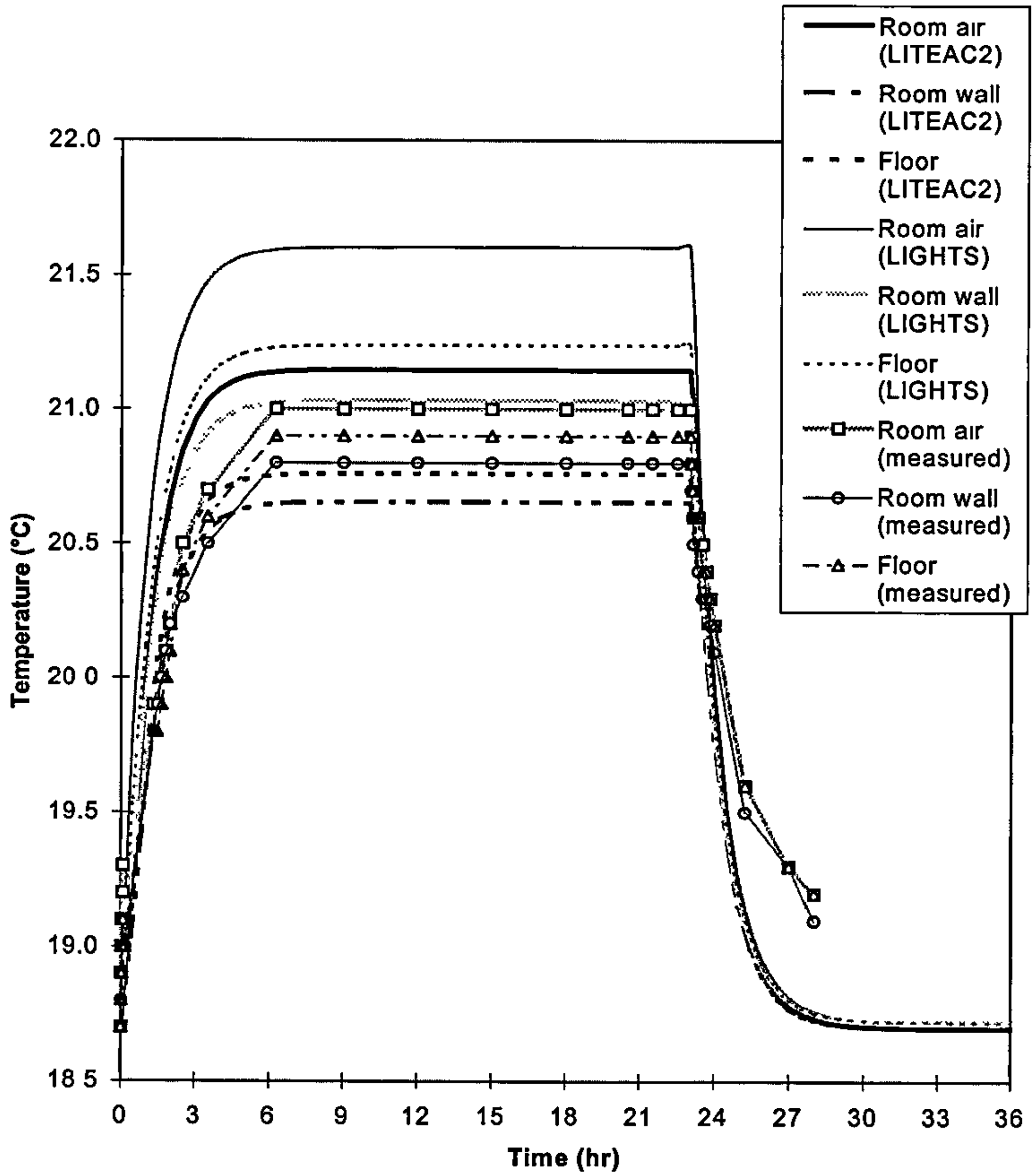

Figure 10.8

Temperatures of three room nodes: room air, room wall and floor surface, in laboratory constructed test cell - comparison between LITEAC2 and LIGHTS predictions, and measured results.

Chapter Eleven

Conclusions

11.1 Summary of the research

The interaction between lighting and HVAC systems has been studied using numerical modelling techniques. This study has generated essentially a numerical model LITEAC2, which represents substantial original work and includes innovative methodologies in several respects, for the simulation of the interaction between lighting and HVAC systems.

LITEAC2 consists of two major components: firstly, a room heat and radiation transfer model which simulates the heat and radiation transfer in a room enclosure; secondly, a fluorescent lamp positive column discharge model which accounts for the conversion of supplied electrical energy into light, long-wave radiation and heat energies together with the dependence of the output energies on lamp parameters such as minimum lamp wall temperature.

The room heat transfer model simulates the heat and radiation (long- and short-wave) transfer inside a room enclosure in which lamps and ballasts are the sources of heat and radiation. Surface temperatures can be predicted at each time step by this room heat transfer model. Heat fluxes can also be calculated. Cooling load can be predicted at each time step in the form of the heat gain to the room air node, the latter being kept at a constant temperature by an ideally-controlled air-conditioning system. This room heat transfer model has been derived from basic heat transfer principles and accounts for radiation, convection and conduction. The computer program of the heat transfer model derived here allows for the use of smaller time steps than those of existing models and hence allows for the inclusion of small thermal capacities in the transient computations without mathematical instability. This represents an improvement on previous models such as Sowell (1989, 1990) in which some nodes have to be assumed massless (i.e. of zero thermal capacity).

The fluorescent lamp positive column model, named LAMPPC, simulates the energy conversion processes inside the fluorescent lamp discharge and their dependence on fluorescent lamp parameters. The electrical input energy to the lamps and ballasts (which are the only power sources considered in LITEAC2) is converted to light (visible radiation), long-wave radiation and heat energies with output energy amounts and proportions depending on the type of lamp and ballast. Since both light and long-wave radiation outputs will not appear immediately as a cooling load to the room air, the relative proportions of each output will have an effect on the rate of build up of cooling load due to lighting. Previous models either assumed arbitrarily a ratio of radiation and convection output from the lamps (Kimura and Stephenson 1968) or allowed for the inputting of a value of the light output from the lamps, calculating the radiation and convection components accordingly (Sowell and O'Brien 1973; Sowell 1990). In LITEAC2, the energy conversion processes inside the discharge of the fluorescent lamp are modelled and the light (visible radiation) output, long-wave radiation output and heat loss by convection are then calculated without the need to input data about the total light output from the lamp nor about the proportions of radiation and convection. LAMPPC is applied, as a subroutine in LITEAC2, to simulate the energy conversion processes inside the fluorescent lamp. LAMPPC calculates the output of the fluorescent lamp discharge, consisting of two ultra-violet lines and several weak visible and invisible lines, which depend on the electric current supplied to the lamp and the mercury vapour pressure inside the discharge tube. The electric current supplied to the lamp, which in turn depends on the lamp-ballast combination, is an input parameter to LAMPPC. The mercury vapour pressure inside the fluorescent lamp tube depends on the minimum lamp wall temperature which is calculated at each time step in the room heat transfer model. Inputting data concerning the spectral power distribution of the phosphors used in the fluorescent lamp allows the calculation of light output from the fluorescent lamp. The spectral power distribution of fluorescent lamps can be obtained from manufacturers. There is also a set of 12 typical fluorescent lamp spectral power distributions published in CIE (1986). Therefore, LITEAC2 not only calculates cooling load and temperatures but also permits the simulation of the variation of light output with the ambient temperature around the lamp which is a well-known effect in fluorescent lighting. The development and inclusion of a fluorescent lamp discharge model within the numerical simulation of the interaction of lighting and HVAC systems, together with the methodologies developed for the calculation of heat and radiation transfer from luminaires and for the calculation of light output and lamp power represent essentially new work; these also represent significant improvements to previous numerical studies of lighting/HVAC interaction published in the relevant literature.

The development of LITEAC2 can be summarised into the following five stages:

(1) In the first stage, a typical office room was modelled by dividing it into three sections: the luminaire, the plenum and the occupied room space (called the 'room' for simplicity) (Chapter 4). Each of these three sections was divided into nodes: an air node and a number of surface nodes. Each node was assumed to be isothermal. A heat balance equation was used to relate the temperature change of each node in one time step to the heat gain or heat loss of the node in that time step. Conduction, convection and radiation heat transfer between nodes were considered, while energy input from an outside source was considered only for lamp and ballast nodes. For radiation transfer, long-wave (or thermal) radiation and short-wave (or visible) radiation were considered separately. For the calculation of cooling load, the room air node was assumed to be kept at a constant temperature by an ideally-controlled air-conditioning system. In this stage the variation of lamp performance (light output and lamp power) was

considered using empirical curves. A FORTRAN program named LITEAC1 was written to encode this model, and this program was tested using a simple configuration for which an analytical solution could be obtained. LITEAC1 can be used for any lamp type, not necessarily fluorescent lamps.

(2) In the second stage of the study, a fluorescent lamp positive column model was developed and used to simulate the conversion of electrical energy input to the fluorescent lamp into light, thermal radiation and heat (Chapters 5). Prior to this study, there have been no previous trials of applying a fluorescent lamp positive column model to the study of the interaction between lighting and HVAC systems. A model with sufficient details was derived in this study to enable the simulation of the conversion of the input electrical energy into light, thermal radiation and heat and to account for the macroscopic behaviour of the fluorescent lamp with respect to a change of thermal environment. The fluorescent lamp positive column model derived in this study uses the same basic hypotheses as those used by previous workers (Waymouth and Bitter 1956; Lama et al. 1982) but considers additional mercury energy levels and transitions. Furthermore, all equations used in the positive column model of this study were derived from first principles using the basic hypotheses; also, these equations were written in a more comprehensive form in this thesis then those published by previous workers. The method of solution of the model equations was also specially derived for this study (Chapter 6). The fluorescent lamp positive column model was encoded and named LAMPPC. LAMPPC can, if wished, be run as a stand-alone program for the simulation of the fluorescent lamp discharge. As a stand-alone program, LAMPPC was tested using experimental measurements reported in the literature (Chapter 7). For the study of lighting/HVAC interaction, LAMPPC was incorporated into the room heat transfer model as a subroutine for the prediction of radiative and convective components of the heat output from the lamp and for the improved simulation of the effect of temperature on lamp performance. This integration generated a new program called LITEAC2.

(3) The third stage of this study was the validation of LITEAC1 and LITEAC2 using experimental data from the literature (Chapter 8). The published data from the NIST full-scale measurements carried out by Treado and Bean (1988, 1992) was used in the validation. Both steady-state and transient results were considered. For most cases, the simulated steady state results deviated from the NIST experimental data by less than 5%. The few cases with higher deviations were explained by the fact that experimental errors might exist in the NIST measurements as shown in the inconsistencies existing in some of the data (Sowell 1990). Discrepancy was also attributed to the fact that detailed properties of materials used in the NIST test cell were not available, so that errors existed in the input data to the model. Transient temperature and cooling load profiles calculated by both LITEAC1 and LITEAC2 also agreed well with experimental data.

(4) In the fourth stage of this study, a simple laboratory test cell was constructed and measurements were taken of temperature and illuminance so as to obtain data for a further validation of the two programs LITEAC1 and LITEAC2 (Chapter 9). The aim of this stage was to test LITEAC1 and LITEAC2 for a cell of different dimensions from the NIST test cell and to obtain more illuminance data for validation to include a wider range of lamp wall temperature than those given in the NIST test cell. Results from this stage of the study showed that both LITEAC1 and LITEAC2 gave good predictions of node temperatures and LITEAC2 gave better predictions of illuminance then LITEAC1.

(5) The fifth stage of the study was a comparison between the simulations carried out with LITEAC2 and the simulations made with LIGHTS (Sowell 1989, 1990) (Chapter 10). The comparison was performed with respect to a selected configuration of the NIST tests and the test configuration carried out in the laboratory test cell. It was found that both models were equally good for the calculation of lighting power, cooling load and temperature. However, LITEAC2 is able to calculate with reasonable accuracy the illuminance on room surfaces;

LIGHTS is incapable of doing this. Furthermore, LITEAC2 runs faster than LIGHTS on a personal computer.

11.2 Application of LITEAC2 in design

Current practice in lighting design does not, in general, consider the effects of temperature on light output. However, since a large proportion of lamps in existing buildings are operating at temperatures higher than the optimum (Verderber et al. 1988), the effects of temperature on light output is receiving more attention. This is shown in IESNA (1993) which states that a non-recoverable light loss factor called the luminaire ambient temperature factor can be used in lighting calculations. However, IESNA (1993) does not give a method for the determination of the luminaire ambient temperature factor; instead it states arbitrarily that for each degree of rise in luminaire ambient temperature above 25°C, the cold-spot temperature of the lamp rises by about 0.6°C. This means that data on the variation of light output with cold-spot temperature has to be obtained before the luminaire ambient temperature factor can be determined. However, manufacturers do not normally give data on the variation of light output with temperature. Hence, LITEAC2 can be used for a simulation during the design stage. The following is a description of how LITEAC2 can be used in design.

In the design of the lighting installation for an office room, a target maintained illuminance is selected according to design guidelines in lighting codes such as the CIBSE Code for Interior Lighting (CIBSE 1994) and the IES Lighting Handbook (IESNA 1993). A luminaire type and a lamp type are then chosen. The 'lumen method' (CIBSE 1994; IESNA 1993) is then used for the determination of the number of luminaires required to give the target illuminance on the working plane. Before using the 'lumen method' formula, a 'maintenance factor' and a 'utilisation factor' have to be determined from the data given by manufacturer (CIBSE 1994); or equivalently, a 'light loss factor' and a 'coefficient of utilisation' are determined when the guidelines in the North American IES Lighting Handbook (IESNA 1993) is followed. The maintenance factor (or light loss factor) is defined as the ratio of maintained illuminance to initial illuminance. The utilisation factor (or coefficient of utilisation) is defined as the ratio of luminous flux incident on the reference plane to the total lamp flux. A suitable luminaire layout is then determined and the spacing to height ratio is checked in order to meet the requirement on uniformity.

To consider the effect of temperature on light output, LITEAC2 can be used to simulate the office room for the planned on/off schedule. Illuminance values predicted by LITEAC2 can be checked with the value calculated by the 'lumen method' but using a maintenance factor or a light loss factor of 1. A unity light loss factor or maintenance factor is used because LITEAC2 does not consider light depreciation due to dirt deposition or due to lamp depreciation; in other words, the initial illuminance is calculated. If the illuminance predicted by LITEAC2 is lower than the 'initial' illuminance calculated by the 'lumen method', then the results show that the lamps are operating at temperatures different from the optimum. To obtain the design target illuminance, either more luminaires have to be installed, or methods have to be applied so as to reduce the luminaire ambient temperature, e.g. by increasing the ventilation rate to the plenum.

After the lighting installation is designed, LITEAC2 can be used to predict the cooling load due to lighting at time intervals determined by the program user. LITEAC2 can also be used to predict the temperatures at room surfaces when the lighting system is the only heat and radiation source in the room. LITEAC2 can be used in its present form by designers who require a numerical tool to verify their designs without the use of 'mock-up' facilities. With further development, the user-friendliness of LITEAC2 can be improved such that it can be routinely used by lighting designers.

11.3 Conclusions

The following conclusions can be drawn from this study:

(1) The two-way interaction between lighting and HVAC systems inside an enclosure can be studied using a newly developed numerical scheme called LITEAC2. LITEAC2 represents an improvement to previous studies published in the literature as it allows not only for the calculation of cooling loads and the temperature changes of room surfaces, but also for the change with ambient temperature of light output levels and power consumed by lamps and ballasts. It permits faster calculations than a recent program called LIGHTS of the transient state cooling loads, temperatures and illuminances without the necessity of assuming that nodes with small thermal capacities are massless (i.e. of zero thermal capacity).

(2) A fluorescent lamp positive column model has been derived and incorporated within a lighting/HVAC simulation model. It permits improved simulation of the variation of light output and lamp power with minimum lamp wall temperature of a fluorescent lamp. This enables the calculation of the conversion of electrical energy input to the fluorescent lamp system into different energy output forms: light, thermal radiation, and heat dissipated from the lamp surface. The incorporation of the fluorescent lamp positive column model into the lighting/HVAC interaction simulation results in more accurate predictions (than models that use only empirical curves to account for variation of light output with temperature) of the dynamic cooling load and temperature changes, as well as illuminances on surfaces, inside the enclosure. This represents a major step forward compared with the previous practice relying on empirical curves to account for the variation of performance of fluorescent lamps with minimum lamp wall temperature.

(3) Validation of LITEAC2 using published data from a full-scale lighting/HVAC interaction test facility was successful. Validation of LITEAC2 using a simple test cell constructed in the laboratory was also successful.

(4) The new numerical solution scheme developed for LITEAC2 allows faster computation of the transient state with the results for cooling load and temperature changes being comparable to those calculated using a numerical lighting/HVAC test cell in the literature. Designers can use LITEAC2 to verify their designs without the need for 'mock-up' facilities. With further work it can be developed into a user-friendly package for everyday use by lighting designers.

(5) LITEAC2 introduces a tool for the research community to investigate seriously into the effect of temperature on the performance of fluorescent lighting systems. LITEAC2, which can calculate the dynamic lighting energy use with the air-conditioning in operation, can be used by building energy researchers to simulate the lighting energy use in buildings for whole building energy simulation with other energy simulation programs.

11.4 Recommended further work

For more accurate predictions of: (i) the cooling load and temperature changes due to lighting, and (ii) the changes in light output, lighting energy consumption and working plane illuminance due to thermal effects, the following further work is recommended:

(1) Use LITEAC2 to perform numerical experiments on an extensive collection of lamps and luminaire types and for different enclosure configurations. These numerical experiments would produce new design data for the calculation of cooling load due to lighting and for the calculation of light loss factors due to thermal effects.

(2) Take a wide range of field measurements for comparison with simulated results from LITEAC2. Although LITEAC2 has been sufficiently validated in this study so as to give confidence in its performance, a range of field measurements would be useful in determining full extent of its applicability. The lamp power, illuminance, lamp temperature, luminaire, plenum and room temperatures should be field tested. A variety of sites should be chosen to represent different combinations of lamps, ballasts and luminaire types, with different room dimensions and configurations.

(3) Numerical experiments could be performed to evaluate the effect of innovative designs of luminaires for keeping the lamp wall temperature at optimum values, such as the thermal bridge method proposed by Verderber et al. (1988) and Packer and Siminovitch (1991). These numerical experiments could reduce the number of physical experiments needed for the assessment of the effectiveness of these innovative luminaire designs. Heat recovery luminaires should also be investigated in this respect.

(4) Physical experiments should be carried out to investigate the heat transfer inside the luminaire. These experiments should be specially directed for the measurement of convection coefficients under the conditions which would normally occur inside luminaires. The convection coefficient over the lamp surface would have a significant effect on the minimum lamp wall temperature which affects the lamp performance. Accurate data for convection coefficients over the lamp surface inside the luminaire compartment are not available at present and this has a beanng on the numerical simulation using LITEAC2.

(5) Experimental measurements should also be performed to investigate the variation of light output and lamp temperature in relation to parameters such as the lamp separation, air flow, luminaire size and construction, and other features of the luminaire.

(6) LITEAC2 can be used to perform simulations of an extensive collection of room and luminaire configurations in order to generate tables of light loss factors due to thermal effects for a wide range of luminaire type, lamp type, room construction and configuration and plenum temperatures. These tables of light loss factors should provide simple-to-use design data for the designers to consider the thermal effects on lighting performance in the design of lighting systems.

Abbreviations

ASHRAE	American Society of Heating, Refrigerating and Air-conditioning Engineers, Inc., U.S.A.
CG	Ceiling grille return
CIE	Commission Internationale de L'Eclairage
CLF	Cooling load factor
CLTD	Cooling load temperature differences
EEDF	Electron energy distribution function
HVAC	Heating, ventilating and air-conditioning
IESNA	Illuminating Engineering Society of North America
LC	Lamp compartment return
LLF	Light loss factor
MLWT	Minimum lamp wall temperature
NIST	National Institute of Standards and Technology, U S. Department of Commerce, U.S.A.
RLE	Relative lighting efficacy
RLO	Relative light output
RLP	Relative lighting power
SCL	Solar cooling load
T12	Tubular fluorescent lamp with diameter equals to 12 × one-eighth of an inch (i.e. 1.5 inch or 38 mm)
T8	Tubular fluorescent lamp with diameter equals to 8 × one-eighth of an inch (i.e. 1 inch or 26 mm)
TA	Time average
TETD	Total equivalent temperature difference
TFL	Thermal factor for light output

TFM	Transfer function method
TFW1	First thermal factor for power
TFW2	Second thermal factor for power
UV	Ultraviolet

Nomenclature

A	Coefficient in the exponential fit of Stephenson and Mitalas (1967) (dimensionless)
A^m	Diagonal matrix of surface area of nodes - in LIGHTS model of Sowell (1989)
A_i	Surface area of node i (m^2)
A_{kj}	Reduced transition coefficient from state k to state j for descending transitions ($k>j$)
B	Coefficient in the index of exponential fit of Stephenson and Mitalas (1967) (h^{-1})
C_{ij}	Heat conductance from node i to node j (W K^{-1})
C_{jk}	Reduced transition coefficient from state j to state k for ascending transitions ($k>j$)
CLF	Cooling load factor (dimensionless)
c or c_{pi}	Specific heat capacity of node i (J $kg^{-1}K^{-1}$)
c_{pa}	Specific capacity of air (J kg^{-1} K^{-1})
$\bar{c}$	Velocity of light ($=3.0\times10^8$ m s^{-1})
D_a	Ambipolar diffusion coefficient
D_e^m	Diffusion coefficients of the electrons
E	Electric field strength (V m^{-1})
E_e	Energy of the electron (J)
E_{el}	Mean energy loss per elastic collision (J)
E_{jk}	Energy gap between j^{th} and k^{th} states (J)
E_{Li}	Long-wave radiation irradiance on node i (W m^{-2})
E_{Si}	Short-wave radiation irradiance on node i (W m^{-2})
e	Electronic charge ($=1.60217733\times10^{-19}$ C)

F	A factor to correct for loss of actinic radiation and emitted light at the ends of lamp
F_{ij}	Radiation form factor (fraction of radiation emitted from node i that falls on node j)
F_{sa}	Lighting special allowance factor, a value to account for the power dissipated by the ballast (dimensionless)
F_{ul}	Lighting use factor, a value from 0 to 1 to account for the proportion of usage of lighting (dimensionless)
$f(E_e)$	Energy distribution function of electrons
g_j	Statistical weight of the j^{th} state
h or h_i	Convective heat transfer coefficient of node i (W $m^{-2}K^{-1}$)
$\bar{h}$	Planck's constant (=6.626×10^{-24} Js)
I	Electric current through positive column (A)
$J^{pl}(T)$	Matrix (N × N) of source radiation at each node in the long-wave band - in LIGHTS model of Sowell (1989)
J^{ps}	Matrix (N × N) of source radiation at each node in the short-wave band - in LIGHTS model of Sowell (1989)
j	Current density (A m^{-2})
K_{ji}	Ionisation rate coefficients of the j^{th} state (j=0,1,...,6) (m^3 s^{-1})
K_{jk}	Transition rate coefficients (m^3 s^{-1}); number of transitions from state j to state k per state j atom per electron per second (j=0,1,...,6)
k	Boltzmann constant (=1.380658×10^{-23} J K^{-1})
k_o	Absorption coefficient at the center of the resonance line (m^{-1})
M	Diagonal matrix of heat capacitances of nodes - in LIGHTS model of Sowell (1989)
M_{Li}	Long-wave radiant exitance (radiosity) of node i (W m^{-2})
M_{Loi}	Long-wave radiant emissive power of node i (W m^{-2})
M_{Si}	Short-wave radiant exitance (radiosity) of node i (W m^{-2})
M_{Soi}	Short-wave radiant emissive power of node i (W m^{-2})

$MLWT$	Minimum lamp wall temperature (°C)
m or m_i	Mass of node i (kg)
m_e	Electron rest mass (=9.1093897×10^{-31} kg)
m_{rg}	Mass of rare gas (kg)
N_e	Electron density (m^{-3})
N_{Hg}	Number density of mercury atoms (m^{-3})
N_j	Number density of the j^{th} state (m^{-3})
N_{rg}	Number density of rare gas (m^{-3})
n_λ	Number of quanta of wavelength λ
p_{Hg}	Partial pressure of mercury vapour (Pa)
Q^o	Vector (column matrix) of source powers at each node - in LIGHTS model of Sowell (1989)
Q_{ej}^m	Momentum transfer cross-section for the elastic collisions between electrons and mercury atoms of the j^{th} state (m^2)
$Q_{jk}(E_e)$	Collision cross-section of the transition from state j to state k (m^2)
Q_θ	Cooling load at time θ (W)
$q(t_n)$	Cooling load from lights at time $t=t_n=n\Delta$ (W)
q_{Ci}	Total (net) conduction heat gain to node i in one time step (J)
q_{el}	Heat gain due to lighting in watts (W)
q_{Gi}	Total (electrical) energy input at node i in one time step (J)
q_{Ha}	Total (net) convection heat gain to the air node in one time step (J)
q_{Hi}	Total (net) convection heat gain to node i in one time step (J)
q_{Li}	Total (net) long-wave radiation heat gain to node i in one time step (J)
q_{Si}	Total (net) short-wave radiation heat gain to node i in one time step (J)
q_θ	Heat gain at time θ (W)
$\dot{q}_{Li}$	Rate of change of long-wave radiation input to node i (W)

$\dot{q}_{Si}$	Rate of change of short-wave radiation input to node i (W)
$\dot{q}_{Hi}$	Rate of change of convection heat input to node i (W)
$\dot{q}_{Ha}$	Rate of heat transfer by convection to the air node (W)
$\dot{q}_{Cai}$	Heat gain of air node 'ai' due to air exchange between air nodes in different sections (W)
$\dot{q}_{Ci}$	Rate of change of conduction heat input to node i (W)
R	Radius of fluorescent lamp tube (m)
$S(\lambda)$	Relative spectral power distribution of light output from fluorescent powder (nm^{-1})
T	Vector of nodal temperatures - in LIGHTS model of Sowell (1989)
T_a	Air node absolute temperature (K)
T_e	Electron temperature (K)
T_g	Absolute temperature of gas inside fluorescent tube (K)
T_i or T_s	Absolute temperature of node i (K)
$\dot{T}$	Vector of the time derivatives of nodal temperatures - in LIGHTS model of Sowell (1989)
t (or t_n)	Time after the lights are turned on (h or s)
$U^c(T)$	N × N matrix (N=number of nodes) of conductive/convective heat transfer coefficients - in LIGHTS model of Sowell (1989)
$V(\lambda)$	Relative spectral luminous efficiency for photopic vision of the standard CIE observer
V^l	Special transfer matrix (N × N) describing inter-reflections and transmissions within the enclosure for long-wave radiation - in LIGHTS model of Sowell (1989)
V^s	Special transfer matrix (N × N) describing inter-reflections and transmissions within the enclosure for short-wave radiation - in LIGHTS model of Sowell (1989)
V_i	Energy level of the ionised state of mercury (eV)

V_i' Average energy level that the mercury atom has to attain for ionisation to take place (eV)

V_{ij} Volume flow rate of air in between air nodes '*ai*' and '*aj*' ($m^3\ s^{-1}$)

V_j Energy level of the j^{th} state (eV)

v Electron drift velocity ($m\ s^{-1}$)

v_e Velocity of the electron ($m\ s^{-1}$)

v_n, w_n (n = 0,1,2....) Coefficients of transfer function

$W(\lambda)$ Power output in wavelength interval λ to λ+dλ per unit wavelength per unit volume of plasma ($W\ nm^{-1}m^{-3}$)

$W(t_n)$ Power input to lights at time $t = t_n = n\Delta$ (W)

W_{185} Power of the 185 nm line per unit volume of plasma ($W\ m^{-3}$)

W_{254} Power of the 254 nm line per unit volume of plasma ($W\ m^{-3}$)

W_{diff} Power loss due to diffusion per unit volume of plasma ($W\ m^{-3}$)

W_{el} Power loss due to elastic collisions per unit volume of plasma ($W\ m^{-3}$)

W_{inel} Power loss due to inelastic collisions per unit volume of plasma ($W\ m^{-3}$)

W_{ion} Power loss due to ionization per unit volume of plasma ($W\ m^{-3}$)

W_{inv} Power of emitted invisible lines per unit volume of plasma ($W\ m^{-3}$)

W_{phos} Total power output of the fluorescent powder in the lamp (W)

W_{sel} Power loss due to super-elastic collisions per unit volume of plasma ($W\ m^{-3}$)

W_{uv} Approximate total power of UV radiation emission per unit volume of plasma ($W\ m^{-3}$)

W_{vis} Power of emitted visible lines per unit volume of plasma ($W\ m^{-3}$)

Δ Time step (s or h)

ΔT Elevation of rare-gas temperature inside the lamp above the minimum lamp wall temperature (°C)

ΔT_i Temperature rise of node i in one time step (K)

Λ Diffusion length (m)

Φ	Luminous flux output per unit volume of positive column (lm m^{-3})
Φ_{lamp}	Total luminous flux output of fluorescent lamp (lm)
δ	Time interval in Transfer Function Method calculation (usually 1 hour)
ε_i	Emissivity of node *i*
η	Quantum efficiency of phosphor
λ	Wavelength (nm)
λ_e	Electron mean free path (m)
μ_e	Electron mobility (m^2 V^{-1}s^{-1})
ν_c	Average frequency of collision between electron and rare-gas atoms per rare-gas atom (s^{-1})
ρ_a	Density of air (kg m^{-3})
ρ_{Li}	Reflectance of node *i* with respect to long-wave radiation
ρ_{Si}	Reflectance of node *i* with respect to short-wave radiation
σ	Stefan-Boltzmann constant (= 5.669×10^{-8} W m^{-2}K^{-4})
τ	Natural life time of radiating state (s)
τ_{eff}	Effective life time of radiating state (s)
τ_j^*	Average effective life time of the j^{th} state (s)
τ_{jk}^*	Effective life time of the spontaneous decay of the j^{th} state to the k^{th} state (j=1,…,6; k=0,…5; $k<j$) (s)

References

1. ASHRAE (1993)
   1993 *ASHRAE Handbook - Fundamentals* Chapter 26

2. ASHRAE (1997)
   1997 *ASHRAE Handbook - Fundamentals* Chapter 28

3. Ball, H.D., and D. Green (1983)
   The impact of lighting fixtures on heating and cooling loads - mathematical model
   ASHRAE Transactions, **89** (2), 236-258.

4. Ballman, T.L., and T. Mueller (1965)
   Fluorescent luminaire calorimetry: principles and procedures.
   ASHRAE Transactions **71**(1): 51-60.

5. Ballman, T.L., R.D. Bradley, and E.C. Hoelscher (1964)
   Calorimetry of fluorescent luminaires.
   Illuminating Engineering Dec. 1964: 779-785.

6. Barnes, B.T. (1960)
   Intensities of 11850 and 12537 in low-pressure mercury vapor lamps with rare gas present
   Journal of Applied Physics, **31** (5), 852-854.

7. Bigio, L. (1988)
   Density measurements of $Hg(6^3P_{0,1,2})$ in a discharge using saturated laser absorption and hook methods
   Journal of Applied Physics, **63** (11), 5259-5269.

8. Bonvallet, G.G. (1963)
   Method of determining energy distribution characteristics of fluorescent luminaires
   Illuminating Engineering Feb. 1963: 69-74.

9. Boyer, L.L. (1966)
   The role of the supply-air plenum in interior zone recessed illumination systems.
   Illuminating Engineering Aug. 1996: 528-533.

10. Boyer, L.L. (1967)
    Thermal environment in perimeter office spaces cooled with ventilating ceilings.
    ASHRAE Transactions **71**(1).

11. Boyer, L.L. (1968)
Radiant panel effects of floor-ceiling assemblies incorporating static, return and supply plenums.
ASHRAE Transactions 74(2): 31-42.

12. California Energy Commission (1993)
Advanced Lighting Guidelines, 2nd edition,
California Energy Commission Publication 400-93-014.

13. Cayless, M.A. (1963)
Theory of the positive column in mercury rare-gas discharges
Brit. J. Appl. Phys., 14, 863-869.

14. Chow W K. and K.T. Chan (1993)
A survey of electrical energy requirement of hotels in Hong Kong
Energy Engineering, 90 (6), 33-41.

15. Chung, T.M. and D.L. Loveday (1998)
Numerical modeling of lighting/HVAC interaction in enclosures: Part I: light and heat transfer in a room
International Journal of Heating, Ventilating, Air-conditioning and Refrigerating Research, 4 (1), 67-84.

16. Chung, T.M. and D.L. Loveday (1998)
Numerical modeling of lighting/HVAC interaction in enclosures: Part II: effect of including a fluorescent lamp positive column model
International Journal of Heating, Ventilating, Air-conditioning and Refrigerating Research, 4 (1), 85-104.

17. CIE (1983)
The Basis of Physical Photometry, 2nd edition.
Publication CIE No. 18.2, Central Bureau of the CIE, Paris.

18. CIE (1986)
Colorimetry, 2nd edition.
Publication CIE No. 15.2, Central Bureau of the CIE, Vienna, Austria.

19. Collins, B.L., S.J. Treado, and M.J. Ouellette (1992)
Evaluation of compact fluorescent lamp performance at different ambient temperatures
National Institute of Standards and Technology Report NISTIR-4935.

20. Dakin, J.T. (1986)
A model of radial variations in the low-pressure mercury-argon positive column
Journal of Applied Physics, 60 (2), 563-570.

21. Dean, J.A. (1992)
Lange's Handbook of Chemistry, 14th edition.
McGraw-Hill, New York.

22. Denneman, J.W., J.J. de Groot, A.G. Jack, and F.A.S. Ligthart (1980)
Insights into the 26mm diameter fluorescent lamp
Journal of the Illuminating Engineering Society, **10**, 2-7.

23. Dorleijn, J.W.F., and A.G. Jack (1985)
Power balances for some fluorescent lamps
Journal of the Illuminating Engineering Society, **15** (1), 75-84.

24. Easley, M.A. (1951)
Probe technique for the measurement of electron temperature
Journal of Applied Physics, **22**, 590-593.

25. Elenbaas, W. (1971)
Fluorescent lamps, 2nd edition, Philips technical library,
Macmillan, London.

26. Energy Efficiency Office (1991)
Energy Efficiency in Offices. Best Practice Programme Energy Consumption Guide No. 19. London, HMSO, UK.

27. Holman, J.P. (1992)
Heat Transfer - seventh edition
McGraw Hill

28. Holstein, T. (1947)
Imprisonment of resonance radiation in gases
Physical Review, **72** (12), 1212-1233.

29. Holstein, T. (1951)
Imprisonment of resonance radiation in gases. II
Physical Review, **83** (6), 1159-1168.

30. Hong Kong Census and Statistics Department (1996)
Hong Kong Energy Statistics - Annual Report 1996 Edition.
Hong Kong Government.

31. Hoyaux, M.F., and E.W. Sucov (1969)
Theoretical analysis of effects of a monoatomic impurity on low-pressure metal arc discharges in a noble gas matrix
Journal of Applied Physics, **40** (8), 3237-3246.

32. IESNA (1984)
IES Lighting Handbook - Reference Edition
Illuminating Engineering Society of North America, New York.

33. IESNA (1993)
IES Lighting Handbook - Reference and Application, 8th Edition, Illuminating Engineering Society of North America, New York.

34. Jerome, C.W. (1953)
The measurement of quantum efficiency of fluorescent lamp phosphors
Journal of the Electrochemical Society, **100**, 586-587.

35. Ji, Y., and R. Davis (1996)
Towards more accurate predictions of energy use and light output for 2 by 4 ft luminaires
Journal of the Illuminating Engineering Society **25** (1), 60-68.

36. Kenty, C. (1950)
Production of 2537 radiation and the role of metastable atoms in an argon-mercury discharge
Journal of Applied Physics, **21** (12), 1309-1318.

37. Kenty, C., M.A. Easley, and B.T. Barnes (1951)
Gas temperatures and elastic losses in low pressure mercury-argon discharges
Journal of Applied Physics, **22** (8), 1006-1011.

38. Kimura, K., and D.G. Stephenson (1968)
Theoretical study of cooling load caused by lights
ASHRAE Transactions, **74** (2), 189-197.

39. Koedam, M., A.A. Kruithof, and J. Riemens (1963)
Energy balance of the low-pressure mercury-argon positive column
Physica, **29**, 565-584.

40. Koedam, M., and A.A. Kruithof (1962)
Transmission of the visible mercury triplet by the low pressure mercury-argon discharge; concentration of the 6^3P states
Physica, **28**, 80-100.

41. Lagushenko, R., and J. Maya (1984)
Positive column Hg-rare gas discharge model applicable to compact fluorescent lamps
Journal of the Illuminating Engineering Society, **14**, 306-314.

42. Lam, J.C. (1995)
Electricity comsumption and built environment in air-conditioned buildings
Energy Engineering, **92** (2), 31-39.

43. Lama, W.L., C.F. Gallo, T.J. Hammond, and P.J. Walsh (1982)
Analytical model for low-pressure gas discharges: application to the Hg+Ar discharge
Applied Optics, **21** (10), 1801-1811.

44. LBL (1979)
DoE-2 Users Guide. *Building Energy Analysis Program - Reference Manual.*
Lawrence Berkeley Laboratory, U.S. Department of Energy.

45. Marlow, W.C. (1967)
Hakenmethode
Applied Optics, **6** (10), 1715-1724.

46. Maya, J., and R. Lagushenko (1990)
Progress in low pressure mercury—rare-gas discharge research
Advances in Atomic, Molecular, and Optical Physics, **26**, 321-373.

47. Mitalas, G.P. (1973a)
Calculating cooling load caused by lights
ASHRAE Journal, June, 37-40.

48. Mitalas, G.P. (1973b)
Cooling load caused by lights
Transactions, Canadian Society for Mechanical Engineering, **2** (3), 169-174.

49. Mitalas, G.P., and D.G. Stephenson (1967)
Room thermal response factors
ASHRAE Transactions, **73** (1).

50. Mitalas, G.P., and K. Kimura (1971)
A calorimeter to determine cooling load caused by lights
ASHRAE Transactions, **77** (2), 65-72.

51. Nevins, R.G., H.E. Straub, and H.D. Ball (1971)
Thermal analysis of heat removal troffers.
ASHRAE Transactions **77**(2): 58-64.

52. Nottage, H.B., and K.S. Park (1969)
Performance of a ventilated luminaire.
ASHRAE Transactions **75**(1): 50-70.

53. Packer, M., and M. Siminovitch (1991)
The application of a thermal bridge to increase light output of a T12 fluorescent fixture system
Conference Record of 1991 IEEE Industry Applications Society Annual Meeting, 1898-1903.

54. Post, H.A. (1986)
Radiative transport at the 184.9-nm Hg resonance line. I. Experiment and theory
Physical Review A, **33** (3), 2003-2016.

55. Post, H A., P. van de Weijer, and R.M.M. Cremers (1986)
Radiative transport at the 184.9-nm Hg resonance line. II. Extensive experiments
Physical Review A, **33** (3), 2017-2024.

56. Rundquist, R.A. (1990)
Consideration in developing a transient heat-from-lights design tool
ASHRAE Transactions, **96** (2), 787-793.

57. Siminovitch, M.J., F.M. Rubinstein, and R.R. Verderber (1984)
Determining lamp/ballast system performance with a temperature-controlled integrating chamber
Journal of the Illuminating Engineering Society, **14** (1), 364-378.

58. Siminovitch, M.J., F.M. Rubinstein, and R.R. Verderber (1988)
The effects of fixture type and HVAC integration on fluorescent lamp/ballast performance
IEEE Transactions on Industry Applications, **24** (3), 365-369.

59. Sowell, E.F. (1989)
LIGHTS User's Guide - A computer program for modeling of thermal and luminous aspects of building lighting systems
Department of Computer Science, California State University, November

60. Sowell, E.F. (1990)
A numerical lighting/HVAC test cell
ASHRAE Transactions, **96** (2), 789-786.

61. Sowell, E.F., and P.F. O'Brien (1973)
The transport of lighting energy
ASHRAE Transactions, **79** (2), 172-182.

62. Stephenson, D.G. and G.P. Mitalas (1967)
Cooling load calculations by thermal response factor
ASHRAE Transactions, **73** (1), III1.1-1.7.

63. Sturrock, W (1938)
Effects of artificial lighting on air conditioning
ASHVE Transactions, **44**, 213-244.

64. Sylvester, G.C. (1964)
Performance of heat-removal troffer with a specific building design.
ASHRAE Transactions **70**: 328-334.

65. Treado, S.J., and J.W. Bean (1988)
The interaction of lighting, heating and cooling systems in buildings - Interim Report
National Institute of Standards and Technology Report NISTIR-883860

66. Treado, S.J., and J.W. Bean (1990)
Experimental evaluation of lighting/HVAC interaction
ASHRAE Transactions, **96** (2), 773-779.

67. Treado, S.J., and J.W. Bean (1992)
The interaction of lighting, heating and cooling systems in buildings
National Institute of Standards and Technology Report NISTIR 4701

68. UIUC (1986)
BLAST 3.0 *Users Manual, The Building Loads Analysis and System Thermodynamics Program*
Support Office, Department of Mechanical and Industrial Engineering, University of Illinois at Urbana-Champaign, Urbana, U.S.A.

69. van de Weijer, P., and M.M. Cremers (1982)
Experimental determination of 6^3P - 6^3P collisional excitation cross sections for line emission in the positive column of dc mercury discharges
Journal of Applied Physics, **53** (3), 1401-1408.

70. van de Weijer, P., and M.M. Cremers (1985)
Determination of the effective radiative lifetime of the 6^3P_1 atomic mercury level in low-pressure mercury discharges
Journal of Applied Physics, **57** (3), 672-677.

71. van de Weijer, P., and M.M. Cremers (1987)
Laser diagnostics for low-pressure mercury discharges
Philips Technical Review, **43** (3), 62-71.

72. Verderber, R.R., F.M. Rubinstein, and M.J. Siminovitch (1988)
Control of lamp wall temperature
Conference Record of 1988 IEEE Industry Applications Society Annual Meeting, **2**, 1848-1851.

73. Verweij, W. (1961)
Probe measurements and determination of electron mobility in the positive column of low-pressure mercury-argon discharges.
Philips Research Reports Supplements, **2**.

74. Vriens, L. (1973)
Energy balance in low-pressure gas discharges
Journal of Applied Physics, **44** (9), 3980-3989.

75. Walsh, P.J. (1959)
Effect of simultaneous Doppler and collision broadening and of hyperfine structure on the imprisonment of resonance radiation
Physical Review, **116** (3), 511-515.

76. Waymouth, J.F. (1971)
Electric Discharge Lamps
MIT Press, Cambridge, Massachusetts.

77. Waymouth, J.F., and F. Bitter (1956)
Analysis of the plasma of fluorescent lamps
Journal of Applied Physics, **27** (2), 122-131.

78. Winkler, R.B., J. Wilhelm, and R. Winkler (1983)
Kinetics of the Ar-Hg plasma of fluorescent lamp discharges
Annalen der Physik (Leipzig), **40**, 90-118; **40**, 119-139.

79. Zissis, G., P. Bénétruy, and I. Bernat (1992)
Modeling the Hg-Ar low-pressure-discharge positive column: A comparative study
Physical Review A, **45** (2), 1135-1148.

Appendix A

Transfer function coefficients for the calculation of cooling load due to lights

A.1 Coefficients determined experimentally by Mitalas

The transfer function coefficients a_1, a_2 and b_1 of equation (2.2) were determined experimentally by Mitalas (1973b) for 26 configurations. These experimentally determined coefficients are shown in Table A.1.

A.2 Design data derived by Mitalas from the experimental results

Mitalas (1973b) derived design values of a_1 by simply grouping the features of the room furnishings, lighting fixtures, and ventilation system into four combinations with each case represented by a single value of a_1. These four groups are given in Table A.2. The design values of b_1 derived by Mitalas (1973b) are listed in Table A.3.

Table A.1

Mitalas' experimental determined Z-transfer coefficients for lights. (Modified from Mitalas 1973b)

Test No.	Ventilation			Furnishing	a_1	a_2	b_1
	Rate (m^3s^{-1})	Supply type	Return type				
1	0.0472	CD-NID	SP-SL	BR	0.44	-0.35	0.91
2, 3	0.0472	CD-NID	RP-SL	BR	0.56	-0.45	0.89
4	0.0472	CD-ID	RP-SL	BR	0.50	-0.40	0.90
5, 6	0.0472	CD-ID	RP-SL	FO	0.55	-0.45	0 90
7, 8	0 0312	CD-ID	RP-SL	FC	0.51	-0.43	0.92
9, 10, 11	0.0661	CD-ID	RP-RLSS	FC	0.63	-0.56	0.93
12, 13	0.0661	CD-ID	RP-RL	FC	0.58	-0.51	0.93
14, 15, 16, 17	0.0312	WFCU	SP-SL	FC	0.53	-0.47	0.94
18	0.0312	WFCU	RP-SL	FC	0.59	-0.52	0.93
19	0.0312	WFCU	RP-RLSS	FC	0.55	-0.47	0.92
20, 21, 22	0.0661	LSS	SP-RL	FC	0.87	-0.80	0.93
23, 24, 25	0.0661	CD-ID	SP-SL	FC	0.59	-0.56	0.97
26	0.0661	CD-ID	SP-SL	BR	0.58	-0.51	0.93

Notes:

Ventilation rate was originally given by Mitalas (1973b) in cfm (cubic feet per minute), the ventilation rates in the above table have been converted to m^3s^{-1}:
0.0312 m^3s^{-1} = 66 cfm; 0.0472 m^3s^{-1} = 100 cfm; 0.0661 m^3s^{-1} = 140 cfm.

Supply type:

CD-NID = Supply air flow is via non-insulated ducts to ceiling diffusers.
CD-ID = Supply air flow is via insulated ducts to ceiling diffusers.
WFCU = Supply air is by wall fan coil units.
LSS = Supply air flow is via insulated ducts to luminaire side slots.

Return type:

SP-SL = Static plenum and static luminaire. The return air passes from the occupied space through wall grilles.
SP-RL = Static plenum and return luminaire. The return air passes from the occupied space through the luminaire and then via insulated ducts through the plenum space.
RP-SL = Return plenum and static luminaire. The return air passes from the occupied space through ceiling grilles and through the plenum.
RP-RL = Return plenum and return luminaire. The return air passes from the occupied space through the luminaire and through the plenum.

Furnishings:

BR = Bare room, no furnitures, no carpet.
FO = Furniture only - table, chair and filing cabinet; no carpet.
FC = Furniture and carpet. Table, chair and filing cabinet, and carpet.

Table A.2

Design values of a_1 coefficient in equation (2.2) derived by Mitalas. (Modified from Mitalas 1973b)

Furnishings	Air supply and return	Type of light fixture	Value of a_1
Heavyweight, single furnishings, no carpet	Low rate; supply and return below ceiling ($V \leq 0.00254\ m^3s^{-1}/m^2$)[a]	Recessed, not vented	0.45
Ordinary furniture, no carpet	Medium to high rate; supply and return below ceiling or through ceiling grille and space ($V \geq 0.00254\ m^3s^{-1}/m^2$)[a]	Recessed, not vented	0.55[b],[c]
Ordinary furniture, with or without carpet	Medium to high rate or fan coil or induction type air conditioning terminal unit; supply through ceiling or wall diffuser; return around light fixtures and through ceiling space ($V \geq 0.00254\ m^3s^{-1}/m^2$)[a]	Vented	0.65[c]
Any type of furniture	Ducted returns through light fixtures	Vented or free-hanging in airstream with ducted returns	0.75 or greater[d]

Notes:

[a] V is the room air supply rate, it was given in units of cfm per sq. ft. of floor area in Mitalas (1973b); $0.00254\ m^3s^{-1}/m^2 = 0.5$ cfm per sq. ft.

[b] Increase a_1 by 0.05 when carpet is used.

[c] The effect on a_1 value by furnishings decreases when light fixtures are used as air supply and/or return registers.

[d] The a_1 value is equal to the fraction of light power input that is picked up by ventilation air at light fixtures or 0.75, whichever is greater.

Table A.3

The b_1 values calculated by Mitalas (1973b) for different room air circulation rates and envelope construction. (Modified from Mitalas 1973b)

Room air circulation[a] and type of supply and return	Room envelope construction[b] 51 mm[c] wood floor	76 mm[c] concrete floor	152 mm[c] concrete floor	203 mm[c] concrete floor	305 mm[c] concrete floor
	Specific mass per unit floor area, kg m^{-2} 49[d]	196[d]	367[d]	587[d]	783[d]
Low	0.88	0.92	0.95	0.97	0.98
Medium	0.84	0.90	0.94	0.96	0.97
High	0.81	0 88	0.93	0.95	0.97
Very High	0.77	0.85	0.92	0.95	0.97
(see Note [b])	0.73	0.83	0.91	0.94	0.96

Notes:

[a] Low: Low ventilation rate - minimum required to cope with cooling load from lights and occupants in interior zone. Supply through floor, wall, or ceiling diffuser. Ceiling space not vented (not used for return air), and h = 2.3 W m^{-2}K^{-1} (where h = inside surface convection coefficient used in the calculation of b_1 value).

Medium: Medium ventilation rate, supply through floor, wall or ceiling diffuser. Ceiling space not vented (not used for return air), and h = 3.4 W m^{-2}K^{-1}.

High: High ventilation rate - room air circulation induced by primary air of induction unit or by fan coil unit. Return through ceiling space and h = 4.5 W m^{-2}K^{-1}.

Very high: High room air circulation used to minimise temperature gradients in a room. Return through ceiling space and h = 6.8 W m^{-2}K^{-1}.

[b] Floor covered with carpet and rubber pad; for a floor covered only with floor tile, take the next b_1 value down the column.

[c] Floor thickness values given in Mitalas (1973b) were in inches.

[d] Specific mass values given in Mitalas (1973b) were in lb/ft^2.

Appendix B

The fluorescent lamp positive column and ambipolar diffusion

Diffusion of electrons and ions takes place in the plasma of the fluorescent lamp discharge. Electrons diffuse to the walls faster than the positive mercury ions due to that electrons have a much smaller mass and higher random thermal velocities. Therefore, there is a charge separation so that an excess of positive ions exists in the centre of the positive column. This results in a positive charge at the centre of the plasma (hence the name positive column is given) and a negative charge near the wall. This charge separation has two effects:

(i) It tends to attract the electrons, slowing down their diffusion rate to the wall.

(ii) It produces a radial electric field, which accelerates the rate of diffusion of positive ions to the wall.

The net effect is that the diffusion of electrons is slowed down and that of ions is accelerated until they both diffuse at the same rate. This phenomenon is called *ambipolar diffusion*. The rate at which electrons and positive ions are diffusing is called the ambipolar diffusion rate.

The ambipolar diffusion coefficient D_a can be calculated from the transport equations for ions and electrons (Waymouth 1971):

$$\Gamma_i = N_i \mu_i E_r - D_i \frac{dN_i}{dr} \tag{B.1}$$

$$\Gamma_e = -N_e \mu_e E_r - D_e \frac{dN_e}{dr} \tag{B.2}$$

where Γ_i and Γ_e are the particle current densities of ions and electrons, N_i and N_e are the ion and electron densities, μ_i and μ_e are the ion and electron mobilities, D_i and D_e are the ion and electron diffusion coefficients, and E_r is the radial electric field due to the excess ion space charge. The quantity E_r can be eliminated between the two equations by noting that $N_i = N_e$ in the positive column (the symbol N_e will be used in the following), and the particle fluxes Γ_i and Γ_e are equal (the symbol Γ will be used in the following) (Waymouth 1971):

$$\frac{1}{\mu_i}\Gamma + \frac{1}{\mu_e}\Gamma = -\left\{\frac{D_i}{\mu_i} + \frac{D_e}{\mu_e}\right\}\frac{dN_e}{dr} \tag{B.3}$$

The diffusion coefficient of a charged particle can be expressed in terms of its mobility by the relationship (Waymouth 1971):

$$D = \frac{\mu kT}{e} \tag{B.4}$$

Also, since $\mu_i << \mu_e$, $\frac{1}{\mu_i} + \frac{1}{\mu_e} \approx \frac{1}{\mu_i}$. Thus:

$$\Gamma = -\frac{\mu_i k(T_e + T_i)}{e}\frac{dN_e}{dr} \tag{B.5}$$

In a low pressure mercury discharge positive column, the ion temperature is low, 300 K to 500 K at most, while T_e is of the order of 10,000 K. Therefore, the following equation is obtained between the electron diffusion flux and the radial gradient of electron density (Waymouth 1971):

$$\Gamma = -\frac{\mu_i kT_e}{e}\frac{dN_e}{dr} = -D_a\frac{dN_e}{dr} \tag{B 6}$$

In equation (B.6), D_a is the ambipolar diffusion coefficient:

$$D_a = \frac{\mu_i k T_e}{e} \tag{B.7}$$

Appendix C

Calculation of convective heat transfer coefficients

For most situations in a typical occupied enclosure, free convection takes place over surfaces inside the enclosure because the velocity of air flow near the surface nodes is not high. In fact, in both LITEAC1 and LITEAC2, the air within a compartment is considered in bulk as a single air node and the air velocity, which is not calculated, is assumed to be very low so that free convection takes place between a surface node and the air node. However, for return air via luminaires, air velocity inside luminaire may be high enough for forced convection to take place on the luminaire and lamp surfaces. Therefore, the programs LITEAC1 and LITEAC2 calculate the convection coefficient based on node geometry and temperature or allow direct input of a convection coefficient for each node which can be calculated elsewhere based on the velocity of air flow through the luminaire.

In both LITEAC1 and LITEAC2, a subroutine CONVEC is used for the calculation of the heat gain/loss due to convective heat transfer between the surface node and the adjacent air. In this subroutine, the convective heat transfer coefficient h_i in equations (4.12) and (4.13) is calculated based on empirical equations for free convection given in Holman (1992) as described below.

A surface node is assumed to be isothermal. For an isothermal surface, Holman (1992) gives the following functional form for the dimensionless Nusselt number to represent the average free-convection heat transfer coefficient for a variety of circumstances:

$$\overline{Nu}_f = C(Gr_f Pr_f)^m \tag{C.1}$$

where $\overline{Nu} = \frac{hL}{k}$ (C.2)

Gr is the Grashof number and Pr is the Prandtl number:

$$Gr = \frac{g\beta(T_w - T_\infty)L^3}{\nu^2} \tag{C.3}$$

$$Pr = \frac{\nu}{\alpha} \tag{C.4}$$

C and m are constants depending on the geometry and range of values of the product $Gr_f Pr_f$.

The subscript f represents that the properties in the dimensionless groups Nu, Gr and Pr are evaluated at the film temperature $T_f = \frac{T_\infty + T_w}{2}$.

In equations (C.2) to (C.4), L is the characteristic length of the surface which depends on the geometry of the surface; k is the thermal conductivity of air; g is the gravitational acceleration; β is volume coefficient of expansion of air; T_w is the surface temperature; T_∞ is the air temperature; ν is the viscosity of air; α is the thermal diffusivity of air.

The product of Gr and Pr is called the Rayleigh number Ra.

$$Ra = \frac{g\beta(T_w - T_\infty)L^3}{\nu^2} Pr \tag{C.5}$$

In the subroutine CONVEC, Ra is calculated first assuming Pr and ν to be constant throughout the range of temperatures considered. The values used are taken from Holman (1992) for a temperature of 300 K:

$Pr_f = 0.708$

$\nu = 15.69 \times 10^{-6}\ m^2 s^{-1}$

Depending on the body type and the range of *Ra*, the subroutine CONVEC uses different values for the constant *C* and the power index *m* in equation (C.1) for the calculation of h_i. The values of *C* and *m* are taken from Holman (1992) and are listed in Table C.1.

In the input data, a number is used to represent the node geometry (body type) of each node; the numbers used for all node geometries considered are listed in Table C.1. The characteristic length is also an input parameter for each node, which should be calculated according to (see Holman 1992):

Horizontal plates: $L = \dfrac{Area}{Perimeter}$

Vertical plates: $L = Height\ of\ plate$

Horizontal cylinder: $L = Diameter\ of\ cylinder$

The Rayleigh number *Ra* is calculated using equation (C.5) at each time step using the calculated node temperature and air temperature at the time step. Then, depending on the body geometry and the range of *Ra*, the constant *C* and power index *m* are determined according to Table C.1. Equation (C.1) is used to calculate the Nusselt number over the node. Finally, equation (C.2) is used to calculate the convective heat transfer coefficient h_i using a value of thermal conductivity of air at the 300 K and the characteristic length of the surface. The calculated h_i will be used for the computation of convective heat transfer between the surface node and the adjacent air node.

Table C.1

Coefficient C and power index m for different geometry used in LITEAC1 and LITEAC2 for the calculation of convective heat transfer coefficient h_l in equation (C.1) and (C.2).

Node geometry	Body type number used in LITEAC1 and LITEAC2	$Ra = Gr_f Pr_f$	C	m
Horizontal plate - heated upper surface	1	$\leq 8 \times 10^6$	0.54	0.25
		$> 8 \times 10^6$	0.15	0.3333
Horizontal plate - cooled upper surface	1	$\leq 1 \times 10^5$	0	0
		$> 1 \times 10^5$	0.27	0.25
Horizontal plate - heated lower surface	2	$\leq 1 \times 10^5$	0	0
		$> 1 \times 10^5$	0.27	0.25
Horizontal plate - cooled lower surface	2	$\leq 8 \times 10^6$	0.54	0.25
		$> 8 \times 10^6$	0.15	0.3333
Vertical plate	3	all	0.59	0.25
Horizontal cylinder	6	$\leq 1 \times 10^2$	1.02	0.148
		$1 \times 10^2 - 1 \times 10^4$	0.85	0.188
		$1 \times 10^4 - 1 \times 10^7$	0.48	0.25
		$> 1 \times 10$	0.125	0.3333
Other body type	7	all	h_l is an input parameter	
Forced convection	7	N.A.	h_l is an input parameter	

Appendix D

Explicit forms of energy dissipation terms in the energy balance equation of the fluorescent lamp discharge

The terms W_{inel}, W_{ion}, W_{el}, W_{diff} and W_{sel} in equation (5.1) can be calculated if the cross-sections of transitions for inelastic collisions (including ionization) and for elastic collisions, the diffusion coefficient of the electrons and the electron energy distribution function are known. These terms can be written in a more explicit form (Zissis et al. 1992) as:

$$W_{inel} = N_e \sum_k \left(\sum_{j<k} N_j E_{jk} \left\langle v_e Q_{jk} \right\rangle \right) \tag{D.1}$$

$$W_{ion} = N_e \sum_j N_j E_{ji} \left\langle v_e Q_{ji} \right\rangle \tag{D.2}$$

$$W_{el} = N_e N_{Hg} \sum_j \frac{N_j}{N_{Hg}} \frac{2m_e}{m_j} \left\langle v_e Q_{ej}^m E_e \right\rangle \tag{D.3}$$

$$W_{diff} = div\left[D_e^m N_{Hg}\, grad\left(\frac{N_e}{N_{Hg}} \right) \right] \left\langle E_e \right\rangle \tag{D.4}$$

$$W_{sel} = N_e \sum_k \left(\sum_{j>k} N_k E_{jk} \left\langle v_e Q_{kj} \right\rangle \right) \tag{D.5}$$

where N_e is the electron density (m^{-3}), i.e. the number of electrons per unit volume of the positive column; N_j is the density (number per unit volume of positive column) of the j^{th} mercury state (m^{-3}); N_{Hg} is the total density of the mercury atoms (m^3); m_e is the electronic mass (kg); m_j is the mass of the j^{th} mercury state (kg); E_{jk} is the energy gap

(J) between j^{th} and k^{th} states; E_e is the energy of the electron (J); v_e is the velocity of the electron (m s^{-1}); Q_{jk} is the cross section (m^2) for the transition between the j^{th} and k^{th} mercury states; Q^m_{ej} represents the momentum-transfer cross section (m^2) for the elastic collisions between electrons and mercury atoms of the j^{th} state; D^m_e is the diffusion coefficient of the electrons. In equations (D.1) to (D.5), quantities written in the form $\langle A \rangle$ represent the average value of A over the electron energy distribution $f(E_e)$, i.e.

$$\langle A \rangle = \frac{1}{N_e} \int_0^\infty A f(E_e) dE_e \tag{D.6}$$

Appendix E

Program LITEAC1

E.1 Description of the program

The computer program LITEAC1 consists of a main program and four subroutines: LWAVE, SWAVE, CONVEC and LPLL. The main program and these four subroutines are described in the following sub-sections.

E.1.1 Main program LITEAC1

The main program reads input data from six data files. Features and data content of these six data files are described in Section E.3. The main program reads the nodal data of area, thermal capacity, long- and short-wave emissivity, reflectance and transmittance, and initial temperature, and also the body type and the characteristic length for each node for the calculation of convective heat transfer coefficient (Appendix C), and a matrix of radiation form factors between pairs of nodes. The main program also reads the number of on-off cycles of the lights, the number of hours with lights on in one cycle and the time step for the simulation. The main program then reads, from the lamp data file, the rated lamp power, the rated lumen output, the rated ballast power, the luminous efficacy of radiation, and a set of data points to represent the empirical curves of lamp power and light output against minimum lamp wall temperature. Using the temperature of the lamp node at the start of each time step (the input initial lamp node temperature for the first time step or the calculated lamp node temperature for other time steps) as input, the main program calls the subroutine LPLL to calculate the lamp power and light output of the lamp node in that time step. From the light output calculated by LPLL, the main program then calculates the short-wave power output of the lamp node using the input value of the luminous efficacy of radiation. If there are more than one lamp nodes defined, then the lamp power and the short-wave radiation power are assumed to be equally divided between all the lamp nodes. The main program then calls LWAVE, SWAVE and CONVEC in turn to calculate the net nodal heat gains due to long-wave radiation, short-wave radiation and convection. The calculation of the conduction heat gain is included in the main program. With all these net heat gains calculated for the time step, the main program then calculates the temperature change of the node in the time step. The calculation is repeated for all nodes. The new set of nodal temperatures will then be used to perform calculations for a successive new time step. The calculations are repeated for the period of simulation specified in the input file 'INDAT' (Section E.3). LITEAC1 gives output at intervals specified in the input file 'INDAT'. The output data, which are written to file names specified in the input file 'INDAT' (Section E.3), consist of nodal temperatures, power gains at each node, cooling load, conductive and convective heat fluxes at each node, long- and short-wave radiation fluxes at each node, illuminance on each nodal surface.

E.1.2 Subroutine LWAVE

LWAVE calculates the long-wave (thermal) radiation exchange between nodes in a compartment. This subroutine requires input, from the main program, the following data: number of nodes, number of 'lens' (i.e. transparent/translucent to long-wave radiation) nodes, the node numbers of all lens nodes, long-wave emissivities of all nodes, reflectances of all nodes, areas of all nodes, temperatures (at start of the time step) of all nodes, and a form factor matrix of the form factors between pairs of nodes. Using a COMMON statement, LWAVE also shares the transmittance data of the nodes in all three sections: the luminaire, the plenum and the room. This is required because LWAVE calculates the long-wave radiation transfer between nodes in an enclosed section, but the lens nodes may transmit long-wave radiation to adjacent sections. An example is that if the diffuser of a luminaire is transparent/translucent to long-wave radiation, it will transmit long-wave radiation from the luminaire compartment to the room compartment and vice versa. Therefore, transparent/translucent nodes need special treatment. With all these data, LWAVE calculates the net heat gain due to long-wave radiation for all nodes according to equations (4.2)-(4.7). It then returns the long-wave radiation heat gains for all nodes to the main program.

E.1.3 Subroutine SWAVE

SWAVE calculates the short-wave (visible) radiation exchange between nodes in a compartment. This subroutine requires input, from the main program, the following data: number of nodes, number of 'lens' (i.e. transparent/translucent to short-wave radiation) nodes, the node numbers of all lens nodes, number of 'lamp' nodes (i.e. nodes generating short-wave radiation), the node numbers of all lamp nodes, short-wave emissivities of all nodes, reflectances of all nodes, areas of all nodes, and a form factor matrix of the form factors between pairs of nodes. Using a COMMON statement, SWAVE also shares the short-wave transmittance data of the nodes in all three sections: the luminaire, the plenum and the room. SWAVE differs from LWAVE in that SWAVE does not require the data of nodal temperatures but requires data of the short-wave power output of the 'lamps' nodes. SWAVE calculates the net heat gain due to short-wave radiation for all nodes according to equations (4.8)-(4.11). It then returns the short-wave radiation heat gains for all nodes to the main program.

E.1.4 Subroutine CONVEC

CONVEC calculates the net heat gain due to convection for all nodes in contact with the air node in the compartment. It also calculates the net convective heat gain of the air node. It requires input from the main program the following data: number of nodes, the body type of each node (Appendix C), the characteristic length of each node (Appendix C), the area of each node, and the temperatures of all nodes. It uses the correlations described in Appendix C for the calculations of the convective heat transfer coefficients. It then calculates the net convective heat gain for all nodes according equations (4.12)-(4.13). It returns to the main program the convective heat gain for all nodes in the compartment in a vector variable.

E.1.5 Subroutine LPLL

This subroutine calculates the lamp power and lamp lumen output using points in empirical curves (Section 4.2.1). It requires input of the following data: number of lamp nodes, temperature of each lamp node, rated lamp power and rated lumen output of the lamp, the number of points (N) in the empirical curves, an $N \times 3$ matrix containing the points in the empirical curves of relative lamp power and relative light output against minimum lamp wall temperature. LPLL compares the temperatures of all lamp nodes and finds the minimum lamp wall temperature as the lowest temperature amongst all the lamp nodes. It then calculates the lamp power and light output by linear interpolation between the two points with temperatures nearest to the minimum lamp wall temperature.

E.2 Program listing

```
      PROGRAM LITEAC1
C
C  TRANSIENT THERMAL MODEL OF AN ENCLOSURE WITH A FLUORESCENT LUMINAIRE
C  AS THE ONLY HEAT AND RADIATION SOURCE AND AN IDEALLY CONTROLLED
C  AIR-CONDITIONING SYSTEM FOR KEEPING ROOM AIR TEMPERATURE CONSTANT
C
C  THE ENCLOSURE IS DIVIDED INTO 3 SECTIONS:
C   1. THE LUMINAIRE SECTION;
C   2. THE PLENUM SECTION;
C   3. THE ROOM SECTION.
C
C  FOR ALL SECTIONS, THE FIRST NODE IS THE AIR NODE
C
C
      REAL AL(20),AP(20),AR(20),CL(20),CP(20),
     1  CR(20),EML(20),EMP(20),EMR(20),FL(20,20),FP(20,20),FR(20,20),
     2  CHARLL(20),CHARLP(20),CHARLR(20),
     3  RHOLL(20),RHOLP(20),RHOLR(20),RHOSL(20),RHOSP(20),RHOSR(20),
     4  TRANSL(20),TRANSP(20),TRANSR(20),TRANLL(20),TRANLP(20),
     5  TRANLR(20),DTIME,LAMPP,LAMPLM,LPMAX,LLMAX,EFFIC,SWPOW,BALPOW,
     6  CHRP,CHRL,CHPL,CKBS(30),OUTIME
```

```
      DOUBLE PRECISION TL(20),TP(20),TR(20),TDUM(5),DTL(20),
     1  DTP(20),DTR(20),QGL(20),QGP(20),QGR(20),QLL(20),QLP(20),
     2  QLR(20),QSL(20),QSP(20),QSR(20),QHL(20),QHP(20),QHR(20),
     3  QCL(20),QCP(20),QCR(20),DQL(20),DQP(20),DQR(20),
     4  ELL(20),ELP(20),ELR(20),RLO(80,3),ESL(20),ESP(20),
     5  ESR(20),QCDUM,TENV
      INTEGER NTIME,NTOFF,NHROFF,NDAY,NTONDT,NTOFFT,IKBS(30,5),
     1  NBTL(20),NBTP(20),NBTR(20),
     2  NLAL,NLAP,NLAR,NLAMPL(5),NLAMPP(5),NLAMPR(5),
     3  NLNL,NLNP,NLNR,NLENSL(5,3),NLENSP(5,3),NLENSR(5,3),
     4  NTYPEL,NTYPEP,NTYPER
      CHARACTER B,HORM
      CHARACTER*12 INPUT1,INPUT2,INPUT3,INPUT4,INPUT5,
     1  OUTPU1,OUTPU2,OUTPU3,OUTPU4
      COMMON /LW/ TRANLL, TRANLP, TRANLR, ELL, ELP, ELR,
     1  /SW/ TRANSL,TRANSP,TRANSR,ESL,ESP,ESR
C
C   FORMAT STATEMENTS
C
   27 FORMAT (1X,F10.2,12F11.5)
C
C   SPECIFYING INPUT AND OUTPUT FILENAMES
C
      OPEN (7,FILE='INDAT',STATUS='OLD')
      READ (7,*) INPUT1,INPUT2,INPUT3,INPUT4,INPUT5,OUTPU1,OUTPU2,
     1  OUTPU3,OUTPU4,B,NTIME,NHROFF,DTIME,OUTIME,HORM
      CLOSE (7)
      IF ((HORM .EQ. 'H') .OR. (HORM .EQ. 'h')) THEN
        OUTIME=OUTIME*3600.
       ELSE IF ((HORM .EQ. 'M') .OR. (HORM .EQ. 'm')) THEN
        OUTIME=OUTIME*60.
       ELSE IF ((HORM .EQ. 'S') .OR. (HORM .EQ. 's')) THEN
        OUTIME=OUTIME
       ELSE
        WRITE (*,*) (' OUTPUT TIME INTERVAL ERROR')
        STOP
      END IF
C
C   READ INPUT DATA
C
      OPEN (8,FILE=INPUT1,STATUS='OLD')
      READ (8,*) NL,NLAL,(NLAMPL(I),I=1,NLAL),NLNL,
     1  ((NLENSL(I,J),J=1,3),I=1,NLNL),NBASTL,(TL(I),I=1,NL),
     2  (AL(I),I=1,NL),(CL(I),I=1,NL),(EML(I),I=1,NL),(RHOLL(I),I=1,NL),
     3  (RHOSL(I),I=1,NL),(TRANLL(I),I=1,NL),(TRANSL(I),I=1,NL),
     4  ((FL(I,J),J=1,NL),I=1,NL),(NBTL(I),I=1,NL),(CHARLL(I),I=1,NL)
      CLOSE (8)
C
      OPEN (9,FILE=INPUT2,STATUS='OLD')
      READ (9,*) NP,NLAP,(NLAMPP(I),I=1,NLAP),NLNP,
     1  ((NLENSP(I,J),J=1,3),I=1,NLNP),(TP(I),I=1,NP),
     2  (AP(I),I=1,NP),(CP(I),I=1,NP),(EMP(I),I=1,NP),(RHOLP(I),I=1,NP),
     3  (RHOSP(I),I=1,NP),(TRANLP(I),I=1,NP),(TRANSP(I),I=1,NP),
     4  ((FP(I,J),J=1,NP),I=1,NP),(NBTP(I),I=1,NP),(CHARLP(I),I=1,NP)
      CLOSE (9)
C
      OPEN (10,FILE=INPUT3,STATUS='OLD')
      READ (10,*) NR,NLAR,(NLAMPR(I),I=1,NLAR),NLNR,
     1  ((NLENSR(I,J),J=1,3),I=1,NLNR),(TR(I),I=1,NR),
     2  (AR(I),I=1,NR),(CR(I),I=1,NR),(EMR(I),I=1,NR),(RHOLR(I),I=1,NR),
     3  (RHOSR(I),I=1,NR),(TRANLR(I),I=1,NR),(TRANSR(I),I=1,NR),
```

```
     4  ((FR(I,J),J=1,NR),I=1,NR),(NBTR(I),I=1,NR),(CHARLR(I),I=1,NR)
      CLOSE (10)
C
      IF ((NLAL .NE. 0) .OR. (NLAP .NE. 0) .OR. (NLAR .NE. 0)) THEN
      OPEN (11,FILE=INPUT4,STATUS='OLD')
      READ (11,*) LPMAX,LLMAX,BALPOW,EFFIC,
     1  NPOINT,((RLO(I,J),J=1,3),I=1,NPOINT)
      CLOSE (11)
      END IF
C
      OPEN (12,FILE=INPUT5,STATUS='OLD')
      READ (12,*) NCOND, ((IKBS(I,J),J=1,5),CKBS(I),I=1,NCOND),
     1  CHRP,CHRL,CHPL,TENV
      CLOSE (12)
C
      AL(1)=1.0
      AP(1)=1.0
      AR(1)=1.0
C
C
      OPEN (13,FILE=OUTPU1,STATUS='NEW')
C
      OPEN (14,FILE=OUTPU2,STATUS='NEW')
C
      OPEN (15,FILE=OUTPU3,STATUS='NEW')
C
      OPEN (16,FILE=OUTPU4,STATUS='NEW')
C
C
      X=0.
      WRITE (13,27) X,(TL(I)-273.,I=1,NL)
      WRITE (14,27) X,(TP(I)-273.,I=1,NP)
      WRITE (15,27) X,(TR(I)-273.,I=1,NR)
      WRITE (16,27) X,LAMPP+QGL(NBASTL),ESR(8)*EFFIC
      IF ((B.EQ.'Y').OR.(B.EQ.'y')) THEN
        NDAY=NTIME
        NTIME=86400
      ELSE
        NDAY=1
        NTIME=NTIME*3600
      END IF
      NTOFF=NHROFF*3600
C
      NTYPEL=1
      NTYPEP=2
      NTYPER=3
C
C   CALCULATE VALUES OF THE POWER INPUT AT NODES
C
      DO 45 I=1,NL
      QGL(I)=0.
   45 CONTINUE
      DO 46 I=1,NP
      QGP(I)=0.
   46 CONTINUE
      DO 47 I=1,NR
      QGR(I)=0.
   47 CONTINUE
      NTONDT=NINT(FLOAT(NTIME)/DTIME)
      NTOFFT=NINT(FLOAT(NTOFF)/DTIME)
      DO 700 LL=1,NDAY
```

```
C
      DO 700 KK=1,NTONDT
      IF (KK .GT. NTOFFT) THEN
         LAMPP=0.
         SWPOW=0.
      ELSE
        DO 50 K=1,NLAL
          TDUM(K)=TL(NLAMPL(K))
   50   CONTINUE
C
        IF (NLAL .NE. 0) THEN
        CALL LPLL(NLAL,NLAMPL,LAMPP,LAMPLM,LPMAX,LLMAX,TL,NPOINT,
     1    RLO)
        SWPOW=LAMPLM/EFFIC
        END IF
      END IF
      IF (NLAL .EQ. 0) GO TO 60
      IF (LAMPP .EQ. 0.) THEN
        QGL(NLAMPL(1))=0.
      ELSE
        QGL(NLAMPL(1))=LAMPP/NLAL
      END IF
      IF (NLAL .GT. 1) THEN
        DO 55 K=2,NLAL
        QGL(NLAMPL(K))=QGL(NLAMPL(1))
   55   CONTINUE
      END IF
C
C  LUMINIARE NODE NBASTL IS THE BALLAST NODE
C
   60 QGL(NBASTL)=BALPOW*LAMPP
C       END IF
      IF (NL .NE. 0) CALL LWAVE(NL,NTYPEL,NLNL,NLENSL,EML,FL,RHOLL,
     1  AL,TL,QLL)
      IF (NP .NE. 0) CALL LWAVE(NP,NTYPEP,NLNP,NLENSP,EMP,FP,RHOLP,
     1  AP,TP,QLP)
      IF (NR .NE. 0) CALL LWAVE(NR,NTYPER,NLNR,NLENSR,EMR,FR,RHOLR,
     1  AR,TR,QLR)
C  ===================================(8/2/95)
      IF (SWPOW .EQ. 0.) THEN
        DO 65 I=1,NL
        QSL(I)=0.
        ESL(I)=0.
   65   CONTINUE
        DO 66 I=1,NP
        QSP(I)=0.
        ESP(I)=0.
   66   CONTINUE
        DO 67 I=1,NR
        QSR(I)=0.
        ESR(I)=0.
   67   CONTINUE
        GOTO 70
      END IF
C  ===================================
      IF (NL .NE. 0) CALL SWAVE(NL,NTYPEL,NLNL,NLENSL,NLAL,NLAMPL,
     1  FL,RHOSL,AL,SWPOW,QSL)
      IF (NP .NE. 0) CALL SWAVE(NP,NTYPEP,NLNP,NLENSP,NLAP,NLAMPP,
     1  FP,RHOSP,AP,SWPOW,QSP)
      IF (NR .NE. 0) CALL SWAVE(NR,NTYPER,NLNR,NLENSR,NLAR,NLAMPR,
     1  FR,RHOSR,AR,SWPOW,QSR)
```

```
C  ==========================================
   70 IF (NL .NE. 0) CALL CONVEC(NL,NBTL,CHARLL,AL,TL,QHL)
      IF (NP .NE. 0) CALL CONVEC(NP,NBTP,CHARLP,AP,TP,QHP)
      IF (NR .NE. 0) CALL CONVEC(NR,NBTR,CHARLR,AR,TR,QHR)
C
      DO 400 I=1,NL
      QCL(I)=0.
  400 CONTINUE
      DO 410 I=1,NP
      QCP(I)=0.
  410 CONTINUE
      DO 420 I=1,NR
      QCR(I)=0.
  420 CONTINUE
C
      DO 450 I=1,NCOND
      IF (IKBS(I,1) .EQ. 1) THEN
        IF (IKBS(I,3) .EQ. 1) THEN
          IF (IKBS(I,5) .EQ. 1 ) THEN
           QCDUM=CKBS(I)*TL(IKBS(I,2))*AL(IKBS(I,2))
          ELSE IF (IKBS(I,5) .EQ. 2) THEN
           QCDUM=CKBS(I)*(TL(IKBS(I,2))-TL(IKBS(I,4)))*AL(IKBS(I,4))
          END IF
          QCL(IKBS(I,4))=QCL(IKBS(I,4))+QCDUM
          QCL(IKBS(I,2))=QCL(IKBS(I,2))-QCDUM
         ELSE IF (IKBS(I,3) .EQ. 2) THEN
          IF (IKBS(I,5) .EQ. 1 ) THEN
           QCDUM=CKBS(I)*TL(IKBS(I,2))*AL(IKBS(I,2))
          ELSE IF (IKBS(I,5) .EQ. 2) THEN
           QCDUM=CKBS(I)*(TL(IKBS(I,2))-TP(IKBS(I,4)))*AP(IKBS(I,4))
          END IF
          QCP(IKBS(I,4))=QCP(IKBS(I,4))+QCDUM
          QCL(IKBS(I,2))=QCL(IKBS(I,2))-QCDUM
         ELSE IF (IKBS(I,3) .EQ. 3) THEN
          IF (IKBS(I,5) .EQ. 1 ) THEN
           QCDUM=CKBS(I)*TL(IKBS(I,2))*AL(IKBS(I,2))
          ELSE IF (IKBS(I,5) .EQ. 2) THEN
           QCDUM=CKBS(I)*(TL(IKBS(I,2))-TR(IKBS(I,4)))*AR(IKBS(I,4))
          END IF
          QCR(IKBS(I,4))=QCR(IKBS(I,4))+QCDUM
          QCL(IKBS(I,2))=QCL(IKBS(I,2))-QCDUM
         ELSE IF (IKBS(I,3) .EQ. 0) THEN
          IF (IKBS(I,5) .EQ. 1 ) THEN
           QCDUM=CKBS(I)*TL(IKBS(I,2))*AL(IKBS(I,2))
          ELSE IF (IKBS(I,5) .EQ. 2) THEN
           QCDUM=CKBS(I)*(TL(IKBS(I,2))-TENV)*AL(IKBS(I,2))
          END IF
          QCL(IKBS(I,2))=QCL(IKBS(I,2))-QCDUM
        END IF
       ELSE IF (IKBS(I,1) .EQ. 2) THEN
        IF (IKBS(I,3) .EQ. 1) THEN
          IF (IKBS(I,5) .EQ. 1 ) THEN
           QCDUM=CKBS(I)*TP(IKBS(I,2))*AP(IKBS(I,2))
          ELSE IF (IKBS(I,5) .EQ. 2) THEN
           QCDUM=CKBS(I)*(TP(IKBS(I,2))-TL(IKBS(I,4)))*AL(IKBS(I,4))
          END IF
          QCL(IKBS(I,4))=QCL(IKBS(I,4))+QCDUM
          QCP(IKBS(I,2))=QCP(IKBS(I,2))-QCDUM
         ELSE IF (IKBS(I,3) .EQ. 2) THEN
          IF (IKBS(I,5) .EQ. 1 ) THEN
           QCDUM=CKBS(I)*TP(IKBS(I,2))*AP(IKBS(I,2))
```

```
    ELSE IF (IKBS(I,5) .EQ. 2) THEN
     QCDUM=CKBS(I)*(TP(IKBS(I,2))-TP(IKBS(I,4)))*AP(IKBS(I,4))
    END IF
    QCP(IKBS(I,4))=QCP(IKBS(I,4))+QCDUM
    QCP(IKBS(I,2))=QCP(IKBS(I,2))-QCDUM
   ELSE IF (IKBS(I,3) .EQ. 3) THEN
    IF (IKBS(I,5) .EQ. 1 ) THEN
     QCDUM=CKBS(I)*TP(IKBS(I,2))*AP(IKBS(I,2))
    ELSE IF (IKBS(I,5) .EQ. 2) THEN
     QCDUM=CKBS(I)*(TP(IKBS(I,2))-TR(IKBS(I,4)))*AR(IKBS(I,4))
    END IF
    QCR(IKBS(I,4))=QCR(IKBS(I,4))+QCDUM
    QCP(IKBS(I,2))=QCP(IKBS(I,2))-QCDUM
   ELSE IF (IKBS(I,3) .EQ. 0) THEN
    IF (IKBS(I,5) .EQ. 1 ) THEN
     QCDUM=CKBS(I)*TP(IKBS(I,2))*AP(IKBS(I,2))
    ELSE IF (IKBS(I,5) .EQ. 2) THEN
     QCDUM=CKBS(I)*(TP(IKBS(I,2))-TENV)*AP(IKBS(I,2))
    END IF
    QCP(IKBS(I,2))=QCP(IKBS(I,2))-QCDUM
   END IF
ELSE IF (IKBS(I,1) .EQ. 3) THEN
 IF (IKBS(I,3) .EQ. 1) THEN
    IF (IKBS(I,5) .EQ. 1 ) THEN
     QCDUM=CKBS(I)*TR(IKBS(I,2))*AR(IKBS(I,2))
    ELSE IF (IKBS(I,5) .EQ. 2) THEN
     QCDUM=CKBS(I)*(TR(IKBS(I,2))-TL(IKBS(I,4)))*AL(IKBS(I,4))
    END IF
    QCL(IKBS(I,4))=QCL(IKBS(I,4))+QCDUM
    QCR(IKBS(I,2))=QCR(IKBS(I,2))-QCDUM
   ELSE IF (IKBS(I,3) .EQ. 2) THEN
    IF (IKBS(I,5) .EQ. 1 ) THEN
     QCDUM=CKBS(I)*TR(IKBS(I,2))*AR(IKBS(I,2))
    ELSE IF (IKBS(I,5) .EQ. 2) THEN
     QCDUM=CKBS(I)*(TR(IKBS(I,2))-TP(IKBS(I,4)))*AP(IKBS(I,4))
    END IF
    QCP(IKBS(I,4))=QCP(IKBS(I,4))+QCDUM
    QCR(IKBS(I,2))=QCR(IKBS(I,2))-QCDUM
   ELSE IF (IKBS(I,3) .EQ. 3) THEN
    IF (IKBS(I,5) .EQ. 1 ) THEN
     QCDUM=CKBS(I)*TR(IKBS(I,2))*AR(IKBS(I,2))
    ELSE IF (IKBS(I,5) .EQ. 2) THEN
     QCDUM=CKBS(I)*(TR(IKBS(I,2))-TR(IKBS(I,4)))*AR(IKBS(I,4))
    END IF
    QCR(IKBS(I,4))=QCR(IKBS(I,4))+QCDUM
    QCR(IKBS(I,2))=QCR(IKBS(I,2))-QCDUM
   ELSE IF (IKBS(I,3) .EQ. 0) THEN
    IF (IKBS(I,5) .EQ. 1 ) THEN
     QCDUM=CKBS(I)*TR(IKBS(I,2))*AR(IKBS(I,2))
    ELSE IF (IKBS(I,5) .EQ. 2) THEN
     QCDUM=CKBS(I)*(TR(IKBS(I,2))-TENV)*AR(IKBS(I,2))
    END IF
    QCR(IKBS(I,2))=QCR(IKBS(I,2))-QCDUM
 END IF
ELSE IF (IKBS(I,1) .EQ. 0) THEN
 IF (IKBS(I,3) .EQ. 1) THEN
    IF (IKBS(I,5) .EQ. 1 ) THEN
     QCDUM=CKBS(I)*TENV*AL(IKBS(I,4))
    ELSE IF (IKBS(I,5) .EQ. 2) THEN
     QCDUM=CKBS(I)*(TENV-TL(IKBS(I,4)))*AL(IKBS(I,4))
    END IF
```

```
         QCL(IKBS(I,4))=QCL(IKBS(I,4))+QCDUM
        ELSE IF (IKBS(I,3) .EQ. 2) THEN
         IF (IKBS(I,5) .EQ. 1 ) THEN
          QCDUM=CKBS(I)*TENV*AP(IKBS(I,4))
         ELSE IF (IKBS(I,5) .EQ. 2) THEN
          QCDUM=CKBS(I)*(TENV-TP(IKBS(I,4)))*AP(IKBS(I,4))
         END IF
         QCP(IKBS(I,4))=QCP(IKBS(I,4))+QCDUM
        ELSE IF (IKBS(I,3) .EQ. 3) THEN
         IF (IKBS(I,5) .EQ. 1 ) THEN
          QCDUM=CKBS(I)*TENV*AR(IKBS(I,4))
         ELSE IF (IKBS(I,5) .EQ. 2) THEN
          QCDUM=CKBS(I)*(TENV-TR(IKBS(I,4)))*AR(IKBS(I,4))
         END IF
         QCR(IKBS(I,4))=QCR(IKBS(I,4))+QCDUM
        END IF
      END IF
  450 CONTINUE
C
      DO 500 I=1,NL
        IF (CL(I) .NE. 0.) THEN
        DQL(I)=QGL(I)+QLL(I)+QSL(I)+QHL(I)+QCL(I)
        DTL(I)=DQL(I)*DTIME/CL(I)
        TL(I)=TL(I)+DTL(I)
        END IF
  500 CONTINUE
      DO 510 I=1,NP
        IF (CP(I) .NE. 0.) THEN
        DQP(I)=QGP(I)+QLP(I)+QSP(I)+QHP(I)+QCP(I)
        DTP(I)=DQP(I)*DTIME/CP(I)
        TP(I)=TP(I)+DTP(I)
        END IF
  510 CONTINUE
C
      DO 515 I=2,NR
        IF (CR(I) .NE. 0.) THEN
        DQR(I)=QGR(I)+QLR(I)+QSR(I)+QHR(I)+QCR(I)
        DTR(I)=DQR(I)*DTIME/CR(I)
        TR(I)=TR(I)+DTR(I)
        END IF
  515 CONTINUE
C
      IF (FLOAT(KK)/ANINT(OUTIME/DTIME) .EQ.
     1  FLOAT(KK/NINT(OUTIME/DTIME))) THEN
        IF ((HORM .EQ. 'H') .OR. (HORM .EQ. 'h')) THEN
         X=FLOAT(KK)*DTIME/3600.
        ELSE IF ((HORM .EQ. 'M') .OR. (HORM .EQ. 'm')) THEN
         X=FLOAT(KK)*DTIME/60.
        ELSE IF ((HORM .EQ. 'S') .OR. (HORM .EQ. 's')) THEN
         X=FLOAT(KK)*DTIME
        END IF
C
C
         IF (NL .NE. 0) WRITE (13,27) X,(TL(I)-273.,I=1,NL)
         IF (NP .NE. 0) WRITE (14,27) X,(TP(I)-273.,I=1,NP)
         IF (NR .NE. 0) WRITE (15,27) X,(TR(I)-273.,I=1,NR)
C
         WRITE (16,27) X,LAMPP,LAMPLM,QGL(NBASTL),ESR(8)*EFFIC,
     1       QCR(1),QHR(1)
      END IF
  700 CONTINUE
```

```
      CLOSE (13)
      CLOSE (14)
      CLOSE (15)
      CLOSE (16)
      STOP
      END
C
      SUBROUTINE LWAVE(N,NTYPE,NLN,NLENS,EM,F,RHOL,A,T,QL)
C
C  THIS IS A SUBROUTINE TO CALCULATE THE LONGWAVE RADIATION EXCHANGE
C
      REAL EM(20),F(20,20),RHOL(20),A(20),EB(20),SIGMA,
     1  TRANLL(20),TRANLP(20),TRANLR(20)
      DOUBLE PRECISION T(20),QL(20),EL(20),EXITL(20),EXDUM(20),
     1  EXLENS,ELL(20),ELP(20),ELR(20),EXITL2(20)
      COMMON /LW/ TRANLL, TRANLP, TRANLR, ELL, ELP, ELR
      INTEGER NLENS(5,3)
      SIGMA=5.669E-8
      DO 100 I=2,N
      EB(I)=EM(I)*SIGMA*T(I)**4.
      EXITL(I)=EB(I)
      EXITL2(I)=0.
C      WRITE (*,*) I, TRANLL(I), TRANLP(I), TRANLR(I)
  100 CONTINUE
C
  150 IF (NLN .EQ. 0) GO TO 180
      DO 160 K=1,NLN
      EXLENS=0.
      IF (NLENS(K,2) .EQ. 1) THEN
       IF (TRANLL(NLENS(K,3)) .NE. 0.)
     1   EXLENS=TRANLL(NLENS(K,3))*ELL(NLENS(K,3))
      ELSE IF (NLENS(K,2) .EQ. 2) THEN
       IF (TRANLP(NLENS(K,3)) .NE. 0.)
     1   EXLENS=TRANLP(NLENS(K,3))*ELP(NLENS(K,3))
      ELSE IF (NLENS(K,2) .EQ. 3) THEN
       IF (TRANLR(NLENS(K,3)) .NE. 0.)
     1   EXLENS=TRANLR(NLENS(K,3))*ELR(NLENS(K,3))
      END IF
      EXITL(NLENS(K,1))=EXITL(NLENS(K,1))+EXLENS
      EXITL2(NLENS(K,1))=EXLENS
C
  160 CONTINUE
C  ==========================================================
  180 DO 250 I=2,N
      EL(I)=0.
      DO 200 J=2,N
      EL(I)=EL(I)+F(I,J)*EXITL(J)
  200 CONTINUE
      EXDUM(I)=EXITL(I)
C
      EXITL(I)=EB(I)+RHOL(I)*EL(I)+EXITL2(I)
  250 CONTINUE
      DO 300 I=2,N
      IF (ABS(EXITL(I)-EXDUM(I)) .GT. 0.0001) GO TO 180
  300 CONTINUE
C
      DO 420 I=2,N
      EL(I)=0.
      DO 420 J=2,N
      EL(I)=EL(I)+F(I,J)*EXITL(J)
  420 CONTINUE
```

```
      DO 460 I=2,N
      QL(I)=A(I)*(EL(I)-EXITL(I))
      DO 450 K=1,NLN
       IF (I .EQ. NLENS(K,1)) THEN
        IF ((NTYPE .EQ. 1) .AND. (TRANLL(I) .NE. 0.)) THEN
         QL(I)=A(I)*(1.-RHOL(I)-TRANLL(I))*EL(I)
        ELSE IF ((NTYPE .EQ. 2) .AND. (TRANLP(I) .NE. 0.)) THEN
         QL(I)=A(I)*(1.-RHOL(I)-TRANLP(I))*EL(I)
        ELSE IF ((NTYPE .EQ. 3) .AND. (TRANLR(I) .NE. 0.)) THEN
         QL(I)=A(I)*(1.-RHOL(I)-TRANLR(I))*EL(I)
        END IF
       END IF
  450 CONTINUE
      IF (NTYPE .EQ. 1) THEN
       ELL(I)=EL(I)
       ELSE IF (NTYPE .EQ. 2) THEN
       ELP(I)=EL(I)
       ELSE IF (NTYPE .EQ. 3) THEN
       ELR(I)=EL(I)
      END IF
  460 CONTINUE
      RETURN
      END
C
      SUBROUTINE SWAVE(N,NTYPE,NLN,NLENS,NLA,NLAMP,F,RHOS,
     1  A,SWPOW,QS)
C
C  THIS IS A SUBROUTINE TO CALCULATE THE SHORT WAVE RADIATION EXCHANGE
C
      REAL F(20,20),RHOS(20),A(20),SWPOW,TRANSL(20),TRANSP(20),
     1  TRANSR(20)
      DOUBLE PRECISION QS(20),EXITS(20),EXDUM(20),
     1  EXLAMP,EXLENS(5),ESL(20),ESP(20),ESR(20),ES(20)
      INTEGER NLENS(5,3),NLAMP(5)
      COMMON /SW/ TRANSL,TRANSP,TRANSR,ESL,ESP,ESR
C  LAMP POWER IS ASSUMED TO BE EQUALLY SHARED AMONG LAMP NODES
      IF (NLA .EQ. 0) GO TO 150
      EXLAMP=SWPOW/NLA
      DO 100 K=1,NLA
      EXITS(NLAMP(K))=EXLAMP/A(NLAMP(K))
  100 CONTINUE
C  =======================================================
C
  150 IF (NLN .EQ. 0) GO TO 180
      DO 160 K=1,NLN
C
      IF (NLENS(K,2) .EQ. 1) THEN
      EXLENS(K)=TRANSL(NLENS(K,3))*ESL(NLENS(K,3))
C
      ELSE IF (NLENS(K,2) .EQ. 2) THEN
      EXLENS(K)=TRANSP(NLENS(K,3))*ESP(NLENS(K,3))
C
      ELSE IF (NLENS(K,2) .EQ. 3) THEN
      EXLENS(K)=TRANSR(NLENS(K,3))*ESR(NLENS(K,3))
C
      END IF
      EXITS(NLENS(K,1))=EXLENS(K)
C
  160 CONTINUE
C  =======================================================
  180 DO 400 I=2,N
```

```
      ES(I)=0.
      DO 200 J=2,N
      ES(I)=ES(I)+F(I,J)*EXITS(J)
  200 CONTINUE
C
      EXDUM(I)=EXITS(I)
C
      EXITS(I)=RHOS(I)*ES(I)
      DO 250 K=1,NLA
      IF (I .EQ. NLAMP(K)) EXITS(I)=EXLAMP/A(I)+RHOS(I)*ES(I)
  250 CONTINUE
      DO 260 K=1,NLN
      IF (I .EQ. NLENS(K,1)) EXITS(I)=EXLENS(K)+RHOS(I)*ES(I)
  260 CONTINUE
  400 CONTINUE
C   ==========================================================
C
      DO 500 I=2,N
      IF (ABS(EXITS(I)-EXDUM(I)) .GT. 0.0001) GO TO 180
  500 CONTINUE
C
  680 DO 700 I=2,N
      ES(I)=0.
      DO 700 J=2,N
      ES(I)=ES(I)+F(I,J)*EXITS(J)
  700 CONTINUE
C
      DO 750 I=2,N
       QS(I)=A(I)*(ES(I)-EXITS(I))
       DO 730 K=1,NLN
       IF (I .EQ. NLENS(K,1)) THEN
         IF (NTYPE .EQ. 1) THEN
           QS(I)=A(I)*(1.-RHOS(I)-TRANSL(I))*ES(I)
         ELSE IF (NTYPE .EQ. 2) THEN
           QS(I)=A(I)*(1.-RHOS(I)-TRANSP(I))*ES(I)
         ELSE IF (NTYPE .EQ. 3) THEN
           QS(I)=A(I)*(1.-RHOS(I)-TRANSR(I))*ES(I)
         END IF
       END IF
  730  CONTINUE
      IF (NTYPE .EQ. 1) THEN
       ESL(I)=ES(I)
       ELSE IF (NTYPE .EQ. 2) THEN
       ESP(I)=ES(I)
       ELSE IF (NTYPE .EQ. 3) THEN
       ESR(I)=ES(I)
      END IF
  750 CONTINUE
      RETURN
      END
C
C
      SUBROUTINE CONVEC(N,NBT,CHARL,A,T,QH)
C
C  THIS IS A SUBROUTINE TO CALCULATE THE CONVECTIVE HEAT EXCHANGE
C
      INTEGER NBT(20)
      REAL A(20),CHARL(20)
      DOUBLE PRECISION T(20),QH(20),RA,HC,TF,PR,DYNVIS
      DO 100 I=2,N
      TF=(T(I)+T(1))/2.
```

```
      IF (TF .GE. 300.) THEN
      DYNVIS=(1.8462+(TF-300.)*0.2288/50.)*1.E-5
      PR=0.708-(TF-300.)*0.011/50.
      ELSE
      DYNVIS=(1.8462-(300.-TF)*0.2472/50.)*1.E-5
      PR=0.708+(300.-TF)*0.014/50.
      END IF
C      RA=5.63694E10*CHARL(I)**3.*ABS(T(I)-T(1))/(T(I)+T(1))
      RA=1221385.175*CHARL(I)**3*ABS(T(I)-T(1))*PR/(TF**3*DYNVIS*DYNVIS)
      IF (RA .EQ. 0.) THEN
      HC=0.
      ELSE
C  RA IS RAYLEIGH NUMBER AND IS EQUAL TO GrPr
C
      IF (NBT(I) .EQ. 1) THEN
       IF (T(I) .GT. T(1)) THEN
        IF (RA .LE. 8.E6) THEN
        HC=0.54*RA**0.25*0.02624/CHARL(I)
        ELSE
        HC=0.15*RA**0.33333333*0.02624/CHARL(I)
C  THE USE OF DIFFERENT EQUATIONS FOR RA LE OR GT 8E6 IS ACCORDING TO
C  HOLMAN
C  THE TWO EQUATIONS HAVE A CROSSOVER AT RA=4.7383843E6
        END IF
       ELSE
        IF (RA .GE. 1.E5) THEN
        HC=0.27*RA**0.25*0.02624/CHARL(I)
        ELSE
        HC=0.
        END IF
       END IF
      ELSE IF (NBT(I) .EQ. 2) THEN
       IF (T(I) .GT. T(1)) THEN
        IF (RA .GE. 1.E5) THEN
        HC=0.27*RA**0.25*0.02624/CHARL(I)
        ELSE
        HC=0.
        END IF
       ELSE
        IF (RA .LE. 8.E6) THEN
        HC=0.54*RA**0.25*0.02624/CHARL(I)
        ELSE
        HC=0.15*RA**0.33333333*0.02624/CHARL(I)
        END IF
       END IF
      ELSE IF (NBT(I) .EQ. 3) THEN
       HC=0.59*RA**0.25*0.02624/CHARL(I)
      ELSE IF ((NBT(I) .EQ. 4) .OR. (NBT(I) .EQ. 5) .OR.
     1  (NBT(I) .EQ. 6)) THEN
C  THE FOLLOWING CORRELATIONS FOR NATURAL CONVECTION FROM HORIZONTAL
C  CYLINDERS IS ACCORDING TO MORGAN 1975
       IF (RA .LE. 1.E2) THEN
        HC=1.02*RA**0.148*0.02624/CHARL(I)
       ELSE IF (RA .LE. 1.E4) THEN
        HC=0.85*RA**0.188*0.02624/CHARL(I)
       ELSE IF (RA .LE. 1.E7) THEN
        HC=0.48*RA**0.25*0.02624/CHARL(I)
       ELSE
        HC=0.125*RA**0.3333*0.02624/CHARL(I)
       END IF
C  ACCORDING TO DATA IN KUEHN AND GOLDSTEIN
```

```
C  Nu=0.78*Nu(AVE) FOR UPPER HALF OF CYLINDER
C  Nu=1.22*Nu(AVE) FOR LOWER HALF OF CYLINDER
        IF (NBT(I) .EQ. 4) THEN
         HC=HC*0.78
        ELSE IF (NBT(I) .EQ. 5) THEN
         HC=HC*1.22
        END IF
      ELSE IF (NBT(I) .EQ. 7) THEN
       HC=CHARL(I)
      ELSE
       HC=0.
      END IF
      END IF
      QH(I)=HC*(T(1)-T(I))*A(I)
  100 CONTINUE
      QH(1)=0.
      DO 200 J=2,N
      QH(1)=QH(1)-QH(J)
  200 CONTINUE
      RETURN
      END
C
C
C
      SUBROUTINE LPLL(NLA,NLAMP,LAMPP,LAMPLM,LPMAX,LLMAX,T,NPT,RLO)
C
C  THIS IS A SUBROUTINE TO CALCULATE THE EFFECT OF MINIMUM LAMP WALL
C  TEMPERATURE ON LAMP POWER AND LAMP LUMEN OUTPUT
C
C  RLO(50,3) IS A MATRIX ON THE RELATIVE LIGHT OUTPUT AND RELATIVE
C  LAMP POWER TO BE READ FROM AN INPUT FILE CONTAINING LAMP DATA
C  THE FIRST DATA OF THIS FILE IS THE NUMBER OF TEMPERATURE POINTS,
C  THE FIRST COLUMN IS THE MINIMUM LAMP WALL TEMPERATURE,
C  THE SECOND COLUMN IS THE RELATIVE LIGHT OUTPUT,
C  THE THIRD COLUMN IS THE RELATIVE LAMP POWER
C
      REAL LAMPP,LAMPLM,LPMAX,LLMAX
      DOUBLE PRECISION TLMIN,T(20),RLO(80,3),RT
      INTEGER NLAMP(5)
      TLMIN=T(NLAMP(1))
      IF (NLA .GT. 1) THEN
        DO 100 I=2,NLA
        TLMIN=DMIN1(TLMIN,T(NLAMP(I)))
  100   CONTINUE
      END IF
C
      IF ((TLMIN .LT. RLO(1,1)) .OR. (TLMIN .GE. RLO(NPT,1))) THEN
        LAMPP=0.
        LAMPLM=0.
      ELSE
        DO 200 I=1,NPT-1
        IF ((TLMIN .GE. RLO(I,1)) .AND. (TLMIN .LT. RLO(I+1,1))) THEN
          RT=(RLO(I+1,1)-TLMIN)/(RLO(I+1,1)-RLO(I,1))
          LAMPP =LPMAX*(RLO(I+1,3)-RT*(RLO(I+1,3)-RLO(I,3)))
          LAMPLM=LLMAX*(RLO(I+1,2)-RT*(RLO(I+1,2)-RLO(I,2)))
          GO TO 300
        END IF
  200 CONTINUE
  300 CONTINUE
      END IF
C
```

```
RETURN
END
```

E.3 List of input data necessary for LITEAC1

Six data files are needed for LITEAC1:

1. A text file named "INDAT" containing the following:

   (i) Input filenames for data of nodes in the three sections - one file for each section.

   (ii) Input filename of lamp data.

   (iii) Input filename of data concerning inter-section conduction and convection.

   (iv) Output filenames: calculated temperature of nodes - one file for each section.

   (v) Output filename for other output.

   (vi) A text variable stating whether on/off cycles are to be simulated: Y or N.

   (vii) Number of cycles (if Y for (vi) above)/Number of hours run (if N for (vi) above).

   (viii) Number of hours lights on.

   (ix) Time step in seconds.

   (x) Output time interval in hours or minutes.

2. A data file for the luminaire section containing the following:

   (i) Number of nodes in the section.

   (ii) Number of lamp nodes in the section.

   (iii) Node numbers of lamp nodes (if any).

   (iv) Number of lens (diffuser) nodes.

   (v) Node number of lens (diffuser) nodes (if any); section and node number of the node opposite to the lens node.

   (vi) Node number of ballast (if any).

   (vii) Initial temperatures of nodes.

   (viii) Area of nodes.

   (ix) Thermal capacity of nodes.

   (x) Emissivity of nodes.

(xi) Reflectivity of nodes for long-wave radiation.

(xii) Reflectivity of nodes for short-wave radiation.

(xiii) Transmission coefficient of nodes for long-wave radiation.

(xiv) Transmission coefficient of nodes for short-wave radiation.

(xv) Form factors - a $N \times N$ matrix.

(xvi) The type of body of each node for the calculation of convective heat transfer coefficient.

(xvii) The characteristic length of each node for the calculation of convective heat transfer coefficient.

3. A data file for the plenum section containing the same items as in the data file for the luminaire section.

4. A data file for the room section containing the same items as in the data file for the luminaire section.

5. A data file for the lamp containing the following:

    (i) Lamp power in Watts.

    (ii) Luminous flux output in lumens.

    (iii) Ballast power.

    (iv) Luminous efficacy of radiation.

    (v) Number of curve points for light output/lamp power vs temperature relationship.

    (vi) A set of three values: temperature, relative light output and relative lamp power.

6. A data file containing the following information for inter-section conduction/ convection:

    (i) Number of conductors.

    (ii) A set of 6 values giving the section and node numbers and the conductance.

    (iii) Air flow rates: supply to room, room to plenum, plenum to supply.

    (iv) Environmental temperature.

Appendix F

Program LITEAC2

F.1 Description of the program

The computer program LITEAC2 consists of a main program and seven subroutines: LWAVE, SWAVE, CONVEC, LAMPPC, GAUSSPIV, SPIV and UNPIV. The subroutines LAMPPC, GAUSSPIV, SPIV and UNPIV form the fluorescent lamp positive column model described in Chapters 5 and 6. The main program and all subroutines are described in the following sub-sections.

F.1.1 Main program LITEAC2

The main program is very similar to that of LITEAC1 (described in Section E.1.1 of Appendix E) with the following differences:

(i) LITEAC2 reads input data from five data files only. The lamp data file used in LITEAC1 is not necessary. Instead, the following data are included in the luminaire data file: total number of lamps, ballast power, the properties of the phosphors in the lamp represented by the integrals $\int_{vis} S(\lambda)V(\lambda)d\lambda$ and $\int_{vis} S(\lambda)\frac{\lambda}{253.7}d\lambda$ in equation (6.39), and the quantum efficiency of the phosphors.

(ii) The main program of LITEAC2 compares the temperatures of all lamp nodes at each time step and finds the minimum lamp wall temperature before calling the subroutine LAMPPC. (This comparison between temperatures of lamp nodes was included in the subroutine LPLL in LITEAC1.)

(iii) The subroutine LAMPPC, which is the fluorescent lamp positive column model, is used in LITEAC2 in place of LPLL.

F.1.2 Subroutines LWAVE, SWAVE and CONVEC

The subroutines LWAVE, SWAVE and CONVEC are the same as those described in Sections E.1.2, E.1.3 and E.1.4, respectively, of Appendix E.

F.1.3 Subroutine LAMPPC

LAMPPC gets the following value from the main program: minimum lamp wall temperature, the quantities represented by the integrals $\int_{vis} S(\lambda)V(\lambda)d\lambda$ and $\int_{vis} S(\lambda)\frac{\lambda}{253.7}d\lambda$ in equation (6 39), and the quantum efficiency of the phosphors. LAMPPC perform calculations according to the steps described in Section 6.5. It returns to the main program the following variables: the total lamp power, the power of visible radiation output from the lamp and total light output of the lamps.

F.1.4 Subroutines GAUSSPIV, SPIV and UNPIV

These are subroutines used in LAMPPC for solving the set of simultaneous equations (6.3)-(6.8) for the number densities of the 6 mercury excited states in the positive column. The subroutine GAUSSPIV is a standard program for solving simultaneous equations in the form of AX=B where A is an $n \times n$ matrix and X (the unknown) and B are column vectors. Gauss elimination with row and column pivoting is the method used in this subroutine. The subroutine SPIV is used by GAUSSPIV to rearrange the order of rows and columns for the fastest gauss elimination for obtaining solution. The subroutine UNPIV is used for undoing the column rearrangements so that the output of GAUSSPIV is in the correct order.

F.2 Program listing

```
      PROGRAM LITEAC2
C
C  TRANSIENT THERMAL MODEL OF AN ENCLOSURE WITH A FLUORESCENT LUMINAIRE
C  AS THE ONLY HEAT AND RADIATION SOURCE AND AN IDEALLY CONTROLLED
C  AIR-CONDITIONING SYSTEM FOR KEEPING ROOM AIR TEMPERATURE CONSTANT
C
C  THE ENCLOSURE IS DIVIDED INTO 3 SECTIONS:
C   1. THE LUMINAIRE SECTION;
C   2. THE PLENUM SECTION;
C   3. THE ROOM SECTION.
C
C  FOR ALL SECTIONS, THE FIRST NODE IS THE AIR NODE
C
C
      REAL AL(20),AP(20),AR(20),CL(20),CP(20),
     1  CR(20),EML(20),EMP(20),EMR(20),FL(20,20),FP(20,20),FR(20,20),
     2  CHARLL(20),CHARLP(20),CHARLR(20),
     3  RHOLL(20),RHOLP(20),RHOLR(20),RHOSL(20),RHOSP(20),RHOSR(20),
     4  TRANSL(20),TRANSP(20),TRANSR(20),TRANLL(20),TRANLP(20),
     5  TRANLR(20),DTIME,LAMPP,LAMPLM,EFFIC,SWPOW,BALPOW,SSLLO2,SSLVL,
     6  QEFFI,CHRP,CHRL,CHPL,CKBS(30),OUTIME
      DOUBLE PRECISION TL(20),TP(20),TR(20),DTL(20),
     1  DTP(20),DTR(20),QGL(20),QGP(20),QGR(20),QLL(20),QLP(20),
     2  QLR(20),QSL(20),QSP(20),QSR(20),QHL(20),QHP(20),QHR(20),
     3  QCL(20),QCP(20),QCR(20),DQL(20),DQP(20),DQR(20),
     4  ELL(20),ELP(20),ELR(20),ESL(20),ESP(20),
     5  ESR(20),QCDUM,TENV
      INTEGER NTIME,NTOFF,NHROFF,NDAY,NTONDT,NTOFFT,IKBS(30,5),
     1  NBTL(20),NBTP(20),NBTR(20),
     2  NLAL,NLAP,NLAR,NLAMPL(5),NLAMPP(5),NLAMPR(5),
     3  NLNL,NLNP,NLNR,NLENSL(5,3),NLENSP(5,3),NLENSR(5,3),
     4  NTYPEL,NTYPEP,NTYPER,NLAMPS
      CHARACTER B,HORM
      CHARACTER*12 INPUT1,INPUT2,INPUT3,INPUT5,
     1  OUTPU1,OUTPU2,OUTPU3,OUTPU4
      COMMON /LW/ TRANLL, TRANLP, TRANLR, ELL, ELP, ELR,
     1  /SW/ TRANSL,TRANSP,TRANSR,ESL,ESP,ESR
C
C   FORMAT STATEMENTS
C
   27 FORMAT (1X,F10.2,12F11.5)
C
C   SPECIFYING INPUT AND OUTPUT FILENAMES
C
      OPEN (7,FILE='INDAT',STATUS='OLD')
      READ (7,*) INPUT1,INPUT2,INPUT3,INPUT5,OUTPU1,OUTPU2,
     1  OUTPU3,OUTPU4,B,NTIME,NHROFF,DTIME,OUTIME,HORM
      CLOSE (7)
      IF ((HORM .EQ. 'H') .OR. (HORM .EQ. 'h')) THEN
        OUTIME=OUTIME*3600.
       ELSE IF ((HORM .EQ. 'M') .OR. (HORM .EQ. 'm')) THEN
        OUTIME=OUTIME*60.
       ELSE IF ((HORM .EQ. 'S') .OR. (HORM .EQ. 's')) THEN
        OUTIME=OUTIME
       ELSE
        WRITE (*,*) (' OUTPUT TIME INTERVAL ERROR')
        STOP
      END IF
```

```
C
C   READ INPUT DATA
C
      OPEN (8,FILE=INPUT1,STATUS='OLD')
      READ (8,*) NL,NLAL,(NLAMPL(I),I=1,NLAL),NLNL,
     1  ((NLENSL(I,J),J=1,3),I=1,NLNL),NBASTL,(TL(I),I=1,NL),
     2  (AL(I),I=1,NL),(CL(I),I=1,NL),(EML(I),I=1,NL),(RHOLL(I),I=1,NL),
     3  (RHOSL(I),I=1,NL),(TRANLL(I),I=1,NL),(TRANSL(I),I=1,NL),
     4  ((FL(I,J),J=1,NL),I=1,NL),(NBTL(I),I=1,NL),(CHARLL(I),I=1,NL),
     5 NLAMPS,BALPOW,SSLLO2,SSLVL,QEFFI
      CLOSE (8)
C
      OPEN (9,FILE=INPUT2,STATUS='OLD')
      READ (9,*) NP,NLAP,(NLAMPP(I),I=1,NLAP),NLNP,
     1  ((NLENSP(I,J),J=1,3),I=1,NLNP),(TP(I),I=1,NP),
     2  (AP(I),I=1,NP),(CP(I),I=1,NP),(EMP(I),I=1,NP),(RHOLP(I),I=1,NP),
     3  (RHOSP(I),I=1,NP),(TRANLP(I),I=1,NP),(TRANSP(I),I=1,NP),
     4  ((FP(I,J),J=1,NP),I=1,NP),(NBTP(I),I=1,NP),(CHARLP(I),I=1,NP)
      CLOSE (9)
C
      OPEN (10,FILE=INPUT3,STATUS='OLD')
      READ (10,*) NR,NLAR,(NLAMPR(I),I=1,NLAR),NLNR,
     1  ((NLENSR(I,J),J=1,3),I=1,NLNR),(TR(I),I=1,NR),
     2  (AR(I),I=1,NR),(CR(I),I=1,NR),(EMR(I),I=1,NR),(RHOLR(I),I=1,NR),
     3  (RHOSR(I),I=1,NR),(TRANLR(I),I=1,NR),(TRANSR(I),I=1,NR),
     4  ((FR(I,J),J=1,NR),I=1,NR),(NBTR(I),I=1,NR),(CHARLR(I),I=1,NR)
      CLOSE (10)
C
C
      OPEN (12,FILE=INPUT5,STATUS='OLD')
      READ (12,*) NCOND, ((IKBS(I,J),J=1,5),CKBS(I),I=1,NCOND),
     1 CHRP,CHRL,CHPL,TENV
      CLOSE (12)
C
      AL(1)=1.0
      AP(1)=1.0
      AR(1)=1.0
C
C
      OPEN (13,FILE=OUTPU1,STATUS='NEW')
C
      OPEN (14,FILE=OUTPU2,STATUS='NEW')
C
      OPEN (15,FILE=OUTPU3,STATUS='NEW')
C
      OPEN (16,FILE=OUTPU4,STATUS='NEW')
C
C
      X=0.
      WRITE (13,27) X,(TL(I)-273.,I=1,NL)
      WRITE (14,27) X,(TP(I)-273.,I=1,NP)
      WRITE (15,27) X,(TR(I)-273.,I=1,NR)
      WRITE (16,27) X,LAMPP,SWPOW,LAMPLM,QGL(NBASTL),ESR(8)*EFFIC
      IF ((B.EQ.'Y').OR.(B.EQ.'y')) THEN
        NDAY=NTIME
        NTIME=86400
      ELSE
        NDAY=1
        NTIME=NTIME*3600
      END IF
      NTOFF=NHROFF*3600
```

```
C
C
      NTYPEL=1
      NTYPEP=2
      NTYPER=3
C
C       IF ((NLAL .NE. 0) .OR. (NLAP .NE. 0) .OR. (NLAR .NE. 0))
C     1  CALL LAMPTC(C)
C
C  CALCULATE VALUES OF THE POWER INPUT AT NODES
C
      DO 45 I=1,NL
      QGL(I)=0.
   45 CONTINUE
      DO 46 I=1,NP
      QGP(I)=0.
   46 CONTINUE
      DO 47 I=1,NR
      QGR(I)=0.
   47 CONTINUE
      NTONDT=NINT(FLOAT(NTIME)/DTIME)
      NTOFFT=NINT(FLOAT(NTOFF)/DTIME)
      DO 700 LL=1,NDAY
C
      DO 700 KK=1,NTONDT
      IF (KK .GT. NTOFFT) THEN
         LAMPP=0.
         SWPOW=0.
         LAMPLM=0.
      ELSE
C
        IF (NLAL .NE. 0) THEN
C
         TLMIN=TL(NLAMPL(1))
         IF (NLAL .GT. 1) THEN
           DO 52 I=2,NLAL
           TLMIN=DMIN1(TLMIN,TL(NLAMPL(I)))
   52      CONTINUE
         END IF
C
C   THE FLUORESCENT LAMP POSITIVE COLUMN MODEL IS USED TO CALCULATE
C   LIGHT OUTPUT AND LAMP POWER
C
         CALL LAMPPC(TLMIN,LAMPP,SWPOW,LAMPLM,SSLLO2,SSLVL,QEFFI)
         LAMPP=NLAMPS*LAMPP
         LAMPLM=NLAMPS*LAMPLM
         SWPOW=NLAMPS*SWPOW
         EFFIC=LAMPLM/SWPOW
        END IF
      END IF
      IF (NLAL .EQ. 0) GO TO 60
      IF (LAMPP .EQ. 0.) THEN
        QGL(NLAMPL(1))=0.
      ELSE
        QGL(NLAMPL(1))=LAMPP/NLAL
      END IF
      IF (NLAL .GT. 1) THEN
        DO 55 K=2,NLAL
        QGL(NLAMPL(K))=QGL(NLAMPL(1))
   55   CONTINUE
      END IF
```

```
C
C  LUMINIARE NODE NBASTL IS THE BALLAST NODE
C
   60 QGL(NBASTL)=BALPOW*LAMPP
C        END IF
       IF (NL .NE. 0) CALL LWAVE(NL,NTYPEL,NLNL,NLENSL,EML,FL,RHOLL,
     1  AL,TL,QLL)
       IF (NP .NE. 0) CALL LWAVE(NP,NTYPEP,NLNP,NLENSP,EMP,FP,RHOLP,
     1  AP,TP,QLP)
       IF (NR .NE. 0) CALL LWAVE(NR,NTYPER,NLNR,NLENSR,EMR,FR,RHOLR,
     1  AR,TR,QLR)
C
       IF (SWPOW .EQ. 0.) THEN
         DO 65 I=1,NL
         QSL(I)=0.
         ESL(I)=0.
   65    CONTINUE
         DO 66 I=1,NP
         QSP(I)=0.
         ESP(I)=0.
   66    CONTINUE
         DO 67 I=1,NR
         QSR(I)=0.
         ESR(I)=0.
   67    CONTINUE
         GOTO 70
       END IF
C  ===================================
       IF (NL .NE. 0) CALL SWAVE(NL,NTYPEL,NLNL,NLENSL,NLAL,NLAMPL,
     1  FL,RHOSL,AL,SWPOW,QSL)
       IF (NP .NE. 0) CALL SWAVE(NP,NTYPEP,NLNP,NLENSP,NLAP,NLAMPP,
     1  FP,RHOSP,AP,SWPOW,QSP)
       IF (NR .NE. 0) CALL SWAVE(NR,NTYPER,NLNR,NLENSR,NLAR,NLAMPR,
     1  FR,RHOSR,AR,SWPOW,QSR)
C  ============================================
   70 IF (NL .NE. 0) CALL CONVEC(NL,NBTL,CHARLL,AL,TL,QHL)
      IF (NP .NE. 0) CALL CONVEC(NP,NBTP,CHARLP,AP,TP,QHP)
      IF (NR .NE. 0) CALL CONVEC(NR,NBTR,CHARLR,AR,TR,QHR)
C
      DO 400 I=1,NL
      QCL(I)=0.
  400 CONTINUE
      DO 410 I=1,NP
      QCP(I)=0.
  410 CONTINUE
      DO 420 I=1,NR
      QCR(I)=0.
  420 CONTINUE
C
C
      DO 450 I=1,NCOND
      IF (IKBS(I,1) .EQ. 1) THEN
        IF (IKBS(I,3) .EQ. 1) THEN
          IF (IKBS(I,5) .EQ. 1 ) THEN
           QCDUM=CKBS(I)*TL(IKBS(I,2))*AL(IKBS(I,2))
          ELSE IF (IKBS(I,5) .EQ. 2) THEN
           QCDUM=CKBS(I)*(TL(IKBS(I,2))-TL(IKBS(I,4)))*AL(IKBS(I,4))
          END IF
          QCL(IKBS(I,4))=QCL(IKBS(I,4))+QCDUM
          QCL(IKBS(I,2))=QCL(IKBS(I,2))-QCDUM
         ELSE IF (IKBS(I,3) .EQ. 2) THEN
```

```
    IF (IKBS(I,5) .EQ. 1 ) THEN
     QCDUM=CKBS(I)*TL(IKBS(I,2))*AL(IKBS(I,2))
    ELSE IF (IKBS(I,5) .EQ. 2) THEN
     QCDUM=CKBS(I)*(TL(IKBS(I,2))-TP(IKBS(I,4)))*AP(IKBS(I,4))
    END IF
    QCP(IKBS(I,4))=QCP(IKBS(I,4))+QCDUM
    QCL(IKBS(I,2))=QCL(IKBS(I,2))-QCDUM
   ELSE IF (IKBS(I,3) .EQ. 3) THEN
    IF (IKBS(I,5) .EQ. 1 ) THEN
     QCDUM=CKBS(I)*TL(IKBS(I,2))*AL(IKBS(I,2))
    ELSE IF (IKBS(I,5) .EQ. 2) THEN
     QCDUM=CKBS(I)*(TL(IKBS(I,2))-TR(IKBS(I,4)))*AR(IKBS(I,4))
    END IF
    QCR(IKBS(I,4))=QCR(IKBS(I,4))+QCDUM
    QCL(IKBS(I,2))=QCL(IKBS(I,2))-QCDUM
   ELSE IF (IKBS(I,3) .EQ. 0) THEN
    IF (IKBS(I,5) .EQ. 1 ) THEN
     QCDUM=CKBS(I)*TL(IKBS(I,2))*AL(IKBS(I,2))
    ELSE IF (IKBS(I,5) .EQ. 2) THEN
     QCDUM=CKBS(I)*(TL(IKBS(I,2))-TENV)*AL(IKBS(I,2))
    END IF
    QCL(IKBS(I,2))=QCL(IKBS(I,2))-QCDUM
  END IF
 ELSE IF (IKBS(I,1) .EQ. 2) THEN
  IF (IKBS(I,3) .EQ. 1) THEN
    IF (IKBS(I,5) .EQ. 1 ) THEN
     QCDUM=CKBS(I)*TP(IKBS(I,2))*AP(IKBS(I,2))
    ELSE IF (IKBS(I,5) .EQ. 2) THEN
     QCDUM=CKBS(I)*(TP(IKBS(I,2))-TL(IKBS(I,4)))*AL(IKBS(I,4))
    END IF
    QCL(IKBS(I,4))=QCL(IKBS(I,4))+QCDUM
    QCP(IKBS(I,2))=QCP(IKBS(I,2))-QCDUM
   ELSE IF (IKBS(I,3) .EQ. 2) THEN
    IF (IKBS(I,5) .EQ. 1 ) THEN
     QCDUM=CKBS(I)*TP(IKBS(I,2))*AP(IKBS(I,2))
    ELSE IF (IKBS(I,5) .EQ. 2) THEN
     QCDUM=CKBS(I)*(TP(IKBS(I,2))-TP(IKBS(I,4)))*AP(IKBS(I,4))
    END IF
    QCP(IKBS(I,4))=QCP(IKBS(I,4))+QCDUM
    QCP(IKBS(I,2))=QCP(IKBS(I,2))-QCDUM
   ELSE IF (IKBS(I,3) .EQ. 3) THEN
    IF (IKBS(I,5) .EQ. 1 ) THEN
     QCDUM=CKBS(I)*TP(IKBS(I,2))*AP(IKBS(I,2))
    ELSE IF (IKBS(I,5) .EQ. 2) THEN
     QCDUM=CKBS(I)*(TP(IKBS(I,2))-TR(IKBS(I,4)))*AR(IKBS(I,4))
    END IF
    QCR(IKBS(I,4))=QCR(IKBS(I,4))+QCDUM
    QCP(IKBS(I,2))=QCP(IKBS(I,2))-QCDUM
   ELSE IF (IKBS(I,3) .EQ. 0) THEN
    IF (IKBS(I,5) .EQ. 1 ) THEN
     QCDUM=CKBS(I)*TP(IKBS(I,2))*AP(IKBS(I,2))
    ELSE IF (IKBS(I,5) .EQ. 2) THEN
     QCDUM=CKBS(I)*(TP(IKBS(I,2))-TENV)*AP(IKBS(I,2))
    END IF
    QCP(IKBS(I,2))=QCP(IKBS(I,2))-QCDUM
   END IF
 ELSE IF (IKBS(I,1) .EQ. 3) THEN
  IF (IKBS(I,3) .EQ. 1) THEN
    IF (IKBS(I,5) .EQ. 1 ) THEN
     QCDUM=CKBS(I)*TR(IKBS(I,2))*AR(IKBS(I,2))
    ELSE IF (IKBS(I,5) .EQ. 2) THEN
```

```
           QCDUM=CKBS(I)*(TR(IKBS(I,2))-TL(IKBS(I,4)))*AL(IKBS(I,4))
          END IF
          QCL(IKBS(I,4))=QCL(IKBS(I,4))+QCDUM
          QCR(IKBS(I,2))=QCR(IKBS(I,2))-QCDUM
         ELSE IF (IKBS(I,3) .EQ. 2) THEN
          IF (IKBS(I,5) .EQ. 1 ) THEN
           QCDUM=CKBS(I)*TR(IKBS(I,2))*AR(IKBS(I,2))
          ELSE IF (IKBS(I,5) .EQ. 2) THEN
           QCDUM=CKBS(I)*(TR(IKBS(I,2))-TP(IKBS(I,4)))*AP(IKBS(I,4))
          END IF
          QCP(IKBS(I,4))=QCP(IKBS(I,4))+QCDUM
          QCR(IKBS(I,2))=QCR(IKBS(I,2))-QCDUM
         ELSE IF (IKBS(I,3) .EQ. 3) THEN
          IF (IKBS(I,5) .EQ. 1 ) THEN
           QCDUM=CKBS(I)*TR(IKBS(I,2))*AR(IKBS(I,2))
          ELSE IF (IKBS(I,5) .EQ. 2) THEN
           QCDUM=CKBS(I)*(TR(IKBS(I,2))-TR(IKBS(I,4)))*AR(IKBS(I,4))
          END IF
          QCR(IKBS(I,4))=QCR(IKBS(I,4))+QCDUM
          QCR(IKBS(I,2))=QCR(IKBS(I,2))-QCDUM
         ELSE IF (IKBS(I,3) .EQ. 0) THEN
          IF (IKBS(I,5) .EQ. 1 ) THEN
           QCDUM=CKBS(I)*TR(IKBS(I,2))*AR(IKBS(I,2))
          ELSE IF (IKBS(I,5) .EQ. 2) THEN
           QCDUM=CKBS(I)*(TR(IKBS(I,2))-TENV)*AR(IKBS(I,2))
          END IF
          QCR(IKBS(I,2))=QCR(IKBS(I,2))-QCDUM
        END IF
       ELSE IF (IKBS(I,1) .EQ. 0) THEN
        IF (IKBS(I,3) .EQ. 1) THEN
          IF (IKBS(I,5) .EQ. 1 ) THEN
           QCDUM=CKBS(I)*TENV*AL(IKBS(I,4))
          ELSE IF (IKBS(I,5) .EQ. 2) THEN
           QCDUM=CKBS(I)*(TENV-TL(IKBS(I,4)))*AL(IKBS(I,4))
          END IF
          QCL(IKBS(I,4))=QCL(IKBS(I,4))+QCDUM
         ELSE IF (IKBS(I,3) .EQ. 2) THEN
          IF (IKBS(I,5) .EQ. 1 ) THEN
           QCDUM=CKBS(I)*TENV*AP(IKBS(I,4))
          ELSE IF (IKBS(I,5) .EQ. 2) THEN
           QCDUM=CKBS(I)*(TENV-TP(IKBS(I,4)))*AP(IKBS(I,4))
          END IF
          QCP(IKBS(I,4))=QCP(IKBS(I,4))+QCDUM
         ELSE IF (IKBS(I,3) .EQ. 3) THEN
          IF (IKBS(I,5) .EQ. 1 ) THEN
           QCDUM=CKBS(I)*TENV*AR(IKBS(I,4))
          ELSE IF (IKBS(I,5) .EQ. 2) THEN
           QCDUM=CKBS(I)*(TENV-TR(IKBS(I,4)))*AR(IKBS(I,4))
          END IF
          QCR(IKBS(I,4))=QCR(IKBS(I,4))+QCDUM
        END IF
      END IF
  450 CONTINUE
C
C
      DO 500 I=1,NL
        IF (CL(I) .NE. 0.) THEN
        DQL(I)=QGL(I)+QLL(I)+QSL(I)+QHL(I)+QCL(I)
        DTL(I)=DQL(I)*DTIME/CL(I)
        TL(I)=TL(I)+DTL(I)
        ELSE
```

```
        TL(I)=TL(1)
        END IF
  500 CONTINUE
      DO 510 I=1,NP
        IF (CP(I) .NE. 0.) THEN
        DQP(I)=QGP(I)+QLP(I)+QSP(I)+QHP(I)+QCP(I)
        DTP(I)=DQP(I)*DTIME/CP(I)
        TP(I)=TP(I)+DTP(I)
        ELSE
        TP(I)=TP(1)
        END IF
  510 CONTINUE
C      IF (CR(1) .EQ. 0.0) THEN
      DO 515 I=1,NR
        IF (CR(I) .NE. 0.) THEN
        DQR(I)=QGR(I)+QLR(I)+QSR(I)+QHR(I)+QCR(I)
        DTR(I)=DQR(I)*DTIME/CR(I)
        TR(I)=TR(I)+DTR(I)
        ELSE
        TR(I)=TR(1)
        END IF
  515 CONTINUE
C
      IF (FLOAT(KK)/ANINT(OUTIME/DTIME) .EQ.
     1  FLOAT(KK/NINT(OUTIME/DTIME))) THEN
        IF ((HORM .EQ. 'H') .OR. (HORM .EQ. 'h')) THEN
         X=FLOAT(KK)*DTIME/3600.
        ELSE IF ((HORM .EQ. 'M') .OR. (HORM .EQ. 'm')) THEN
         X=FLOAT(KK)*DTIME/60.
        ELSE IF ((HORM .EQ. 'S') .OR. (HORM .EQ. 's')) THEN
         X=FLOAT(KK)*DTIME
        END IF
C
C
         IF (NL .NE. 0) WRITE (13,27) X,(TL(I)-273.,I=1,NL)
         IF (NP .NE. 0) WRITE (14,27) X,(TP(I)-273.,I=1,NP)
         IF (NR .NE. 0) WRITE (15,27) X,(TR(I)-273.,I=1,NR)
C
         WRITE (16,27) X,LAMPP,SWPOW,LAMPLM,QGL(NBASTL),ESR(8)*EFFIC,
     1      QCR(1),QHR(1)
      END IF
  700 CONTINUE
      CLOSE (13)
      CLOSE (14)
      CLOSE (15)
      CLOSE (16)
      STOP
      END
C
      SUBROUTINE LWAVE(N,NTYPE,NLN,NLENS,EM,F,RHOL,A,T,QL)
C
C  THIS IS A SUBROUTINE TO CALCULATE THE LONGWAVE RADIATION EXCHANGE
C
      REAL EM(20),F(20,20),RHOL(20),A(20),EB(20),SIGMA,
     1  TRANLL(20),TRANLP(20),TRANLR(20)
      DOUBLE PRECISION T(20),QL(20),EL(20),EXITL(20),EXDUM(20),
     1  EXLENS,ELL(20),ELP(20),ELR(20),EXITL2(20)
      COMMON /LW/ TRANLL, TRANLP, TRANLR, ELL, ELP, ELR
      INTEGER NLENS(5,3)
      SIGMA=5.669E-8
      DO 100 I=2,N
```

```
      EB(I)=EM(I)*SIGMA*T(I)**4.
      EXITL(I)=EB(I)
      EXITL2(I)=0.
C
  100 CONTINUE
C  =======================================================
C
  150 IF (NLN .EQ. 0) GO TO 180
      DO 160 K=1,NLN
      EXLENS=0.
      IF (NLENS(K,2) .EQ. 1) THEN
       IF (TRANLL(NLENS(K,3)) .NE. 0.)
     1   EXLENS=TRANLL(NLENS(K,3))*ELL(NLENS(K,3))
      ELSE IF (NLENS(K,2) .EQ. 2) THEN
       IF (TRANLP(NLENS(K,3)) .NE. 0.)
     1   EXLENS=TRANLP(NLENS(K,3))*ELP(NLENS(K,3))
      ELSE IF (NLENS(K,2) .EQ. 3) THEN
       IF (TRANLR(NLENS(K,3)) .NE. 0.)
     1   EXLENS=TRANLR(NLENS(K,3))*ELR(NLENS(K,3))
      END IF
      EXITL(NLENS(K,1))=EXITL(NLENS(K,1))+EXLENS
      EXITL2(NLENS(K,1))=EXLENS
C
  160 CONTINUE
C  =======================================================
  180 DO 250 I=2,N
      EL(I)=0.
      DO 200 J=2,N
      EL(I)=EL(I)+F(I,J)*EXITL(J)
  200 CONTINUE
      EXDUM(I)=EXITL(I)
C
      EXITL(I)=EB(I)+RHOL(I)*EL(I)+EXITL2(I)
C
  250 CONTINUE
      DO 300 I=2,N
      IF (ABS(EXITL(I)-EXDUM(I)) .GT. 0.0001) GO TO 180
  300 CONTINUE
C
C
      DO 420 I=2,N
      EL(I)=0.
      DO 420 J=2,N
      EL(I)=EL(I)+F(I,J)*EXITL(J)
  420 CONTINUE
      DO 460 I=2,N
      QL(I)=A(I)*(EL(I)-EXITL(I))
      DO 450 K=1,NLN
       IF (I .EQ. NLENS(K,1)) THEN
        IF ((NTYPE .EQ. 1) .AND. (TRANLL(I) .NE. 0.)) THEN
         QL(I)=A(I)*(1.-RHOL(I)-TRANLL(I))*EL(I)
        ELSE IF ((NTYPE .EQ. 2) .AND. (TRANLP(I) .NE. 0.)) THEN
         QL(I)=A(I)*(1.-RHOL(I)-TRANLP(I))*EL(I)
        ELSE IF ((NTYPE .EQ. 3) .AND. (TRANLR(I) .NE. 0.)) THEN
         QL(I)=A(I)*(1.-RHOL(I)-TRANLR(I))*EL(I)
        END IF
       END IF
  450 CONTINUE
      IF (NTYPE .EQ. 1) THEN
       ELL(I)=EL(I)
       ELSE IF (NTYPE .EQ. 2) THEN
```

```
      ELP(I)=EL(I)
      ELSE IF (NTYPE .EQ. 3) THEN
      ELR(I)=EL(I)
     END IF
 460 CONTINUE
     RETURN
     END
C
     SUBROUTINE SWAVE(N,NTYPE,NLN,NLENS,NLA,NLAMP,F,RHOS,
    1  A,SWPOW,QS)
C
C  THIS IS A SUBROUTINE TO CALCULATE THE SHORT WAVE RADIATION EXCHANGE
C
C
     REAL F(20,20),RHOS(20),A(20),SWPOW,TRANSL(20),TRANSP(20),
    1  TRANSR(20)
     DOUBLE PRECISION QS(20),EXITS(20),EXDUM(20),
    1  EXLAMP,EXLENS(5),ESL(20),ESP(20),ESR(20),ES(20)
     INTEGER NLENS(5,3),NLAMP(5)
     COMMON /SW/ TRANSL,TRANSP,TRANSR,ESL,ESP,ESR
C  LAMP POWER IS ASSUMED TO BE EQUALLY SHARED AMONG LAMP NODES
     IF (NLA .EQ. 0) GO TO 150
     EXLAMP=SWPOW/NLA
     DO 100 K=1,NLA
     EXITS(NLAMP(K))=EXLAMP/A(NLAMP(K))
 100 CONTINUE
C  ========================================================
C
 150 IF (NLN .EQ. 0) GO TO 180
     DO 160 K=1,NLN
C
     IF (NLENS(K,2) .EQ. 1) THEN
     EXLENS(K)=TRANSL(NLENS(K,3))*ESL(NLENS(K,3))
C
     ELSE IF (NLENS(K,2) .EQ. 2) THEN
     EXLENS(K)=TRANSP(NLENS(K,3))*ESP(NLENS(K,3))
C
     ELSE IF (NLENS(K,2) .EQ. 3) THEN
     EXLENS(K)=TRANSR(NLENS(K,3))*ESR(NLENS(K,3))
C
     END IF
     EXITS(NLENS(K,1))=EXLENS(K)
C
 160 CONTINUE
C  ========================================================
 180 DO 400 I=2,N
     ES(I)=0.
     DO 200 J=2,N
     ES(I)=ES(I)+F(I,J)*EXITS(J)
 200 CONTINUE
C
     EXDUM(I)=EXITS(I)
C
     EXITS(I)=RHOS(I)*ES(I)
     DO 250 K=1,NLA
     IF (I .EQ. NLAMP(K)) EXITS(I)=EXLAMP/A(I)+RHOS(I)*ES(I)
 250 CONTINUE
     DO 260 K=1,NLN
     IF (I .EQ. NLENS(K,1)) EXITS(I)=EXLENS(K)+RHOS(I)*ES(I)
 260 CONTINUE
 400 CONTINUE
```

```
C  ==========================================================
C
      DO 500 I=2,N
      IF (ABS(EXITS(I)-EXDUM(I)) .GT. 0.0001) GO TO 180
  500 CONTINUE
C
C
  680 DO 700 I=2,N
      ES(I)=0.
      DO 700 J=2,N
      ES(I)=ES(I)+F(I,J)*EXITS(J)
  700 CONTINUE
C
C
      DO 750 I=2,N
       QS(I)=A(I)*(ES(I)-EXITS(I))
       DO 730 K=1,NLN
       IF (I .EQ. NLENS(K,1)) THEN
         IF (NTYPE .EQ. 1) THEN
           QS(I)=A(I)*(1.-RHOS(I)-TRANSL(I))*ES(I)
         ELSE IF (NTYPE .EQ. 2) THEN
           QS(I)=A(I)*(1.-RHOS(I)-TRANSP(I))*ES(I)
         ELSE IF (NTYPE .EQ. 3) THEN
           QS(I)=A(I)*(1.-RHOS(I)-TRANSR(I))*ES(I)
         END IF
       END IF
  730  CONTINUE
      IF (NTYPE .EQ. 1) THEN
       ESL(I)=ES(I)
       ELSE IF (NTYPE .EQ. 2) THEN
       ESP(I)=ES(I)
       ELSE IF (NTYPE .EQ. 3) THEN
       ESR(I)=ES(I)
      END IF
  750 CONTINUE
      RETURN
      END
C
C
C
      SUBROUTINE CONVEC(N,NBT,CHARL,A,T,QH)
C
C  THIS IS A SUBROUTINE TO CALCULATE THE CONVECTIVE HEAT EXCHANGE
C
      INTEGER NBT(20)
      REAL A(20),CHARL(20)
      DOUBLE PRECISION T(20),QH(20),RA,HC,TF,PR,DYNVIS
      DO 100 I=2,N
      TF=(T(I)+T(1))/2.
      IF (TF .GE. 300.) THEN
      DYNVIS=(1.8462+(TF-300.)*0.2288/50.)*1.E-5
      PR=0.708-(TF-300.)*0.011/50.
      ELSE
      DYNVIS=(1.8462-(300.-TF)*0.2472/50.)*1.E-5
      PR=0.708+(300.-TF)*0.014/50.
      END IF
C      RA=5.63694E10*CHARL(I)**3.*ABS(T(I)-T(1))/(T(I)+T(1))
      RA=1221385.175*CHARL(I)**3*ABS(T(I)-T(1))*PR/(TF**3*DYNVIS*DYNVIS)
      IF (RA .EQ. 0.) THEN
      HC=0.
      ELSE
```

```
C  RA IS RAYLEIGH NUMBER AND IS EQUAL TO GrPr
C  5.63694E10=9.8*.708*2/15.69E-6**2
C  1221385.175=9.8*(1.0132E5/287)**2
C  NBT(I)=1 MEANS HORIZONTAL PLATE UPPER SURFACE
C  NBT(I)=2 MEANS HORIZONTAL PLATE LOWER SURFACE
C  NBT(I)=3 MEANS VERTICAL PLATE
C  NBT(I)=4 MEANS HORIZONTAL CYLINDER UPPER HALF
C  NBT(I)=5 MEANS HORIZONTAL CYLINDER LOWER HALF
C  NBT(I)=6 MEANS HORIZONTAL CYLINDER WHOLE
C  NBT(I)=7 MEANS OTHERS
      IF (NBT(I) .EQ. 1) THEN
       IF (T(I) .GT. T(1)) THEN
        IF (RA .LE. 8.E6) THEN
        HC=0.54*RA**0.25*0.02624/CHARL(I)
        ELSE
        HC=0.15*RA**0.33333333*0.02624/CHARL(I)
C  THE USE OF DIFFERENT EQUATIONS FOR RA LE OR GT 8E6 IS ACCORDING TO
C  HOLMAN
C  THE TWO EQUATIONS HAVE A CROSSOVER AT RA=4.7383843E6
        END IF
       ELSE
        IF (RA .GE. 1.E5) THEN
        HC=0.27*RA**0.25*0.02624/CHARL(I)
        ELSE
        HC=0.
        END IF
       END IF
      ELSE IF (NBT(I) .EQ. 2) THEN
       IF (T(I) .GT. T(1)) THEN
        IF (RA .GE. 1.E5) THEN
        HC=0.27*RA**0.25*0.02624/CHARL(I)
        ELSE
        HC=0.
        END IF
       ELSE
        IF (RA .LE. 8.E6) THEN
        HC=0.54*RA**0.25*0.02624/CHARL(I)
        ELSE
        HC=0.15*RA**0.33333333*0.02624/CHARL(I)
        END IF
       END IF
      ELSE IF (NBT(I) .EQ. 3) THEN
       HC=0.59*RA**0.25*0.02624/CHARL(I)
      ELSE IF ((NBT(I) .EQ. 4) .OR. (NBT(I) .EQ. 5) .OR.
     1  (NBT(I) .EQ. 6)) THEN
C  THE FOLLOWING CORRELATIONS FOR NATURAL CONVECTION FROM HORIZONTAL
C  CYLINDERS IS ACCORDING TO MORGAN 1975
       IF (RA .LE. 1.E2) THEN
        HC=1.02*RA**0.148*0.02624/CHARL(I)
       ELSE IF (RA .LE. 1.E4) THEN
        HC=0.85*RA**0.188*0.02624/CHARL(I)
       ELSE IF (RA .LE. 1.E7) THEN
        HC=0.48*RA**0.25*0.02624/CHARL(I)
       ELSE
        HC=0.125*RA**0.3333*0.02624/CHARL(I)
       END IF
C  ACCORDING TO DATA IN KUEHN AND GOLDSTEIN
C  Nu=0.78*Nu(AVE) FOR UPPER HALF OF CYLINDER
C  Nu=1.22*Nu(AVE) FOR LOWER HALF OF CYLINDER
       IF (NBT(I) .EQ. 4) THEN
        HC=HC*0.78
```

```
      ELSE IF (NBT(I) .EQ. 5) THEN
       HC=HC*1.22
      END IF
     ELSE IF (NBT(I) .EQ. 7) THEN
      HC=CHARL(I)
     ELSE
      HC=0.
     END IF
     END IF
     QH(I)=HC*(T(1)-T(I))*A(I)
 100 CONTINUE
     QH(1)=0.
     DO 200 J=2,N
     QH(1)=QH(1)-QH(J)
 200 CONTINUE
     RETURN
     END
C
C
C
C ===================================================================
subroutine lamppc(tcsa,wlampt,waviso,lamplm,ssllo2,sslvl,qeffi)
c
c  This is a subroutine of a positive column model of a fluorescent lamp
c
c  Defining variables:
c  tcs - cold spot temperature in C
c  trg - rare-gas temperature in K
c  trgc - rare-gas temperature in C
c  te - electron temperature
c  kte - kb*te
c  phg - mercury vapour pressure
c  prg - rare-gas vapour pressure
c  dn0 - mercury ground state density
c  dn1 - mercury 1st excited state 6-3P0 density
c  dn2 - mercury 2nd excited state 6-3P1 density
c  dn3 - mercury 3rd excited state 6-3P2 density
c  dn4 - mercury 6-1P1 density
c  dn5 - mercury 7-3S1 density
c  dn6 - mercury upper level density
c  dnrg - rare-gas density
c  dne - electron density
c  ue - electron mobility
c  ui - ion mobility
c  ambi - ambipolar diffusion coefficient
c  vi - mercury ionization level
c  v1 - mercury 6-3P0 state level
c  v2 - mercury 6-3P1 state level
c  v3 - mercury 6-3P2 state level
c  v4 - mercury 6-1P1 state level
c  v5 - mercury 7-3S1 state level
c  v6 - mercury upper state level
c  coeion - ionization coefficient
c  rate(i,j) - transition rate from state i to j , 7 denoting ionized
c              state
c  ratemr - 6-3P2 to 6-3P1 transition rate
c  ratem0 - 6-3P2 to 6-1S0 transition rate
c  rater0 - 6-3P1 to 6-1S0 transition rate
c  raterm - 6-3P1 to 6-3P2 transition rate
c  rate0r - 6-1S0 to 6-3P1 transition rate
c  gamma - 6-3P2 population fraction
```

```
c  w254 - 253.7 nm uv radiation power
c  efs - electric field
c  wesl - elastic scattering loss
c  pci - positive column current
c  me - electron mass
c  mrg - mass of rare-gas atom
c  mfp - mean free path
c  wil - ionization loss
c  w185 - 184.9 nm uv radiation power
c  woth - other radiation power - assumed to be equal to w185
c  wlamp - lamp power
c  effi - lamp efficacy
c
      real kb, tcs, trg, te, phg, dnrg, dne, dn0, dn1, dn2, dn3, dn4,
     1 dn5, dn6, ue, ui, vi, v1, v2, v3, v4, v5, v6, tau2, tau4,
     2 tau5, tau6, rate(0:7,0:7), a(6,6), b(6), x(6), w254, efs, wesl,
     3 pci, kte, me, mrg, mfp, w254pm, weslpm, mfp0, ui0, prg,
     4 wil, wilpm, wlamp, wlampt, tubel, rad, effi, wvis, wnv, wothpm,
     5 w185, w185pm, te1, efs1, kboe, kteoe, rate17, rate27, rate37,
     6 ambior, kteoep, c(0:7,0:7), trgd, dn1n, dn2n, dn3n, dn4n,
     7 waviso, wphos, lamplm, tcsa, wvispm, wnvpm, ssllo2, sslvl, qeffi
      integer icol(6)
c
c  defining constants
c
      pi=3.1415927
      rad=0.018
      tubel=1.2
      kb=1.380658e-23
      e=1.6021773e-19
      kboe=8.6174e-5
      prg=400.
      dnrg=prg/(kb*298.)
      me=9.1093897e-31
      mrg=6.63e-26
      mfp0=1.43e19
      mfp=mfp0/dnrg
      vi=10.44
      v1=4.66
      v2=4.87
      v3=5.43
      v4=6.68
      v5=7.70
      v6=8.85
      ue0=1.24e25
      ue=ue0/dnrg
c
      ui0=4.45e21
      ui=ui0/dnrg
c
      pci=0.42
c
      te=11500.
      tcs=42.
      trgd=50.
      dne=2.1e17
c
      dn1=1.845e17
      dn2=1.558e17
      dn3=2.952e17
c
```

```
      dn4=1.8e16
      dn5=1.5e14
      dn6=5.1e13
c
      phg=10.**(10.025-3110.14/(tcs+267.42))
      trg=tcs+273.+trgd
      dn0=phg/(kb*trg)
c
      tau2=5./8.*2.23e-16*dn0*rad*1.2e-7/sqrt(trg)*sqrt(pi*
     1  alog(2.23e-16*dn0*rad/sqrt(trg)))
      tau4=5./8.*71.8e-16*dn0*rad*1.3e-9/sqrt(trg)*sqrt(pi*
     1  alog(71.8e-16*dn0*rad/sqrt(trg)))
c
      tau5=tau4
      tau6=tau5
      efs=pci/(pi*rad**2*e*ue*dne)
      kte=kb*te
      kteoe=kte/e
      kteoep=kteoe**1.5
c
      rate(0,1)=2.95e34/(dn0*dne)
      rate(0,2)=1.6e35/(dn0*dne)
      rate(0,3)=1.57e35/(dn0*dne)
      rate(0,4)=7.41e33/(dn0*dne)
      rate(0,5)=2.7e33/(dn0*dne)
      rate(0,6)=1.08e33/(dn0*dne)
    5 rate(1,0)=5.9e33/(dn1*dne)
      rate(1,2)=6.56e34/(1.45*dn1*dne)
      rate(1,3)=8.e34/(1.45*dn1*dne)
      rate(1,4)=3.47e33/(1.45*dn1*dne)
      rate(1,5)=1.08e33/(1.45*dn1*dne)
c
      rate(1,6)=1.08e33/(1.45*dn1*dne)
c
      rate(1,7)=6.e32/(1.45*dn1*dne)
      rate(2,0)=1.85e34/(1.45*dn2*dne)
      rate(2,1)=4.19e34/(1.45*dn2*dne)
      rate(2,3)=1.29e35/(1.45*dn2*dne)
      rate(2,4)=5.87e33/(1.45*dn2*dne)
      rate(2,5)=1.91e33/(1.45*dn2*dne)
      rate(2,6)=6.56e32/(1.45*dn2*dne)
      rate(2,7)=3.e32/(1.45*dn2*dne)
      rate(3,0)=4.56e34/(1.45*dn3*dne)
      rate(3,1)=8.e34/(1.45*dn3*dne)
      rate(3,2)=2.2e35/(1.45*dn3*dne)
      rate(3,4)=1.57e34/(1.45*dn3*dne)
      rate(3,5)=7.14e33/(1.45*dn3*dne)
      rate(3,6)=2.6e33/(1.45*dn3*dne)
      rate(3,7)=2.1e33/(1.45*dn3*dne)
c
      rate(4,5)=1.e31/(1.45*dn4*dne)
      rate(4,6)=1.e31/(1.45*dn4*dne)
      rate(4,7)=0
      rate(5,6)=1.e31/(1.45*dn5*dne)
      rate(5,7)=0
      rate(6,7)=0
c
      rate(4,0)=7.9e32/(1.45*dn4*dne)
      rate(4,1)=6.0e32/(1.45*dn4*dne)
      rate(4,2)=2.02e33/(1.45*dn4*dne)
      rate(4,3)=2.91e33/(1.45*dn4*dne)
```

```
c
c
      rate(5,0)=rate(0,5)*exp(v5/kteoe)/3.
      rate(5,1)=rate(1,5)*exp((v5-v1)/kteoe)/3.
      rate(5,2)=rate(2,5)*exp((v5-v2)/kteoe)
      rate(5,3)=rate(3,5)*exp((v5-v3)/kteoe)*5./3.
      rate(5,4)=rate(4,5)*exp((v5-v4)/kteoe)
      rate(6,0)=rate(0,6)*exp(v6/kteoe)/5.
      rate(6,1)=rate(1,6)*exp((v6-v1)/kteoe)/5.
      rate(6,2)=rate(2,6)*exp((v6-v2)/kteoe)*3./5.
      rate(6,3)=rate(3,6)*exp((v6-v3)/kteoe)
      rate(6,4)=rate(4,6)*exp((v6-v4)/kteoe)*3./5.
      rate(6,5)=rate(5,6)*exp((v6-v5)/kteoe)*3./5.
c
      a(1,1)=rate(1,0)+rate(1,2)+rate(1,3)
     1  +rate(1,4)+rate(1,5)+rate(1,6)+rate(1,7)
      a(1,2)=-1.*rate(2,1)
      a(1,3)=-1.*rate(3,1)
      a(1,4)=-1.*rate(4,1)
      a(1,5)=-1.*rate(5,1)
      a(1,6)=-1.*rate(6,1)
      b(1)=rate(0,1)*dn0/1.45
      a(2,1)=-1.*rate(1,2)
      a(2,2)=rate(2,0)+rate(2,1)+rate(2,3)+rate(2,4)
     1  +rate(2,5)+rate(2,6)+rate(2,7)+1.e13/(1.45*dne*tau2)
      a(2,3)=-1.*rate(3,2)
      a(2,4)=-1.*rate(4,2)
      a(2,5)=-1.*rate(5,2)
      a(2,6)=-1.*rate(6,2)
      b(2)=rate(0,2)*dn0/1.45
      a(3,1)=-1.*rate(1,3)
      a(3,2)=-1.*rate(2,3)
      a(3,3)=rate(3,0)+rate(3,1)+rate(3,2)
     1  +rate(3,4)+rate(3,5)+rate(3,6)+rate(3,7)
      a(3,4)=-1.*rate(4,3)
      a(3,5)=-1.*rate(5,3)
      a(3,6)=-1.*rate(6,3)
      b(3)=rate(0,3)*dn0/1.45
      a(4,1)=-1.*rate(1,4)
      a(4,2)=-1.*rate(2,4)
      a(4,3)=-1.*rate(3,4)
      a(4,4)=rate(4,0)+rate(4,1)+rate(4,2)+rate(4,3)
     1  +rate(4,5)+rate(4,6)+rate(4,7)+1.e13/(1.45*dne*tau4)
      a(4,5)=-1.*rate(5,4)
      a(4,6)=-1.*rate(6,4)
      b(4)=rate(0,4)*dn0/1.45
      a(5,1)=-1.*rate(1,5)
      a(5,2)=-1.*rate(2,5)
      a(5,3)=-1.*rate(3,5)
      a(5,4)=-1.*rate(4,5)
      a(5,5)=rate(5,0)+rate(5,1)+rate(5,2)+rate(5,3)+rate(5,4)
     1  +rate(5,6)+rate(5,7)+1.e13/(1.45*dne*tau5)
      a(5,6)=-1.*rate(6,5)
      b(5)=rate(0,5)*dn0/1.45
      a(6,1)=-1.*rate(1,6)
      a(6,2)=-1.*rate(2,6)
      a(6,3)=-1.*rate(3,6)
      a(6,4)=-1.*rate(4,6)
      a(6,5)=-1.*rate(5,6)
      a(6,6)=rate(6,0)+rate(6,1)+rate(6,2)+rate(6,3)+rate(6,4)
     1  +rate(6,5)+rate(6,7)+1.e13/(1.45*dne*tau6)
```

```
      b(6)=rate(0,6)*dn0/1.45
c
      call gausspiv(a,b,x,icol,6)
      dn1n=x(1)
      dn2n=x(2)
      dn3n=x(3)
      dn4n=x(4)
      dn5n=x(5)
      dn6n=x(6)
c
      if ((abs(dn1n-dn1)/dn1 .gt. 0.001) .or.
     1 (abs(dn2n-dn2)/dn2 .gt. 0.001) .or.
     2 (abs(dn3n-dn3)/dn3 .gt. 0.001) .or.
     3 (abs(dn4n-dn4)/dn4 .gt. 0.001) .or.
     4 (abs(dn5n-dn5)/dn5 .gt. 0.001) .or.
     5 (abs(dn6n-dn6)/dn6 .gt. 0.001)) then
        dn1=dn1n
        dn2=dn2n
        dn3=dn3n
        dn4=dn4n
        dn5=dn5n
        dn6=dn6n
       go to 5
      end if
c
c
      c(0,1)=rate(0,1)/(kteoep*(1.+0.5*v1/kteoe)*exp(-v1/kteoe))
      c(0,2)=rate(0,2)/(kteoep*(1.+0.5*v2/kteoe)*exp(-v2/kteoe))
      c(0,3)=rate(0,3)/(kteoep*(1.+0.5*v3/kteoe)*exp(-v3/kteoe))
      c(0,4)=rate(0,4)/(kteoep*(1.+0.5*v4/kteoe)*exp(-v4/kteoe))
      c(0,5)=rate(0,5)/(kteoep*(1.+0.5*v5/kteoe)*exp(-v5/kteoe))
      c(0,6)=rate(0,6)/(kteoep*(1.+0.5*v6/kteoe)*exp(-v6/kteoe))
      c(1,2)=rate(1,2)/(kteoep*(1.+0.5*(v2-v1)/kteoe)
     1  *exp((v1-v2)/kteoe))
      c(1,3)=rate(1,3)/(kteoep*(1.+0.5*(v3-v1)/kteoe)
     1  *exp((v1-v3)/kteoe))
      c(1,4)=rate(1,4)/(kteoep*(1.+0.5*(v4-v1)/kteoe)
     1  *exp((v1-v4)/kteoe))
      c(1,5)=rate(1,5)/(kteoep*(1.+0.5*(v5-v1)/kteoe)
     1  *exp((v1-v5)/kteoe))
      c(1,6)=rate(1,6)/(kteoep*(1.+0.5*(v6-v1)/kteoe)
     1  *exp((v1-v6)/kteoe))
      c(1,7)=rate(1,7)/(kteoep*(1.+0.5*(vi-v1)/kteoe)
     1  *exp((v1-vi)/kteoe))
      c(2,3)=rate(2,3)/(kteoep*(1.+0.5*(v3-v2)/kteoe)
     1  *exp((v2-v3)/kteoe))
      c(2,4)=rate(2,4)/(kteoep*(1.+0.5*(v4-v2)/kteoe)
     1  *exp((v2-v4)/kteoe))
      c(2,5)=rate(2,5)/(kteoep*(1.+0.5*(v5-v2)/kteoe)
     1  *exp((v2-v5)/kteoe))
      c(2,6)=rate(2,6)/(kteoep*(1.+0.5*(v6-v2)/kteoe)
     1  *exp((v2-v6)/kteoe))
      c(2,7)=rate(2,7)/(kteoep*(1.+0.5*(vi-v2)/kteoe)
     1  *exp((v2-vi)/kteoe))
      c(3,4)=rate(3,4)/(kteoep*(1.+0.5*(v4-v3)/kteoe)
     1  *exp((v3-v4)/kteoe))
      c(3,5)=rate(3,5)/(kteoep*(1.+0.5*(v5-v3)/kteoe)
     1  *exp((v3-v5)/kteoe))
      c(3,6)=rate(3,6)/(kteoep*(1.+0.5*(v6-v3)/kteoe)
     1  *exp((v3-v6)/kteoe))
      c(3,7)=rate(3,7)/(kteoep*(1.+0.5*(vi-v3)/kteoe)
```

```
     1   *exp((v3-vi)/kteoe))
c
      c(4,5)=rate(4,5)/(kteoep*(1.+0.5*(v5-v4)/kteoe)
     1   *exp((v4-v5)/kteoe))
      c(4,6)=rate(4,6)/(kteoep*(1.+0.5*(v6-v4)/kteoe)
     1   *exp((v4-v6)/kteoe))
      c(4,7)=rate(4,7)/(kteoep*(1.+0.5*(vi-v4)/kteoe)
     1   *exp((v4-vi)/kteoe))
      c(5,6)=rate(5,6)/(kteoep*(1.+0.5*(v6-v5)/kteoe)
     1   *exp((v5-v6)/kteoe))
      c(5,7)=rate(5,7)/(kteoep*(1.+0.5*(vi-v5)/kteoe)
     1   *exp((v5-vi)/kteoe))
      c(6,7)=rate(6,7)/(kteoep*(1.+0.5*(vi-v6)/kteoe)
     1   *exp((v6-vi)/kteoe))
c
c
      c(1,0)=rate(1,0)*kteoe
      c(2,0)=rate(2,0)*kteoe
      c(2,1)=rate(2,1)*kteoe
      c(3,0)=rate(3,0)*kteoe
      c(3,1)=rate(3,1)*kteoe
      c(3,2)=rate(3,2)*kteoe
      c(4,0)=rate(4,0)*kteoe
      c(4,1)=rate(4,1)*kteoe
      c(4,2)=rate(4,2)*kteoe
      c(4,3)=rate(4,3)*kteoe
      c(5,0)=rate(5,0)*kteoe
      c(5,1)=rate(5,1)*kteoe
      c(5,2)=rate(5,2)*kteoe
      c(5,3)=rate(5,3)*kteoe
      c(5,4)=rate(5,4)*kteoe
      c(6,0)=rate(6,0)*kteoe
      c(6,1)=rate(6,1)*kteoe
      c(6,2)=rate(6,2)*kteoe
      c(6,3)=rate(6,3)*kteoe
      c(6,4)=rate(6,4)*kteoe
      c(6,5)=rate(6,5)*kteoe
      c(7,0)=0.
      c(7,1)=0.
      c(7,2)=0.
      c(7,3)=0.
      c(7,4)=0.
      c(7,5)=0.
      c(7,6)=0.
c
c
      tcs=tcsa-273.
   10 trgc=tcs+trgd
   15 trg=trgc+273.
      phg=10.**(10.025-3110.14/(tcs+267.42))
      dn0=phg/(kb*trg)
c
c
      tau2=5./8.*2.23e-16*dn0*rad*1.2e-7/sqrt(trg)*sqrt(pi*
     1  alog(2.23e-16*dn0*rad/sqrt(trg)))
c
      tau4=5./8.*71.8e-16*dn0*rad*1.3e-9/sqrt(trg)*sqrt(pi*
     1  alog(71.8e-16*dn0*rad/sqrt(trg)))
c
      tau5=tau4
      tau6=tau5
```

```
c
c
      efs=80.-0.3*tcs
   20 dne=pci/(pi*rad**2*e*ue*efs)
      te=12000.
   30 kte=kb*te
      kteoe=kboe*te
      kteoep=kteoe**1.5
c
      rate(0,1)=c(0,1)*kteoep*(1.+0.5*v1/kteoe)*exp(-v1/kteoe)
      rate(0,2)=c(0,2)*kteoep*(1.+0.5*v2/kteoe)*exp(-v2/kteoe)
      rate(0,3)=c(0,3)*kteoep*(1.+0.5*v3/kteoe)*exp(-v3/kteoe)
      rate(0,4)=c(0,4)*kteoep*(1.+0.5*v4/kteoe)*exp(-v4/kteoe)
      rate(0,5)=c(0,5)*kteoep*(1.+0.5*v5/kteoe)*exp(-v5/kteoe)
      rate(0,6)=c(0,6)*kteoep*(1.+0.5*v6/kteoe)*exp(-v6/kteoe)
      rate(1,2)=c(1,2)*kteoep*(1.+0.5*(v2-v1)/kteoe)*
     1  exp((v1-v2)/kteoe)
      rate(1,3)=c(1,3)*kteoep*(1.+0.5*(v3-v1)/kteoe)*
     1  exp((v1-v3)/kteoe)
      rate(1,4)=c(1,4)*kteoep*(1.+0.5*(v4-v1)/kteoe)*
     1  exp((v1-v4)/kteoe)
      rate(1,5)=c(1,5)*kteoep*(1.+0.5*(v5-v1)/kteoe)*
     1  exp((v1-v5)/kteoe)
      rate(1,6)=c(1,6)*kteoep*(1.+0.5*(v6-v1)/kteoe)*
     1  exp((v1-v6)/kteoe)
      rate(1,7)=c(1,7)*kteoep*(1.+0.5*(vi-v1)/kteoe)*
     1  exp((v1-vi)/kteoe)
      rate(2,3)=c(2,3)*kteoep*(1.+0.5*(v3-v2)/kteoe)*
     1  exp((v2-v3)/kteoe)
      rate(2,4)=c(2,4)*kteoep*(1.+0.5*(v4-v2)/kteoe)*
     1  exp((v2-v4)/kteoe)
      rate(2,5)=c(2,5)*kteoep*(1.+0.5*(v5-v2)/kteoe)*
     1  exp((v2-v5)/kteoe)
      rate(2,6)=c(2,6)*kteoep*(1.+0.5*(v6-v2)/kteoe)*
     1  exp((v2-v6)/kteoe)
      rate(2,7)=c(2,7)*kteoep*(1.+0.5*(vi-v2)/kteoe)*
     1  exp((v2-vi)/kteoe)
      rate(3,4)=c(3,4)*kteoep*(1.+0.5*(v4-v3)/kteoe)*
     1  exp((v3-v4)/kteoe)
      rate(3,5)=c(3,5)*kteoep*(1.+0.5*(v5-v3)/kteoe)*
     1  exp((v3-v5)/kteoe)
      rate(3,6)=c(3,6)*kteoep*(1.+0.5*(v6-v3)/kteoe)*
     1  exp((v3-v6)/kteoe)
      rate(3,7)=c(3,7)*kteoep*(1.+0.5*(vi-v3)/kteoe)*
     1  exp((v3-vi)/kteoe)
c
      rate(4,5)=c(4,5)*kteoep*(1.+0.5*(v5-v4)/kteoe)*
     1  exp((v4-v5)/kteoe)
      rate(4,6)=c(4,6)*kteoep*(1.+0.5*(v6-v4)/kteoe)*
     1  exp((v4-v6)/kteoe)
      rate(4,7)=c(4,7)*kteoep*(1.+0.5*(vi-v4)/kteoe)*
     1  exp((v4-vi)/kteoe)
      rate(5,6)=c(5,6)*kteoep*(1.+0.5*(v6-v5)/kteoe)*
     1  exp((v5-v6)/kteoe)
      rate(5,7)=c(5,7)*kteoep*(1.+0.5*(vi-v5)/kteoe)*
     1  exp((v5-vi)/kteoe)
      rate(6,7)=c(6,7)*kteoep*(1.+0.5*(vi-v6)/kteoe)*
     1  exp((v6-vi)/kteoe)
c
      rate(3,2)=c(3,2)/kteoe
      rate(3,1)=c(3,1)/kteoe
```

```
      rate(3,0)=c(3,0)/kteoe
      rate(2,1)=c(2,1)/kteoe
      rate(2,0)=c(2,0)/kteoe
      rate(1,0)=c(1,0)/kteoe
c
c
      rate(4,0)=c(4,0)/kteoe
      rate(4,1)=c(4,1)/kteoe
      rate(4,2)=c(4,2)/kteoe
      rate(4,3)=c(4,3)/kteoe
c
      rate(5,0)=c(5,0)/kteoe
      rate(5,1)=c(5,1)/kteoe
      rate(5,2)=c(5,2)/kteoe
      rate(5,3)=c(5,3)/kteoe
      rate(5,4)=c(5,4)/kteoe
      rate(6,0)=c(6,0)/kteoe
      rate(6,1)=c(6,1)/kteoe
      rate(6,2)=c(6,2)/kteoe
      rate(6,3)=c(6,3)/kteoe
      rate(6,4)=c(6,4)/kteoe
      rate(6,5)=c(6,5)/kteoe
c
c
   33 a(1,1)=rate(1,0)+rate(1,2)+rate(1,3)
     1  +rate(1,4)+rate(1,5)+rate(1,6)+rate(1,7)
      a(1,2)=-1.*rate(2,1)
      a(1,3)=-1.*rate(3,1)
      a(1,4)=-1.*rate(4,1)
      a(1,5)=-1.*rate(5,1)
      a(1,6)=-1.*rate(6,1)
      b(1)=rate(0,1)*dn0/1.45
      a(2,1)=-1.*rate(1,2)
      a(2,2)=rate(2,0)+rate(2,1)+rate(2,3)+rate(2,4)
     1  +rate(2,5)+rate(2,6)+rate(2,7)+1.e13/(1.45*dne*tau2)
      a(2,3)=-1.*rate(3,2)
      a(2,4)=-1.*rate(4,2)
      a(2,5)=-1.*rate(5,2)
      a(2,6)=-1.*rate(6,2)
      b(2)=rate(0,2)*dn0/1.45
      a(3,1)=-1.*rate(1,3)
      a(3,2)=-1.*rate(2,3)
      a(3,3)=rate(3,0)+rate(3,1)+rate(3,2)
     1  +rate(3,4)+rate(3,5)+rate(3,6)+rate(3,7)
      a(3,4)=-1.*rate(4,3)
      a(3,5)=-1.*rate(5,3)
      a(3,6)=-1.*rate(6,3)
      b(3)=rate(0,3)*dn0/1.45
      a(4,1)=-1.*rate(1,4)
      a(4,2)=-1.*rate(2,4)
      a(4,3)=-1.*rate(3,4)
      a(4,4)=rate(4,0)+rate(4,1)+rate(4,2)+rate(4,3)
     1  +rate(4,5)+rate(4,6)+rate(4,7)+1.e13/(1.45*dne*tau4)
      a(4,5)=-1.*rate(5,4)
      a(4,6)=-1.*rate(6,4)
      b(4)=rate(0,4)*dn0/1.45
      a(5,1)=-1.*rate(1,5)
      a(5,2)=-1.*rate(2,5)
      a(5,3)=-1.*rate(3,5)
      a(5,4)=-1.*rate(4,5)
      a(5,5)=rate(5,0)+rate(5,1)+rate(5,2)+rate(5,3)+rate(5,4)
```

```
     1  +rate(5,6)+rate(5,7)+1.e13/(1.45*dne*tau5)
      a(5,6)=-1.*rate(6,5)
      b(5)=rate(0,5)*dn0/1.45
      a(6,1)=-1.*rate(1,6)
      a(6,2)=-1.*rate(2,6)
      a(6,3)=-1.*rate(3,6)
      a(6,4)=-1.*rate(4,6)
      a(6,5)=-1.*rate(5,6)
      a(6,6)=rate(6,0)+rate(6,1)+rate(6,2)+rate(6,3)+rate(6,4)
     1  +rate(6,5)+rate(6,7)+1.e13/(1.45*dne*tau6)
      b(6)=rate(0,6)*dn0/1.45
c
c
      call gausspiv(a,b,x,icol,6)
      dn1=x(1)
      dn2=x(2)
      dn3=x(3)
      dn4=x(4)
      dn5=x(5)
      dn6=x(6)
c
c Calculate electron temperature using balance of ion creation and decay
c
      rate17=c(1,7)*1.e-13*kteoep*(1.+0.5*5.78/kteoe)*exp(-0.77/kteoe)
      rate27=c(2,7)*1.e-13*kteoep*(1.+0.5*5.57/kteoe)*exp(-0.56/kteoe)
      rate37=c(3,7)*1.e-13*kteoep*(1.+0.5*5.01/kteoe)
   35 ambi=ui*kteoe
c
      ambior=ambi/(rad/2.4)**2
      te1=(vi-v3)/(kboe*alog((rate17*dn1+rate27*dn2+rate37*dn3)
     1  /ambior))
c
      if (abs(te1-te) .lt. 1.) go to 60
      te=(te1+te)/2.
c
      go to 30
   60 continue
c
      w254=e*v2*dn2/tau2
      w185=e*v4*dn4/tau4
      wesl=8.*sqrt(me/3.)*kte**1.5*dne/(mrg*mfp)
      vi1=vi+1.5*kteoe
      wil=(rate(1,7)*dn1*(vi1-v1)+rate(2,7)*dn2*(vi1-v2)+
     1  rate(3,7)*dn3*(vi1-v3))*dne*e*1.45e-13
      wvis=e*(v5-v2)*dn5/tau5
      wnv=e*(v6-v2)*dn6/tau6
      wlamp=w254+w185+wesl+wil+wvis+wnv
      efs1=sqrt(wlamp/(e*ue*dne))
c
      if (abs(efs1-efs) .lt. .1) go to 80
      efs=efs1
      go to 20
  80  continue
c
c
      effi=w254/wlamp
      w254pm=w254*pi*rad**2
      w185pm=w185*pi*rad**2
      weslpm=wesl*pi*rad**2
      wilpm=wil*pi*rad**2
      wvispm=wvis*pi*rad**2
```

```
      wnvpm=wnv*pi*rad**2
      wothpm=wvispm+wnvpm
      wlampt=wlamp*pi*rad**2*tubel
c
c  Assume value of 62.15 from Jerome (1953) (Standard cool white)
c  Value for 185 nm calculated from 62.15*253.7/184.9
c  Variables sellou=sum of Elambda*lambda/253.7 and
c  selyba=sum of Elambda*y-bar incorporated so that the program can be
c  used for other lamp types
c
c  Variables ssllo2=sum of S(lambda)*lambda/253.7 and
c  sslvl=sum of S(lambda)*V(lambda)
c  qeffi=quantum efficiency
c
      wuv=tubel*(253.7*w254pm+185.*w185pm)/253.7
      wphos=qeffi*wuv/ssllo2
c
c  Above expression is not absolutely correct as ssllo2 obtained from
c  Jerome (1953) is not normalised. This does not affect the calculation
c  of lamplm but affects that of waviso.
c
      lamplm=683.*(0.75*wphos*sslvl+0.5*0.388*wvispm*tubel)
      waviso=0.75*wphos+0.5*wvispm*tubel
c
c
      return
      end
c
*-----------------------------------------------------------------
*-----------------------------------------------------------------
      SUBROUTINE GAUSSPIV(A,B,X,ICOL,N)
C
C  GAUSS ELIMINATION SOLVE AX=B WITH ROW AND COLUMN PIVOTING
C
C  A = INPUT REAL ARRAY OF N X N COEFFICIENTS, IS DESTROYED
C  B = INPUT REAL ARRAY, N RIGHT HAND SIDES, IS DESTROYED
C  X = OUTPUT REAL SOLUTION ARRAY DIMENSION N
C  ICOL = WORKING INTEGER ARRAY DIMENSION N
C  N = INPUT INTEGER VALUE, NUMBER OF EQUATIONS
C
C
      REAL A(N,N),B(N),X(N)
      INTEGER ICOL(N)
C  FIRST INITIALIZE ICOL
      DO 5 K=1,N
    5 ICOL(K)=K
C  OUTER LOOP - ELIMINATE COLUMN
      DO 30 K=1,N-1
C  FIND THE BEST PIVOT ELEMENT
      CALL SPIV(A,B,N,K,ICOL)
C  THIS LOOP - ROW TO OPERATE ON
      DO 20 I=K+1,N
C  THIS LOOP ACTUALLY DOES IT
      Z=A(I,K)
      DO 10 J=K,N
   10 A(I,J)=A(I,J)-A(K,J)*Z
C  OPERATE ALSO ON B
   20 B(I)=B(I)-B(K)*Z
   30 CONTINUE
C  NOW BACK-SUBSTITUTE
      X(N)=B(N)/A(N,N)
```

```
C  TAKE ROWS IN REVERSE ORDER
      DO 50 K=N-1,1,-1
C  SUM OVER KNOWN RESULTS
      SUM=B(K)
      DO 40 J=K+1,N
   40 SUM=SUM-X(J)*A(K,J)
   50 X(K)=SUM
C  FINALLY UNDO REORDERING
      CALL UNPIV(X,B,N,ICOL)
      END
C
C
      SUBROUTINE SPIV(A,B,N,K,ICOL)
C
C  SUBROUTINE TO PIVOT EQUATIONS A
C
C  SEARCH N X N REAL ARRAY A FOR LARGEST ABSOLUTE VALUE A(I,J)
C  FOR I,J .GE. K. THEN SWITCH ROWS AND COLUMNS TO BRING THIS TO
C  A(K,K).  ALSO SWITCH RIGHT HAND SIDE VECTOR B AND COLUMN
C  MEMORY ARRAY ICOL.
C
      REAL A(N,N),B(N)
      INTEGER ICOL(N)
      IF (K .GE. N) RETURN
C  SEARCH A FOR LARGEST A(I,J)
      ABSMX=0.
      IMAX=K
      JMAX=K
      DO 10 J=K,N
        DO 10 I=K,N
          ABSA=ABS(A(I,J))
          IF (ABSA .GT. ABSMX) THEN
          ABSMX=ABSA
          IMAX=I
          JAMX=J
        END IF
   10 CONTINUE
C  SWITCH ROWS K AND IMAX IN A,B
      DO 20 J=1,N
        TEMP=A(K,J)
        A(K,J)=A(IMAX,J)
   20   A(IMAX,J)=TEMP
      TEMP=B(K)
      B(K)=B(IMAX)
      B(IMAX)=TEMP
C  SWITCH COLUMNS K ,JMAX IN A, ICOL
      DO 30 I=1,N
        TEMP=A(I,K)
        A(I,K)=A(I,JMAX)
   30 A(I,JMAX)=TEMP
      IT=ICOL(K)
      ICOL(K)=ICOL(JMAX)
      ICOL(JMAX)=IT
C  SCALE ROW K
      Z=A(K,K)
      DO 40 J=K,N
   40 A(K,J)=A(K,J)/Z
      B(K)=B(K)/Z
      END
C
C
```

```
      SUBROUTINE UNPIV(X,B,N,ICOL)
C
C  UNDO COLUMN REARRANGEMENTS
C
C  ON INPUT X IS REAL SOLUTION VECTOR LENGTH N WHICH HAS BEEN REORDERED.
C  INTEGER ARRAY ICOL ON INPUT TELLS DESIRED ORDER, B IS USED AS WORKING
C  SPACE. ON OUTPUT X IS THE SOLUTION IN THE CORRECT ORDER.
C
      REAL X(N), B(N)
      INTEGER ICOL(N)
      DO 10 J=1,N
        ITRUE=ICOL(J)
10      B(ITRUE)=X(J)
      DO 20 J=1,N
20    X(J)=B(J)
      END
```

F.3 List of input data necessary for LITEAC2

Five data files are needed for LITEAC2:

1. A text file named "INDAT" containing the following:

   (i) Input filenames for data of nodes in the three sections - one file for each section.

   (ii) Input filename of data concerning inter-section conduction and convection.

   (iii) Output filenames: calculated temperature of nodes - one file for each section.

   (iv) Output filename for other output.

   (v) A text variable stating whether on/off cycles are to be simulated: Y or N.

   (vi) Number of cycles (if Y for vi above)/Number of hours run (if N for vi above).

   (vii) Number of hours lights on.

   (viii) Time step in seconds.

   (ix) Output time interval in hours or minutes.

2. A data file for the luminaire section containing the following:

   (i) Number of nodes in the section.

   (ii) Number of lamp nodes in the section.

   (iii) Node numbers of lamp nodes (if any).

   (iv) Number of lens (diffuser) nodes.

(v) Node number of lens (diffuser) nodes (if any); section and node number of the node opposite to the lens node.

(vi) Node number of ballast (if any).

(vii) Initial temperatures of nodes.

(viii) Area of nodes.

(ix) Thermal capacity of nodes.

(x) Emissivity of nodes.

(xi) Reflectivity of nodes for long-wave radiation.

(xii) Reflectivity of nodes for short-wave radiation.

(xiii) Transmission coefficient of nodes for long-wave radiation.

(xiv) Transmission coefficient of nodes for short-wave radiation.

(xv) Form factors - a N × N matrix. (N = number of nodes in the section)

(xvi) The type of body of each node for the calculation of convective heat transfer coefficient.

(xvii) The characteristic length of each node for the calculation of convective heat transfer coefficient.

(xviii) Total number of lamps in the section.

(xix) Ballast power.

(xx) Property of the phosphor: the quantity $\int_{vis} S(\lambda)\frac{\lambda}{253.7}d\lambda$ in equation (6.39).

(xxi) Property of the phosphor: the quantity $\int_{vis} S(\lambda)V(\lambda)d\lambda$ in equation (6.39).

(xxii) Quantum efficiency of the phosphor.

3. A data file for the plenum section containing items (i)-(xvii) as in the data file for the luminaire section.

4. A data file for the room section containing items (i)-(xvii) as in the data file for the luminaire section.

5. A data file containing the following information for inter-section conduction/ convection:

   (i) Number of conductors.

   (ii) A set of 6 values giving the section and node numbers and the conductance.

   (iii) Air flow rates: supply to room, room to plenum, plenum to supply.

   (iv) Environmental temperature.

Appendix G

Input data for the NIST test cell

The data used in the input files for the validation runs of the programs LITEAC1 and LITEAC2 using the NIST test results are listed in Tables G.1-G.8. In Tables G.1, G.3 and G.5, data concerning initial temperatures, surface areas, thermal capacities, emissivities and reflectivities were obtained from the NIST reports (Treado and Bean 1988, 1992). Transmittance values were assumed (see Section 8.3). Some of the thermal capacity data were calculated from the materials property data in the ASHRAE Handbook (ASHRAE 1993) using dimension and mass information given in the NIST reports. The body type and characteristic length were obtained from information in the NIST reports and these data are used for the determination of convective heat transfer coefficients by the correlations given in Holman (1992). Radiation form factors (in Tables G.2, G.4 and G.6) were calculated using the view factor program 'VF' and 'FACTS' included in 'LIGHTS' (Sowell 1989). The lamp data (in Table G.7) concerning the relative lamp power and relative light output were obtained from Siminovitch et al. (1984). The conductance data (in Table G.8) were obtained from information given in Treado and Bean (1988).

Table G.1

Nodal data for the luminaire section used in the validation runs of LITEAC1 and LITEAC2 described in Chapter 8.

	Luminaire air	Lamp	Diffuser top	Ballast	Luminaire housing
Initial Temperature (K)	296.9	296.9	296.9	296.9	296.9
Surface Area (m^2)	1	1.1674	2.9729	0.1236	4.831
Thermal capacity (J/K)	294.36	2123.1	2734.7	11394.6	16123.4
Emissivity	0	0.9	0.9	0	0.9
Reflectivity for long-wave radiation	0	0.1	0.1	0	0.1
Reflectivity for short-wave radiation	0	0.9	0.1	0.7	0.8
Transmission coefficient for long-wave radiation	0	0	0	0	0
Transmission coefficient for short-wave radiation	0	0	0.8	0	0
Body type (see note below)	0	6	1	0	2
Characteristic length (m)	0	0.038	0.9	0	0.9

Body type:
0 = Not applicable
1 = horizontal plate upper surface
2 = horizontal plate lower surface
3 = vertical plate
4 = horizontal cylinder upper half
5 = horizontal cylinder lower half
6 = horizontal cylinder (whole cylinder)

Table G.2

Form factors for calculation of radiation transfer between luminaire nodes - used in the validation runs of LITEAC1 and LITEAC2 described in Chapter 8.

Form factor matrix	Luminaire air	Lamp	Diffuser top	Ballast	Luminaire housing
Luminaire air	0	0	0	0	0
Lamp	0	0.01156	0 40336	0	0.58508
Diffuser top	0	0.1584	0	0	0.8416
Ballast	0	0	0	1	0
Luminaire housing	0	0 14139	0.51791	0	0 3407

Table G.3

Nodal data for the plenum section used in the validation runs of LITEAC1 and LITEAC2 described in Chapter 8.

	Plenum air	Luminaire housing top	Plenum steel	East plenum wall	South plenum wall	West plenum wall	North plenum wall	Ceiling	Suspended ceiling top
Initial Temperature (K)	295 9	296 9	296 9	296 2	296 2	296 2	296 2	295 9	296 9
Surface Area (m^2)	1	4 831	2 7871	3 2516	2 7871	2 7871	3 2516	15 6077	12 6438
Thermal capacity (J/K)	15401 7	16123 4	300817 4	30955 3	71596 1	30955 3	27726 9	341268 3	25125 1
Emissivity	0	0 9	0 9	0 9	0 9	0 9	0 9	0 9	0 9
Reflectivity for long-wave radiation	0	0 1	0 1	0 1	0 1	0 1	0 1	0 1	0 1
Reflectivity for short-wave radiation	0	0 7	0 2	0 3	0 3	0 3	0 3	0 3	0 5
Transmission coefficient for long-wave radiation	0	0	0	0	0	0	0	0	0
Transmission coefficient for short-wave radiation	0	0	0	0	0	0	0	0	0
Body type (see note below)	0	1	3	3	3	3	3	2	1
Characteristic length (m)	0	0 9	0 38	0 76	0 76	0 76	0 76	3 97	1 69

Body type:
0 = Not applicable
1 = horizontal plate upper surface
2 = horizontal plate lower surface
3 = vertical plate
4 = horizontal cylinder upper half
5 = horizontal cylinder lower half
6 = horizontal cylinder (whole cylinder)

Table G.4

Form factors for calculation of radiation transfer between plenum nodes - used in the validation runs of LITEAC1 and LITEAC2 described in Chapter 8.

Form factor matrix	Plenum air	Luminaire housing top	Plenum steel	East plenum wall	South plenum wall	West plenum wall	North plenum wall	Ceiling	Suspended ceiling top
Plenum air	0	0	0	0	0	0	0	0	0
Luminaire housing top	0	0 01997	0 10382	0 03857	0 06140	0 03857	0 06140	0 49792	0 17836
Plenum steel	0	0 17995	0 39359	0 03440	0 01244	0 02393	0 00197	0 27231	0 08142
East plenum wall	0	0 06685	0 03440	0	0 08231	0 03334	0 08231	0 38728	0 31352
South plenum wall	0	0 09122	0 01066	0 07055	0	0 07055	0 04722	0 39226	0 31754
West plenum wall	0	0 06685	0 02393	0 03334	0 08231	0	0 09277	0 38728	0 31352
North plenum wall	0	0 09122	0 00169	0 07055	0 04722	0 07952	0	0 39226	0 31754
Ceiling	0	0 15412	0 04863	0 06916	0 08172	0 06916	0 08172	0	0 49550
Suspended ceiling top	0	0 06820	0 01796	0 06916	0 08172	0 06916	0 08172	0 61209	0

Table G.5

Nodal data for the room section used in the validation runs of LITEAC1 and LITEAC2 described in Chapter 8.

	Room air	Diffuser bottom	Suspended ceiling bottom	East wall	South wall	West wall	North wall	Carpet surface	Floor surface
Initial Temperature (K)	296 9	296 9	296 9	296 2	296 2	296 2	296 2	295 7	295 7
Surface Area (m^2)	1	2 9729	12 6438	8 9187	10 4051	8 9187	10 4051	15 6077	15 6077
Thermal capacity (J/K)	0	2734 7	25125 1	98753 2	230550 7	98753 2	115275 4	13852 5	682536 5
Emissivity	0	0 9	0 9	0 9	0 9	0 9	0 9	0 9	0 9
Reflectivity for long-wave radiation	0	0 1	0 1	0 1	0 1	0 1	0 1	0 1	0 1
Reflectivity for short-wave radiation	0	0 1	0 7	0 5	0 5	0 5	0 5	0 3	0
Transmission coefficient for long-wave radiation	0	0	0	0	0	0	0	0	0
Transmission coefficient for short-wave radiation	0	0 8	0	0	0	0	0	0	0
Body type (see note below)	0	2	2	3	3	3	3	1	0
Characteristic length (m)	0	0 9	1 69	2 44	2 44	2 44	2 44	3 97	0

Body type:
0 = Not applicable
1 = horizontal plate upper surface
2 = horizontal plate lower surface
3 = vertical plate
4 = horizontal cylinder upper half
5 = horizontal cylinder lower half
6 = horizontal cylinder (whole cylinder)

Table G.6

Form factors for calculation of radiation transfer between room nodes - used in the validation runs of LITEAC1 and LITEAC2 described in Chapter 8.

Form factor matrix	Room air	Diffuser bottom	Suspended ceiling bottom	East wall	South wall	West wall	North wall	Carpet surface	Floor surface
Room air	0	0	0	0	0	0	0	0	0
Diffuser bottom	0	0	0	0 11785	0 15780	0 11785	0 15780	0 44870	0
Suspended ceiling bottom	0	0	0	0 15818	0 18196	0 15818	0 18196	0 31972	0
East wall	0	0 03928	0 22409	0	0 17769	0 11788	0 17769	0 26337	0
South wall	0	0 04508	0 22095	0 15231	0	0 15231	0 16331	0 26604	0
West wall	0	0 03928	0 22409	0 11788	0 17769	0	0 17769	0 26337	0
North wall	0	0 04508	0 22095	0 15231	0 16331	0 15231	0	0 26604	0
Carpet surface	0	0 08547	0 25881	0 15050	0 17736	0 15050	0 17736	0	0
Floor surface	0	0	0	0	0	0	0	0	1

Table G.7

Lamp data used in the validation of LITEAC1 described in Chapter 8.

Rated lamp power	320 W (8 lamps × 40 W)
Luminous flux output	24800 lumens (8 lamps × 3100 lm)
Ballast power	55 W (6.9 W per lamp)
Luminous efficacy of radiation emitted by lamp	340 lm W^{-1}

Points for defining relative light output (RLO) and relative lamp power (RLP):
[Data obtained from Siminovitch et al. (1984)]

MLWT (K)	RLO	RLP
0	0	0
286	0.521	0.9433
289	0.660	0.9902
292	0.777	0.9966
295	0.870	0.9976
298	0.936	0.9886
301	0.974	0.9814
304	0.990	0.9691
307	0.998	0.9632
310	0.994	0.9546
313	0.983	0.9450
316	0.964	0.9304
319	0.939	0.9155
322	0.909	0.8971
325	0.876	0.8808
328	0.840	0.8644
331	0.805	0.8465
334	0.774	0.8302
337	0.742	0.8159
473	0	0

Table G.8

Conductance data used in the validation runs of LITEAC1 and LITEAC2 described in Chapter 8.

From node	To node	Conductance (W m^{-2}K^{-1})	One-way or two-way
Luminaire node: diffuser top	Room node: diffuser bottom	53.33	2
Luminaire node: ballast	Luminaire node: housing	631 87	2
Luminaire node. housing	Plenum node. luminaire housing top	1263 73	2
Plenum node: suspended ceiling top	Room node: suspended ceiling bottom	4 8	2
Plenum node: ceiling	Room node· floor surface	9 818	2
Room node· carpet surface	Room node: floor surface	2.73	2

Appendix H

Input data for the laboratory test cell

The data used in the input files for the validation runs of the programs LITEAC1 and LITEAC2 using the laboratory test cell results are listed in Tables H.2-H.9. In Tables H.2, H.4 and H.6, data concerning surface areas, thermal capacities, emissivities and reflectivities were calculated from the cell dimensions and the materials property data (listed in Table H.1) obtained from the ASHRAE Handbook (ASHRAE 1993) and Holman (1992). Radiation form factors (in Tables H.3, H.5 and H.7) were calculated using the view factor program 'VF' and 'FACTS' included in 'LIGHTS' (Sowell 1989). The lamp data (in Table H.8) concerning the relative lamp power and relative light output were obtained from Siminovitch et al. (1984). The conductance data (in Table H.9) were obtained from the conductivity data of materials in ASHRAE (1993) and Holman (1992).

Table H.1

Materials data used for the calculation of the input data for the laboratory test cell.

Nodes	Material	Density (kg m^{-3})	Specific heat capacity (J $kg^{-1}K^{-1}$)	Thermal conductivity (W $m^{-1}K^{-1}$)	Data source
Ceiling All plenum nodes Suspended ceiling All room nodes Floor	Plywood	540	1210	0.12	ASHRAE (1993)
Luminaire housing	Nickel steel	7933	460	19	Holman (1992)
Ballast	Iron	7897	452	73	Holman (1992)
Lamp wall	Glass	2470	750	1.0	ASHRAE (1993)
All air nodes	Air at 300K	1.177	1005.7	-	Holman (1992)

Table H.2

Nodal data for the luminaire section used in the validation runs of LITEAC1 and LITEAC2 using the laboratory test cell (described in Chapter 9).

	Luminaire air	Lamp upper	Lamp lower	Diffuser top	Ballast	Luminaire housing
Initial Temperature (K)	291.7	291.7	291.7	291.7	291.7	291.7
Surface Area (m^2)	0	0 0716	0.0716	0 216	0 003456	0 4644
Thermal capacity (J/K)	23 455	132 6915	132 6915	849.2	81.55	909.1
Emissivity	0	0 9	0.9	0.9	0	0 9
Reflectivity for long-wave radiation	0	0.1	0.1	0.1	0	0.1
Reflectivity for short-wave radiation	0	0 9	0.9	0.1	0.7	0.8
Transmission coefficient for long-wave radiation	0	0	0	0	0	0
Transmission coefficient for short-wave radiation	0	0	0	0 8	0	0
Body type (see note below)	0	4	5	1	0	2
Characteristic length (m)	0	0 038	0 038	0.2032	0	0 2032

Body type:
0 = Not applicable
1 = horizontal plate upper surface
2 = horizontal plate lower surface
3 = vertical plate
4 = horizontal cylinder upper half
5 = horizontal cylinder lower half
6 = horizontal cylinder (whole cylinder)

Table H.3

Form factors for calculation of radiation transfer between luminaire nodes - used in the validation runs of LITEAC1 and LITEAC2 using the laboratory test cell (described in Chapter 9).

Form factor matrix	Luminaire air	Lamp upper	Lamp lower	Diffuser top	Ballast	Luminaire housing
Luminaire air	0	0	0	0	0	0
Lamp upper	0	0	0	0	0	1
Lamp lower	0	0	0	0.7048	0	0.2952
Diffuser top	0	0	0 2336	0	0	0 7664
Ballast	0	0	0	0	1	0
Luminaire housing	0	0 1542	0 0455	0.3565	0	0.4438

Table H.4

Nodal data for the plenum section used in the validation runs of LITEAC1 and LITEAC2 using the laboratory test cell (described in Chapter 9).

	Plenum air	Luminaire housing top	East plenum wall	South plenum wall	West plenum wall	North plenum wall	Ceiling	Suspended ceiling top
Initial Temperature (K)	291 7	291 7	291 7	291 7	291 7	291 7	291 7	291 7
Surface Area (m^2)	0	0 4644	0 2	0 3	0 2	0 3	1 5	1 28
Thermal capacity (J/K)	363 985	909 1	1244 7	1867 1	1244 7	1867 1	9258 3	3995 5
Emissivity	0	0 9	0 9	0 9	0 9	0 9	0 9	0 9
Reflectivity for long-wave radiation	0	0 1	0 1	0 1	0 1	0 1	0 1	0 1
Reflectivity for short-wave radiation	0	0 7	0 3	0 3	0 3	0 3	0 3	0 5
Transmission coefficient for long-wave radiation	0	0	0	0	0	0	0	0
Transmission coefficient for short-wave radiation	0	0	0	0	0	0	0	0
Body type (see note below)	0	1	3	3	3	3	2	1
Characteristic length (m)	0	0 2032	0 762	0 762	0 762	0 762	0 9847	0 4148

Body type:
0 = Not applicable
1 = horizontal plate upper surface
2 = horizontal plate lower surface
3 = vertical plate
4 = horizontal cylinder upper half
5 = horizontal cylinder lower half
6 = horizontal cylinder (whole cylinder)

Table H.5

Form factors for calculation of radiation transfer between plenum nodes - used in the validation runs of LITEAC1 and LITEAC2 using the laboratory test cell (described in Chapter 9).

Form factor matrix	Plenum air	Luminaire housing top	East plenum wall	South plenum wall	West plenum wall	North plenum wall	Ceiling	Suspended ceiling top
Plenum air	0	0	0	0	0	0	0	0
Luminaire housing top	0	0	0 0336959	0 0523831	0 0336959	0 0523831	0 5980013	0 2298407
East plenum wall	0	0 0782419	0	0 089441	0 0150947	0 089441	0 3851389	0 3426425
South plenum wall	0	0 0810890	0 0596273	0	0 0596273	0 0438008	0 4046174	0 3512382
West plenum wall	0	0 0782419	0 0150947	0 089441	0	0 089441	0 3851389	0 3426425
North plenum wall	0	0 0810890	0 0596273	0 0438008	0 0596273	0	0 4046174	0 3512382
Ceiling	0	0 1851412	0 0513519	0 0809235	0 0513519	0 0809235	0	0 5503080
Suspended ceiling top	0	0 0833891	0 0535379	0 0823214	0 0535379	0 0823214	0 6448923	0

Table H.6

Nodal data for the room section used in the validation runs of LITEAC1 and LITEAC2 using the laboratory test cell (described in Chapter 9).

	Room air	Diffuser bottom	Suspended ceiling bottom	East wall	South wall	West wall	North wall	Floor surface
Initial Temperature (K)	291 7	291 7	291 7	291 7	291 7	291 7	291 7	291 7
Surface Area (m^2)	0	0 216	1 28	0 8	1 2	0 8	1 2	1 5
Thermal capacity (J/K)	1556 8236	849 2	3995 5	4978 9	7468 4	4978 9	7468 4	9258 3
Emissivity	0	0 9	0 9	0 9	0 9	0 9	0 9	0 9
Reflectivity for long-wave radiation	0	0 1	0 1	0 1	0 1	0 1	0 1	0 1
Reflectivity for short-wave radiation	0	0 1	0 7	0 5	0 5	0 5	0 5	0 3
Transmission coefficient for long-wave radiation	0	0	0	0	0	0	0	0
Transmission coefficient for short-wave radiation	0	0 8	0	0	0	0	0	0
Body type (see note below)	0	2	2	3	3	3	3	1
Characteristic length (m)	0	0 2032	0 4148	2 4384	2 4384	2 4384	2 4384	0 9847

Body type.
0 = Not applicable
1 = horizontal plate upper surface
2 = horizontal plate lower surface
3 = vertical plate
4 = horizontal cylinder upper half
5 = horizontal cylinder lower half
6 = horizontal cylinder (whole cylinder)

Table H.7

Form factors for calculation of radiation transfer between room nodes - used in the validation runs of LITEAC1 and LITEAC2 using the laboratory test cell (described in Chapter 9).

Form factor matrix	Room air	Diffuser bottom	Suspended ceiling bottom	East wall	South wall	West wall	North wall	Floor surface
Room air	0	0	0	0	0	0	0	0
Diffuser bottom	0	0	0	0 1285107	0 1836662	0 1285107	0 1836662	0 3756462
Suspended ceiling bottom	0	0	0	0 1347953	0 2093741	0 1347953	0 2093741	0 3116612
East wall	0	0 0346979	0 2163464	0	0 2029125	0 0920864	0 2029125	0 2510443
South wall	0	0 0330599	0 2240303	0 135275	0	0 135275	0 2152694	0 2570904
West wall	0	0 0346979	0 2163464	0 0920864	0 2029125	0	0 2029125	0 2510443
North wall	0	0 0330599	0 2240303	0 135275	0 2152694	0 135275	0	0 2570904
Floor surface	0	0 0540930	0 2667818	0 1338903	0 2056723	0 1338903	0 2056723	0

Table H.8

Lamp data used in the validation of LITEAC1 using laboratory test cell described in Chapter 9.

Rated lamp power	40 W
Luminous flux output	3400 lumens
Ballast power	6 9 W
Luminous efficacy of radiation emitted by lamp	340 lm W^{-1}

Points for defining relative light output (RLO) and relative lamp power (RLP)

MLWT (K)	RLO	RLP	MLWT (K)	RLO	RLP
0	0	0	312	0 988	0.9488
286	0.521	0 9433	313	0.983	0 9450
287	0 562	0.9598	314	0.978	0.9420
288	0 610	0.9728	315	0.971	0 9362
289	0 660	0.9902	316	0.964	0 9304
290	0 695	0 9932	317	0 957	0 9255
291	0 738	0.9942	318	0 948	0.9205
292	0.777	0.9966	319	0 939	0 9155
293	0 810	0.9990	320	0.931	0.9113
294	0 843	1.0000	321	0.919	0 9033
295	0 870	0 9976	322	0.909	0 8971
296	0 893	0.9910	323	0 898	0 8899
297	0 917	0.9900	324	0.888	0.8873
298	0.936	0.9886	325	0.876	0 8808
299	0 952	0.9881	326	0.864	0 8751
300	0.964	0.9836	327	0 852	0.8694
301	0 974	0 9814	328	0.840	0 8644
302	0 981	0.9802	329	0 829	0.8568
303	0.986	0.9731	330	0.817	0.8517
304	0 990	0.9691	331	0.805	0 8465
305	0 993	0 9642	332	0.795	0 8397
306	0 995	0.9632	333	0.783	0 8343
307	0 998	0.9632	334	0.774	0 8302
308	0.999	0.9623	335	0.762	0 8228
309	0.998	0.9594	336	0.752	0 8194
310	0 994	0.9546	337	0.742	0 8159
311	0 991	0 9517	473	0	0

Table H.9

Conductance data used in the validation runs of LITEAC1 and LITEAC2 using the laboratory test cell described in Chapter 9.

From node	To node	Conductance (W $m^{-2}K^{-1}$)	One-way or two-way
Luminaire node: diffuser top	Room node: diffuser bottom	44.79	2
Luminaire node ballast	Luminaire node: housing	631.87	2
Luminaire node ballast	Plenum node: luminaire housing top	631.87	2
Luminaire node: housing	Plenum node luminaire housing top	1263.73	2
Plenum node: suspended ceiling top	Room node: suspended ceiling bottom	12.6	2
Plenum node: east plenum wall	Ambient environment	1.887	2
Plenum node: south plenum wall	Ambient environment	1.887	2
Plenum node: west plenum wall	Ambient environment	1.887	2
Plenum node: north plenum wall	Ambient environment	1.887	2
Plenum node: ceiling	Ambient environment	1.949	2
Room node: east wall	Ambient environment	1.887	2
Room node: south wall	Ambient environment	1.887	2
Room node: west wall	Ambient environment	1.887	2
Room node: north wall	Ambient environment	1.887	2
Room node: suspended ceiling bottom	Ambient environment	1.795	2

Appendix I

Publications originated from this work

Numerical Modeling of Lighting/HVAC Interaction in Enclosures Part I: Light and Heat Transfer in a Room

Tse-Ming Chung
Member ASHRAE

D.L. Loveday, Ph.D.

A numerical model based on heat transfer equations was developed for the dynamic simulation of a room with lamps in luminaires as the only power source. The model was used to consider heat transfer by conduction, convection and radiation between surfaces in the luminaire, the plenum space and the room space. Also, it was used to calculate temperatures, cooling loads, and lighting levels at each time step. It was designed to be flexible so that different room configurations could be simulated. The main differences between this model and previous models in the literature are that, firstly, this model does not assume that some nodes are massless; secondly, it calculates illuminance on room surfaces; and thirdly, a fluorescent lamp positive column model can be incorporated at a later stage for improved simulation of lighting levels for a room, these differences represent an improvement on similar existing models. The present model was validated, using the experimental results reported by Treado and Bean (1988, 1992), and using further experimental measurements obtained from a laboratory-constructed test cell. Further validation was conducted using the numerical test cell developed by Sowell (1990). Results predicted by the model agreed well with experimental results from both the NIST test cell and the laboratory test cell. The incorporation of a fluorescent lamp positive column model is presented in Part II.

INTRODUCTION

Electric lighting and air-conditioning are the two major consumers of electrical energy in most modern office buildings. They are essential in modern, deep plan office buildings, particularly in tropical regions and in metropolitan areas where natural ventilation is precluded for reasons of air quality and noise. The actual proportions of electricity used by lighting and air-conditioning depend on the design of lighting and heating, ventilation and air-conditioning (HVAC) systems, and these proportions also vary geographically and seasonally with changes in climate. Lighting or air-conditioning alone can account for 20-50% of the total electricity consumption in a modern office building. As a result, a small percentage saving of lighting and/or HVAC energy consumption can result in a substantial saving of money.

Although lighting and HVAC are separate systems in a building and provide different functions, they mutually affect one another when they are operating simultaneously. Lighting imposes a heat gain which must be removed by the air-conditioning in order to maintain occupant thermal comfort; at the same time, air-conditioning affects the fluorescent lamp operating temperature, which, in turn, is closely related to the light output of the lamp.

It is the relationship between lamp and HVAC operation which is the subject of study in this paper. A numerical model that can simulate the mutual interaction between lighting and HVAC was developed. The model integrates a fluorescent lamp positive column model with a room

Tse-Ming Chung is an assistant professor in the Department of Building Services Engineering, The Hong Kong Polytechnic University, Kowloon, Hong Kong D.L. Loveday is a reader in Civil and Building Engineering, Loughborough University, Leicestershire, U K

model, the latter comprised of a luminaire, a plenum, an occupied space and ventilation inlets and outlets. In this way, the model could be used to simulate both the transient and the steady-state cooling load caused by lights, as well as the variation of lighting levels with time on both the working plane and the other room surfaces

The goal of this research is to develop a numerical model for the simulation of the mutual interaction between HVAC and lighting which will find applications in areas such as design calculations of cooling load and light output, building energy analysis, and the evaluation of the performance of lighting systems as affected by room characteristics and HVAC system designs Initial designs of new luminaire appliances can also be evaluated by this numerical tool so that the necessity of experimental evaluation can be minimized In this sense, the model can be used to aid the future design of luminaires.

Details of the room model are discussed in this paper with the objective of describing how the mathematical model was constructed from the fundamental heat balance equations; the fluorescent lamp positive column model itself will be discussed in Part II. Before we discuss the mathematical model of a room containing luminaires, we begin with a review of the background to this field and describe previous studies of the cooling loads caused by lighting.

COOLING LOAD CAUSED BY LIGHTING

Lighting power is a large source of heat gain in buildings because the energy consumed by electric lighting appears ultimately as heat in building interiors, even if it has been converted to visible radiation. In fact, in interior zones of office buildings where solar heat gain is absent, lighting is the major source of heat gain. This heat gain may be beneficial to occupants in buildings located in cold climates, but for hot climates and the cooling season of temperate climates this heat gain adds to the cooling load of the air-conditioning system.

Even for the most efficient light source, a large proportion of the power input to the luminaire is converted to heat directly and is manifested as a rise in temperature of the lamp and ballast surfaces The remaining power is radiated out from the lamp as electromagnetic radiation in both the visible and infrared wavelengths. Hence, power input to lighting becomes heat gain to the space in two forms· One form is the convective or conductive heat gain due to the raised temperature of the lamp and ballast surfaces; these add heat to the space instantaneously. The second form is radiation emitted from the lamps. This radiant energy is first absorbed by room and furniture surfaces, causing an increase in their surface temperatures This temperature increase finally adds heat to the space through convection after a time lag. At steady state, the space heat gain due to lights is equal to the lighting power input if all the lighting radiation is trapped within the space (e.g. for an interior zone with no windows). However, steady state conditions are not normally attained due to these on/off cycles, since most offices lights are usually switched off outside office hours, and some energy-conscious occupants may turn off the lights when the room is unoccupied. The instantaneous heat gain from lights therefore depends on many factors, including: the on/off schedule of the lighting, the configuration of the room, room surface and furniture thermal properties, room ventilation rate, etc.

PREVIOUS STUDIES

Perhaps the first model of heat transfer in lighting was produced by Kimura and Stephenson (1968). They used a simple model of a room with a ceiling plenum, a recessed luminaire and a heat-storing floor slab. Lighting power was split arbitrarily into "upward" (released to plenum space) and "downward" (released to room space) fractions. Each of these fractions was assumed to be equally divided into convective and radiative heat transfer. Using the response factor method developed by Stephenson and Mitalas (1967), they showed that the instantaneous cooling load due to lights can be expressed in terms of two coefficients. Subsequently, Mitalas and

Kimura (1971) built a calorimeter to determine the values of these coefficients. Mitalas (1973a, 1973b) further showed, using Z-transfer functions, that the cooling load at time t_n, which is a whole number multiple of a fixed time step after lights on, i.e. $t = t_n = n\Delta$, where n is a whole number and Δ is a time step interval, is given by:

$$q(t_n) = v_1 W(t_{n-1}) + v_2 W(t_{n-2}) + w_1 q(t_{n-1}) \tag{1}$$

where

$q(t_n)$ = cooling load due to lights at $t = n\Delta$

$W(t_n)$ = power input to lights at $t = n\Delta$

v_1, v_2 and w_1 are coefficients of transfer function with $v_2 = 1 - w_1 - v_1$

Based on the experimental study of Mitalas and Kimura (1971), design values of v_1 and w_1 were derived by Mitalas (1973a, 1973b) These values were used in the transfer function method for cooling load calculation in the 1993 *ASHRAE Handbook* However, this handbook uses the following equation for the calculation of cooling load from lights:

$$q(t_n) = v_0 W(t_n) + v_1 W(t_{n-1}) + w_1 q(t_{n-1}) \tag{1a}$$

This relates the cooling load due to the lights at the current hour (t_n), to the power input to lights at the current hour (t_n) and 1 hour beforehand (t_{n-1}) Values of the coefficient v_0 used by ASHRAE (1993) in Equation (1a) are exactly the same as those of v_1 originally derived by Mitalas. The authors noted also that an earlier edition of *ASHRAE Handbook* (ASHRAE 1981) used v_1 and v_2 coefficients in the same way as derived by Mitalas (1973a, 1973b).

Sowell and O'Brien (1973) constructed a detailed analytical model representing the building unit cell with a fluorescent luminaire recessed into the plenum The unit cell was discretized into a number of nodes and the heat transfer modes of conduction, convection and radiation between nodes were considered. In the steady-state condition, a heat balance equation in vector-matrix form was obtained This vector-matrix equation was solved numerically and a set of steady-state nodal temperatures was obtained to enable the prediction of the effects of the lighting system on the thermal environment in the living space

Ball and Green (1983), report results from an ASHRAE-sponsored study, using mathematical modeling of the transient energy transfer caused by lighting. Their model simulated primarily the conditions in the test room facility used by Mitalas and Kimura (1971), with the room, the plenum and the luminaire being considered separately. The model was used to generate the transfer function coefficients v_1 and w_1 in Equation (1) for the experimental conditions used by Mitalas and Kimura. Some good and some poor agreements were found. However, with a caveat for the case in which a large discrepancy was found in the v_1 value, they made recommendations for the use of the model generated transfer coefficients for cooling load calculations

Sowell (1990) added dynamic simulation to his earlier steady-state model so that the heat balance equation had an additional term comprising the product of heat capacitance and rate of temperature change. This vector-matrix equation was solved by partitioning it into nodes with finite thermal mass and nodes that were assumed to be massless. He also added the effect of lamp wall temperature on lamp and ballast power, and on luminous output, using empirical curves. Sowell called his model a "numerical lighting/HVAC test cell" and he argued that the use of his numerical test cell had advantages over the use of full-scale physical test cells. His numerical test cell was implemented in the C programming language and called the LIGHTS program (Sowell 1989). The LIGHTS program was validated by a number of simple examples with known solutions Comparisons were also made with results from the NIST physical test cell (Treado and

Bean 1988, 1990, 1992); however, agreement was generally poor. Sowell (1990) attributed the discrepancies between the model and the NIST data to model deficiencies or experimental error

MODEL EQUATIONS

The room model developed in our study is a dynamic mathematical model for simulating transient heat flow and temperature for a room with luminaires and a plenum. The model uses heat balance equations for the nodes based on fundamental heat transfer principles. It differs from the previous models by other researchers in three main aspects; firstly, it solves the dynamic heat balance equations without assuming any node to be massless; secondly, it calculates illuminance on room surfaces; and thirdly, a fluorescent lamp positive column model can be incorporated to simulate the variation of light output with ambient temperature. Hence, the model calculates not only the dynamic temperature variation but also the dynamic lighting levels in a room with both air-conditioning and lighting on.

To conform with most modern offices, the room model was comprised of three separate sections (compartments): the luminaire, the plenum (ceiling void) and the room (conditioned space). Each section is divided into a number of nodes The model was designed to be flexible so that it could simulate different room configurations; to achieve this, the number of nodes in each of the three sections could be varied A node represents an isothermal surface For most cases the walls, floor and ceiling of the room (and plenum) could be assumed to be isothermal surfaces and each is represented by one surface node. Lamp and luminaire surfaces are usually non-isothermal. The model allowed a non-isothermal surface to be divided into smaller elements to form different nodes (each with a different temperature) provided that the physical properties of all nodes, the radiation form factors and the conduction coupling between adjacent nodes are known It is anticipated that in most simulations, due to the complexity when too many nodes are used, luminaire and lamp surfaces have to be assumed isothermal. Figure 1 shows a schematic diagram of the three sections and the distribution of some nodes.

For each node, the following equation can be made for the heat balance: (This equation relates the temperature rise of each node in one time step to the total net heat gain of that node in one time step)

$$m_i c_{pi} \Delta T_i = q_{Gi} + q_{Li} + q_{Si} + q_{Hi} + q_{Ci} \tag{2}$$

where

m_i = mass of node i
c_{pi} = specific heat capacity of node i
ΔT_i = temperature rise of node i in one time step
q_{Gi} = total (electrical) energy input at node i in one time step
q_{Li} = total (net) long-wave radiation heat gain to node i in one time step
q_{Si} = total (net) short-wave radiation heat gain to node i in one time step
q_{Hi} = total (net) convection heat gain to node i in one time step
q_{Ci} = total (net) conduction heat gain to node i in one time step

As shown in this heat balance equation, the net heat gain to a node consists of five components: energy input (for lamp and ballast nodes only), long-wave (infrared) radiation, short-wave (visible) radiation, convection, and conduction. Each of these components is calculated separately, as described below.

Energy Input at a Node

As the purpose of this model was to study the interaction between lighting and air-conditioning, the only energy input considered was the electrical energy consumed at the lamp and ballast

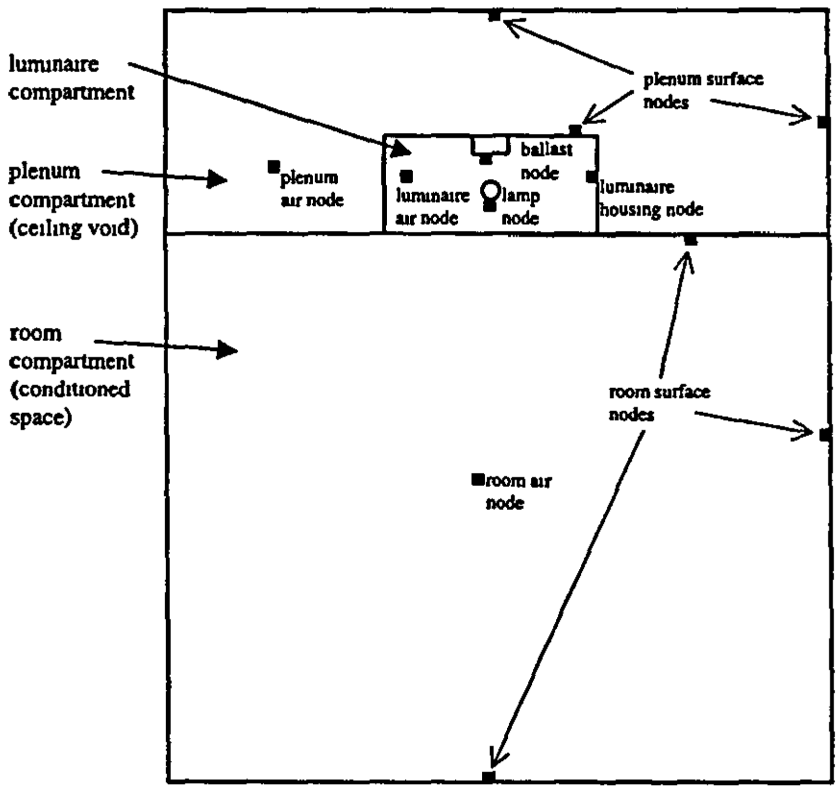

Figure 1. Schematic diagram of the three sections and the distribution of some typical nodes.

nodes, no other power sources were considered. Fluorescent lamp power input, as well as the light output, depend on the minimum lamp wall temperature (also called the cold-spot temperature which is the temperature of the coldest spot on the lamp wall) which in turn depends on the operating environment. Therefore, when modeling the fluorescent lamp power input one cannot simply use the rated power of the lamp. As the lamp power depends on the discharge current inside the fluorescent tube, a positive column model of the fluorescent lamp (see, for example, Waymouth (1971)) was used to calculate the variation of lamp power under different operating conditions. This positive column model could be incorporated into the room model for improved simulation of the variation of light output with ambient temperature.

The positive column model was added in the form of a subroutine so that it could be substituted (for comparison purposes) by other methods of calculation of the variation of lamp power and light output with ambient temperature such as the use of empirical curves. In this paper, the results obtained from a room model simulation calculated using empirical curves were compared with results from the LIGHTS program Details of the positive column model are described in Part II.

The power consumed at the ballast depends on the quality of the ballast. For calculation purposes it is usually assumed to be a fraction (e.g. 0.15) of the lamp power. The power input at nodes other than the lamp and the ballast is assumed to be zero.

Net Long-Wave Radiation

The net rate of long-wave radiation flow to node i is obtained by subtracting the radiant exitance (radiosity) of i from the irradiance on i as follows:

$$q_{Li} = (E_{Li} - M_{Li})A_i \tag{3}$$

where E_{Li}, M_{Li}, and A_i are, respectively, the irradiance, radiant exitance (radiosity), and area with reference to node i (all symbols with a subscript L refer to long-wave radiation). Using radiation form factors F_{ji}, reflectances ρ_{Li}, and emissivities ε_i, etc. E_L and M_L are given as follows:

$$E_{Li} = \sum_j \frac{A_j F_{ji} M_{Lj}}{A_i} = \sum_j F_{ij} M_{Lj} \tag{4}$$

where the last equality in Equation (4) uses the reciprocity relation of radiation form factors

$$M_{Li} = M_{Loi} + \rho_{Li} E_{Li} = M_{Loi} + \rho_{Li} \sum_j F_{ij} M_{Lj} \tag{5}$$

where M_{Loi} is the radiant emissive power from a gray surface, and is given by the Stefan-Boltzmann law·

$$M_{Loi} = \varepsilon_i \sigma T_i^4 \tag{6}$$

Equation (5) is actually a set of simultaneous linear equations that can be solved by an iteration process such as the Jacobi or Gauss-Seidel iteration method.

Combining Equations (3), (4), (5) and (6):

$$\begin{aligned} \dot{q}_{Li} &= (E_{Li} - \varepsilon_i \sigma T_i^4 - \rho_{Li} E_{Li}) A_i \\ &= [(1 - \rho_{Li}) E_{Li} - \varepsilon_i \sigma T_i^4] A_i \\ &= A_i (1 - \rho_{Li}) \sum_j F_{ij} M_{Lj} - A_i \varepsilon_i \sigma T_i^4 \end{aligned} \tag{7}$$

and assuming all surfaces to be diffuse grey, then $\rho_{Li} = 1 - \varepsilon_i$ and Equation (7) becomes:

$$\dot{q}_{Li} = A_i \varepsilon_{Li} \left(\sum_j F_{ij} M_{Lj} - \sigma T_i^4 \right) \tag{8}$$

Net Short-wave Radiation

If all surfaces (including the light-emitting surfaces) are assumed to be diffuse, then equations similar to Equations (3), (4), and (5) above also apply to short-wave radiation. Fluorescent tubes have more or less a diffuse emission, and the assumption of diffuse surfaces is a good one for all surfaces in a normal office environment, except that there may be a reflector which has a large specular component inside the luminaire Using symbols similar to the long-wave radiation terms but with a subscript S denoting short-wave radiation, the following equation gives the net short-wave radiation heat gain:

$$\dot{q}_{Si} = (E_{Si} - M_{Si})A_i \tag{9}$$

E_{Si} and M_{Si} are given, respectively, by:

$$E_{Si} = \sum_j \frac{A_j F_{ji} M_{Sj}}{A_i} = \sum_j F_{ij} M_{Sj} \tag{10}$$

and

$$M_{Si} = M_{Soi} + \rho_{Si} E_{Si} = M_{Soi} + \rho_{Si} \sum_j F_{ij} M_{Sj} \tag{11}$$

where M_{Soi} is the luminous power per unit area emitted from surface i, and is zero except for the lamp and diffuser nodes. In a fluorescent lamp, the luminous power emission M_{Soi} is related to the property (quantum efficiency and spectral distribution) of the fluorescent powder in the lamps and the discharge intensity inside the lamp. The discharge intensity, in turn, is related to the mercury vapor pressure inside the lamp. As mercury vapor inside the lamp condenses at the coldest spot, the discharge intensity and hence the luminous flux emission depend on the minimum lamp wall temperature. A fluorescent lamp positive column model can be used to calculate M_{Soi} for the lamp nodes (to be described in a further paper). Otherwise, M_{Soi} for the lamp nodes can be calculated from the lumen output of the lamp by assuming a luminous efficacy of radiation emitted from the lamp.

Similar to Equation (5), Equation (11) is also a set of simultaneous equations which can be solved by an iteration process such as the Jacobi or Gauss-Seidel iteration method.

Combining Equations (9), (10), and (11), the short-wave radiation heat gain of node i is then given by.

$$\dot{q}_{Si} = A_i \left[(1 - \rho_{Si}) \sum_j F_{ij} M_{Sj} - M_{Soi} \right] \tag{12}$$

Convection

For surfaces in contact with an air node there is convection heat exchange between the surface and the air node. The convection heat gain of node i is:

$$\dot{q}_{Ha} = A_i h_i (T_a - T_i) \tag{13}$$

where h_i is the convective heat transfer coefficient of node i, T_a is the temperature of the air node adjacent to node i, and T_i is the node temperature.

The convection to the air node is then:

$$\dot{q}_{Hi} = \sum_i h_i (T_i - T_a) A_i \tag{14}$$

where the sum is taken over all nodes in contact with the air node.

In the computer program developed for the model, the convective heat transfer coefficient h_i was calculated based on empirical equations for free convection given in Holman (1992). The geometry and dimensions of a node were input parameters for the calculation of convection coefficient. For example, the geometry of the lamp was a horizontal cylinder, walls are vertical surfaces, floor and ceiling are horizontal surfaces, and the ballast is assumed to be an irregular solid. A surface (node) was assumed to be isothermal and the temperature difference between the surface and adjacent air was calculated at each time step With this temperature difference, the convective heat transfer coefficient was calculated using appropriate empirical equations and correlation constants, as given in Table 7-1 of Holman (1992). All nodes in the model are treated separately, yielding separate convection coefficient values. The computer program also allowed input of the convective heat transfer coefficient directly, where this is known, e.g through experimental determination. For cases in which air return is through the luminaire compartment, forced convection may happen and the convective coefficients over lamp and luminaire surfaces then have to be determined either by calculation using known empirical equations such as those given in Holman (1992), or by experimental measurements.

If there is air exchange in between air nodes in different sections, then the convection heat gain of air node ai due to this air exchange is calculated from:

$$\dot{q}_{Cai} = \sum_{j \neq i} V_{ij}\rho_a c_{pa}(T_{aj} - T_{ai}) \tag{15}$$

where V_{ij} is the volume flow rate of air in between air nodes ai and aj and ρ_a and c_{pa} are the density and specific heat capacity of air, respectively, which are assumed to be constant over the range of air temperatures concerned.

Conduction

For nodes in contact with each other, there is a conduction heat transfer between them. The total conductive heat transfer to node i is calculated from:

$$q_{Ci} = \sum_j C_{ji}(T_j - T_i) \tag{16}$$

where C_{ji} is the conductance from node j to node i and the sum is taken over all nodes in contact with node i

SOLUTION SCHEME

In order to get a solution, the mass, heat capacity, reflectivity, emissivity and initial temperature of each node had to be known or assumed. A time step was then selected The rates of heat gain by different modes were then calculated one by one using Equations (3)–(16) with nodal temperatures equal to that at the beginning of the time step. In the calculation, consideration was given not only to heat exchange between nodes within a section but also to heat exchange by short wave radiation transmitted from one section to another, by conduction between adjacent nodes of different sections, and by air exchange between sections. These rates of heat gain to each node by different modes were then added together. This total rate of heat gain to a node was then multiplied by the time step and divided by the heat capacity of the node to get the temperature change of the node during the time step period, as given by Equation (2). This temperature change was then added to the nodal temperature prevailing at one time step before. In other words, the model used the forward finite difference method in the calculation of the nodal temperatures one time step forward. It was assumed that the room air was kept at a constant temperature by an ideally-controlled air-conditioning system; therefore, the heat convected to the room air node was equal to the cooling load due to lighting. From the short-wave radiation falling on a nodal surface, the illuminance on the surface could be calculated using the CIE relative spectral sensitivity curve (CIE 1983), and either knowing or assuming the spectral distribution of the light.

The Gauss-Seidel iteration method was used to solve the simultaneous equations [Equations (5) and (11)] for fast convergence. Stability and convergence of the numerical scheme used in the model caused some concern in the development of the model. In fact, the stability of the numerical scheme depends very much on the input values of the parameters, such as areas, heat capacities and heat transfer coefficients. In Sowell's LIGHTS program (Sowell 1989), nodal heat capacities smaller than a certain value (user defined) are assumed to be 'massless', so that the transient problem becomes a steady-state one, and in this way the problem of instability due to small mass and large conductances is eliminated. In the present numerical model, the maximum time step to ensure numerical stability depends on the relative thermal masses of the nodes To include nodes with small thermal masses such as the lamp node but not assuming them to be 'massless', a small time step (of the order of seconds) has to be used to ensure numerical stability. In the validation run (described next), a time step of 1.0 second was used to ensure stability. Since the program will not be used directly for simulation on an annual basis, the short time step interval will not increase the computational time unduly. For building energy simulation on an annual basis, the model can be used as a "pre-processor" to generate weighting factors and lighting energy distribution fractions These pre-processor results are then used in building energy analysis programs. The numerical model was coded in FORTRAN77, and therefore could be compiled using any FORTRAN77 compiler. It has also been compiled and run successfully on several recent models of desktop computers.

MODEL VALIDATION

The model described previously was validated using experimental data and a numerical test cell (Sowell's LIGHTS program, 1989) Sowell's model uses an empirical curve in place of the positive column model to account for the variation of light output with lamp-wall temperature. In order to make direct comparison with the LIGHTS program, simulations were performed using the room model as described in this paper but without the inclusion of the positive column model of the fluorescent lamp. For identification purposes, this version of our numerical model is termed LITEAC1. The version incorporating the positive column model is termed LITEAC2, and will be discussed in Part II Two sets of experimental data were used for the validation exercise The first set consisted of measurements in a full-scale room taken at the US National Institute of Standards and Technology (NIST), and published in two NIST reports (Treado and Bean 1988, 1992). The second set was a series of measurements taken in a specially-constructed laboratory-scale test cell containing a luminaire. The following describes the results of these validation exercises.

The NIST Test Cell

Treado and Bean (1988, 1990, 1992) reported on full-scale measurements of the interaction between lighting and HVAC carried out at NIST's Building and Fire Research Laboratory They used a test room of dimensions 4.27 m long and 3 66 m wide, with a conditioned room space height of 2.44 m, and a plenum height of 0.76 m. Four luminaires, each 0 6 m wide by 1 2 m long, were recessed into the plenum. In the case considered here, each of the luminaires contained two 40 W lamps and an acrylic diffuser. It was configured with air return through a ceiling grille to the plenum. Supply air flow rate was 0 0944 m^3/s. In the validation work conducted here, the NIST test room was divided into 23 nodes: 5 luminaire nodes, 9 plenum nodes and 9 room nodes. This division is similar to that used in the NIST numerical model (Treado and Bean 1988) with the following changes: 2 nodes are added: the carpet surface and the base of the luminaire diffuser; in addition, four NIST nodes were eliminated: middle floor and middle ceiling. These were actually the same node and considered unnecessary in the current validation exercise· ceiling top and floor surface, which were actually the same node, and were combined into a single node, and ceiling bottom and floor bottom (which are also the same node and are also combined into a single node in this validation exercise)

Data concerning the dimensions, the heat capacity, the emissivity and the reflectivity of nodes were obtained either from the NIST reports or were calculated from data in ASHRAE (1993). Radiation form factors were calculated using the view factor programs VF and FACTS included in LIGHTS (Sowell 1989). Convective heat transfer coefficients were calculated according to empirical equations for free convection given in Holman (1992). Conductance values were obtained from ASHRAE (1993)

In this study, as the fluorescent lamp positive column model was not included, lamp data concerning the relative power and relative light output was obtained from Siminoritch et al. (1984); lamp power balances and luminous efficacies were obtained from Dorleijn and Jack (1985). The transmittance of the prismatic diffusers used in the NIST test cell is not available in the published reports According to IESNA (1993), the transmittance of clear prismatic lens has a range between 0.7 and 0 92 and it is reasonable in the calculations here to assume the transmittance to be 0 8.

To facilitate comparison with the results published in the NIST reports (Treado and Bean 1988, 1992), two kinds of simulation tests, namely, the "lights on" test and "lighting on/off cycles" test, are reported here

Lighting ON Test

Simulations were conducted, using both the present model and Sowell's LIGHTS model, for the NIST test cell where all the lamps were switched on at time zero, and then were kept on at all times. Initial temperatures of the nodes are as those given in the NIST reports (Treado and Bean 1988, 1992). In the simulations, the node temperatures, cooling load and lighting power were calculated for each time step.

The results are shown in Figures 2 and 3. In Figure 2 the lamp temperature is compared against time, as predicted by simulations using the present model LITEAC1 along with those from the LIGHTS model. Also shown in this figure is the lamp temperature measured in the NIST test, and the lamp temperature predicted by LIGHTS (Sowell 1990). This figure shows that the lamp temperature rose to its equilibrium value within the first two hours. There is very good agreement between the simulation results of both the LITEAC1 model, the LIGHTS model, and the NIST experimental results, with differences of less than 1°C between simulated and measured temperatures. While there is no significant difference between the simulation results from the LITEAC1 model and those from the LIGHTS model, significant differences did occur, however, between the computation times required. Namely, using a fixed time step of one second, a simulated period of 96 hours, and running on a personal computer with an Intel Pentium-100MHz processor, the LITEAC1 model required nine minutes of computation time, whereas the LIGHTS model required three hours and 37 minutes of computation time. The LIGHTS model can run faster if the time step is allowed to vary between a minimum and a maximum Even with a minimum time step of 0.36 seconds and a maximum time step of 18 seconds, 15 minutes of computation time was required for LIGHTS to complete a simulation run with the same configuration.

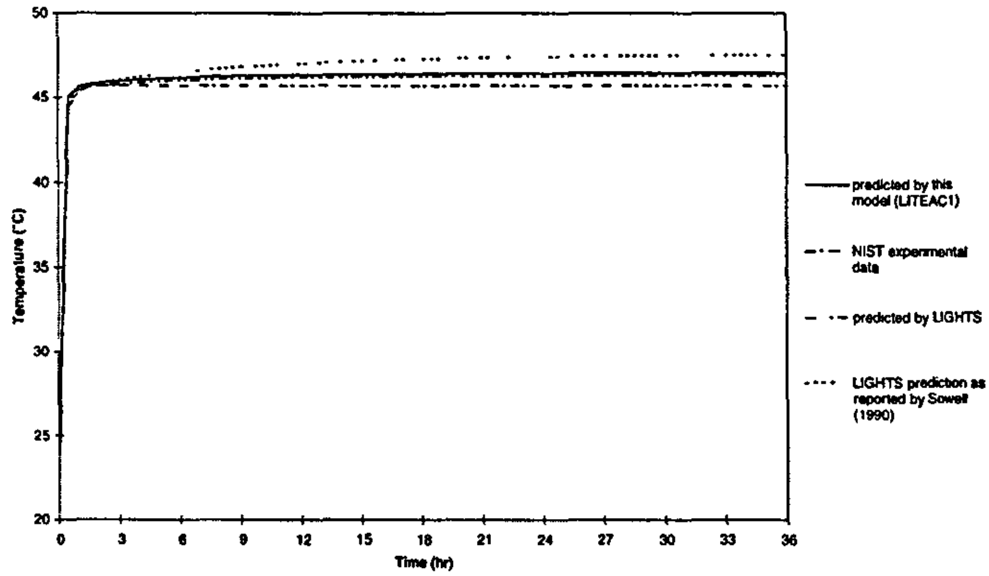

Figure 2. Lamp node temperatures of NIST test cell—comparison between LITEAC1, LIGHTS, and measured results

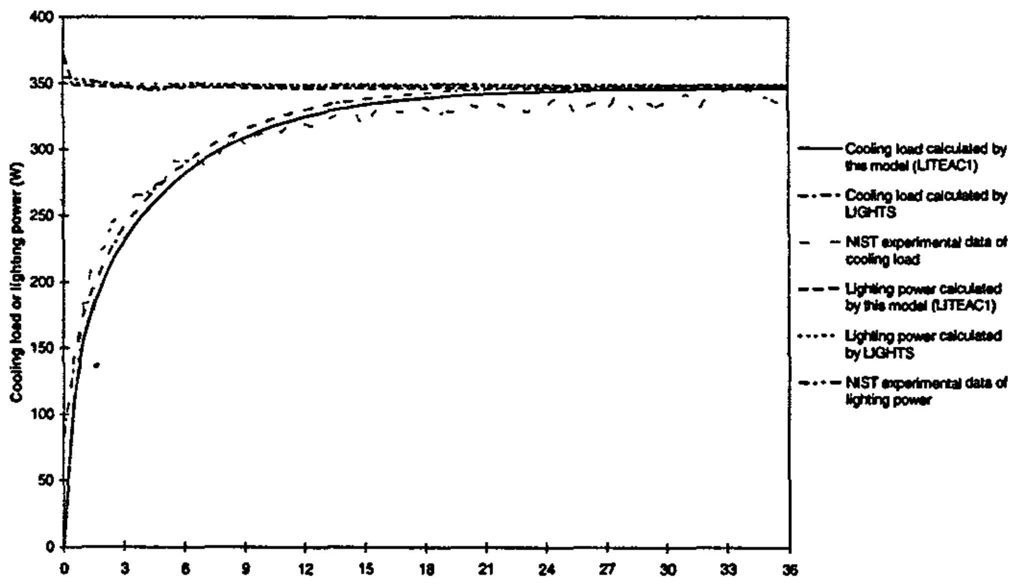

Figure 3. Cooling load and lighting power of NIST test cell—comparison between LITEAC1, LIGHTS, and measured results

Figure 3 shows a comparison of the lighting power and cooling load simulated by LITEAC1, the NIST test data, and the simulated results from the LIGHTS model. Good agreement is shown between the three cooling load curves; that is, between the predicted result of the current model, the predicted result of the LIGHTS model, and the NIST experimental results. For lighting power, the agreement between the simulated results of the two models and the NIST experimental result was excellent.

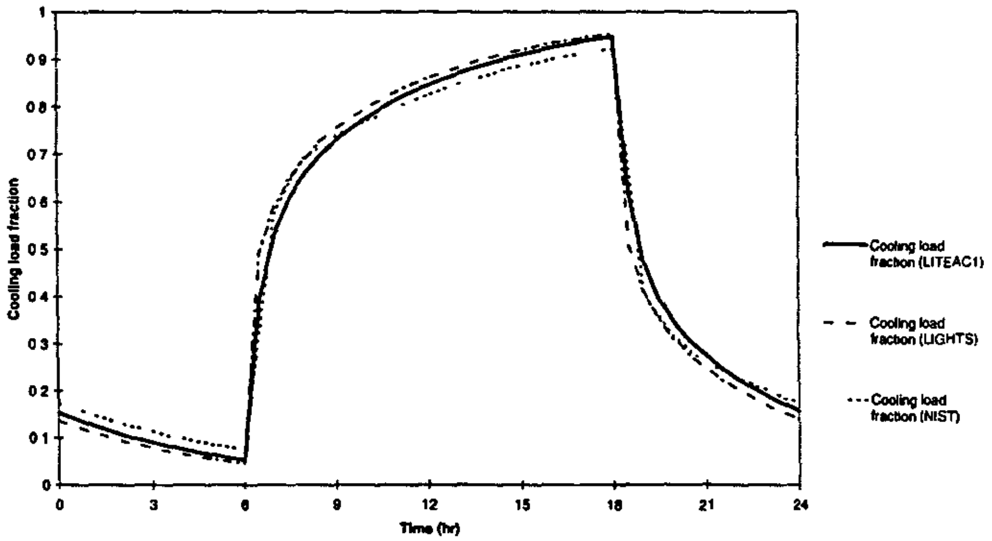

Figure 4. Cooling load fraction of NIST test cell—comparison between LITEAC1, LIGHTS, and measured results

Lighting On/Off Cycles

Further simulations were conducted, using both LITEAC1 and LIGHTS, assuming a period of five days, with lamps on for 12 hours (lamps switched on at hour 0) and lamps off for 12 hours (lamps switched off at hour 12) each day. Figure 4 shows The LITEAC1 and LIGHTS simulation results of the cooling load profile as a fraction of the lighting power over a 24-hour period, starting at hour 18 of day three are shown in Figure 4 Also shown in Figure 4 are the NIST test results (Treado and Bean 1990) for the same configuration. The figure shows that the simulated results agree well with each other and with the NIST test results.

The Laboratory Test Cell

For further validation of the model, a laboratory test cell containing a fluorescent luminaire, a plenum or ceiling void, and a room space was constructed. This cell was not a scaled-down model of an office, but a room with small dimensions. This set-up could be used to validate the model because the model is designed such that it can be used for different dimensions, provided that suitable values for heat transfer coefficients and radiation form factors are inserted as appropriate

The cell was 1.5 m long, 1 m wide, and 1 m high It was constructed of 9 5 mm thick plywood, and insulated on the outside with expanded polystyrene The height of the cell was divided by a suspended ceiling into a ceiling void of 0.2 m in height and a room space of 0 8 m in height Figure 5 illustrates how a 1200 mm × 300 mm fluorescent luminaire was installed at the center of the 'suspended ceiling', with its axis along the length of the cell, and holding a 1200 mm long fluorescent lamp To measure node temperatures, thermocouples were attached to the lamp and luminaire surfaces, and to the walls, floor and ceiling, as shown in Figure 5 Temperature measurement uncertainty was estimated to be ±1.0°C. Three lux meters, consisting of color and cosine corrected silicon photocells were used to measure illuminance on the floor The uncertainty of the photocells were estimated to be ±2% of the reading. An air-conditioning laboratory unit was used to supply cool air to the cell.

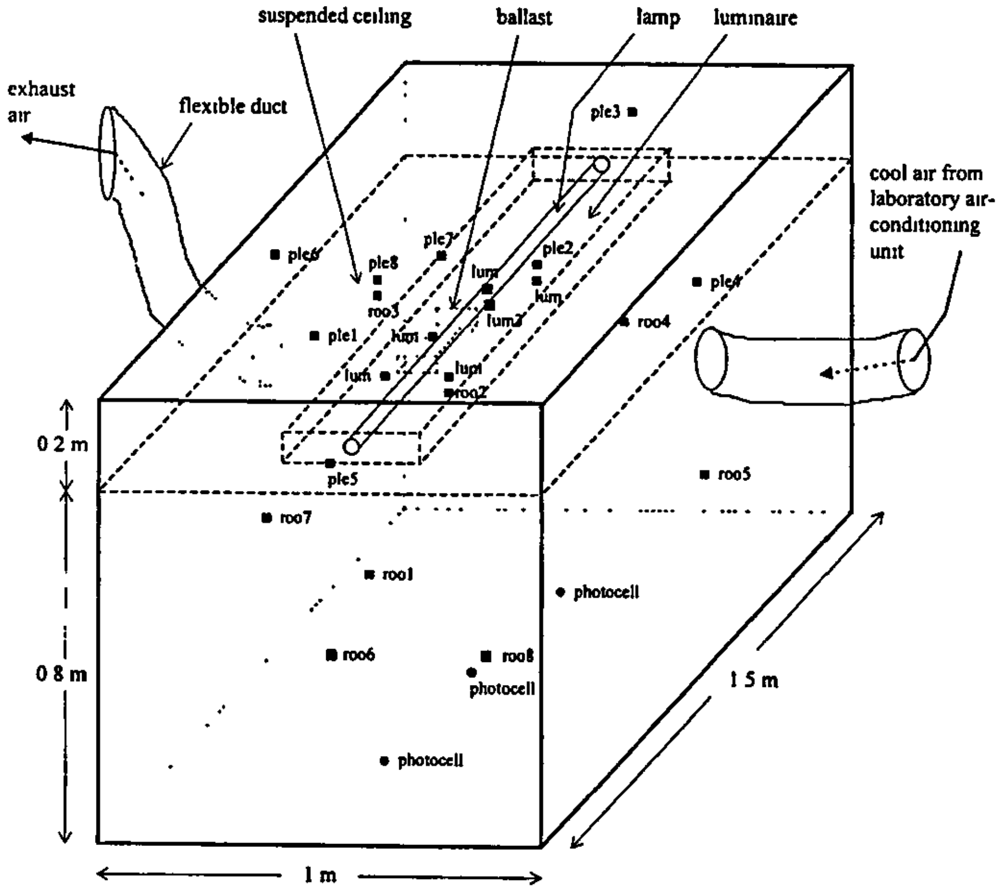

■ Positions of thermocouples for measurement of node temperatures with node code indicated

•' Positions of photocells for measurement of floor illuminance

Nodes

lum1	luminaire air	roo1	conditioned space air
lum2	lamp upper	roo2	luminaire diffuser bottom (outside luminaire)
lum3	lamp lower	roo3	suspended ceiling bottom
lum4	luminaire diffuser top (inside luminaire)	roo4	east wall
lum5	ballast	roo5	south wall
lum6	luminaire housing bottom (inside luminaire)	roo6	west wall
ple1	plenum air	roo7	north wall
ple2	luminaire housing top (outside luminaire)	roo8	floor surface
ple3	east plenum wall		
ple4	south plenum wall		
ple5	west plenum wall		
ple6	north plenum wall		
ple7	ceiling		
ple8	suspended ceiling top (plenum side)		

Figure 5. Cooling load fraction of NIST test cell—comparison between LITEAC1, LIGHTS, and measured results

From the cell physical dimensions and its construction materials, data for the heat capacity, emissivity, and reflectivity of the nodes were obtained from ASHRAE (1993). Radiation form factors were calculated from the physical dimensions using the view factor programs VF and FACTS, which are included in LIGHTS (Sowell 1989). Approximations were used in the calculation of form factors for surfaces inside the luminaire. Convective heat transfer coefficients were estimated for the geometries concerned according to equations given in Holman (1992) Conductance values were obtained from ASHRAE (1993)

To include both the "lights on" and "lights off" tests, experimental measurements were made for the case when the lamp was switched on for 23 hours, and then switched off Measurements of temperatures at node surfaces were taken every minute for the first ten minutes after the lamp was switched on, then at every 10 minutes throughout the rest of the "lamp on" period; this was repeated at every minute for the first ten minutes after the lamp was switched off and then at every 10 minutes for up to 10 hours after the lamp was switched off. During the test, the ambient air temperature around the test cell was 18 7°C.

The preceding situation was simulated using both the LITEAC1 and LIGHTS models, and the comparisons are shown in Figures 6 to 10. Figure 6 shows the temperatures of the two nodes for the lamp. The temperatures for the lamp upper node predicted using LITEAC1 agreed very closely with the experimentally measured values. However, the lamp's lower node temperatures that were calculated with LITEAC1 were about 2.8°C higher than the measured values. This can be explained by the fact that the calculated lamp lower node temperature represents the average temperature over the entire lower half of the lamp, while the measured lamp lower node temperature was taken at a single point only, which could be unrepresentative of the overall temperature. The lamp upper temperatures predicted using the LIGHTS program were about 2°C higher than the experimentally measured values, while for the lamp lower temperatures, values predicted using the LIGHTS program were about 6°C higher than the experimental values. Thus, for the simulation of lamp temperatures, LITEAC1 gives results closer to the experimental values than those given by the LIGHTS program. Figure 7 shows the temperatures of two other luminaire nodes: luminaire air and luminaire housing. Both LITEAC1 and LIGHTS gave similar results for luminaire air and for luminaire housing temperatures, both of which were lower than the corresponding experimentally-measured values by between 2 and 2.5°C. This discrepancy may be due to the assumption that an isothermal surface is not good enough for the lamp and

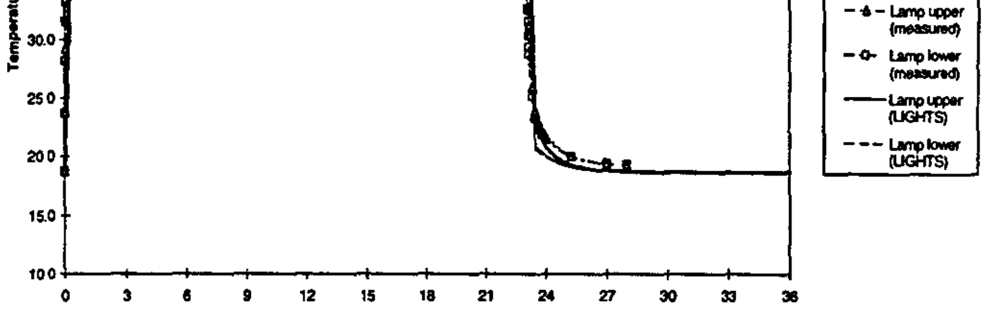

Figure 6. Lamp node temperatures of laboratory test cell—comparison between LITEAC1, LIGHTS, and measured results

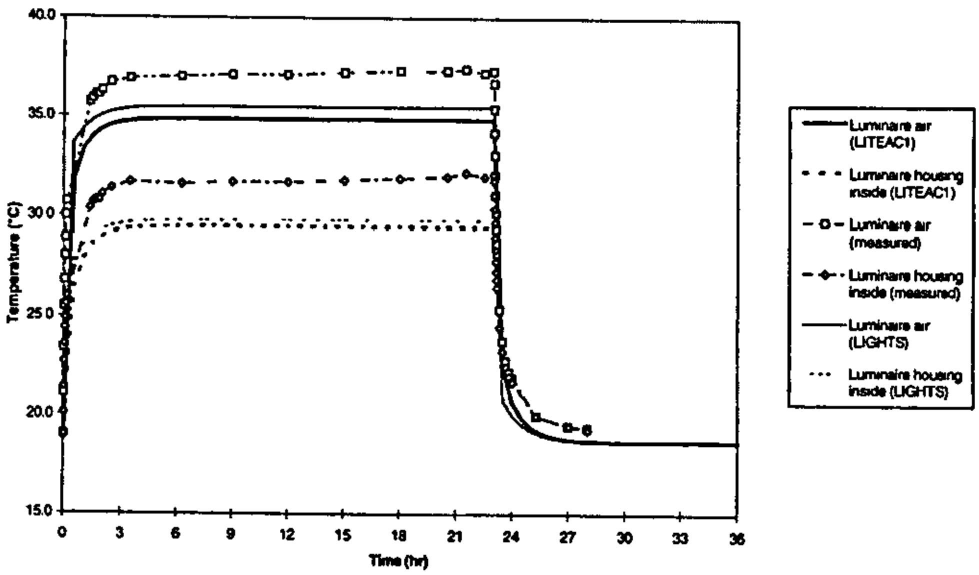

Figure 7. Other luminaire node temperatures of laboratory test cell—comparison between LITEAC1, LIGHTS, and measured results

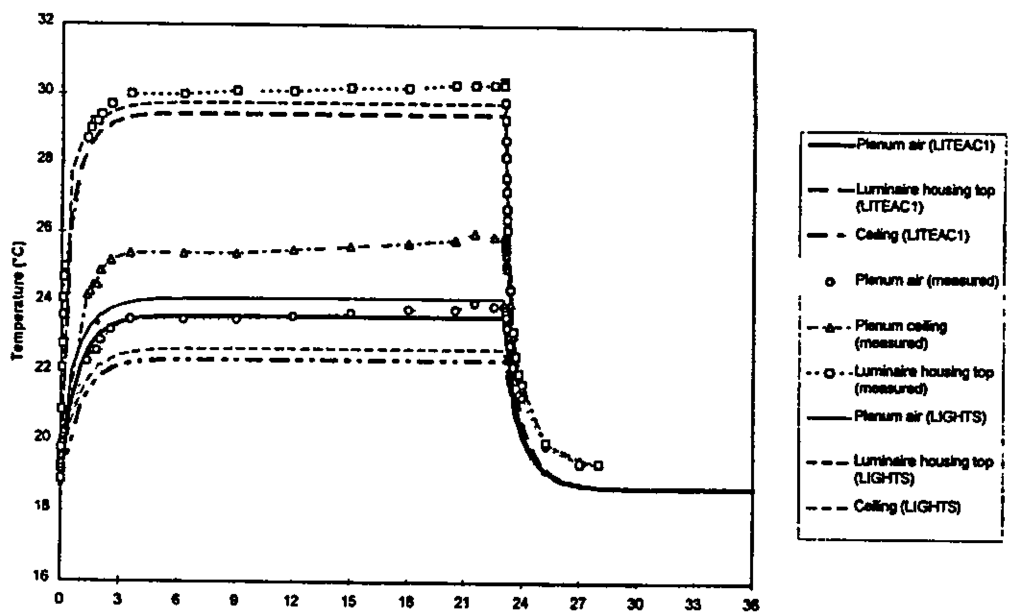

Figure 8. Plenum node temperatures of laboratory test cell—comparison between LITEAC1, LIGHTS, and measured results

luminaire housing, and/or inaccuracies in the input data of the heat transfer coefficients used in the simulations.

The temperature of three plenum nodes. plenum air, luminaire housing top and ceiling are shown in Figure 8. The figure shows that both the LITEAC1 and LIGHTS models predict values for plenum air temperatures and luminaire housing top temperatures which match very closely

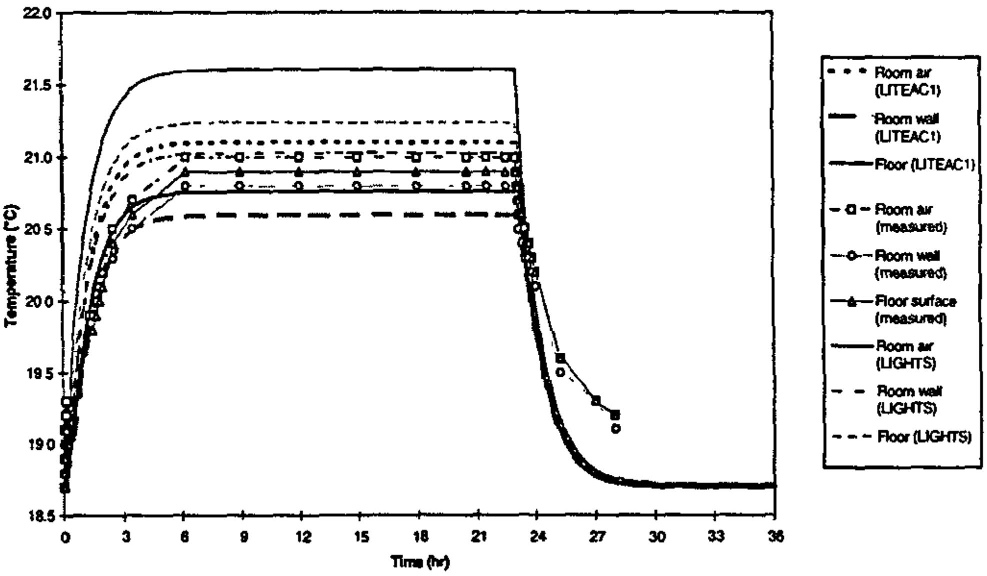

Figure 9. Room node temperatures of laboratory test cell—comparison between LITEAC1, LIGHTS, and measured results

with the measured values. LITEAC1 and LIGHTS also gave very similar results for the ceiling temperatures However, there is a mis-match between the simulated and measured results of the ceiling temperature The cause of this discrepancy is thought to be due to experimental error in the measurement of the ceiling temperature or to inadequate insulation.

Figure 9 shows the temperature of three room nodes: room air, walls and floor The figure shows that there is good agreement between the simulated results of both models and with the measured results Both the simulated and the measured results show that the room air temperature is higher than the floor temperature which is in turn higher than the wall temperature However, the results from LITEAC1 were closer than those from LIGHTS to the experimentally measured results.

Figure 10 shows a comparison of the floor illuminance calculated by LITEAC1, and that measured experimentally It can be seen that there are deviations of about 10% between the calculated and measured illuminance values It will be shown in Part II that the match between calculated and measured illuminance values can be improved by incorporating a fluorescent lamp positive column model in LITEAC1. The LIGHTS program does not include an output of the illuminance of room surfaces so that this comparison cannot be made

CONCLUSIONS

A mathematical model was derived based on heat transfer principles for the simulation of the effects of interior lighting on the cooling load in enclosed spaces, as well as simulating the change in lighting level. A computer program based on the model equations was written in FORTRAN and called LITEAC1. This program was compared with Sowell's LIGHTS program (Sowell 1989), and was found to give very similar results but to run much faster on a personal computer. Comparison of the simulated results from LITEAC1 with the experimental measurements from the NIST test cell (constructed specifically for the study of the interaction between HVAC and lighting) indicates good agreement The model was further validated using a laboratory constructed test cell containing a fluorescent luminaire. Comparison of predicted tempera-

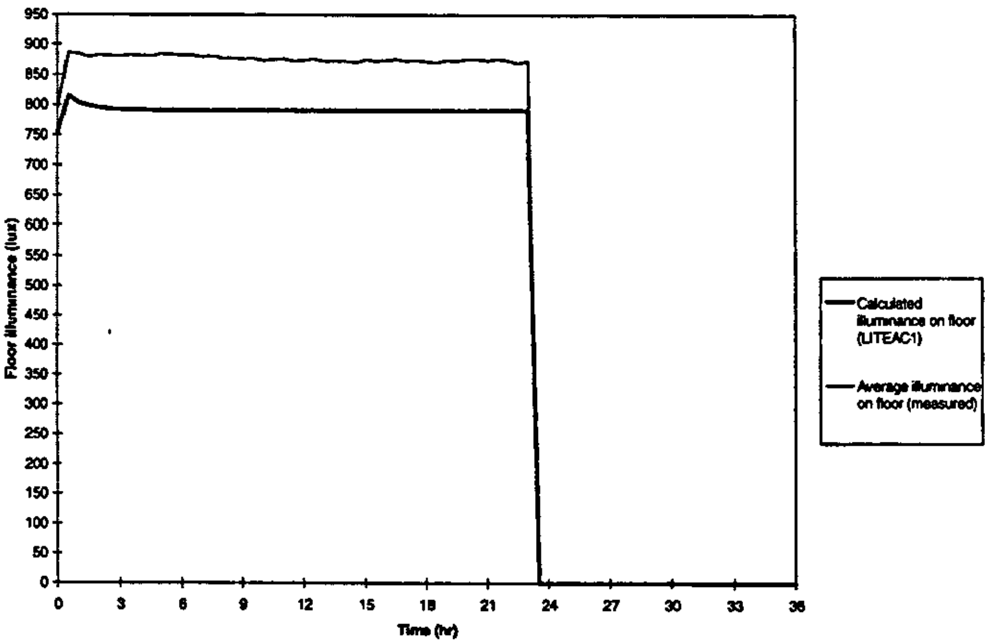

Figure 10. Floor illuminance of laboratory test cell—comparison between LITEAC1 and measured results

tures from LITEAC1 with measured results from this laboratory test cell revealed good agreement Prediction of floor illuminance by LITEAC1 was found to give only moderate agreement with experimental results. A positive column model has been incorporated into LITEAC1 with the aim of improving the simulation of lighting outputs; details of the positive column model will be discussed in Part II. It is not possible to predict illuminance with LIGHTS, and so LITEAC1 represents an advancement on previous models in that respect.

NOMENCLATURE

σ	Stefan-Boltzmann constant = 5 669 × 10^{-8} W/(m^2 K^4)
Δ	Time step, s or h
ε_i	Emissivity of node *i*
ρ_{Li}	Reflectance of node *i* with respect to long-wave radiation
ρ_{Si}	Reflectance of node *i* with respect to short-wave radiation
A_i	Surface area of node *i*, m^2
C_{ij}	Heat conductance from node *i* to node *j*, W/K
c_{pi}	Specific heat capacity of node *i*, J/(kg·K)
ΔT_i	Temperature rise of node *i* in one time step, K
E_{Li}	Long-wave radiation irradiance on node *i*, W/m^2
E_{Si}	Short-wave radiation irradiance on node *i*, W/m^2
F_{ij}	Radiation form factor (fraction of radiation emitted from node *i* that falls on node *j*)
h_i	Convective heat transfer coefficient of node *i*, W/(m^2 K)
m_i	Mass of node *i*, kg
M_{Li}	Long-wave radiant exitance (radiosity) of node *i*, W/m^2
M_{Loi}	Long-wave radiant emissive power of node *i*, W/m^2
M_{Si}	Short-wave radiant exitance (radiosity) of node *i*, W/m^2
M_{Soi}	Short-wave radiant emissive power of node *i*, W/m^2
$q(t_n)$	Cooling load from lights at time $t = t_n = n\Delta$, W
q_{Ci}	Total (net) conduction heat gain to node *i* in one time step, J or W s

q_{Gi}	Total (electrical) energy input at node i in one time step, J or W s	q_{Si}	Total (net) short-wave radiation heat gain to node i in one time step, J or W s
q_{Hi}	Total (net) convection heat gain to node i in one time step, J or W s	T_a	Air node absolute temperature, K
q_{Ha}	Total (net) convection heat gain to the air node in one time step, J or W s	T_i	Absolute temperature of node i, K
q_{Li}	Total (net) long-wave radiation heat gain to node i in one time step, J or W s	v_1, v_2, w_1	Coefficients of transfer function
		V_{ij}	Volume flow rate of air in between air nodes a_i and a_j, m^3/s
		$W(t_n)$	Power input to lights at time $t = t_n = n\Delta$, W

REFERENCES

ASHRAE. 1981. Table 32: Coefficients of Room Transfer Functions, pp 26 39 *ASHRAE Handbook—1981 Fundamentals*. Atlanta. ASHRAE.

ASHRAE. 1993 Nonresidential Air-Conditioning Cooling and Heating Load 1993 *ASHRAE Handbook—Fundamentals*. Atlanta. ASHRAE.

Ball, H D., and D. Green. 1983 The Impact of Lighting Fixtures on Heating and Cooling Loads—Mathematical Model. *ASHRAE Transactions* 89(2): 236-258.

CIE 1983. *The Basis of Physical Photometry. Publication CIE No. 18 2 (TC-1.2)* Paris: Commission Internationale de L'Eclairage.

Dorleijn, J.W.F., and A G. Jack. 1985. Power Balances for Some Fluorescent Lamps. *Journal of the Illuminating Engineering Society* 15(1): 75-84.

Holman, J P 1992 *Heat Transfer*, Seventh edition. New York: McGraw Hill

IESNA. 1993 *IES Lighting Handbook—Reference and Application*, Eighth edition. New York. Illuminating Engineering Society of America

Kimura, K., and D G. Stephenson 1968 Theoretical Study of Cooling Load Caused by Lights. *ASHRAE Transactions* 74(2): 189-197.

Mitalas, G P. 1973a. Calculating Cooling Load Caused by Lights. *ASHRAE Journal* 5(6) 37-40.

Mitalas, G P. 1973b. Cooling Load Caused by Lights. *Transactions, Canadian Society for Mechanical Engineering* 2(3): 169-174

Mitalas, G P., and K. Kimura. 1971. A Calorimeter to Determine Cooling Load Caused by Lights *ASHRAE Transactions* 77(2). 65-72.

Siminovitch, M.J., F.M. Rubinstein, and R.R. Verderber. 1984. Determining Lamp/Ballast System Performance with a Temperature-Controlled Integrating Chamber. *Journal of IES* 14(1): 364-378

Sowell, E F. 1989. LIGHTS User's Guide—A Computer Program for Modeling of Thermal and Luminous Aspects of Building Lighting Systems. Fullerton: Department of Computer Science, California State University

Sowell, E.F. 1990. A Numerical Lighting/HVAC test cell. *ASHRAE Transactions* 96(2) 780-786

Sowell, E F., and P F. O'Brien. 1973. The Transport of Lighting Energy. *ASHRAE Transactions* 79(2) 172-182.

Stephenson, D.G and G P. Mitalas. 1967. Cooling Load Calculations by Thermal Response Factor *ASHRAE Transactions* 73(1), III1.1-1.7.

Treado, S.J., and J.W. Bean. 1988 *The Interaction of Lighting, Heating and Cooling Systems in Buildings—Interim Report* NISTIR-883860. Gaithersburg: National Institute of Standards and Technology

Treado, S.J., and J.W. Bean 1990 Experimental Evaluation of Lighting/HVAC Interaction. *ASHRAE Transactions* 96(2): 773-779.

Treado, S.J., and J W. Bean 1992 *The Interaction of Lighting, Heating and Cooling Systems in Buildings Report* NISTIR 4701. Gaithersburg: National Institute of Standards and Technology.

Waymouth, J F. 1971. *Electric Discharge Lamps* Cambridge: MIT Press

Numerical Modeling of Lighting/HVAC Interaction in Enclosures Part II: Effect of Including a Fluorescent Lamp Positive Column Model

Tse-Ming Chung
Member ASHRAE

D.L. Loveday, Ph.D.

A numerical model of the fluorescent lamp positive column suitable for use in simulating the interaction between lighting and HVAC systems in enclosures is presented. The model was modified from existing models in the literature to include only sufficient details for simulating the conversion of electric energy into light and heat. Details of the fluorescent lamp positive column model are described. The model presented was incorporated within an existing model, LITEAC1 (described in Part I), that had been used for modeling the interaction between lighting and HVAC systems in enclosures. The resulting model, called LITEAC2, was tested by simulating the performance of a fluorescent lamp in a laboratory constructed test cell. It was found that the positive column model enabled better predictions for the lighting/air-conditioning interaction, and improved the modeling of illuminance on room surfaces.

INTRODUCTION

In Part I, the authors presented a model described the mutual interaction between lighting and air-conditioning systems It was stated that the model was used to calculate not only the effect of heat output from lighting on the cooling load in an enclosure, but also the effect of the ambient thermal environment upon the performance of the lighting system itself. To do this requires a knowledge of how the light output, lamp power and lamp efficacy vary with the ambient thermal environment in the enclosure.

Fluorescent lamps are low pressure mercury discharge lamps. A typical fluorescent lamp consists of a long glass tube of diameter either 38 mm (T12) or 26 mm (T8) with two electrodes, one at each end of the tube. Smaller tube diameters are used in compact fluorescent lamps. The electrodes are coated with alkaline earth oxides to facilitate the emission of electrons. The tube is filled with a rare-gas, such as argon or krypton or a mixture of argon and krypton, at a pressure of about 300 to 500 Pa. A small amount of mercury is introduced into the tube so that at normal room temperatures there is a mercury vapor pressure of about 0.8 to 1 3 Pa. A potential difference applied across the two electrodes accelerates the electrons emitted from the electrodes. These electrons collide inelastically with the mercury atoms in the tube, losing kinetic energy, thereby exciting the mercury atoms to higher energy levels. As the excited mercury atoms relax back to the ground state or an intermediate metastable state, the energy which they absorbed during excitation is dissipated as quanta of electromagnetic radiation. This process occurs in a region called the positive column of the discharge which occupies over 95% of the length of the tube. The radiation emitted consists of two resonance lines in the ultraviolet (UV)

Tse-Ming Chung is an assistant professor in the Department of Building Services Engineering, The Hong Kong Polytechnic University, Kowloon, Hong Kong **D.L. Loveday** is a reader in Civil and Building Engineering, Loughborough University, Leicestershire, U K

band, at 253.7 nm and 185 0 nm with some other weak lines in the visible and invisible bands of wavelengths. Fluorescent powder, or phosphor, on the inside surface of the tube wall converts the UV radiation to visible light for various lighting applications.

The number of inelastic collisions in the discharge depends on the mobility of electrons and the density of mercury atoms. The number of excitations to the resonance and upper energy states depends on the energy distribution of the electrons. The radiation emitted during de-excitation of mercury atoms suffers from self absorption within the positive column. This self absorption, often called radiation trapping or imprisonment of radiation (Holstein 1947, 1951), increases with the density of mercury atoms. Since there is an excess amount of mercury inside the tube, the density of mercury atoms is determined by the saturated vapor pressure of mercury at the cold spot temperature of the tube wall Hence, for a fixed lamp-ballast system, the variable affecting the light output of a fluorescent lamp is the minimum lamp wall temperature (also called the cold-spot temperature) which is the temperature of the coldest spot on the lamp wall The two competing processes of increasing UV quanta emitted, and increasing self-absorption with density of mercury atoms, give rise to the phenomenon that the light output has a maximum with respect to changes in the minimum lamp wall temperature; i e. there is an optimum value of the minimum lamp wall temperature at which the light output is at a maximum.

Previous models of the interaction between lighting and zone cooling systems, such as that of Sowell (1989, 1990), made use of empirical curves of the light output and lamp power against minimum lamp wall temperature in order to account for this effect. However, the use of empirical curves gives no physical insight into the mechanism that converts electrical energy into light and heat within the fluorescent lamp. Furthermore, it is necessary to use different curves for lamps of different type and different size. In order to obtain a physical insight and to calculate the conversion of electric power into light and heat from first principles, a mathematical model of the discharge process inside the fluorescent tube has to be used. In a fluorescent lamp discharge model, the energy balance is considered in relation to the density of mercury atoms which in turn depends on the ambient temperature.

In this paper is described the effect of including a fluorescent lamp positive column model, in which the effect of ambient temperature on lamp performance is treated from first principles, in our existing model LITEAC1 for describing the lighting/HVAC interaction as elaborated in Part I

FLUORESCENT LAMP ENERGY BALANCE

Electrical energy input to the fluorescent lamp discharge becomes principally the kinetic energy of the electrons due to acceleration of electrons by the electric field within the plasma The kinetic energy of the electrons is dissipated in one of the following processes: (i) inelastic collisions with mercury atoms which results in emission of radiation; (ii) ionization of the mercury atoms, and (iii) elastic collision with the rare-gas atoms

An energy balance equation can be written as follows·

$$Ej = W_{inel} + W_{ion} + W_{el} \tag{1}$$

where E is the electric field across the discharge tube, j is the electric current density, W_{inel} is the inelastic collision loss per unit volume of plasma, W_{ion} is the ionization loss per unit volume and W_{el} is the elastic collision loss per unit volume.

The inelastic collision loss is dissipated mainly as radiation emissions in the ultraviolet wavelengths 253 7 nm and 185 nm with some weak emissions in the visible and invisible bands of wavelengths. The ionization and elastic collision losses are finally dissipated as heat in the tube wall and in the plasma

The inelastic collision loss W_{inel} can be subdivided into terms that give the power losses of radiation emissions in different wavelengths:

$$W_{inel} = W_{254} + W_{185} + W_{vis} + W_{nv} \tag{2}$$

where W_{254} and W_{185} are the losses (per unit volume) due to emissions in the two ultraviolet wavelengths 253.7 nm and 185 nm respectively, W_{vis} and W_{nv} are the power losses (per unit volume) due to weak emissions in the visible and invisible bands resulting from excitations of mercury atoms to energy states higher than the resonance states These radiation losses occur in the form of emission of quanta of energy and each quantum has an energy equals to the product of the electronic charge and the energy level difference in electron volts between the excited state and the final state of the transition. The number of quanta that can escape the plasma in unit time per unit volume is equal to the number density of the excited state in the plasma divided by the effective life time of the state in the plasma The following equations give the radiation power loss terms W_{254}, W_{185}, W_{vis}, and W_{nv}.

$$W_{254} = eV_2\frac{N_2}{\tau_2^*} \tag{3}$$

$$W_{185} = eV_4\frac{N_4}{\tau_4^*} \tag{4}$$

$$W_{vis} = e(V_5 - V_2)\frac{N_5}{\tau_5^*} \tag{5}$$

$$W_{nv} = e(V_6 - V_2)\frac{N_6}{\tau_6^*} \tag{6}$$

These power loss terms depend on the density and energy distribution of electrons, the densities of all species of mercury atoms, the rate of ionization of mercury atoms, the rate of re-combination 'at the tube wall and the density of rare-gas in the tube. If the electron energy distribution in the plasma and the collision cross sections between the electrons and the different species of mercury atoms are known or can be assumed, then the number densities of the mercury states can be found by solving a set of simultaneous equations.

THE FLUORESCENT LAMP POSITIVE COLUMN MODEL USED IN THIS STUDY

As already stated, a model of the positive column is important for understanding the mechanism in converting electrical energy into light energy inside a fluorescent lamp. In our study, the aim was to investigate the macroscopic behavior of the fluorescent lamp with respect to a change of thermal environment, rather than to investigate the detailed processes occurring inside the fluorescent tube; we did not, therefore, use a rigorous and detailed fluorescent lamp positive column model, in which the radial variation of mercury excited state densities, for example, were considered Instead, in developing the model the following were considered the major mercury excited states, the literature values of transition rates between different states, and radiation trapping with a simple formulation. The radial variation of discharge properties and the excitation of rare-gas atoms were ignored In this way, the processes taking place within the fluorescent tube were modeled in sufficient detail so as to advance the current status of HVAC/lighting interaction modeling beyond the level of reliance upon simple empirical curves.

Mercury atom energy levels considered in the model

A simplified picture of mercury atom energy levels was used in this model. This simplified mercury energy level diagram consists of only eight levels, as shown in Figure 1:

Equations relating the densities of mercury states

At equilibrium, the rate of change of the ground state density is equal to zero

$$-\sum_{j=1}^{6} K_{0j} N_e N_0 - K_{0i} N_e N_0 + \sum_{j=1}^{6} K_{j0} N_e N_j + \sum_{j=1}^{6} \frac{N_j}{\tau_{j0}^{*}} + \frac{D_a N_e}{\Lambda^2} = 0 \tag{7}$$

In the above equation, the first term represents the excitation of the ground state to the six excited states, the second term represents ionization from the ground state, the third term repre-

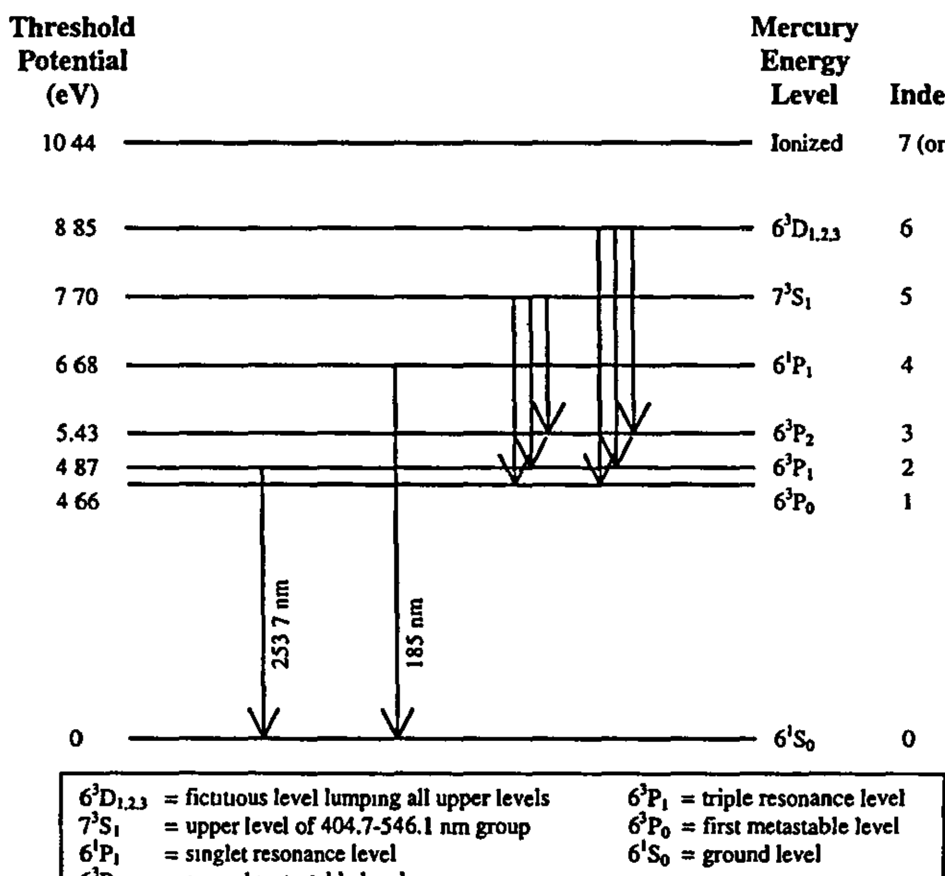

Figure 1. Simplified energy diagram of the mercury atom. Transitions that produce radiation are shown as dotted lines with arrow heads. No other transitions are shown.

sents the inelastic decay of the six excited states to the ground state, the fourth term represents the spontaneous decay of the six excited states with emission of a photon, the last term represents the rate of recombination of ions and electrons, which is assumed to be purely an ambipolar diffusion phenomenon.

Again, at equilibrium, the rate of change of the k^{th} state density is equal to zero. Therefore, for the k^{th} excited state:

$$-\sum_{j=k+1}^{6} K_{kj} N_e N_k - K_{ki} N_e N_k + \sum_{j=0}^{k-1} K_{jk} N_e N_j + \sum_{j=k+1}^{6} K_{jk} N_e N_j - \sum_{j=0}^{k-1} K_{kj} N_e N_k - \frac{N_k}{\tau_{k0}^{*}} = 0 \quad (8)$$

This represents a set of six equations, one for each of the six excited states $k = 1$ to 6. The first term represents the k^{th} state loss due to inelastic collisions causing excitation to higher levels. The second term represents loss due to ionization. The third and fourth terms represent, respectively, the increase in the k^{th} state due to excitation from lower states, and the inelastic de-excitation of higher states. The fifth term represents loss due to inelastic de-excitation of the k^{th} state. The last term represents the spontaneous decay of the k^{th} state with emission of a photon.

Electron Density and Ionized State Density

At equilibrium, electrons are assumed to come only from the ionization of mercury atoms; hence, the electron density and the ionized state density are equal. Assuming that there is no recombination of electrons and ions within the plasma, then the loss of electrons and ions takes place only by ambipolar diffusion to the tube wall, where they recombine Therefore, the rate of creation of electron-ion pairs is equal to the rate of loss due to recombination at the tube wall

$$\sum_{j=1}^{6} K_{ji} N_e N_j - \frac{D_a N_e}{\Lambda^2} = 0 \quad (9)$$

This is called the ambipolar diffusion equation. The first term is the sum of the rate of ionization from the ground state and the six excited states. The second term is the ambipolar diffusion rate to the tube wall.

Electric Current Density

$$j = N_e e v = N_e e \mu_e E \quad (10)$$

The electric current density is governed by the electron mobility and the electric field across the positive column Waymouth and Bitter (1956) used a hypothesis that the electron mobility is determined solely by collisions with rare gas atoms and estimated the electron mobility as a function of electron temperature from integrals of collision probability over the electron distribution. Verweij (1961) did an experimental measurement of electron mobility in mercury-rare-gas positive columns, this data was used in the model under discussion.

Model Equations

Equations (7) and (10), together with the energy balance Equation (1), form the set of model equations. This set of equations can be solved for the number densities of mercury states by using some approximations which are elaborated in Appendix A and an iteration method described in Appendix B. After solving for the mercury state densities, the power radiated from the discharge in the UV, visible and invisible bands can be calculated when the effective life times of the corresponding states are known.

VALIDATION OF THE POSITIVE COLUMN MODEL

It is possible to validate our positive column model by comparing calculated results of electron temperature, electric field strength, electron density and resonance state density with experimental data quoted in the literature. As quoted above, Verweij's article (1961) relating to positive column measurement includes very reliable data used by many authors for comparison with model results.

Figure 2 shows the variation of electron temperature with minimum lamp wall temperature as predicted by our model; also plotted are the measurements obtained by Verweij As seen in the figure, the agreement is very good.

Figure 3 shows the model-predicted electric field strength plotted against the minimum lamp wall temperature; Verweij's experimental results are also plotted in the same figure. The agreement between the model-predicted and measured values is not very good. However, the model does predict a decrease in electric field strength as the minimum lamp wall temperature increases, and the order of magnitude of the electric field strength is correct.

Figure 4 shows the electron density plotted against minimum lamp wall temperature. The figure shows not only the calculated results of this model and Verweij's experimental data but also the results predicted by the model of Dakin (1986) The figure shows that the current model gives a better fit to the experimental data then does the model of Dakin.

Figure 5 compares the resonance state density as predicted by our model with two sets of measured data, one by Koedam and Kruithof (1962) and the other by Bigio (1988), the model results of Dakin (1986) are also shown for comparison. It can be seen that the calculated resonance state density agrees well with the measured data by Koedam and Kruithof (1962) More recent measurements by Bigio (1988) gave higher resonance state densities at 20, 30 and 40° C and the calculated results of current model agree better to these points than do the results calculated by Dakin (1986)

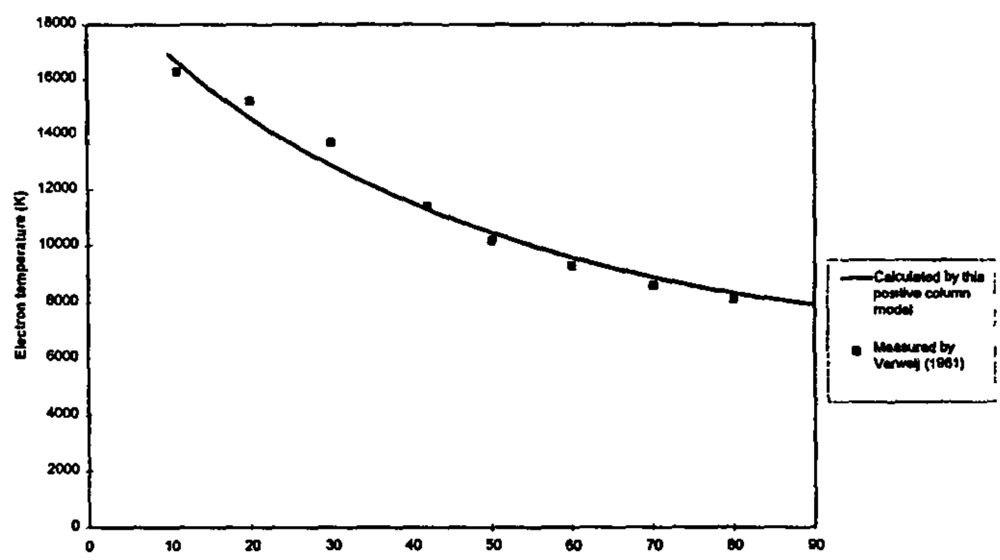

Figure 2. Electron temperature versus minimum lamp wall temperature.

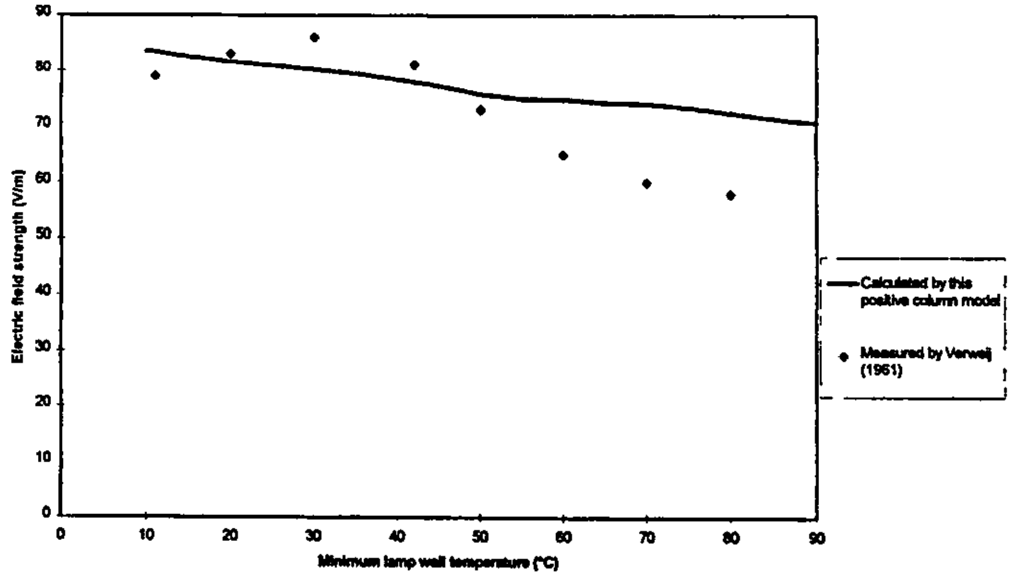

Figure 3. Electric field versus minimum lamp wall temperature.

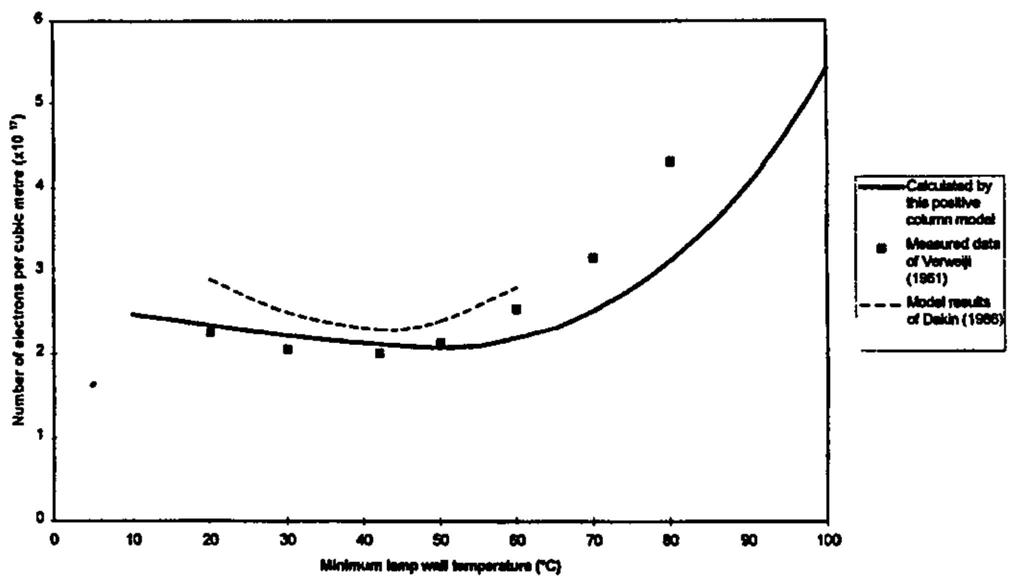

Figure 4. Electron density versus minimum lamp wall temperature.

It can be concluded that the model presented here can simulate the fluorescent lamp positive column to a good degree of accuracy; further, it gives better agreement with experiment than previous models. Next, the new model can be incorporated into the lighting and air-conditioning interaction model LITEAC1, already described Part I of this paper, and it can be determined whether there is an improvement in simulating the effects of air-conditioning on light output.

CALCULATION OF LIGHT OUTPUT FROM FLUORESCENT LAMP

After the radiation power terms have been calculated using the positive column model, the light output from the lamp can be derived from a knowledge of the relative spectral power out-

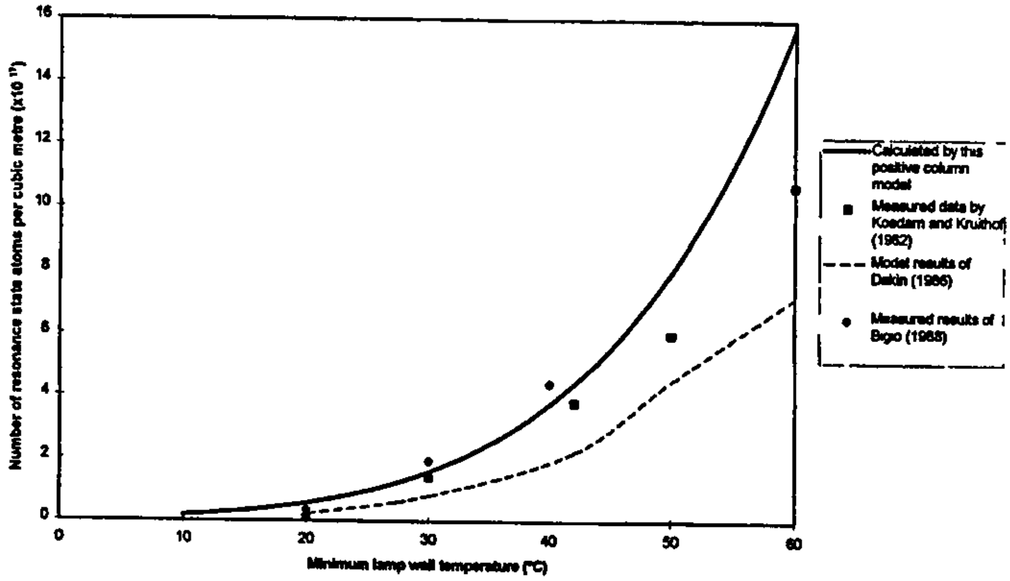

Figure 5. Resonance state (6^3P_1) density versus minimum lamp wall temperature.

put $S(\lambda)$ of the fluorescent powder in the lamp. Here, the relative spectral power output $S(\lambda)$ is defined such that $\int S(\lambda)d\lambda = 1$, i.e. the power output per unit wavelength, per unit volume of the positive column, of light from the fluorescent powder in wavelength interval λ to $\lambda + d\lambda$ is $W(\lambda) = S(\lambda)W_{phos}$ where W_{phos} is the total output power per unit volume of the positive column of the fluorescent powder in the lamp.

The quantum efficiency of the lamp phosphor η can be defined as the ratio of the number of quanta of visible light emitted from the phosphor to the total number of quanta of UV radiation reaching the tube wall, i.e.:

$$\eta = \frac{\int n_\lambda d\lambda}{n_{254} + n_{185}} \tag{11}$$

where n_λ is the quanta, per unit wavelength interval per unit volume of the positive column per unit time, emitted from the phosphors in the wavelength interval λ to $\lambda + d\lambda$; n_{254} and n_{185} are the quanta of the 253.7 nm and 185.0 nm emission from the positive column that reach the tube wall per unit volume of the positive column per unit time, respectively.

It can be shown that the quantum efficiency η is given by the following expression:

$$\eta = \frac{W_{phos}}{W_{uv}}\int S(\lambda)\frac{\lambda}{253.7}d\lambda \tag{12}$$

where

$$W_{uv} = \frac{253.7W_{254} + 185W_{185}}{253.7} \tag{13}$$

Then, the visible light output from the phosphors per unit volume of the positive column due to UV radiation emitted from the positive column is:

$$\Phi = F683W_{phos}\int S(\lambda)V(\lambda)d\lambda \tag{14}$$

Combining Equations (12) and (14) gives:

$$\Phi = F683\eta W_{uv}\frac{\int S(\lambda)V(\lambda)d\lambda}{\int S(\lambda)\frac{\lambda}{253.7}d\lambda} \tag{15}$$

In the above two equations, F is a factor to correct for loss of emitted light at the ends of the lamp and absorption of light by the phosphor and glass bulb. F is quoted by Jerome (1953) to be 0 75 which is a representative value for most lamps. The factor 683 is the maximum luminous efficacy of radiation, which is 683 lm/W, occurring at a wavelength of 555 nm $V(\lambda)$ is the relative spectral luminous efficiency for photopic vision of the human eye of the CIE (1983).

CIE (1986) gives the relative spectral power distributions for 12 types of typical fluorescent lamps, representing standard, broad-band, and three-narrow-band fluorescent lamps. From these spectral power distributions, the integrals and can be evaluated Using literature values of the quantum efficiency (Jerome 1953), the light output due to UV radiation Φ can be calculated using Equation (15).

There is a small light output due to the visible emission of the discharge directly. This is calculated by assuming that half of the visible emission can escape through the phosphor coating and that the only visible lines emitted are 404 6 nm, 435 8 nm, and 546.1 nm so that the mean $V(\lambda)$ is 0 334. Hence, the total luminous flux output of the fluorescent lamp is calculated by the following formula:

$$\Phi_{lamp} = 683\left(0.75\eta W_{uv}+\frac{\int S(\lambda)V(\lambda)d\lambda}{\int S(\lambda)\frac{\lambda}{253.7}d\lambda}+0.5W_{vis}0\ 334\right)L\pi\frac{d^2}{4} \tag{16}$$

In the above equation, L is the length of the positive column and d is the diameter of the lamp. The first term is the light output from the UV activated phosphors and the second term is the light output due to the visible lines in the discharge.

HVAC/LIGHTING SIMULATION: RESULTS AND VALIDATION

Existing HVAC/lighting simulation models rely on empirical curves for predicting lamp performance. We now include a fluorescent lamp positive column model in such a simulation. The fluorescent lamp positive column model, as described above, was incorporated into the lighting and air-conditioning interaction model LITEAC1 as a subroutine replacing the existing subroutine which calculates the variation of light output with minimum lamp wall temperature from empirical curves. The modified lighting and air-conditioning interaction model incorporating with the positive column model is called LITEAC2. In order to validate LITEAC2 and to determine the level of improvement (if any) over LITEAC1, the laboratory-constructed test cell used in the previous validation exercise for LITEAC1 (See Part I of this paper for details) is used again.

Measurements in the test cell were taken for the case with the lamp switched on for 23 hours, and then switched off (for further details, refer to Part I of this paper). Simulations were performed using LITEAC1 and LITEAC2, and the results are shown in Figures 6 to 10.

In Figure 6 is shown the temperature of the two lamp nodes plotted against time for the simulation results of LITEAC2 and LITEAC1, and for the experimental results. It can be seen from this figure that the lamp node temperatures calculated by LITEAC2 do not show a significant difference from the corresponding lamp node temperatures calculated by LITEAC1. The lamp upper node temperature matches very well with the measured data, whilst the lamp lower temperature is about 2.8°C higher than the measured data. As discussed in Part I, this can be explained by the fact that the calculated lamp lower node temperature represents the average temperature over the entire lower half of the lamp, whereas the measured lamp lower node temperature is the temperature at one point only.

Figure 7 shows the comparison of LITEAC2 with LITEAC1 and with the experimental data for two other luminaire node temperatures: luminaire air and luminaire housing. This figure shows again that there is no significant difference between the calculated results of LITEAC2 and LITEAC1.

Figure 8 shows the comparison of simulation results from LITEAC2 of three plenum node temperatures with the corresponding predictions of LITEAC1, and with the experimental data Again, there is no significant difference between the results of LITEAC2 and LITEAC1. Figure 9 shows the simulated and experimental results of three room nodes. Again, there is no significant difference between the results of LITEAC2 and LITEAC1.

Figure 10 shows a comparison of the floor illuminance predicted by LITEAC2 with that predicted by LITEAC1, and with the measured floor illuminance. It can be seen from this figure that LITEAC2 gives a remarkably good match with the experimental data, while LITEAC1 gives an illuminance value about 10% lower than the experimental value.

From the results given above, it can be concluded that the lighting and air-conditioning interaction model LITEAC1 gives good predictions when compared with experimental data. For

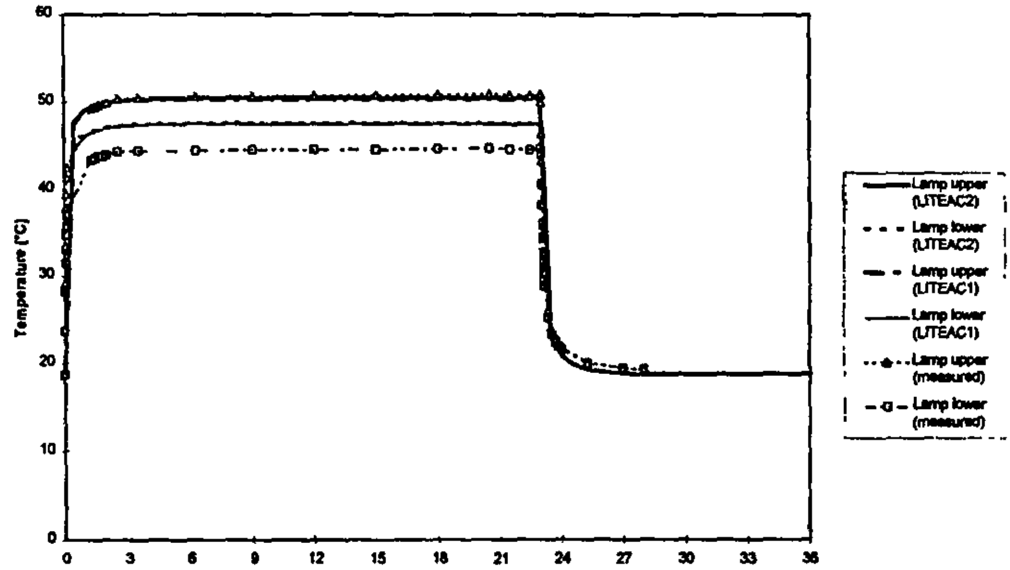

Figure 6. Lamp node temperatures—comparison between LITEAC1, LITEAC2, and measured results

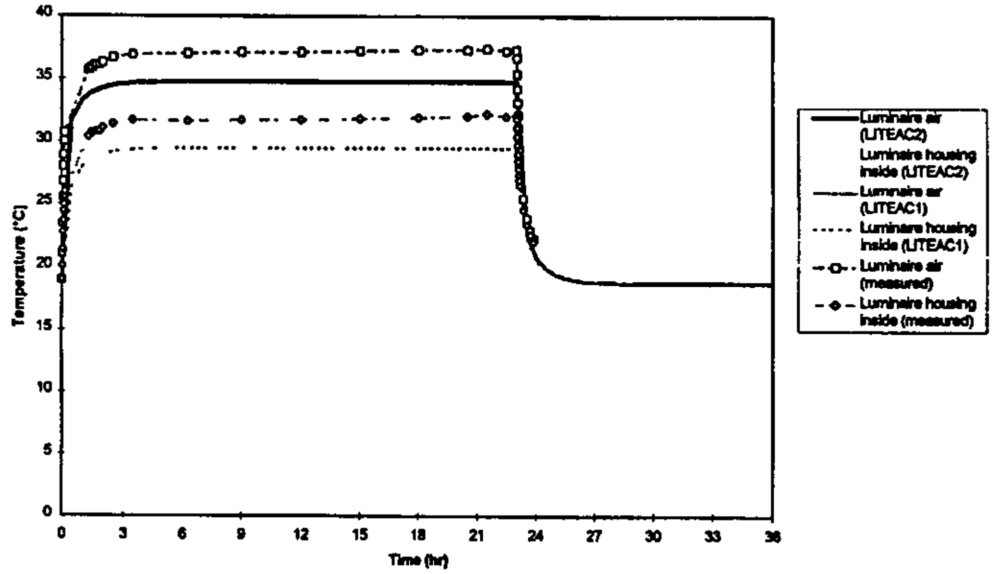

Figure 7. Luminaire air and housing temperatures—comparison between LITEAC1, LITEAC2, and measured results

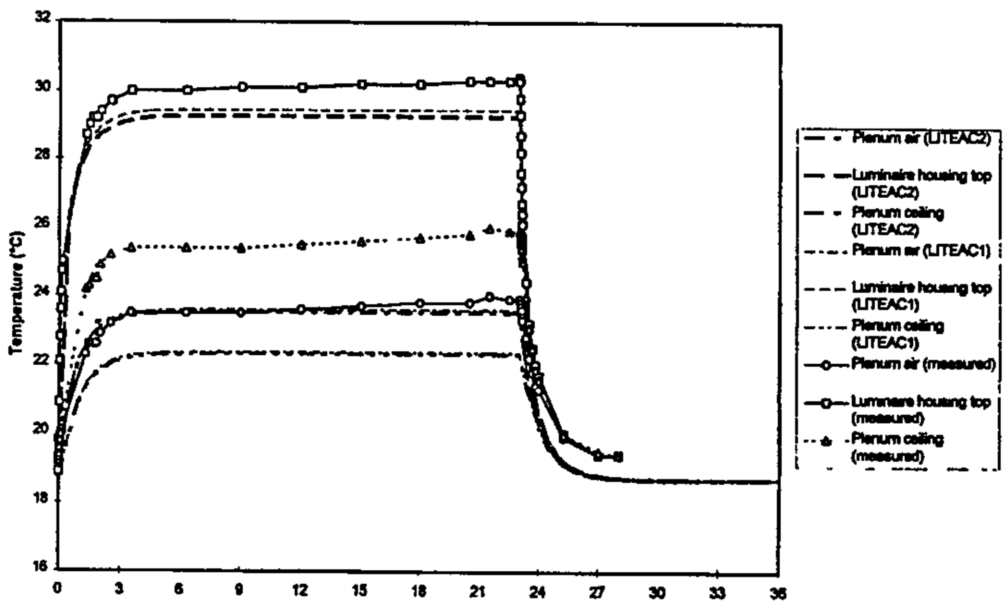

Figure 8. Plenum node temperatures—comparison between LITEAC1, LITEAC2, and measured results

LITEAC1 to give good predictions, good empirical curves to represent the change of lamp power and light output with lamp wall temperature must be obtained as input data. Lamp manufacturers do not normally include these data in the lamp data sheet or manual. The incorporation of a fluorescent lamp positive column model into the lighting and air-conditioning interaction

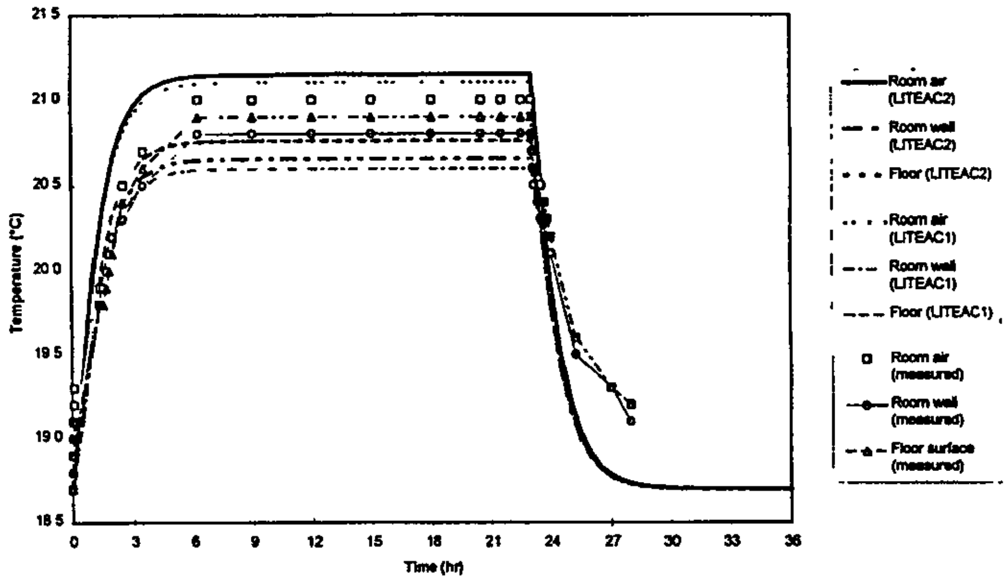

Figure 9. Room node temperatures—comparison between LITEAC1, LITEAC2, and measured results

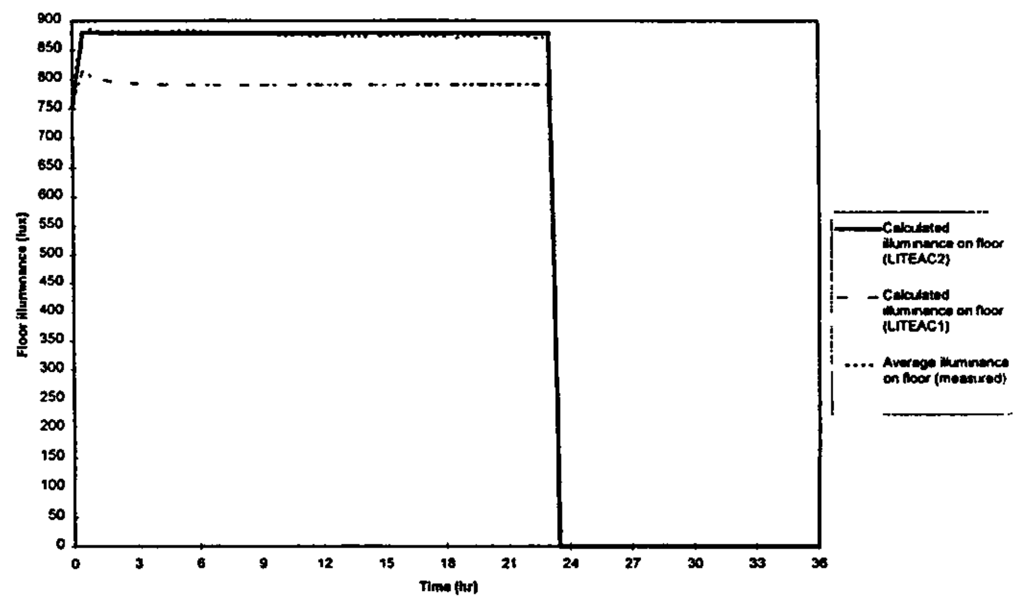

Figure 10. Floor illuminance—comparison between LITEAC1, LITEAC2, and measured results

model LITEAC2 avoids the use of these empirical curves and gives improved predictions of luminous flux output from lamps and hence room surface illuminances, though there is little effect on predictions of temperature. The positive column model also permits a better understanding of the conversion of electrical energy into visible and invisible radiation, and then into heat.

CONCLUSIONS

A mathematical model of the fluorescent lamp positive column was developed. Calculation results of the electron temperature, electric field strength, electron density and resonance state density by the positive column model agreed well with published experimental data. The positive column model was successfully incorporated into a lighting and air-conditioning interaction model, and experimental data from a laboratory-constructed cell containing a single fluorescent luminaire were used for the validation of the model. The agreement between the simulated and experimental results was remarkably good While inclusion of the positive column model had little effect on predictions of zone temperature there was a significant improvement in predictions of zone illuminance. Calculated floor illuminances by the lighting/air-conditioning interaction model incorporating the positive column model agreed much better with the experimental data than did the illuminances calculated by a model without the positive column model. It is therefore concluded that the numerical model presented of the interaction between lighting and air-conditioning can be used for the simulation of the two way interaction between lighting and air-conditioning in a room, and can lead to better simulation of the effect on light output of fluorescent lamps due to variations of the ambient temperature.

APPENDIX A

Approximations used to solve the set of model equations

In solving the set of model equations, several hypotheses described below were employed The main hypotheses were:

1 The electron energy distribution was chosen to be Maxwellian, and the electron temperature wass independent of radial position. In numerical models of the fluorescent lamp positive column, the electron energy is usually assumed to follow a Maxwell-Boltzmann distribution (Waymouth and Bitter 1956, Cayless 1963, Lamma et al. 1982), in which the electron energy is described by a single electron temperature. Some recent models used a two-temperature group electron energy distribution (Vriens 1973, Dakin 1986) or a non-Maxwell electron energy distribution function (Lagushenko and Maya 1984, Zissis et al 1992). The authors think that, for their purposes, it was sufficient to assume a Maxwellian electron energy distribution, and that the transition rates are dependent on the electron temperature as described in a sub-section below.
2. Only mercury was assumed to be ionized and excited, whilst inelastic collisions with rare-gas atoms were completely ignored This assumption is justified since the ionization and excitation of rare-gas atoms needs a much higher energy than the kinetic energy acquired by most of the electrons.
3. All ionization was assumed to take place by two-stage processes, direct ionization from the ground state could be neglected. Furthermore, ionization from levels higher than the 6^3P_2 metastable level could also be neglected. Again, this is justified by the fact that there is a very small amount of high energy electrons for the direct ionization of mercury atoms.
4. Loss of electrons and ions was assumed to take place purely by ambipolar diffusion to the tube wall, where they recombine. Recombination within the positive column is negligible.
5 The excited mercury atoms were assumed to be de-excited by the spontaneous emission of photons, and by inelastic collisions with electrons. Losses due to diffusion of excited atoms to the tube wall, and de-excitation by collisions with rare-gas atoms, were ignored.
6 The positive column was assumed to be uniform and free of striations.

The above hypotheses are the same as those used by earlier investigators, e g. Waymouth and Bitter (1956), Cayless (1963), and Lama et al. (1982). These investigators also assumed that electron and ion mobilities were determined by the rare-gas only but they stated that this assumption was not completely valid especially at high mercury pressures. For the purposes of the present study, Verweij's (1961) measurement results for electron mobility were adopted, and an empirical dependence of the electron mobility on the mercury density was used.

In addition to the above hypotheses, some further approximations were used in solving the set of model equations. The first of these approximations is that the mercury ground state density is assumed to be equal to the density of mercury atoms. This approximation is justified because the mercury ground state density is about 2 to 3 orders of magnitude greater than the densities of the excited states.

$$N_0 = N_{Hg} \tag{17}$$

Hypothesis (3) implies that the transition rates K_{0i}, K_{4i}, K_{5i}, and K_{6i} are all equal to zero. It is further assumed that excitation to the 7^3S_1 and $6^3D_{1,2,3}$ levels comes only from the ground and the triplet $6^3P_{0,1,2}$ levels; and the decay of these levels can only take place with the release of quanta of radiation. Using these approximations, Equations (7) to (9) can be rewritten as:

$$-\sum_{j=1}^{6} K_{0j}N_eN_0 + \sum_{j=1}^{6} K_{j0}N_eN_j + \sum_{j=1}^{6} \frac{N_j}{\tau_{j0}^*} + \frac{D_aN_e}{\Lambda^2} = 0 \tag{18}$$

$$K_{01}N_eN_0 + K_{21}N_eN_2 + K_{31}N_eN_3 - \left(K_{10} + \sum_{j=2}^{7} K_{1j}\right)N_eN_1 = 0 \tag{19}$$

$$K_{02}N_eN_0 + K_{12}N_eN_1 + K_{32}N_eN_3 - \left(K_{20} + K_{21} + \sum_{j=3}^{7} K_{2j}\right)N_eN_2 - \frac{N_2}{\tau_2^*} = 0 \tag{20}$$

$$K_{03}N_eN_0 + K_{13}N_eN_1 + K_{23}N_eN_2 - \left(\sum_{j=0}^{2} K_{3j} + \sum_{j=4}^{7} K_{3j}\right)N_eN_3 = 0 \tag{21}$$

$$K_{04}N_eN_0 + K_{14}N_eN_1 + K_{24}N_eN_2 + K_{34}N_eN_3 - \sum_{j=0}^{3} K_{4j}N_eN_4 - \frac{N_4}{\tau_4^*} = 0 \tag{22}$$

$$K_{05}N_eN_0 + K_{15}N_eN_1 + K_{25}N_eN_2 + K_{35}N_eN_3 - \frac{N_5}{\tau_5^*} = 0 \tag{23}$$

$$K_{06}N_eN_0 + K_{16}N_eN_1 + K_{26}N_eN_2 + K_{36}N_eN_3 - \frac{N_6}{\tau_6^*} = 0 \tag{24}$$

$$K_{17}N_eN_1 + K_{27}N_eN_2 + K_{37}N_eN_3 - \frac{D_aN_e}{\Lambda^2} = 0 \tag{25}$$

The above simplified Equations (17) to (25) are solved, together with the energy balance Equation (1), using the scheme described in Appendix B. There are some approximations used in the transition rate coefficients, effective life times, and ionization and elastic collision losses These approximations are discussed in the following paragraphs.

Transition rate coefficients

The transition rate coefficients in the above equations K_{jk} can be obtained by an integration of the collision cross section over the electron energy distribution function as follows:

$$K_{jk} = \left(\frac{2e}{m_e}\right)^{1/2}\int_0^\infty UQ_{jk}(U)f(U)dU \tag{26}$$

In order to simplify the solution process, and due to the scarcity of reliable data on the cross sections for transitions between the various mercury states are sparse, and the electron energy distribution is assumed to be Maxwellian described by a single electron temperature, we do not perform the above integration, but instead follow the method of Hoyaux and Sucov (1969) to determine the transition rate coefficients. Here, it was assumed that the transition rate coefficients K_{jk} were dependent on the electron temperature T_e as follows.

For ascending transitions ($k>j$):

$$K_{jk} = C_{jk}\left(\frac{kT_e}{e}\right)^{\frac{3}{2}}\left(1+\frac{e(V_k-V_j)}{2kT_e}\right)\exp\left(-\frac{e(V_k-V_j)}{kT_e}\right) \tag{27}$$

where the coefficients C_{jk} are constants, to be determined using experimental values of transition rates and electron temperature, as quoted in the literature.

Hoyaux and Sucov (1969) used a simple inverse dependence of transition rates on electron temperature for all descending transitions:

$$K_{kj} = A_{kj}\frac{e}{kT_e} \tag{28}$$

where the coefficients A_{kj} are constants derived by them using the results of Kenty (1950). However, the authors propose that it is easier and more consistent to use the following relationship which applies directly to the transition rate coefficients for downward transitions:

$$K_{kj} = \frac{g_j}{g_k}\exp\left(\frac{e(V_k-V_j)}{kT_e}\right)K_{jk} \tag{29}$$

The above relationship comes from the Klein-Rosseland relationship and is based on detailed balancing of excitation and de-excitation by electron collisions. As discussed by Hoyaux and Sucov (1969), this relationship is generally valid as long as the electron energy distribution is Maxwellian.

Transition rates used for the calculation are those corresponding to a minimum lamp wall temperature of 42°C and are taken from Winkler et al. (1983). Using the experimentally measured electron temperature of 11500 K for 42°C lamp wall temperature, the set of continuity equations for the particle densities is solved iteratively to obtain a convergence solution of the particle densities at the lamp wall temperature of 42°C. These particle densities are then used to calculate the constant coefficients C_{jk}. These constants C_{jk} are then used to calculate the transition rate coefficients K_{jk} at different electron temperatures.

Effective life times

The effective life times of the radiating states are also very important for the adequate explanation of the observed emission of radiation from the discharge. The resonance states emit photons which suffer from self-absorption whilst traveling through the discharge plasma. The repeated absorptions and re-emissions of photons on the way to the tube wall increase the effective mean life times of the mercury resonance states. Accurate knowledge of the effective life times is essential for the numerical modeling of the emission, absorption and re-emission of radiation by the resonance states In our model, the effective life times for the resonance states 6^3P_1 and 6^1P_1 as well as the 7^3S_1 and $6^3D_{1,2,3}$ states are needed in order to solve the set of balance equations.

The magnitude of the effective life time is influenced by many factors, amongst which are the mercury atom density, the broadening of the hyperfine structure of the resonance lines due to thermal motion of the atoms (Doppler broadening), and the interaction of the mercury atoms with mercury and argon atoms (collision broadening). Holstein (1947, 1951) performed an analysis of the effective life time by considering Doppler broadening and collision broadening separately, and then obtaining different relations for each of the two cases. Walsh (1959) investigated the combined effects of both Doppler and collision broadening However, there still remain unsolved problems concerning the hyperfine structure of the lines, and researchers are still active in this subject; examples of recent work include those of van de Weijer and Cremers (1985), Post (1986) and Post et al. (1986).

In order to keep the analysis as simple as possible, Holstein's theory for a pure Doppler broadening (Holstein, 1947) was used in our model. The expression giving the effective life time is as follows:

$$\tau_{eff} = \frac{k_o R[\pi \ln(k_o R)]^{1/2} \tau}{1.6} \tag{30}$$

where k_o is the absorption coefficient at the center of the resonance line, R the radius of the discharge tube, and τ the natural life time of the radiating state Following Winkler et al. (1983), we use the following expressions for the absorption coefficient of the two resonance lines 253.7 nm and 185 nm.

$$k_{02} = 2.23 \times 10^{-16} N_0 T^{-1/2} m^{-1} \tag{31}$$

$$k_{04} = 71.8 \times 10^{-16} N_0 T^{-1/2} m^{-1} \tag{32}$$

The values of the natural lifetime are discussed in various articles such as van de Weijer and Cremers (1985). A natural lifetime was used of 120 ns and 1.3 ns for the 6^3P_1 and 6^1P_1 states, respectively.

Ionization and Elastic Collision Losses

As stated previously, we ignore ionization from states other than the triplet $6^3P_{0,1,2}$ states Following Hoyaux and Sucov (1969), we assume further that the average energy level corresponding to the ionized state is $V_i + 3kT_e/2_e$ rather than simply V_i. Then, the ionization loss is calculated by the following equation:

$$W_{ion} = K_{17}N_eN_1e\left(V_i + \frac{3kT_e}{2e} - V_1\right) + K_{27}N_eN_2e\left(V_i + \frac{3kT_e}{2e} - V_2\right) + K_{37}N_eN_3e\left(V_i + \frac{3kT_e}{2e} - V_3\right) \tag{33}$$

The elastic collision loss rate is the product of energy loss per electron per collision, the collision frequency and the electron density. According to Waymouth (1971), the electron loses on average a fraction of its energy equal to $8m_e/3m_{rg}$. Also, according to Lamma et al. (1982), if the average electron kinetic energy is kT_e and the average electron speed is $(3kT_e/m_e)^{1/2}$, then the elastic collision loss is:

$$W_{el} = \frac{8\left(\frac{m_e}{3}\right)^{1/2} N_{rg}N_e(kT_e)^{3/2}}{m_{rg}\lambda_e^o} \tag{34}$$

APPENDIX B

Solution Scheme

To solve the above set of Equations (7)–(14), the following steps were taken:

1. The ground state density N_0 was calculated using Equation (17) and Dalton's Law of partial pressure:

$$N_0 = N_{Hg} = \frac{p_{Hg}}{kT_g} \tag{35}$$

where p_{Hg} is the mercury vapor pressure at the minimum lamp wall temperature and T_g is the gas temperature inside the lamp in kelvins.

In LITEAC2, the minimum lamp wall temperature was the lowest temperature of all lamp nodes. The gas temperature inside the lamp was assumed to be given by the elevation ΔT above the minimum lamp wall temperature, using the indirectly measured values of Kenty, Easley and Barnes (1951). DT is larger for a lower minimum lamp wall temperature (MLWT), e g. ΔT = 15.8°C when MLWT = 60°C and ΔT = 42.7°C when MLWT = 17°C.

2. The electron density N_e was then calculated using Equation (10) in the following form and a estimated value of electric field strength E:

$$I = N_e e\mu_e E\pi R^2 \tag{36}$$

In the above equation, the positive column current I was assumed to be constant, and can be obtained from the lamp data provided by the manufacturer.

3. The electron temperature T_e was then calculated, using an iteration method. An initial value of T_e was estimated, then all the transition rates K_{jk} and K_{kj} were calculated using this estimated value of T_e and the Equations (27) and (29).

4. Using the set of transition rates from step 3, the set of simultaneous Equations (19)–(21) was solved for the number densities N_1, N_2, and N_3 of the mercury triplet states 6^3P_0, 6^3P_1, and 6^3P_2, respectively.
5. T_e was then calculated using the ambipolar diffusion Equation (25) This equation is rewritten by taking out the common factor of the first three terms $\exp(-4.97e/kT_e)$:

$$(K'_{17}N_1 + K'_{27}N_2 + K'_{37}N_3)\exp\left(-\frac{4.97e}{kT_e}\right) = \frac{D_a}{\Lambda^2} \tag{37}$$

where

$$K'_{17} = C_{17}\left(\frac{kT_e}{e}\right)^{3/2}\left(1+\frac{5.76e}{2kT_e}\right)\exp\left(-\frac{0.79e}{kT_e}\right) \tag{38}$$

$$K'_{27} = C_{27}\left(\frac{kT_e}{e}\right)^{3/2}\left(1+\frac{5.54e}{2kT_e}\right)\exp\left(-\frac{0.57e}{kT_e}\right) \tag{39}$$

$$K'_{37} = C_{37}\left(\frac{kT_e}{e}\right)^{3/2}\left(1+\frac{4.97e}{2kT_e}\right) \tag{40}$$

Re-arrangement of Equation (37) gives the following expression for T_e:

$$T_e = \frac{4.97e}{k\log\left(\frac{K'_{17}N_1 + K'_{27}N_2 + K'_{37}N_3}{D_a/\lambda^2}\right)} \tag{41}$$

6 The newly calculated T_e was compared with the estimated T_e. If the difference is larger than a pre-set value, say 1 K, then the new T_e value is used to calculate all the transition rates K_{jk} and K_{kj} again, from Equations (27) and (29). This new set of transition rates was used to calculate the densities of the triplet states, as described in step 4. Using the new triplet state densities, a new value for T_e was calculated again, as described in step 5. This process was repeated until Te converges to a certain value.
7. The converged value for T_e was then used to calculate the transition rates in the set of Equations (19)–(25), according to Equations (27) and (29). Using these transition rates, the set of Equations (19)–(21) was solved for the densities, N_1, N_2, and N_3, of the triplet states. The densities of the 6^1P_1, 7^3S_1 and $6^3D_{1,2,3}$ states, N_4, N_5, and N_6, were then calculated using Equations (22), (23), and (24).
8. After obtaining T_e, N_e, N_0, N_1, N_2, N_3, N_4, N_5, and N_6, the energy balance Equation (1) was used to calculate the electric field E again. This value of E was then compared with the initially assumed electric field (in step 2) If the difference between the newly calculated and the initially assumed value of electric field strength is greater than a preset value, say 0.1 V/m, then the calculations are repeated from step 2 until convergence.
9. On convergence of both E and T_e, the set of equations were solved and all the unknowns E, T_e, N_e, N_0, N_1, N_2, N_3, N_4, N_5, and N_6 were found. The power of UV lines 253.7 nm and

185 nm were then calculated using Equations (3) and (4) The visible and invisible radiation output power from the 7^3S_1 and $6^3D_{1,2,3}$ states were estimated by Equations (5) and (6).

10 The light output was then calculated from Equation (16), with values for W_{uv} and W_{vis} derived from Equations (13) and (5), respectively. The illuminance on room surfaces was then calculated by multiplying the light output with the ratio of short-wave radiation falling on the surface to that emitted from the lamps.

ACKNOWLEDGEMENT

This research was made possible by the support of the Staff Development Fund of The Hong Kong Polytechnic University. The authors are also very grateful to Prof E. Sowell of California State University for providing the LIGHTS program.

NOMENCLATURE

Λ Diffusion length, m
Φ Luminous flux output per unit volume of positive column, lm m^3
Φ_{lamp} Total luminous flux output of fluorescent lamp, lm
τ Natural life time of radiating state, s
τ_{eff} Effective life time of radiating state, s
τ_j^* Average effective life time of the j^{th} state, s
τ_{jo}^* Effective life time of the spontaneous decay of the j^{th} state to the ground state, s
η Quantum efficiency of phosphor
λ Wavelength, nm
μ_e Electron mobility, m^2/(V s)
A_{kj} Reduced transition coefficient from state k to state j for descending transitions ($k > j$)
C_{jk} Reduced transition coefficient from state j to state k for ascending transitions ($k > j$)
D_a Ambipolar diffusion coefficient
E Electric field strength, V/m
e Electronic charge = 1 60217733 $\times 10^{-19}$ C
F A factor to correct for loss of actinic radiation and emitted light at the ends of lamp
$f(U)$ Energy distribution function of electrons
g_j Statistical weight of the i^{th} state
I Electric current through positive column, A
j Current density, A/m^2
k Boltzmann constant = 1.380658 $\times 10^{-23}$ J K^{-1}
K_{jk} Transition rate coefficients m^3 s^{-1}
k_o Absorption coefficient at the center of the resonance line
m_e Electron rest mass = 9 1093897 $\times 10^{-31}$ kg
mrg Mass of rare gas, kg
n_λ Number of quanta of wavelength λ
N_e Electron density, m^3
N_{Hg} Number density of mercury atoms, m^3
N_j Number density of the j^{th} state, m^3
N_{rg} Number density of rare gas, m^3
p_{Hg} Partial pressure of mercury vapor, Pa
$Q_{jk}(U)$ Collision cross-section of the transition from state j to state k
R Radius of fluorescent lamp tube, m
$S(\lambda)$ Relative spectral power distribution of light output from fluorescent powder, 1/mm
T_e Electron temperature, K
T_g Absolute temperature of gas inside fluorescent tube, K
U Electron energy, eV
v Electron drift velocity, m/s
$V(\lambda)$ Relative spectral luminous efficiency for photopic vision of standard CIE observer
V_j Energy level of the j^{th} state, eV
$W(\lambda)$ Power output in wavelength interval λ to $\lambda + d\lambda$ per unit wavelength per unit volume of plasma, W/(nm m^3)
W_{185} Power of the 185 nm line per unit volume of plasma, W/m^3
W_{254} Power of the 254 nm line per unit volume of plasma, W/m^3
W_{el} Power loss due to elastic collisions per unit volume of plasma, W/m^3
W_{inel} Power loss due to inelastic collisions per unit volume of plasma, W/m^3
W_{ion} Power loss due to ionization per unit volume of plasma, W/m^3
W_{nv} Power of emitted invisible lines per unit volume of plasma, W/m^3
W_{phos} Total power output of the fluorescent powder in the lamp, W
W_{vis} Power of emitted visible lines per unit volume of plasma, W/m^3

REFERENCES

Bigio, L 1988 Density Measurements of $Hg(6^3P_{0,1,2})$ in a Discharge Using Saturated Laser Absorption and Hook Methods. *Journal of Applied Physics* 63(11)· 5259-5269.

Cayless, M A. 1963. Theory of the Positive Column in Mercury Rare-Gas Discharges. *Brit. J. Appl Phys* 14· 863-869

Chung, T M., and D L Loveday. 1998 A Room Model for the Numerical Modeling of Lighting—Part 1· HVAC Interaction in Enclosures. *Companion Paper*

CIE. 1983 *The Basis of Physical Photometry. Publication CIE No.* 18.2. Paris· CIE

CIE. 1986 *Colorimetry.* 2nd edition. *Publication CIE No.* 15 2 Vienna· Central Bureau of the CIE.

Dakin, J.T. 1986. A Model of Radial Variations in the Low-Pressure Mercury-Argon Positive Column *Journal of Applied Physics* 60(2): 563-570

Easley, M A. 1951. Probe Technique for the Measurement of Electron Temperature. *Journal of Applied Physics* 22: 590-593.

Holstein, T 1947. Imprisonment of Resonance Radiation in Gases. *Physical Review* 72(12). 1212-1233

Holstein, T 1951. Imprisonment of Resonance Radiation in Gases. II *Physical Review* 83(6). 1159-1168

Hoyaux, M F., and E.W. Sucov. 1969. Theoretical Analysis of Effects of a Monoatomic Impurity on Low-Pressure Metal arc Discharges in a Noble Gas Matrix. *Journal of Applied Physics* 40(8)· 3237-3246.

Jerome, C.W. 1953 The Measurement of Quantum Efficiency of Fluorescent Lamp Phosphors *Journal of the Electrochemical Society* 100. 586-587.

Kenty, C. 1950. Production of 2537 Radiation and the Role of Metastable Atoms in an Argon-Mercury Discharge. *Journal of Applied Physics* 21(12). 1309-1318.

Kenty, C , M.A. Easley, and B T. Barnes. 1951. Gas Temperatures and Elastic Losses in Low Pressure Mercury-Argon Discharges. *Journal of Applied Physics* 22(8). 1006-1011.

Koedam, M , and A.A. Kruithof. 1962. Transmission of the Visible Mercury Triplet by the Low Pressure Mercury-Argon Discharge, concentration of the 6^3P states. *Physica* 28: 80-100

Lagushenko, R., and J. Maya. 1984. Positive Column Hg-rare Gas Discharge Model Applicable to Compact Fluorescent Lamps. *Journal of IES* 14. 306-314.

Lama, W L., C.F. Gallo, T J. Hammond, and P J. Walsh. 1982. Analytical Model for Low-Pressure Gas Discharges: Application to the Hg+Ar Discharge. *Applied Optics* 21(10). 1801-1811.

Post, H A 1986. Radiative Transport at the 184 9-nm Hg Resonance Line I. Experiment and Theory *Physical Review A* 33(3): 2003-2016

Post, H A , P. van de Weijer, and R.M M. Cremers. 1986 Radiative Transport at the 184.9-nm Hg Resonance Line. II. Extensive Experiments. *Physical Review A* 33(3) 2017-2024.

Sowell, E F. 1989. *LIGHTS User's Guide—A Computer Program for Modeling of Thermal and Luminous Aaspects of Building Lighting Systems* Fullerton. Department of Computer Science, California State University.

Sowell, E F. 1990 A Numerical Lighting/HVAC Test Cell. *ASHRAE Transactions* 96(2): 780-786.

Treado, S J., and J.W. Bean. 1988 *The Interaction of Lighting, Heating and Cooling Systems in Buildings—Interim* Report NIST IR-883860 Gaithersburg: National Institute of Standards and Technology

Treado, S J , and J.W. Bean 1992 *The Interaction of Lighting, Heating and Cooling Systems in Buildings Report* NIST IR 4701. Gaithersburg· National Institute of Standards and Technology

Verweij, W. 1961. Probe Measurements and Determination of Electron Mobility in the Positive Column of Low-Pressure Mercury-Argon Discharges. *Philips Research Reports Supplements* 2.

Vriens, L. 1973. Energy Balance in Low-Pressure Gas Discharges. *Journal of Applied Physics* 44(9): 3980-3989.

Walsh, P.J 1959. Effect of Simultaneous Doppler and Collision Broadening and of Hyperfine Structure on the Imprisonment of Resonance Radiation. *Physical Review* 116(3): 511-515.

Waymouth, J F. 1971. *Electric Discharge Lamps* Cambridge, Massachusetts· MIT Press.

Waymouth, J F, and F Bitter. 1956 Analysis of the Plasma of Fluorescent Lamps. *Journal of Applied Physics* 27(2) 122-131.

van de Weijer, P., and M M. Cremers. 1985. Determination of the Effective Radiative Lifetime of the 6^3P_1 Atomic Mercury Level in Low-Pressure Mercury Discharges *Journal of Applied Physics* 57(3) 672-677

Winkler, R B , J. Wilhelm, and R. Winkler. 1983. Kinetics of the Ar-Hg Plasma of Fluorescent Lamp Discharges. *Annalen der Physik (Leipzig)*, 40: 90-118; 40: 119-139.

Zissis, G , P. Bénétruy, and I. Bernat. 1992. Modeling the Hg-Ar Low-Pressure-Discharge Positive Column· A Comparative Study *Physical Review A* 45(2): 1135-1148.

Numerical Simulation of the Ambient Thermal Effect on Light Output of Fluorescent Luminaires in an Enclosure

T.M. Chung
(The Hong Kong Polytechnic University)

Abstract

The light output of fluorescent lamps is sensitive to changes of ambient temperature and/or air flow rate around the lamps. This is due to that the radiant power of resonance UV radiation generated in the low-pressure mercury discharge depends on the mercury vapour pressure inside the discharge tube The mercury vapour pressure inside the fluorescent lamp tube changes with the minimum lamp wall temperature because mercury condenses on the cold-spot of the lamp wall In this study, a numerical model of the low-pressure mercury rare-gas discharge positive column is applied to simulate the effect of tube wall temperature on the light output of the fluorescent lamp A numerical model of the heat transfer in an enclosure is used to simulate the heat transfer inside the luminaire compartment This heat transfer model calculates the lamp wall temperature which is then used in the positive column model for the calculation of light output The heat transfer model, which considers radiation, conduction and convection, can also include heat transfer in the ceiling plenum and in the room space. This paper discusses how the fluorescent positive column numerical model is incorporated into a numerical model of the heat transfer in a compartment This combined positive column and heat transfer model will find applications in the design of fluorescent luminaires so as to ensure that fluorescent lamps inside the luminaire compartment are operating under optimum ambient thermal conditions which will give maximum light output

1. INTRODUCTION

It is well known that the light output of a fluorescent lamp depends on the lamp wall temperature which in turn depends on changes of ambient thermal conditions around the lamp. There is an optimum lamp wall temperature for which fluorescent lamps give maximum light output. Fluorescent lamps which are put inside an enclosed luminaire compartment may operate at a temperature much higher than the optimum resulting in a decrease in light output and efficiency. On the other hand, if the return air flows through the lamps in an air-handling luminaire, it is possible that the lamps are cooled too far below the optimum temperature, again resulting a decrease in light output and efficiency.

Previous numerical models developed for the simulation of the interaction between lighting and air-conditioning, such as that of Sowell [1,2], made use of empirical curves of the light output and lamp power against minimum lamp wall temperature in order to account for the temperature effect on light output. However, the use of empirical curves gives no physical insight into the mechanism of conversion of electrical energy into light and heat within the fluorescent lamp. Furthermore, it is necessary to use different curves for lamps of different type and different size. In order to obtain a physical insight and to calculate the conversion of electrical power into light and heat from first principles, a mathematical model of the discharge process inside the fluorescent lamp has to be used

In view of the above, a numerical model has been developed to simulate the mutual interaction between fluorescent lamps and the ambient thermal environment The model combines a fluorescent lamp discharge model with a heat transfer model in an enclosure The fluorescent lamp positive column model simulates the process of conversion of electrical energy to light and heat. The heat transfer model simulates the heat transfer between surfaces inside an enclosure which can be just a single luminaire compartment, or a room enclosure comprising a luminaire, a plenum, an occupied space and ventilation inlets and outlets. The three modes of heat transfer, conduction, convection and radiation are all considered in the model This heat transfer model calculates the lamp wall temperature which is then used in the positive column model for the calculation of light output.

The goal of the research is to develop a numerical model for the simulation of the mutual interaction between lighting and air-conditioning which will find applications in areas such as.

(i) evaluation of performance of the lighting system as affected by room characteristics and design of the air-conditioning system
(ii) design calculations of cooling load due to lights and light output due to changes in thermal conditions

(iii) building energy analysis

The first item of the above can include evaluation of new luminaire designs to ensure that fluorescent lamps inside the luminaire compartment are operating under optimum ambient thermal conditions. The use of this numerical tool can minimize the necessity of experimental evaluation

In this model, the fluorescent lamp is the only source of energy input to the room, i e all other sources of energy input are not considered. For applications such as annual building energy analysis, this model can be used as a "pre-processor" to generate lighting load weighting factors and lighting energy distribution fractions for input to building energy analysis programs.

2. THE FLUORESCENT LAMP POSITIVE COLUMN MODEL

In the fluorescent lamp positive column model, energy balance is examined in relation to the densities of different species of mercury atoms which in turn depend on the lamp wall temperature. The model first calculates how the mercury densities change with changes in minimum lamp wall temperature and then how changes in mercury densities affect the energy balance. In the following description of the fluorescent lamp positive column model, the energy balance in the discharge is first described followed by a description of the balance of mercury species.

2.1 Fluorescent lamp energy balance

The function of an electric lamp is to convert electrical energy into light energy. In a fluorescent lamp, this conversion occurs through a number of processes within the lamp discharge tube

Electrical energy input to the fluorescent lamp discharge becomes principally the kinetic energy of the electrons due to acceleration of electrons by the electric field within the plasma. The kinetic energy of the electrons is dissipated in one of the following processes

(i) inelastic collisions with mercury atoms causing excitation to higher energy levels;
(ii) ionization of the mercury atoms;
(iii) elastic collisions with the rare-gas atoms; and
(iv) diffusion to the tube wall and recombination with excited atoms there.

The electrons may also collide with excited mercury atoms causing de-excitation which results in the excitation energy being released back to the electrons. This process is called superelastic collisions or sometimes referred to as elastic collisions of the second kind

An energy balance equation for the electrons in the positive column can be written as follows:

$$E \cdot j - W_{inel} - W_{ion} - W_{el} - W_{diff} + W_{sel} = 0 \qquad (1)$$

where E is the electric field across the discharge tube, j is the electric current density, and the W terms denote the local energy gains or losses per unit time per unit volume of the positive column The subscripts *inel*, *ion*, *el*, *diff*, and *sel* denote inelastic collision, ionization, elastic collision, diffusion, and super-elastic collisions, respectively. In equation (1), it is assumed that the recombination of electrons with ions within the plasma is negligible and that the thermal flux conducted through the electron gas is zero The last assumption follows from the fact that the electron temperature T_e is taken to be constant throughout the positive column in this study.

The net radiation loss W_{rad} of the discharge is given by the difference between the inelastic collision loss W_{inel} and the super-elastic collision loss W_{sel}. This is because the excited atoms can either decay spontaneously with emission of radiation or collide super-elastically with an electron transferring their extra energy back to the electron Hence, the net radiation power loss of the positive column per unit volume is given by:

$$W_{rad} = W_{inel} - W_{sel} \qquad (2)$$

The radiation emission from the discharge contains mainly the two ultra-violet wavelengths 253.7 and 185 nm with some weak lines in the visible and invisible wavelengths. Therefore, the radiation loss can be written as

$$W_{rad} = W_{254} + W_{185} + W_{vis} + W_{inv} \qquad (3)$$

where W_{254} and W_{185} are the losses (per unit volume) due to emissions in the two ultra-violet wavelengths 253 7 and 185 nm respectively; W_{vis} and W_{inv} are the power losses (per unit volume) due to weak emissions in the visible and invisible bands resulting from excitations of mercury atoms to energy states higher than the resonance states These radiation losses occur in the form of emission of quanta of energy and each quantum has an energy equals to the product of the electronic charge and the energy level difference in electron volts between the excited state and the final state of the transition. The number of quanta that can escape the plasma in unit time per unit volume is equal to the number density of the excited state in the plasma divided by the effective life time of the state (τ_j^*) in the plasma. The radiation power is then equal to the number of quanta escaping the plasma per unit time per unit volume multiplied by the energy gap of the transition.

$$W_{254} = eV_2 \frac{N_2}{\tau_2^*} \quad (4)$$

$$W_{185} = eV_4 \frac{N_4}{\tau_4^*} \quad (5)$$

$$W_{ms} = e(V_5 - V_2)\frac{N_5}{\tau_5^*} \quad (6)$$

$$W_{mv} = e(V_6 - V_2)\frac{N_6}{\tau_6^*} \quad (7)$$

In equations (4)-(7), e is the electronic charge and V_j denotes the energy level of the jth state

The power loss terms (W terms) all depend on the density of all species of mercury atoms, cross-sections of ionization and excitation of mercury atoms, the rate of re-combination at the tube wall and the density of rare-gas in the tube. A continuity equation can be set up for each species of the mercury atom. The set of continuity equations for all species of the mercury atom together with the energy balance equation form the equation set of a positive column model of the fluorescent lamp. Simplifications and approximations have to be made in order that the set of model equations becomes solvable

2.2 Continuity equations

The ground state density is governed by the following continuity equation:

$$-\sum_{j=1}^{6} K_{0j}N_eN_0 - K_{0i}N_eN_0 + \sum_{j=1}^{6} K_{j0}N_eN_j + \sum_{j=1}^{6}\frac{N_j}{\tau_{j0}^*} + \frac{D_aN_e}{\Lambda^2} = 0 \quad (8)$$

In the above equation, K_{jk} denotes the transition rate coefficient from state j to state k, N_e denotes the electron density, N_0 the ground state density and N_j the jth excited state density; τ_{j0}^* denotes the effective life time of the spontaneous decay of the j^{th} state to the ground state, D_a denotes the ambipolar diffusion coefficient; and Λ is the diffusion length.

The first term in equation (8) represents the excitation of the ground state to the six excited states, the second term represents ionization from the ground state, the third term represents the super-elastic decay of the six excited states to the ground state, the fourth term represents the spontaneous decay of the six excited states to the ground state with emission of a photon, the last term represents the rate of recombination of ions and electrons which is assumed to be purely an ambipolar diffusion phenomenon.

Again, at equilibrium, the kth excited state is governed by the following continuity equation:

$$-\sum_{j=k+1}^{6} K_{kj}N_eN_k - K_{ki}N_eN_k + \sum_{j=0}^{k-1} K_{jk}N_eN_j + \sum_{j=k+1}^{6} K_{jk}N_eN_j - \sum_{j=0}^{k-1} K_{kj}N_eN_k - \sum_{j=0}^{k-1}\frac{N_k}{\tau_{kj}^*} = 0 \quad (9)$$

In this model 6 excited states are considered, therefore equation (9) represents a set of 6 equations, one for each of the 6 excited states k=1 to 6. The first term represents loss of the kth state due to inelastic collisions causing excitation to higher levels. The second term represents loss due to ionization. The third and fourth terms represent the increase in the kth state due to excitation from lower states and super-elastic de-excitation of higher states respectively The fifth term represents loss due to super-elastic de-excitation of the kth state. The last term represents the spontaneous decay of the kth state with emission of a photon, this term is written in general form in equation (9) that includes decay transitions to all lower states, however, there are only several 'permissible' transitions that emit photons.

At equilibrium, the rate of creation of electron-ion pairs is equal to the rate of loss due to recombination at tube wall which is the same as the rate of ambipolar diffusion to the tube wall. Therefore, the electron density and the ionized state density are governed by the following equation which is called the ambipolar equation.

$$\sum_{j=0}^{6} K_{ji}N_eN_j - \frac{D_aN_e}{\Lambda^2} = 0 \quad (10)$$

The first term of equation (10) is the sum of the rate of ionization from the ground state and the six excited states The second term is the ambipolar diffusion rate to the tube wall which represents the rate of loss of electrons and mercury ions

2.3 Electric current density

The electric current density is equal to the product of the electron density N_e, the electronic charge e and the electron velocity v which is governed by the electron mobility μ_e and the electric field E across the positive column

$$j = N_eev = N_ee\mu_eE \quad (11)$$

2 4 Solution scheme

Equations (1) to (11) form the set of equations of the fluorescent lamp positive column model. In deriving the above equations and in order to solve this set of equations some approximations have to be employed Due to limitation of space, the approximations and the modified set of equations are not given here. More details of the approximations used with full discussions will be published in a research paper.

In the solution processes, the electron temperature is first calculated using an iteration method Then the transition rates K_{jk} and K_{kj} in equations (8)-(10) are calculated using the value of electron temperature Using this set of transition rates, the set of simultaneous equations (8)-(10) is solved for the number densities N_e, N_0, N_1, N_2, N_3, N_4, N_5 and N_6 With these number densities, equations (4)-(5) are used to calculate the power output of the 253.7 nm and 185 nm UV lines and also equations (6)-(7) are used to calculate the visible and non-visible radiation output. All terms in the energy balance equation (1) can also be calculated.

2 5 Calculation of light output

The light output from the lamp can be derived from a knowledge of the relative spectral power output $S(\lambda)$ of the fluorescent powder in the lamp. In here, the relative spectral power output $S(\lambda)$ is defined such that

$$\int S(\lambda)d\lambda = 1 \tag{12}$$

i e. the power output in wavelength interval λ to $\lambda+d\lambda$ is

$$W(\lambda) = S(\lambda)\ W_{phos} \tag{13}$$

where W_{phos} is the total output power of the fluorescent powder in the lamp.

Using the quantum efficiency of the lamp phosphor η which is defined such that

$$\eta = \frac{\int n_\lambda d\lambda}{n_{254} + n_{185}} \tag{14}$$

it can be shown that the quantum efficiency η is equal to the following expression

$$\eta = \frac{W_{phos}}{W_{uv}} \int S(\lambda)\frac{\lambda}{253\,7}d\lambda \tag{15}$$

In equation (14), n_λ is the number of quanta of the wavelength λ; n_{254} and n_{185} are the numbers of quanta of the 253.7 nm and 185.0 nm emission from the positive column, respectively. In equation (15),

$$W_{uv} = \frac{253\,7W_{254} + 185W_{185}}{253\,7} \tag{16}$$

Then the visible light output from the phosphors due to UV radiation emitted from the positive column is

$$\Phi = F\ 683\ W_{phos}\int S(\lambda)V(\lambda)d\lambda \tag{17}$$

Substituting for η with the expression given above

$$\Phi = F\cdot 683\ \eta\cdot W_{uv}\frac{\int S(\lambda)V(\lambda)d\lambda}{\int S(\lambda)\frac{\lambda}{253\,7}d\lambda} \tag{18}$$

In equations (17) and (18), F is a factor to correct for loss of radiation and emitted light at the ends of the lamp and absorption of light by the phosphor and glass bulb. F is quoted by Jerome [3] to be 0 75 which is a representative value for most lamps. The factor 683 is the maximum luminous efficacy of radiation which is 683 lm/W occurring at a wavelength of 555 nm $V(\lambda)$ is the CIE relative spectral luminous efficiency for photopic vision of the human eye.

CIE publication No. 15.2 [4] gives relative spectral power distributions of 12 types of typical fluorescent lamps representing standard, broad-band and three-narrow-band fluorescent lamps. From these spectral power distributions the integrals

$$\int S(\lambda)V(\lambda)d\lambda \tag{19}$$

$$\text{and}\ \int S(\lambda)\frac{\lambda}{253.7}d\lambda \tag{20}$$

can be evaluated. Using literature values of the quantum efficiency [3], the light output due to UV radiation Φ can be calculated by equation (18)

There is a small light output due to the visible emission of the discharge directly. This is calculated by assuming that half of the visible emission can escape through the phosphor coating and that the only visible lines emitted are 404.6 nm, 435 8 nm and 546 1 nm so that the mean $V(\lambda)$ is 0 334 Hence, the total luminous flux output per unit volume of the positive column of the discharge of the fluorescent lamp is calculated by the following formula:

$$\Phi = 683\left(0.75\ \eta\ W_{uv}\frac{\int S(\lambda)V(\lambda)d\lambda}{\int S(\lambda)\frac{\lambda}{253.7}d\lambda} + 0.5\ W_{vis}\cdot 0.334\right) \tag{21}$$

In the above equation, the first term is the light output from the UV activated phosphors and the second term is the light output due to the visible lines in the discharge.

The total luminous flux output of the fluorescent lamp is then equal to the expression of (21) multiplied by the length L and the cross-sectional area of the discharge tube (with d equals to the diameter of the tube).

$$\Phi_{lamp} = \Phi \cdot L \cdot \pi \cdot \frac{d^2}{4} \qquad (22)$$

3. THE HEAT TRANSFER MODEL OF AN ENCLOSURE

3.1 The enclosure

The enclosure considered in the heat transfer model can be a single enclosure, such as a luminaire compartment, or a room comprising luminaires, a plenum (ceiling void) and an occupied room space. The enclosure is divided into a number of nodes. Each node represents an isothermal surface.

3.2 The model heat transfer equations

This model uses fundamental heat transfer principles in heat balance equations for the nodes. The three modes of heat transfer between nodes are considered. For radiation heat transfer, short-wave radiation (mainly visible light) and long-wave radiation are calculated separately. For each node, the following heat balance equation holds. This equation relates the temperature rise of each node in one time step to the total net heat gain of that node in one time step.

$$m_i c_{pi} \Delta T_i = q_{in} + q_{Li} + q_{Si} + q_{Hi} + q_{Ci} \qquad (23)$$

where
- m_i = mass of node i,
- c_{pi} = specific heat capacity of node i,
- ΔT_i = temperature rise of node i in one time step,
- q_{in} = total (electrical) energy input at node i in one time step,
- q_{Li} = total (net) long-wave radiation heat gain to node i in one time step,
- q_{Si} = total (net) short-wave radiation heat gain to node i in one time step,
- q_{Hi} = total (net) convection heat gain to node i in one time step,
- q_{Ci} = total (net) conduction heat gain to node i in one time step.

As shown in this heat balance equation (23), the net heat gain to a node consists of five components: energy input (for lamp and ballast nodes only), long-wave (infrared) radiation, short-wave (visible) radiation, convection and conduction. Each of these components is calculated separately as described below.

The energy input at node i, q_{in}, for the lamp and ballast nodes is calculated by the fluorescent lamp model described above. This depends on the lamp used and the lamp wall temperature.

The rate of net long-wave radiation to node i is obtained by subtracting the radiant exitance (radiosity) of i from the irradiance on i as follows.

$$q_{Li} = (E_{Li} - M_{Li}) A_i \qquad (24)$$

where E_{Li}, M_{Li} and A_i are respectively the irradiance, radiant exitance (radiosity) and area with reference to node i (all symbols with a subscript L refer to long-wave radiation). Using form factors F_{ij}, and emissivities ε_i etc, equation (24) can be written as follows

$$q_{Li} = A_i \varepsilon_i (\sum_j F_{ij} M_{Lj} - \sigma T_i^4) \qquad (25)$$

where σ is the Stefan-Boltzmann constant and T_i is the absolute temperature of the ith node.

Using similar treatment as above for the short-wave radiation and assuming all surfaces within the enclosure are perfectly diffuse, then the rate of net short-wave radiation to node i can be written as:

$$\dot{q}_{Si} = A_i [(1 - \rho_{Si}) \sum_j F_{ij} M_{Sj} - M_{Sni}] \qquad (26)$$

where ρ_{Si} is the short-wave reflectance of the ith surface and M_{Sni} is the luminous power per unit area emitted from the ith surface. M_{Sni} is zero except for the lamp and diffuser nodes. In a fluorescent lamp the luminous power emission M_{Sni} is related to the property (quantum efficiency and spectral distribution) of the fluorescent powder in the lamps and the discharge intensity inside the lamp. The fluorescent lamp positive column model described above is used to calculate M_{Sni} for the lamp nodes. Consideration of the visible radiation can be divided into a number of wavelength bands if reflectance etc. are known for each surface for each wavelength band. This division into different wavelength bands will make the calculation of illuminance more accurate.

For surfaces in contact with an air node there is convection heat exchange between the surface and the air node. The convection heat gain of node i is:

$$\dot{q}_{Hi} = A_i h_i (T_a - T_i) \qquad (27)$$

where h_i is the convective heat transfer coefficient of node i, and T_a is the temperature of the air node adjacent to node i

The convection to the air node is then given by

$$q_{Ha} = \sum_i h_i (T_i - T_a) A_i \quad (28)$$

where the sum is taken over all nodes in contact with the air node

For nodes in contact with each other, there is a conduction heat transfer between them. The total conductive heat transfer to node i is calculated by

$$\dot{q}_{Ci} = \sum_j C_{ji} (T_j - T_i) \quad (29)$$

where C_{ji} is the conductance from node j to node i and the sum is taken over all nodes in contact with node i

3 3 Solution scheme

In order to get a solution, the mass, heat capacity, reflectivity, emissivity and initial temperature of each node must be known or assumed A time step is then selected. The rates of heat gain by different modes are then calculated one by one using equations (24) to (29) with nodal temperatures equal to that at the beginning of the time step. The power on the lamp node and the short-wave radiation emitted from the lamp node are calculated using the fluorescent lamp positive column model with the temperature of the lamp node as input. Equation (23) is then used to calculate the temperature change in one time step This temperature change is then added to the nodal temperature prevailing at one time step before. In other words, the model uses the forward finite difference method in the calculation of the nodal temperatures one time step forward. From the short-wave radiation falling on a nodal surface, the illuminance on the surface can be calculated using the CIE relative spectral sensitivity curve, and either knowing or assuming the spectral distribution of the light.

4. PRELIMINARY RESULTS

This model has been validated using experimental results reported in literature. Further validation has also been done using a laboratory constructed test cell with a simple luminaire installed. Results show good agreement of calculated values with experimental data both for light levels and temperatures. It is found that with the incorporation of a fluorescent lamp positive column model in a heat transfer model, the lighting/air-conditioning interaction is better predicted together with an improvement in the modeling of illuminance on room surfaces. The results of the validation runs of this model will be discussed in detailed research papers which are being prepared and will be published in an international research journal.

5. CONCLUSION

A mathematical model of the fluorescent lamp positive column can be used to simulate the effect of the thermal environment inside luminaire compartments within enclosures on the light output and power input to the lamp This fluorescent lamp positive column model can also be incorporated into a heat transfer model of an enclosure to simulate the mutual interaction of lighting and the thermal environment which may include effects on the air-conditioning Investigations on the possible applications of the mathematical model are being done

References

[1] Sowell, E F. 1989. LIGHTS User's Guide Fullerton: Department of Computer Science, California State University.

[2] Sowell, E F. 1990 A numerical lighting/HVAC test cell *ASHRAE Transactions* 96(2) 780-786

[3] Jerome, C.W. 1953. The measurement of quantum efficiency of fluorescent lamp phosphors. *Journal of the Electrochemical Society* 100. 586-587.

[4] CIE. 1986. *Colorimetry 2nd edition Publication CIE No 15 2.* Vienna, Austria Central Bureau of the CIE

Acknowledgment

This research reported here forms part of the author's PhD study at Loughborough University. The study is supported by staff development fund of The Hong Kong Polytechnic University.

Author:	CHUNG, Tse-ming
Address:	Department of Building Services Engineering, The Hong Kong Polytechnic University, Hung Hom, Kowloon, HONG KONG.
Tel	(852) 2766 5844
Fax.	(852) 2774 6146
E-mail:	betmchng@polyu edu hk